Assessment of diffuse pollution originating from estuarine historical landfills

Francis Timothy O'Shea

A thesis submitted in partial fulfilment of the requirements of the degree of Doctor of Philosophy.

School of Geography, Queen Mary, University of London

2016

I, Francis Timothy O'Shea, confirm that the research included within this thesis is my own work or that where it has been carried out in collaboration with, or supported by others, that this is duly acknowledged below and my contribution indicated. Previously published material is also acknowledged below.

I attest that I have exercised reasonable care to ensure that the work is original, and does not to the best of my knowledge break any UK law, infringe any third party's copyright or other Intellectual Property Right, or contain any confidential material.

I accept that the College has the right to use plagiarism detection software to check the electronic version of the thesis.

I confirm that this thesis has not been previously submitted for the award of a degree by this or any other university.

Signature:

Date:

Details of collaborations:

Michelle Morris, Queen Mary University of London, performed Mercury analysis at the Biotron Centre for Climate Change, University of Western Ontario, Canada, during April 2014. The raw data is presented within Section 4.4.2, data analysis and interpretation was undertaken by myself.

Professor Andrew Cundy, University of Brighton, performed ^{210}Pb and ^{137}Cs gamma spectrophotometry on 17 sediment samples. These data are presented in Section 4.4.2. All interpretation was undertaken by myself.

This work was supported by a Natural Environment Research Council CASE studentship in association with Arcadis N.V. (Grant number NE/I018212/1).

Acknowledgements

Firstly, I would like to thank my supervisors, Dr. Kate Spencer, Professor James Brasington, Mark Webb and Katy Baker for their support, inspiration, understanding and general willingness to work with me for the last 3(+) years! I owe you all a lot!

I am also indebted to past and present laboratory staff at QMUL; Simon Dobinson, Michelle Day, Laura Cox, Kate Peel, Natalie Ludgate and Maggie Fitzherbert, to name but a few. It has been a pleasure working with you all, and thank you for your patience over the last few years!

Thanks also go to Dr. Emma Shuttleworth, Niall Lehane, Professor Andrew Cundy and Professor Andy Plater. You have all played key roles in the last few years, through either scientific discussion, method explanations, sample analysis or equipment loan.

In addition, I am thankful to Dr. James Rothwell for my initial introduction into contaminant geochemistry, Ray Howarth for your enthusiasm towards physical geography, and to examiners Dr. Neil Rose and Dr. Mark Scrimshaw.

To everyone from 224, Kieran Stanley, Michelle Morris, Eleanor Webster, James Holloway, Joe James, and further afield in 104, John Groves, Cianna Wyshnytzky, James Brand, Anna March, Ginny Benardout and Harold Lovell. I have made some incredible friends over the past few years, with whom I have shared a lot of stories, experiences, coffees and beers. You have made this process even more enjoyable!

Finally, I would like to thank my mum, Shelagh, and my brother, Tom, for their support throughout the PhD process, and of course Anna Glover, for your unconditional and often well timed encouragement, without whom I would not have been so happy and well fed!

Thank you.

Abstract

The UK contains 5000 unlined historical landfills in the coastal zone currently at risk of erosion within the next 50 years. These rely on natural attenuation in surrounding sediment to reduce the contaminant load to the environment. This thesis investigates the extent and magnitude of sediment metal contamination from historical estuarine landfills.

An intensive investigation of Newlands historical landfill, Essex, indicated elevated metal concentrations in surface and sub-surface sediments. Surface sediment concentrations were similar to other industrially impacted estuaries, whilst peak metal concentrations at c. 50 cm depth were indicative of industrial activity in the mid-20th Century. Below this depth, sediments were enriched with Pb (EF > 2) and Zn (EF = 1.5) indicative of an historic leachate plume that extends c. 15 m from the landfill site boundary. These sediments present a secondary source of diffuse pollution and a site contamination load of c. 1200 kg Pb.

In-situ XRF was demonstrated as a rapid contamination screening tool for Fe, Pb, Sr and Zn enabling a broad-scale investigation of historical landfills across SE England. Sediment cores from eight sites containing both hazardous and inert waste were screened. Concentrations and EFs of Pb and Zn at depth were significantly higher in hazardous sites compared to inert sites. Spatial distributions of Pb and Zn were comparable to Newlands historical landfill. This indicates that diffuse pollution from historical landfill sites with similar chemical and physical attributes to Newlands is likely to present a regional, if not national problem, with UK historical landfills presenting contaminated sediments, comprising a significant, previously unidentified and unquantified diffuse pollution source in the coastal zone.

Contents

List of Figures

List of Tables

List of Equations

List of Appendices

Chapter 1 Introduction

The UK has a rich history of landfilling; having disposed of waste in the ground for centuries (Bagchi, 1994) and first regulating landfill disposal in the early 19th Century (Read *et al.*, 1997). The UK still commits around 57 million tonnes, or 43% of all waste produced to the ground, disposing more waste to landfill than any other EU nation (Davies, 2012). The introduction of legislation such as the Control of Pollution Act (1974), the Environmental Protection Act (1990) and Landfill Regulations (2002) has helped to provide guidance and frameworks to control, investigate and reduce the effects of landfilling on the environment, leading to a 36% reduction in landfilled waste by the end of the 20th Century. However, prior to the introduction of the Landfill Regulations (2002), the burial of waste within the environment was not subject to the strict management, waste acceptance criteria and engineering controls of today's more engineered sites. Historically, our estuaries and coasts would have frequently been the locations for these landfills, as low-lying coastal land, prone to tidal flooding had low economic and agricultural value and hence provided suitable locations for waste disposal proximal to urban areas. As a result, there are approximately 20000 landfills situated on low-lying land within the inter-tidal, coastal zone in the UK (Cooper, 2012; Environment Agency, 2012).

These coastal historic landfills were commonly engineered without basal or side wall liners, and they relied upon the natural attenuation capacity of surrounding fine-grained mudflat and salt marsh sediments to sorb contaminants, such as heavy metals or inorganic salts, before any leachates interacted with saline groundwater or surface waters (Bagchi, 1987; Njue *et al.*, 2012). Therefore, sediments adjacent to the coastal landfills may have been historically polluted and could now present a secondary diffuse source of contamination in the coastal zone.

Climate change predictions state that within the next 50 years, both the frequency and intensity of high energy storm events will increase (Solomon *et al.*, 2007), as well as increased saline intrusion (Field, 1995) and declines in salt marsh area (Craft *et al.*, 2009) as a result of shoreline retreat (Kennish, 2002), and coastal erosion (Bromhead and Ibsen, 2006). It is forecast that coastal sediments, including those impacted by landfill contamination will be eroded as a result of these climate change predictions. Erosion of contaminated sediments (Cooper, 2001) may result in the remobilisation of contaminants into the local environment, placing ecosystems at risk. There is a duty of care for contaminated land managers and land owners to adequately manage historic landfills, as climate change driven redistribution of contaminated sediments could result in failure to comply with regulations such as the Water Framework Directive.

To date, there have been few studies examining the magnitude and extent of contamination from historic landfills within the coastal zone, however it has been reported that sediments surrounding landfills can be impacted by trace metals, ammonium and organic compounds (Michalak and Kitanidis, 2002; Njue *et al.*, 2012; Gooddy *et al.*, 2014). Subsequently, as the requirements for local authorities, landfill managers and stake holders to effectively manage coastal areas increase in light of the inception of the Water Framework Directive (2000/60/EC), Shoreline Management Plans (DEFRA, 2006) and the requirements for Environmental Impact and risk assessments, there is an increased necessity to comprehensively understand the nature and extent of contamination within the coastal zone.

The overall aim of this PhD thesis is to investigate the potential that historical, coastal landfills within the United Kingdom have to contaminate both adjacent sediment bodies and the further environment, such as biota. This was achieved by addressing a number of research aims and associated research objectives.

Research Aim 1: To establish whether Newlands Landfill has created a legacy source of contamination.

Objective 1a: To assess the magnitude of metal concentrations within sediments and establish whether they pose an environmental threat.

Objective 1b: To examine the spatial distribution of contamination to support an investigation into the behaviour of metals.

Objective 2: To understand the potential pathway and behaviour of metals in the sediment.

Research Aim 2: To assess whether in-situ X-ray Fluorescence (XRF) analysis can be used to generate rapid, accurate and precise sediment contamination data within coastal sediments suitable for onsite investigations.

Objective 1: To examine the influence of moisture content on X-ray suppression and determine a moisture correction factor that can be applied to field wet *in-situ* sediment samples.

Objective 2: To undertake and examine the accuracy of *in-situ* sample moisture measurements.

Objective 3: To determine whether moisture corrected *in-situ* XRF analysis provides analytically accurate data for a range of metals, in comparison to *ex-situ* ICP-OES analysis.

Research Aim 3: To investigate whether historic contaminant release from Newlands landfill and resultant contamination of surrounding sediments is representative of other sites in SE England and hence, whether historic landfills present a significant problem in the South East and more widely in the whole of the UK.

Objective 1: To identify potentially hazardous historical landfill sites using publicly available secondary data.

Objective 2: To use *in-situ* XRF as a rapid screening tool to identify the presence and extent of sub-surface contaminated sediments indicative of a legacy leachate plume and attenuation within surrounding coastal sediments.

Objective 3: To provide a recommended 'next step' and worked example for the assessment of risk from historical landfills.

Chapter 2 Thesis Outline

This PhD thesis will begin by presenting an overview of the literature, primarily focused around landfilling, landfill design, leachates, waste degradation, the estuarine environment and the role of metals within these areas as well as the hazards and risk assessment methods for environment contamination (Chapter 3).

Chapters 4 to 6 are self-contained research chapters, comprising their own methods, results and discussions. Chapter 4 is an in-depth intensive investigation into the contamination distribution surrounding Newlands, an historic landfill within Essex, UK, to establish whether the landfill is impacting adjacent sediments. Chapter 5 presents a novel technique for the accurate quantification of contamination within wet sediment using X-Ray Fluorescence analysis, in order to develop a rapid screening method for contamination surrounding other landfills. The extensive investigation is subsequently presented in Chapter 6, where eight landfills situated on coastal sediments within the South East were visited and their contamination distribution examined. The implications of the findings are then presented and a method for the estimation of risk from these sites is offered.

Finally, Chapter 7 presents a summary of the findings from the project, as well as considering identified research gaps relating to the effective assessment of contamination risks from historic landfills within the coastal zone.

Chapter 3 Literature Review

3.1. Landfilling

The UK places more than 57 million tonnes of waste (around 43% of the total produced) into landfills every year (Davies, 2012), making it the most dominant, yet least favourable waste disposal route for waste management (DEFRA, 2011c). Landfilling has been utilised for waste disposal for centuries (Bagchi, 1994), however it was only in 1875 that guidelines were first established for the control of public waste, introducing requirements for public storage of refuse (Read *et al.*, 1997). From this point, various waste acts have been introduced, notably the Public Health Act in 1936, the Town and Country Planning Act in 1947, the Control of Pollution Act in 1974 and the Environmental Protection Act (1990) which tightened the guidance and controls of the waste industry. The introduction of the Landfill Directive 1999 (1999/31/EC) outlined specific requirements for landfilling, ensuring protective provisions to reduce pollution potential as far as possible. As a result, landfills constructed after 16th July 2001 are subject to strict design, licensing, monitoring and post-closure controls, which aim to control the pollutant potential from the 4000 landfills which currently have waste disposal licences within the UK (Williams, 2005). However, there are still an estimated 20000 landfill sites in the UK (Cooper, 2012) which were constructed prior to 2001 and are not required to comply with the Landfill Regulations and are defined as 'historical landfills' (Mouser *et al.*, 2005).

3.1.1. Landfill Design

Waste contained within both modern licenced and historical landfills requires control. Pollution prevention and control legislation requires modern sites to have impermeable layers on both the base and sides of the site as well as collection points for leachates (Landfill Directive (1999)(1999/31/EC)) (Section 3.1.2). This is referred to as a containment site design (Figure 3.1), where wastes are entirely separated from surrounding soils and sediments. As these sites are controlled under the Landfill Regulations, they pose little hazard to the environment when stable, as the waste is physically contained within the site.

Conversely, historical landfill site design was commonly based on the theory of natural attenuation (Figure 3.1), the process through which the magnitude of contaminants within a landfill is reduced through the slow release of leachate into surrounding sediments, relying on the dilution and dispersion capacity of the surrounding saturated and unsaturated zones (Shukla and Rai, 2009). Contaminated leachate (Section 3.1.2) released from the landfill initially migrates through the unsaturated vadose zone and then through groundwater via advection and dispersion (McCarthy and Zachara, 1989), physically diluting contaminants

(Njue *et al.*, 2012), yet not reducing the actual contaminant load available to sensitive environmental receptors. Chemical processes are responsible for reducing the contaminant availability and therefore the availability to receptors. These processes; sorption, biodegradation, and transformation will be discussed in more detail within Section 3.3. The release of contaminants from a landfill and subsequent natural attenuation has the potential to result in the formation of a secondary source of pollution within nearby surrounding sediments.

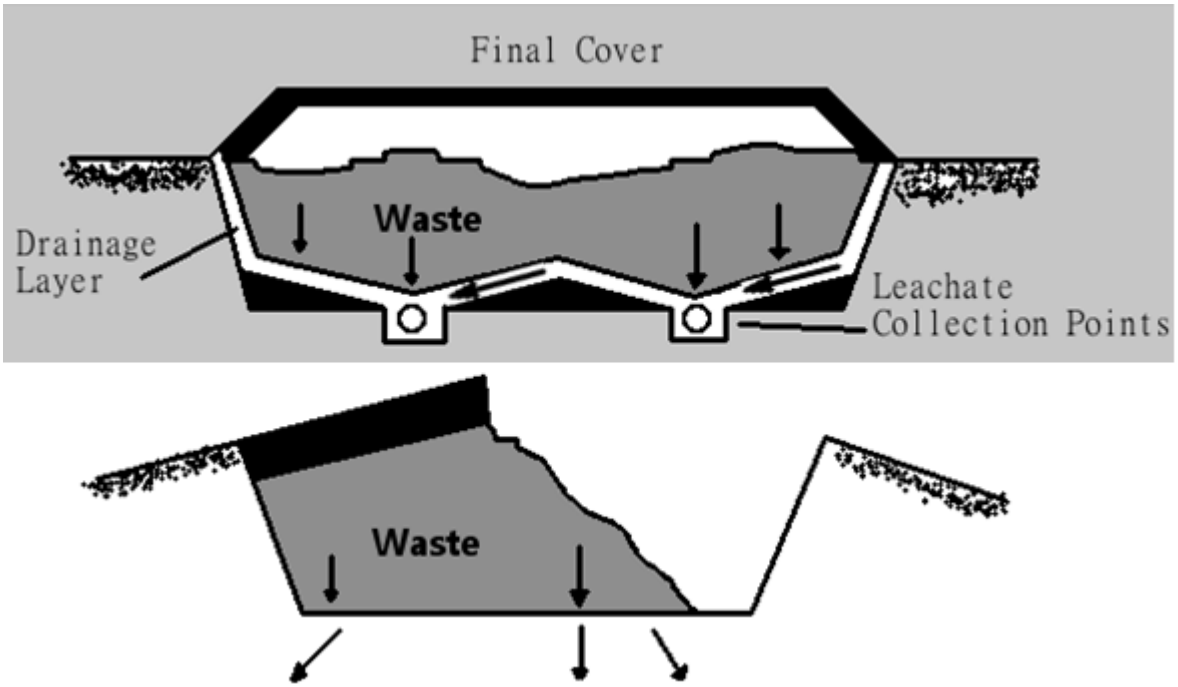

Figure 3.1: Different landfill types. Top: A modern containment landfill with leachate collection points to ensure waste is not in contact with surrounding sediment. Bottom: A Natural Attenuation landfill showing leakage from the waste into surrounding substrata. Adapted from Bagchi (1994).

In compliance with the Landfill Regulations, modern sites are subject to strict monitoring and management requirements. However, prior to the introduction of these regulations, there was no requirement to keep records and therefore data regarding waste composition, volume and age of historic landfills, where available, must be approached with caution. The data do however indicate that there are over 20000 known instances of historic landfilling within England and Wales, with over 5000 of these being situated within the coastal zone and along estuary banks, predicted to be at risk of flooding with a 1 in 50 chance in a given year (Environment Agency, 2012) An example of the number of coastal landfills within the Thames estuary is given in Figure 3.2.

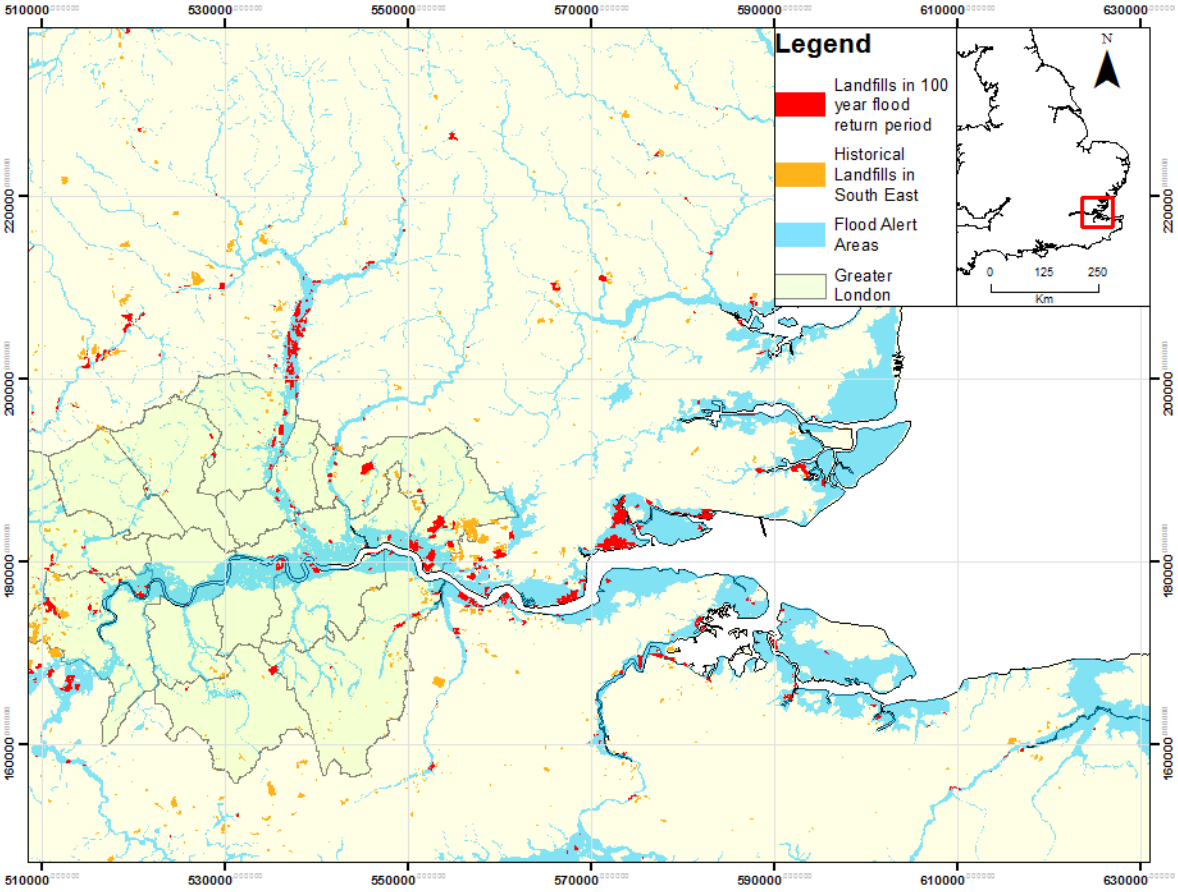

Figure 3.2: The abundance of landfills within the Environment Agency flood alert area on the Thames Estuary, South East England (Environment Agency, 2014).

These sites, commonly situated on repurposed, low value, possibly uninhabitable land, such as exhausted agricultural or marsh lands, are prevalent within major urban estuarine areas such as the Lower Thames, with easy access from both river and road enabling transport of waste to the sites. Some historical UK sites have been investigated under Part IIa of the Environmental Protection Act (Environmental Protection Act, 1990), finding contamination records of both landfill gases and anthropogenic metals (Njue *et al.*, 2012). Other work has found sites with elevated levels of cyclic organic compounds (Michalak and Kitanidis, 2002) and ammonium (Gooddy *et al.*, 2014). These studies indicate that this waste has the ability to impact the environment and, as such, requires further investigation of their potential hazard.

3.1.2. Leachate Composition and Generation

Landfill leachates are a water-based solution, generated by landfills from the infiltration of water as well as internal moisture (Williams, 2005), comprising a mix of organic and inorganic compounds (Table 3.1) that reflect both the composition and degradation stage of the waste (Slack *et al.*, 2005). Leachates are the medium through which potentially polluting elements/compounds are transferred from the landfill into surrounding soils, sediments and groundwater and in some cases, eventually surface waters.

Table 3.1: Common leachate contaminants. From Christensen *et al.* (2001)

- Dissolved Organic Matter - Expressed as the leachate Chemical Oxygen Demand (COD) or Total Organic Carbon (TOC). Also includes methane, volatile fatty acids and fulvic compounds.
- Inorganic Macrocomponents - Ca, Mg, Na, K, Fe, Mn, Cl, NH_4^+, SO_4^{2-} and HCO_3^- .
- Heavy Metals – Cd, Cr, Cu, Pb, Ni and Zn.
- Xenobiotic Organic Compounds – Hydrocarbons, Phenols and Chlorinated Aliphatics.

Controls on Leachate Composition

Leachate quality is chiefly governed by the composition of the waste, directly reflecting the constituents of the waste material (Johnson *et al.*, 1999). Additional factors, such as waste degradation state, degree of compaction, temperature and moisture content all play major roles in the composition of leachates. For example, inert and non-hazardous waste landfills produce less hazardous leachate than industrial or hazardous waste (Williams, 2005). Pulped or shredded waste will present a higher surface area, and therefore increased microbial activity, whereas waste which is highly compact may inhibit the free flow of nutrients or water, inhibiting initial aerobic degradation and slowing the overall degradation process (Williams, 2005). Average leachate composition from a domestic municipal landfill can be seen in Table 3.2. The table also shows the variation in leachate composition, notably metals such as Pb and Zn, with time.

Table 3.2: Average leachate composition values (mg L^{-1}) for contaminants from a (1) young landfill (Williams, 2005) and a (2) mature landfill (Lopez et al., 2004).

Constituent	Young (Hydrolysis) Landfill mean(mg L^{-1})(1)	Mature (Methanogenic) Landfill mean(mg L^{-1}) (2)
pH	6.73	8.2
Na	1371	3970
Mg	384	24.1
Fe	653.8	2.7
Ni	0.42	0.31
Cu	0.130	
Zn	17.37	0.16
Cd	0.02	<0.02
Pb	0.28	<0.03
Hg	0.0004	

Waste degradation has a major effect on leachate composition due to the significant physicochemical changes that occur within the waste immediately after landfill disposal (Williams, 2005). The key stages, as well as the major physical, chemical and microbial characteristics of waste decomposition are outlined below:

Stage I: Hydrolysis/Aerobic Degradation. Immediately after deposition, high organic matter concentrations and an abundance of oxygen within the waste provide constituents for initial aerobic metabolism. Aerobic micro-organisms use this organic matter and produce carbon dioxide (CO_2), water and heat, with the potential for waste temperatures to reach 90 °C. The duration of aerobic degradation is short (Erses *et al.*, 2008), commonly up to a month, however it is dependent on waste compaction, depth of waste and the waste cover as they all influence oxygen concentration and availability (Waste Management Paper 26B, 1995).

Stage II: Hydrolysis and Fermentation. Once oxygen is depleted, facultative anaerobes increase and anaerobic degradation become dominant (Kulikowska and Klimiuk, 2008). Large levels of ammonia (NH_3), CO_2 and carboxylic acids are produced by the deamination of proteins. As this stage is not as exothermic as aerobic degradation, the waste temperature drops to around 30 °C (Waste Management Paper 26B, 1995).

Stage III: Acetogenesis. During this stage, acetogens (micro-organisms producing acetate) convert the high concentrations of carboxylic acids from Stage II into acetic acid. The production of this acid, as well as the presence of chloride, ammonium and phosphate ions, reduce the pH within the waste, subsequently increasing the solubility of metal ions (Yusof *et al.*, 2009). This stage is referred to as the acid formation phase, and is reflected within leachate composition (Figure 3.3), which will contain a discrete spike of metal concentrations, indicating the phase of acetogenic degradation (Williams, 2005).

Stage IV: Methanogenesis. This is the main anaerobic degradation stage and the dominant stage of landfill gas production, capable of lasting tens of years before the slow, temperature dependant reactions have completed (CAPCOA, 1990). CH_4 is generated from both the organic acids from previous stages as well as microbial conversion of H^+ and CO_2 and can constitute 50% of the gas from the waste (Warith and Sharma, 1998). The production of these gasses neutralises the acidic conditions produced within the acetogenic stage, restoring the waste pH, reducing metal solubility and as a result, reducing metal concentrations present within leachates (Figure 3.3).

Stage V: Oxidation. The final stage of degradation is aerobic, and commonly referred to in the literature as 'Final Maturation' (Pohland *et al.*, 1985; Onay and Pohland, 1998; Morris *et al.*, 2003; He and Shen, 2006). However, the processes outlined in this stage are theoretical as there are a limited number of landfills sufficiently old enough to be undergoing this degradation. Controlled experimentation suggests that when landfill gas production exhausts available acids, aerobic microorganisms will slowly replace anaerobic organisms, stabilising the waste. This may be shown by a change from CH_4 to CO_2 production, as well as generation of water (Williams, 2005).

As well as the rate of degradation being time dependent, factors which further influence

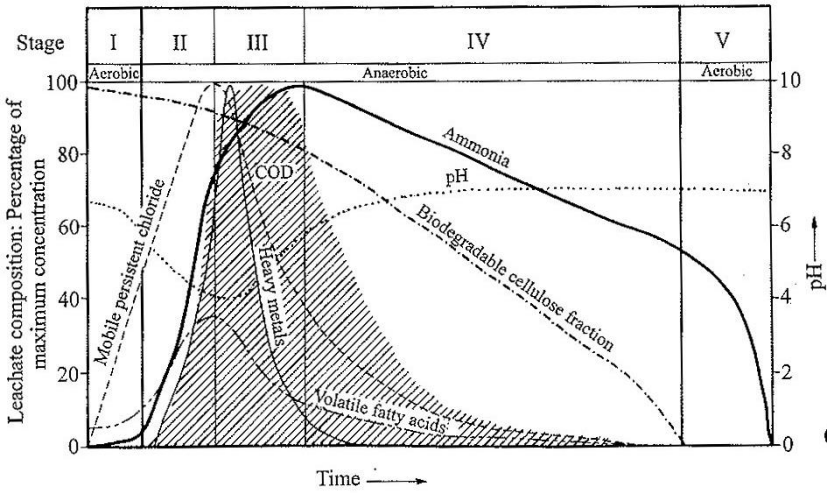

Figure 3.3: Leachate composition over various stages of waste degradation. From Williams (2005).

leachate composition, such as an increased ambient temperature, will have the effect of increasing microbial activity and accelerating the rates of decomposition (Williams, 2005). Additionally, water content has shown to consistently promote rapid degradation as decomposition in sites situated within arid climates is slower than those in areas receiving 500 – 1000 mm rainfall per year (Kjeldsen *et al.*, 2002).

This waste degradation behaviour shows that landfill age is critical and must be considered in order to establish the risk potential from any landfill site. It is likely that collecting and analysing leachates from an historic landfill will contain little or no inorganic contaminants

(Njue *et al.*, 2012), as any contamination within the waste will have already been mobilised during acetogenic degradation, releasing it within the leachates.

Leachate Generation

Whilst the volume of leachate is primarily dependant on the moisture content of the waste exceeding the field capacity (El-Fadel *et al.*, 2002), the source and levels of moisture will vary on a site by site basis. Leachate generation can be estimated using Equation 3.1:

Equation 3.1: Estimating leachate generation (L_o) as a function of rainfall (R) liquid waste (LW) surface infiltration (IRA) and leachate discharge (LTP) waste absorption (aW) and basal seepage (DL). Derived from Williams, 2005).

$$L_o = [R + LW + IRA] - [LTP + aW + DL]$$

Rainfall (R) has the largest impact on leachate production (Baucom and Ruhl, 2013), and is therefore controlled in modern, operational landfills by daily capping (Cassiani *et al.*, 2008). Liquid within the waste (LW), will transfer to the leachate under compressive stresses of waste compaction. Surface infiltration (IRA) represents moisture entering the waste through capping materials (Williams, 2005).

3.2. The Estuarine Environment

Estuarine areas are the tidal interface between both riverine and marine environments (Dhanakumar, 2013), where fresh water dilutes saline sea waters, resulting in a salinity of neither 0 gL^{-1} (freshwater) nor 34 gL^{-1} (fully saline) (Chapman and Wang, 2001). Sediments within estuarine zones are sourced from periodical flooding and deposition of both terrigenous and marine sediments, commonly forming fine grained (<63 µm) mudflat floodplains (Pande and Nayak, 2013) which through continuous sedimentation may accumulate and become vegetated with halophytic species, trapping sediment and eventually forming a salt marsh (Allen, 2000). The sediments themselves are of immense importance to social, economic and ecological systems (Apitz, 2012); providing crucial habitats for avifaunal and fish communities (Boyes and Allen, 2007), acting as nutrient sources, improving water quality through storage of sediment and sediment-bound contaminants, as well as natural coastal defences (Williams, 1993) due to the effective wave attenuation of vegetated salt marshes (Möller *et al.*, 2014).

Daily flooding of estuarine sediments and salt marshes makes them predominantly depositional environments, providing suitable conditions for the rapid storage of heavy metals and nutrients within the sediments (Williams, 1993; Henry and Jefferies, 2003). As many estuaries are situated downstream of large industrial areas (Clark, 2001), such as the Scheldt (Du Laing *et al.*, 2002) or a mining legacy, such as Dulas Bay in Anglesey (Whiteley and Pearce, 2003), their sediments generally receive significant anthropogenic inputs of metals such as Pb, Zn and Cu from both point and diffuse sources (Chapman and Wang, 2001), with values up to 2500 times the natural background level (Vernet, 1991; Rubio *et al.*, 2000). However, not all elevated metal concentrations are a result of anthropogenic activity. The weathering of bedrocks (Castro *et al.*, 2013) and atmospheric deposition (Çevik *et al.*, 2009) are the main natural sources of trace metals in the environment. The concentrations are commonly low, reflecting only the metal rich sediment fractions, such as clays (Windom *et al.*, 1989). Contaminants are transferred through either dissolved or particulate form, which will then be transferred to salt marsh surface sediments (Zwolsman *et al.*, 1996) reflecting present day water quality (Spencer, 2002). The abundance of fine-grained material and organic matter adds to the storage ability of estuarine sediments (Cundy *et al.*, 2005). Numerous studies have observed the contaminant record present within the sediments, in order to reproduce past pollutant inputs (Zwolsman *et al.*, 1993; Cochran *et al.*, 1998; Álvarez-Iglesias *et al.*, 2007) or measure contaminant distribution and behaviour (Emmerson *et al.*, 2000; Zoumis *et al.*, 2001; Spencer *et al.*, 2003; McIntosh *et al.*, 2012).

However, any contaminant accumulation within sediments cannot be considered permanent (ElBishlawi *et al.*, 2013), and metals may be re-released to the water column via diagenetic remobilisation (Shaw *et al.*, 1990; Whiteley and Pearce, 2003) (Section 3.3), or physical/biological reworking of sediment (Cundy *et al.*, 2003; Wolters *et al.*, 2005a). Salt marshes in south east England, particularly in major estuaries (such as the Thames) have been suffering from sediment and vegetation losses due to pollution exposure (O'Reilly Wiese *et al.*, 1995), land reclamation (Gedan *et al.*, 2009), embankment construction (Wolters *et al.*, 2005b) and increased wave energy (van der Wal and Pye, 2004). This erosion has led to an estimated loss of 1000 ha of sediment during the late 20th Century (Cooper, 2001) with an average net salt marsh loss of 3 ha year $^{-1}$ in the Thames estuary (van der Wal and Pye, 2004). This erosion leads to physical loss of sediment and the potential for chemical conditions to release any stored contaminants that may be bound, such as those sorbed to sediments as a result of the natural attenuation of landfill leachate.

This overview suggests that estuarine sediments are crucial to the deposition and storage of anthropogenic contamination, however they are an indefinite sink as conditions may arise that promote the release stored contamination long after initial deposition (Pande and Nayak, 2013).

3.2.1. The Thames Estuary

The Thames estuary is the major focus of this thesis. It is an example of a major urbanised estuary (Trimmer *et al.*, 2003), situated downstream from Greater London. The tidal area covers approximately 131 km^2, from Teddington Weir to Southend, Essex, draining a catchment of approximately 14000 km^2 (Figure 3.4). The funnel shaped estuary is macrotidal, with spring and neap tides of 6 and 3 m respectively (Trimmer *et al.*, 2000). The underlying geology in the area is sedimentary clay and sands, deposited in the Palaeogene and Eocene, approximately 50 M years ago (Smith *et al.*, 1973). The estuary lies to the south of the London Basin syncline, created during the Alpine Orogeny, which exposes older, Cretaceous chalks on the south of the river. The coastline is home to approximately 4000 ha of fringing and open marshes (van der Wal and Pye, 2004) acting, as previously mentioned, as efficient scavengers for the abundance of nutrients, xenobiotics and heavy metals which have been discharged into the water over London's rich history of pollution (Fletcher *et al.*, 1994).

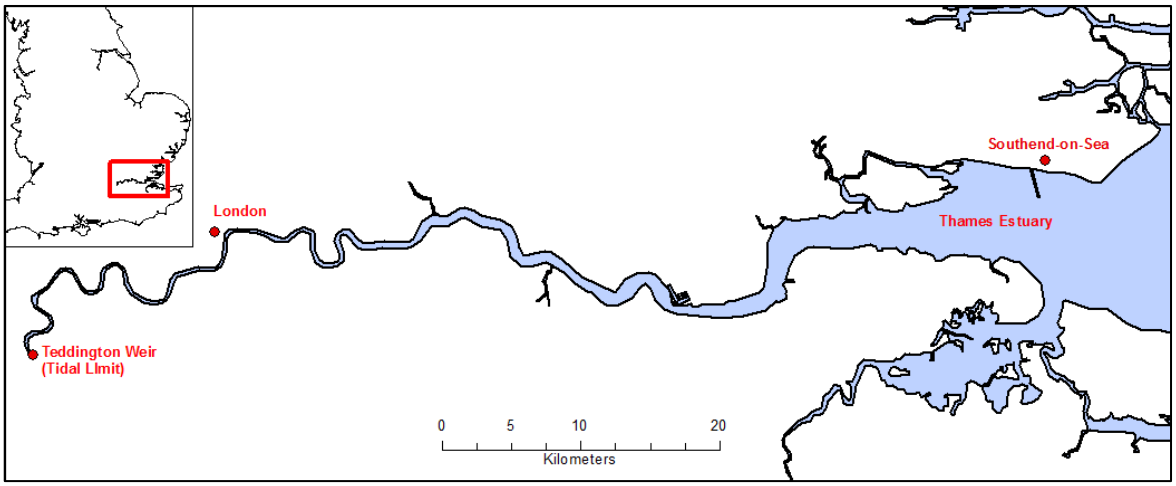

Figure 3.4: Thames Estuary in South East England.

The first evidence of pollution in the River Thames is as early as the 14th Century, where the river was used as a conduit for public effluence discharge (Wheeler, 1969). The rise of industry in the UK brought the industrial revolution, increasing London's importance as a centre of commerce, vastly expanding the city. In the early 19th Century, oxygen depleting human wastes and industrial effluent were pumped directly into the water, leading to a period of severely degraded water quality, with 1858 being referred to as "The Year of the Great Stink" (Attrill, 1998).

There are currently numerous brickworks, steel manufacturers, battery recycling centres, gas works (O'Reilly Wiese *et al.*, 1997b), sewage treatment plants and outfalls (Trimmer *et al.*, 2000) located on the main channel. The quality of the Thames water and sediments have received significant attention over the years, with studies focusing on quantifying contamination and associated biological implications. Within the 20th Century, the Thames river water has had a documented legacy of Pb, Cd (Power *et al.*, 1999), As (Millward *et al.*, 1997) and Sn (Harino *et al.*, 2003) contamination, PCBs entering biota (Yamaguchi *et al.*, 2003; Jürgens *et al.*, 2015) contamination, as well as an oxygen sag within the middle estuary (Araújo *et al.*, 2000) reducing O_2 saturation to ~20% during summer months (Trimmer *et al.*, 2003). The river is also home to an abundance of physical plastic and sanitary contamination (Morritt *et al.*, 2014) both on the surface and within bed sediments.

Surface sediments contain Ag, As, Cd, Cr, Cu, Hg, Mn, Ni, Pb, Sn and V (Smith *et al.*, 1973; Attrill, 1995) concentration elevated above geochemical background, whilst sediment cores have provided well-documented records of historically elevated levels of As, Cd, Hg, Pb, Se (Fletcher *et al.*, 1994) and PCBs (Scrimshaw *et al.*, 1996). These show a clear record of early 20th Century industrial contamination, with a decrease towards the surface due to the introduction of environmental legislation in the late 20th Century, resulting in less contaminated sediments overlying impacted ones (O'Reilly Wiese *et al.*, 1995). The pollution record within the Thames is similar to that found within other industrialised estuaries (Attrill, 1995), suggesting that anthropogenic contamination is a large scale problem, impacting global sediment quality (Table 3.3).

Table 3.3: Average Estuarine sediment concentrations (mg kg^{-1}) 1. (Attrill, 1995), 2. (Bai et al., 2011a), 3. (Zwolsman et al., 1996), 4. (Bryan and Langston, 1992).

	Ag	As	Cd	Cr	Cu	Fe	Hg	Mn	Ni	Pb	Sn	Zn
Medway[1]	1.5	18	1.1	53	55	32216	1	418	26	86	3	220
Mersey[1]	0.7	42	1.2	84	84	27326	3	1169	29	124	8	379
Scheldt[3]	-	10	0.8	130	15	-	0.3	-	10	27	-	98
Severn[4]	0.4	8	0.6	55	38	28348	0.5	686	33	89	8	259
Thames[1]	4.7	15	1.3	59	61	28228	0.6	552	34	179	16	219
Tyne[1]	1.6	25	2.2	46	9.2	28206	0.9	395	34	187	5	421
Yellow River[2]	-	38	0.8	64	31	-	-	-	28	29	-	96

3.2.2. Coastal Erosion in the Thames and South East

The Thames Estuary, however, is currently under pressure. The majority of London was developed on low lying marshland, reclaimed and occupied for industrial, agricultural and domestic purposes (Lavery and Donovan, 2005). Twinned with the isostatic rebound from melting of the Late Devensian Ice Sheet (Lambeck, 1991), the Thames is under threat from climate change as a result of rising sea levels and increased storm intensity (Lavery and Donovan, 2005). Experimental modelling suggests that in the future, areas of up to 1000 km^2 may be regularly flooded, costing up to £98 billion in damages (Dawson *et al.*, 2005). As a direct result of the devastating floods in 1953, tidal defences on the Thames have been improved, by constructing the Thames Barrier (Lavery and Donovan, 2005), however this does not provide any protection to sediments in the lower estuary. Consequently, the majority of coastal sediments within the estuary are within the Environment Agency flood alert area, and are at risk from erosion/reworking (Figure 3.5).

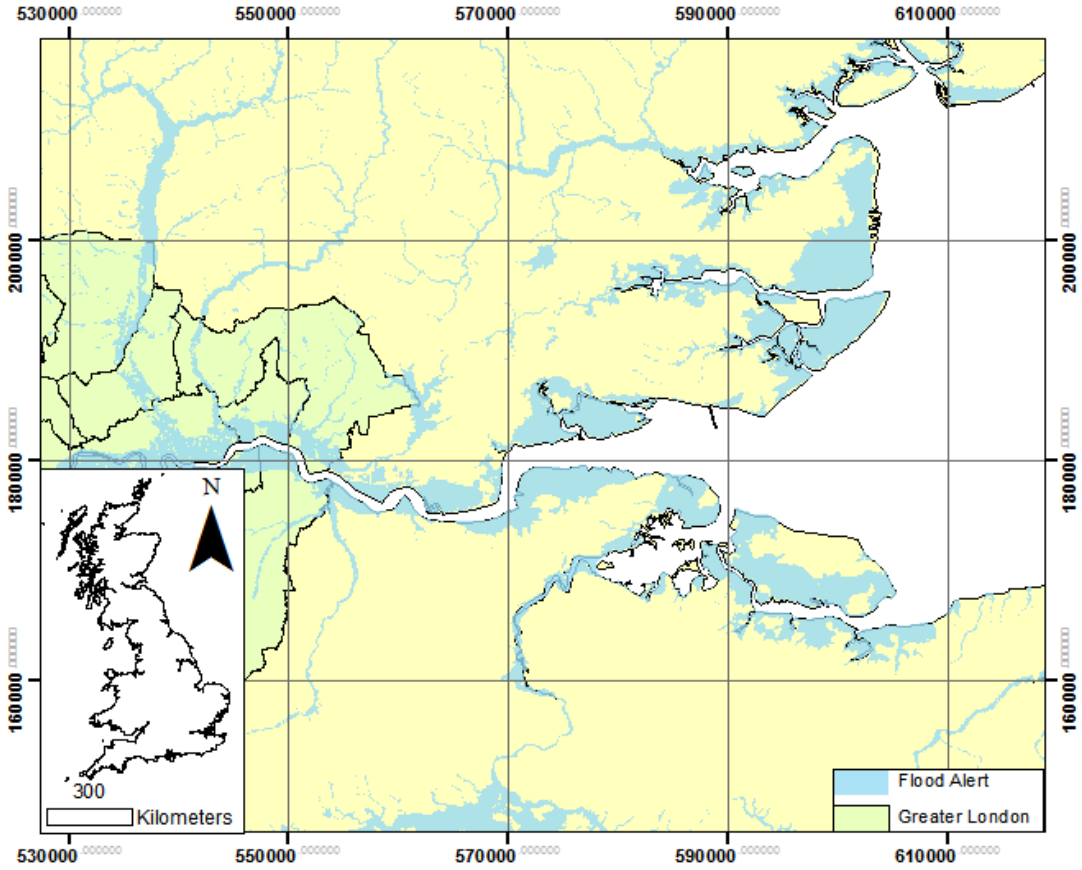

Figure 3.5: Extent of flooding risk within the South East and Thames area (Environment Agency, 2012).

3.3. Metals in the Estuarine Environment

This thesis focuses on major and trace metals within the environment. Lighter metals, such as ^{25}Mn to ^{30}Zn are essential for metabolic life at lower concentrations, yet may cause toxicological damage above certain concentrations (Waldron, 1980). Conversely, heavier elements such as ^{48}Cd, ^{80}Hg and ^{82}Pb are not required for metabolic activity and are toxic at low concentrations (Mil-Homens *et al.*, 2013). Metals exist in many forms within the environment, affecting their behaviour and bioavailability, specifically as water soluble metals, exchangeable metals (free ions or inorganic/organic complexes), metal carbonates, oxides and hydroxides (adsorbed to high molecular weight humic substances such as organic matter, or Fe/Mn oxides), precipitated as sulphide compounds or metals bound within the lattice of primary materials (Du Laing *et al.*, 2009). The presence of these metals can be considered a hazard, however their form, behaviour and therefore bioavailability is variable and not permanent. With sediment concentrations being up to 5 orders of magnitude higher than the overlying water column, even a small change in mobility can release a vast quantity of metals, resulting in detrimental effects to the surrounding environment (Bryan and Langston, 1992).

Metals commonly enter salt marsh environments through riverine discharges or atmospheric deposition. The most common form of the metals at this point is either in solution, either as free ions such as Fe^{2+} (Hopwood *et al.*, 2014) or less soluble complexes with ligands such as natural organic matter (Rose, 2003). They can also be in particulate form, bound to the surface or within solids such as carbonates, clay minerals or organic matter (Luoma and Rainbow, 2008).

Metals such as Cu, Zn and Pb become associated with particulate phases within coastal sediments through adsorption (Lion *et al.*, 1982). The degree to which estuarine sediments attract and adsorb trace metals is dependent on the sediment Cation Exchange Capacity (CEC), or the ability for negatively charged surfaces of organic matter, clay particles, Fe and Al oxides to attract positively charged metal ions (Du Laing *et al.*, 2009). Estuarine areas contain high levels of fine grained material, defined as clay and silt with diameters of <3.9 µm and 3.9 - 63 µm respectively (Wentworth, 1922). These sediments can increase concentrations of sediment-bound metals (Ackermann *et al.*, 1983) due to their negative surface charge, and a surface area c. 1000 x larger per gram than their sandy counterparts, increasing the number of available binding sites (Baird, 2012). This ‘grain size effect’ has significant impact on sediment metal concentrations and therefore needs to be taken into consideration when undertaking comparative analysis of differing grain sizes (Kersten and Smedes, 2002).

Additionally, precipitation occurs when the concentration of a metal is higher than the solubility of the least soluble compound that can be formed by the reaction of the metal and the anion (Bryan, 1971). Within estuarine waters, metals are readily precipitated, or co-precipitate with carbonates (Sundaray *et al.*, 2011), hydroxyl, chlorides and sulphides to form solid complexes with a new molecular unit (Sposito, 1987). The reaction between 2 soluble compounds such as Zn^{2+} and CO_3^{2-} results in the precipitation of an insoluble precipitate and a soluble by-product. Equation 3.2 Shows an example of Iron (III) Oxide precipitating as an oxide ion as the system is not in equilibrium in respect to the solubility product of H_2O (Du Laing *et al.*, 2009).

Equation 3.2: Solubility of Iron (III) Oxide. The reaction shows precipitation of $2Fe^{2+}$ (right to left) into the solid phase and dissolution of Fe_2O_3 (left to right) into the aqueous phase. From Du Laing et al. (2009)

$$Fe_2O_3(s) + 2e^- + 6H^+(aq) \leftrightarrow 2Fe^{2+}(aq) + 3\ H_2O\ (l)$$

3.3.1. Processes Affecting Mobility

Once metals are deposited in the environment, they may undergo diagenetic changes, a series of biological, physical and chemical processes which may re-release them back into the water column (Spencer *et al.*, 2003). Williams (1993) cites salt marsh hydrology as the most important factor regulating metal bioavailability within salt marshes, as the periodic flooding and inundation with saltwater regularly varies both salinity and oxygen supply within sediments.

Within estuarine sediments, oxygen is rapidly utilised within surface sediments (top few mm), due to both high levels of microbial activity and the presence of relatively impermeable clay minerals (Kostka *et al.*, 2002). As the sediment is periodically waterlogged, there is a limited oxygen supply to micro-organisms at depth, promoting a series of redox reactions utilising successively more reduced alternative electron sinks; nitrogenous compounds (NO_3^-), reduced Mn (MnO_2) and Fe ($Fe(OH)_3$), sulphate (SO_4^{2-}) and methane (CH_4) (Williams, 1993). Figure 3.6 provides examples of various redox zones occurring at increased depths within marsh sediments and the changes to electron receptors, promoting either binding or dissolution of metals under different scenarios.

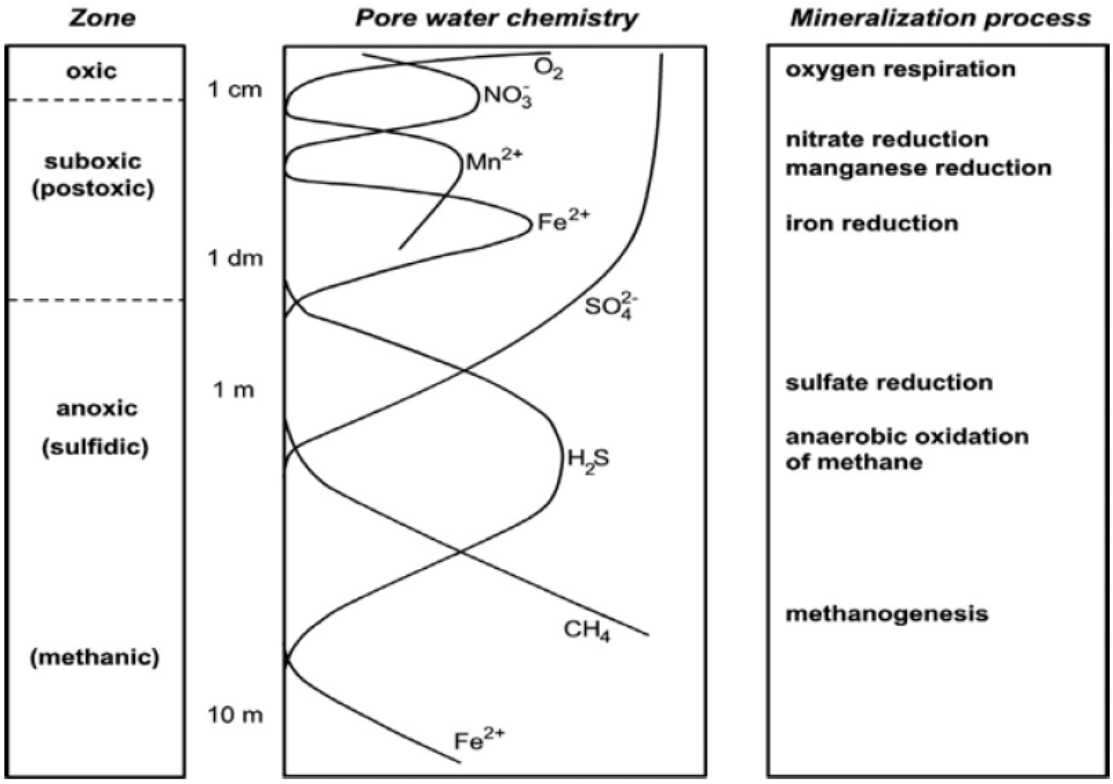

Figure 3.6: Biogeochemical zonation within estuarine/marine sediments, showing main redox reactions and processes occurring at depth. From Jørgensen and Kasten (2006).

This anoxic binding/ dissolution of metals is not permanent. Within aerobic conditions, the effective metal scavengers, Fe and Mn oxides are considered insoluble (Luoma and Rainbow, 2008), but easily undergo dissolution when reduced (Fe^{3+} to Fe^{2+} and Mn^{4+} to Mn^{2+}) due to their weaker outer sphere electrostatic attraction, leading to the remobilisation of any adsorbed metals (Zwolsman *et al.*, 1993). Mn is more easily reduced, therefore preferentially utilised, than Fe, and is considered more mobile, resulting in typically shallower enrichment than Fe (Figure 3.6). However, as well as these releases, reduction also converts Cr(IV) into Cr(III) and Cu(II) into Cu(I), both of which are less toxic species (Pardu *et al.*, 1995; Simpson *et al.*, 2000). The change in redox potential at depth also as an effect on sediment pH, as protons are consumed during reduction (Du Laing *et al.*, 2009). The resultant pH increase is likely to reduce mobilisation, transferring metals to the sediment, the opposite effect to when reduced sediments are oxidised, releasing metals such as Cu and Pb (Calmano *et al.*, 1993). In areas dominated by calcareous minerals, carbonates are likely to exhibit a buffering effect on any pH changes (Vranken *et al.*, 1990). However, decalcification may occur as a result of FeS oxidation and organic matter decomposition, leading to acidification and subsequent release of metals at depth (Du Laing *et al.*, 2009). This results in the typical enrichment profiles found within salt marsh sediments (Anderson *et al.*, 1986; Spencer *et al.*, 2003).

At greater depths, metal mobility is affected by the presence of metal sulphides, produced by bacterial reduction of sulphate sources from inundated material (Du Laing *et al.*, 2009). Fe is the most predominant sulphide-generating element, forming FeS (Billon *et al.*, 2001) or FeS_2 (Luther III and Church, 1988), however metals such as Pb, Cu, Zn and Cd can form insoluble, stable sulphides in anoxic sediment (Giblin *et al.*, 1986). FeS can then co-precipitate with trace metals, reducing their solubility (Lord III and Church, 1983).

Within salt marsh sediments, tidal inundation will also increase salinity, which will form soluble chloro-complexes, increasing the solubility of metals such as Cd, Mn, Cu and Pb (Zhao *et al.*, 2013). This formation will increase metal mobility, reducing metal sediment accumulation (Speelmans *et al.*, 2007).

Physical disturbances, such as bioturbation (Simpson *et al.*, 1998), re-suspension due to more turbulent flow (Zoumis *et al.*, 2001) or erosion (Spencer, 2002) can lead to oxidation of anoxic estuarine sediments. Oxidation is likely to result in the increased mobility of trace metals, due to the oxidation of sulphides to sulphates reducing sediment pH, resulting in the release of any co-precipitated metals (Du Laing *et al.*, 2009). Despite salt marsh sediment root structures inhibiting reworking (Zwolsman *et al.*, 1996) and anaerobic conditions at depth limiting bioturbation activity (Spencer *et al.*, 2003), any sediment

disturbances, such as those predicted for sediment in the South East, have the ability to oxidise sediment, redistributing any stored contaminants as a result of physical advection, to the surrounding water column, contributing a hazard to both biota and humans (Yao *et al.*, 2015).

3.3.2. Bioavailability

All metals, both essential and non-essential, have the potential to be toxic to biota above taxa specific thresholds (Rainbow, 1995). However, it is their bioavailability, or the metal fraction available for biological uptake (Olaniran *et al.*, 2013), that controls the potential transfer of those metals to the food chain and human life (Paller and Knox, 2013). Metal bioavailability is a function of a complex set of both geochemical parameters, such metal speciation (Section 3.3.1) and local environmental parameters such as pH, redox and salinity, as well as certain biological factors, such as taxa physiology (Mayer *et al.*, 1996) or feeding position of marine organisms (Paller and Knox, 2013). The main uptake route from contaminated soils and sediments to biota is through plant uptake, where metals are transferred from the sediment into the plant root, into the plant cells, into the xylem, ending up in either leaves, seeds, tubers or fruit (John and Leventhal, 1995). Direct uptake via sediment and feeding on contaminated waters can lead to metal accumulation within muscles, gills and bones of fish (Ben Salem *et al.*, 2014).

There are multiple negative consequences of metal accumulation within the environment, if organisms are exposed to metals outside their healthy concentration range, or 'window of essentiality' (Hopkin, 1989). Transition metals, such as Zn, are essential to biological productivity in low concentrations, and are regularly transported as mobile cations around aqueous systems, however they have been found to accumulate within shellfish, and can cause acute harm, such as reduced growth or mortality at high concentrations (Clark, 2001). Conversely, metalloids are not required for metabolic activity and can be toxic at low concentrations. Metals such as Cd, Pb and Hg have been found at toxic levels within mussels (Pan and Wang, 2012). These may readily cause organism mortality and be transferred to the human food chain.

Bioaccumulation can pose a significant hazard and therefore even small concentrations of contamination can manifest itself at levels capable of causing harm to biota (Clark, 2001) and human life (Järup, 2003). For example, marine organisms can bio-magnify contaminants, threatening the health of organisms up the food chain (Casado-Martinez *et al.*, 2012), resulting in in metal concentrations within predator species being millions of times larger than surface waters (Lavoie *et al.*, 2013). Metals such as Hg, Cd and Pb which are likely to bio-accumulate (Kalman *et al.*, 2014), have well known documented detrimental effects on biota (Chandra Sekhar *et al.*, 2004; Louriño-Cabana *et al.*, 2011).

Soil and sediment quality guidelines have been developed as a method by which the potential for adverse ecological effects can be gauged (Burton, 2002). Commonly implemented screening values have been published by the Canadian Council of Ministers

of the Environment for the protection of aquatic life (CCME, 2002), the Dutch Government (Crommentuijn, 1997) and NOAA (Buchman, 2008). Despite a number of the guidelines delineating screening values for both terrestrial and marine sediments (Environmental Quality Standards Directive (2008/105/EC), as well as strategies to reduce metal inputs to the North Sea (OSPAR, 2001), there is no single set of values focusing on estuarine sediments (Chapman and Wang, 2001).

The accurate assessment of toxicity is more complex than simply measuring contaminant magnitude due to the intricate interactions of geochemical and biological processes affecting bioavailability. The measurement of Acid Volatile Sulphides (AVS) is a proxy for bioavailability (Ribeiro *et al.*, 2013), and is based on the prevalence of FeS within anaerobic sediments. If metals are present, they are likely to displace the FeS, resulting in their removal from the water column (Paller and Knox, 2013). A more recent approach, and one which is making a positive impact within regulatory agencies (de Polo and Scrimshaw, 2012), are biotic ligand models (BLM). These models are essentially chemical equilibrium models, focusing on the chemical interactions of the metal and the physiology of an organism (Paquin *et al.*, 2002) (Figure 3.7).

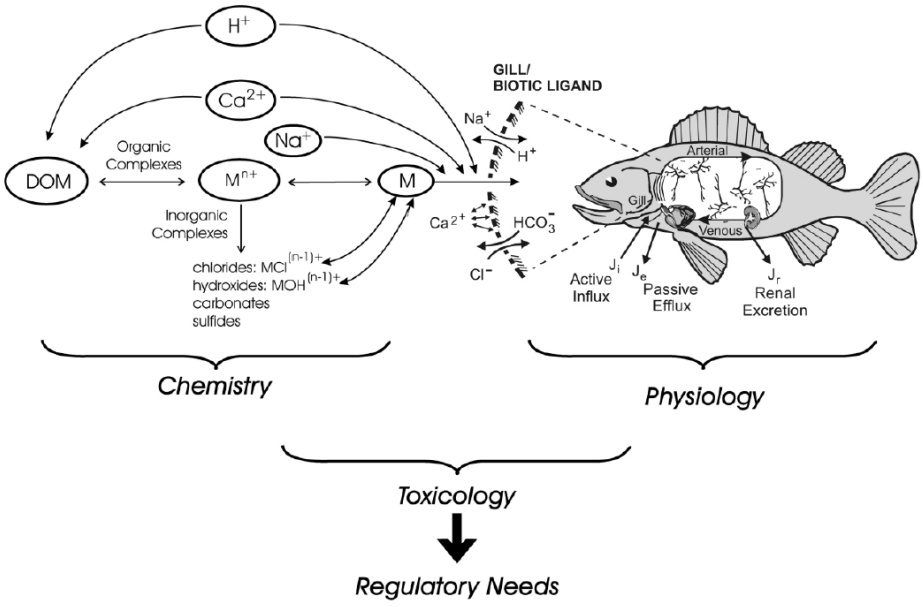

Figure 3.7: Biotic Ligand Model, showing the link between chemistry, physiology and toxicology (Paquin, 2002).

These models can then be used to predict species toxicity with success (Constantino *et al.*, 2011), to an extent where the recent amendments of the environmental quality standards in the field of water policy legislation use BLM calculations for EQS concentrations (Council Directive, 2013/39/EU), resulting in a change from average permissible surface Pb concentrations from 7.2 to 1.3 µg L^{-1}.

3.4. Approaches to Contaminated Land Risk Assessment

Legislation such as the Water Framework Directive (2000/60/EC) and the Marine Strategy Framework Directive (2008/56/EC) increase the requirement to develop a method to understand fully the risks associated with contamination within the environment (CDOIF, 2013). However, the majority of risk assessment strategies presently used by shareholders and site managers lack the scientific underpinning, such as detailed understanding of contaminant uptake by different organisms, required to confidently undertake assessment (Energy Institute, 2013). Significant research has been conducted on groundwater flow modelling (Bear and Verruijt, 1987), leachate plume assessments (Brun and Engesgaard, 2002; Hung *et al.*, 2009), capping design (Go *et al.*, 2009) and empirical speciation modelling (Sauve *et al.*, 2000; Trivedi, 2000) to assess contaminant risks at operational landfill sites. However, there is a distinct omission of a robust framework for the assessment of the risk for historical landfill sites, including an assessment of both the likelihood and consequence of a hazard occurring.

A common method for understanding contamination linkages within the environment is to adopt the Source-Pathway-Receptor method (Butt and Oduyemi, 2003; Sneddon *et al.*, 2009; Driscoll *et al.*, 2013; Schnug and Lottermoser, 2013). This theory is based on the fundamental assumption that risk can only exist if an identified hazard at a site (Source) is in either direct or indirect contact with a sensitive receptor via an environmental pathway (Figure 3.8).

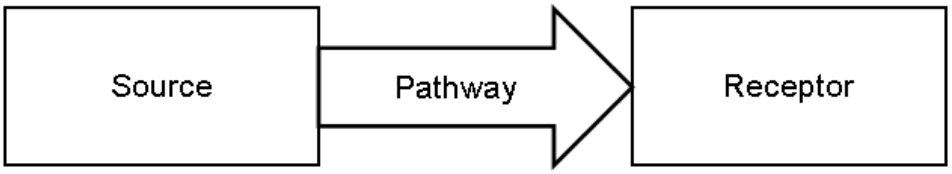

Figure 3.8: The 'Source-Pathway-Receptor' approach. From Butt and Oduyemi (2003).

This approach is the cornerstone of most contaminated land studies, and forms the template for Conceptual Site Model (CSM) development. A CSM is a representative schematic of the site under investigation and allows all site data to be gathered and an initial assessment of the SPR linkages to be made (DEFRA, 2011b). In order for the CSM to illustrate fully potential risks, all potential interactions between sources, pathways and receptors must be illustrated (Table 3.4) requiring a detailed knowledge of the mechanics controlling their presence (Critto *et al.*, 2003). Initial CSM's are developed based on a qualitative/informative basis to reduce over complication, and may include the whole site or just a single SPR linkage (DEFRA, 2011b). Only once a CSM has been drafted and a potential pollutant linkage exists is, quantitative (site specific) data used to form a more complex

understanding of risk (Bevan, 2004). The main objective of this stage however is to assess the status of SPR linkages and to address what needs to be dealt with under the initial objective of the investigation.

Table 3.4: Example CSM parameters for the assessment of contaminated land (Energy Institute, 2013).

Parameter	SPR component	Description
Contaminant Type	(Source)	- A list of present compounds as well as potential for bioaccumulation and availability.
Contaminant Distribution	(Source)	- Lateral and vertical distribution (if known), as well as potential sources and background levels
Hydrodynamics	(Pathway)	- Sediment type, the depositional environment, tidal system (if applicable), sediment dynamics over time.
Receptors	(Receptor)	- Individual species and the ecosystem, members within the food chain, sensitive species, exposure methods.

A linkage must exist between the source and receptor in order for contamination to present a risk (Cooper, 2012). This is outlined in Figure 3.9, which shows 3 scenarios in which; (a) contamination presents a potential risk to a sensitive receptor, (b) there is no pathway through which a source could impact a receptor and (c) a scenario in which there are no sensitive receptors present.

This information would all be within an initial CSM, helping the appraisal of risk. Once a risk has been identified, remediation can then be undertaken based on the site characteristics. The main remediation options consist of either doing nothing, continued surveillance of the site, removing the source, breaking the pathway or removing the receptor from the source of risk (Energy Institute, 2013).

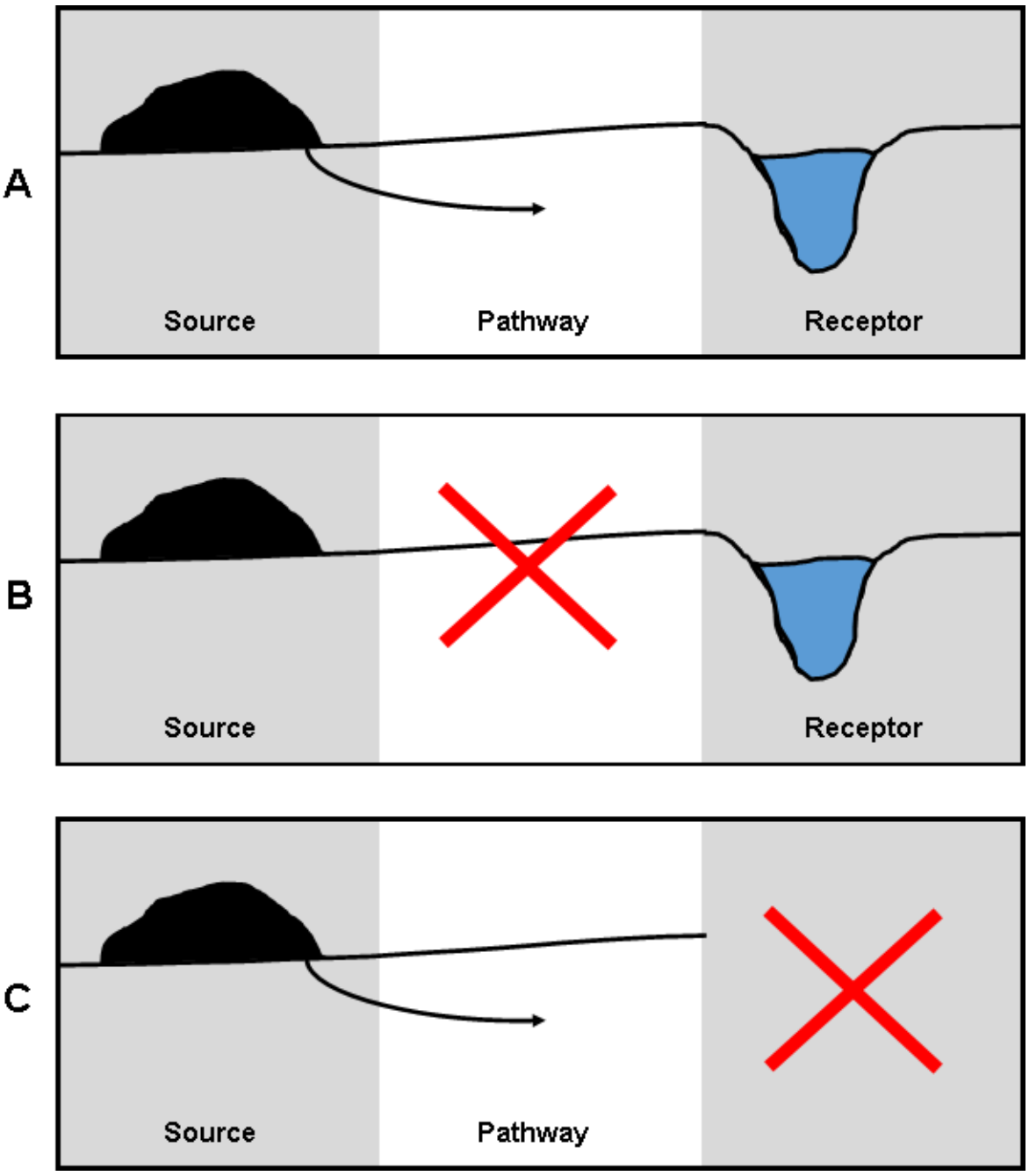

Figure 3.9: Theoretical SPR land contamination scenarios, a) a SPR linkage showing a continuum between the source and receptor, b) a contamination hazard presenting no risk as there is no environmental pathway, and c) where contamination has a pathway but there are no sensitive receptors within the area.

3.5. Legal Context of Historical Coastal Landfills

Risk or contaminated land assessments will only be undertaken if the presence of contamination is likely to breach an environmental law. While there is no single piece of legislation within the EU concerning investigation and remediation of contaminated sediments, many pieces of legislation cover the requirement to address them (Energy Institute, 2013).

Part IIa of the Environmental Protection Act (1990) introduced the UK to mandatory identification and remediation of contaminated land. The Act defines a contamination event as causing significant harm to human health, animals or controlled waters. The Water Resources Act (1991) introduced the polluter pays principle, requiring industrial operators to pay for unlicensed discharges leading to contamination. Water Environment Regulations (2003) sit beside the Water Framework Directive (2000/60/EC) which aims to protect and improve the ecological status of all waters within the UK by 2015, achieved through the introduction of quality standards based on status objectives. Despite the WFD not explicitly including sediments, they play a significant role in the quality of aquatic life and should ultimately be included within assessment of ecological quality (SedNet, 2004). A major outcome of the Water Framework Directive is the implementation of Shoreline Management Plans, an assessment of the large-scale risks associated with predicted coastal processes, therefore reducing the risks to people and the environment (DEFRA, 2006). The main priority of the plan is to address and monitor the fate of the coastline via 4 policies (Table 3.5).

Table 3.5: Shoreline Management Plan policies available to shoreline managers (DEFRA, 2006).

SMP Policy	
Hold the existing line	The existing defence line is not moved, but is maintained or updated, including rebuilding seawall toes.
Advance the line	The defence line is moved seawards by the construction of new defences, allowing land reclamation.
Managed Realignment	Allowing the shoreline to move, with new management to control the limit.
No Intervention	No investment in coastal defences.

The Landfill Directive (1999/31/EC) introduced a tighter control on waste types and land disposal through the introduction of waste categories and disposal procedures. This was brought into act in the UK with the Landfill Regulations (2002) which specified licencing requirements through monitoring guidelines, waste acceptance criteria and site design, which were not mandatory until this time. Other directives such as the Habitats Directive (92/43/EEC) have impacted sediment investigation through the establishment of Special

Areas of Conservation within the UK. These areas are set up to protect sensitive species by ensuring a favourable status is maintained (Natural England, 2014).

It is clear that sediment contamination is not specifically addressed within any current legislation, meaning that the management of historical landfills or surrounding sediments contaminated by historical landfills remains a challenge. There are, however, emerging guidance documents which aim to appraise the hazards associated with coastal contamination. 'Management of landfill sites on low lying coastlines' from CIRIA (Construction Industry Research and Information Association) utilises the wealth and complexity of legislation to compile a methodology for the assessment of coastal risk as well as management and monitoring of that risk in compliance with Part IIa of the EPA (1990), the Landfill Directive (1999/31/EC), Water Resources Act (1991) and the Environmental Damage Regulations (2009) (Cooper, 2012).

3.6. Conclusion

There is increasing evidence to suggest that historic landfills have the potential to pollute the environment (Njue *et al.*, 2012; Green *et al.*, 2014) but data are limited. The original intention of natural attenuation landfilling was to produce a passive method, through which any pollutants present within landfill leachate would become associated with the solid phase due to rapid physicochemical changes in surrounding sediments (Lee *et al.*, 2005). It is, however, likely that this has generated a secondary source of contamination within sediments surrounding the landfills.

Conservative estimations suggest there are around 20000 of these landfills within the UK, 5000 of which are within the coastal zone with flood return periods of 50 years. Climate predictions state that the frequency and intensity of coastal storm events will increase by the year 2050. Therefore, these landfills and the surrounding sediments that occupy the inter-tidal zone are vulnerable to inundation and erosion, with the potential to remobilise or redistribute any legacy contamination contained within sediments. This is of particular pertinence within the South East and the Thames Estuary.

To date, no research has been undertaken to examine the magnitude, nature or spatial extent of contamination surrounding historic landfills, and therefore this risk is not being represented within coastal flood design or shoreline management plans. Additionally, the implications of contaminated sediment release to the environment due to coastal erosion are poorly understood.

Chapter 4 Metal Distribution in Sediments Adjacent to an Historical Landfill.

Abstract

Landfills were historically constructed without basal or side-wall engineering, which allowed attenuation of contaminated leachate within surrounding sediments. There is therefore potential for these sediments to act as a present day contamination source, which may pose a major threat within eroding coastal sediments. This chapter examines whether Newlands Landfill, Essex, UK has created a legacy source of contamination within surrounding marsh sediments.

A detailed programme of surface samples and sediment core collection was conducted around the landfill. Elevated levels of metal contamination were identified in both surface and subsurface sediments. While an environmental concern, surface contamination was at similar levels to comparable industrial areas and not a result of the landfill. Analysis of the subsurface, via a transect of sediment cores from the landfill boundary, indicated enrichment of anthropogenic metals at depth, such as Pb (EF > 2) and Zn (EF = 1.5), likely to be associated with the historical leachate plume. Enrichment was spatially contained within 15 m of the site boundary, but represented Cu, Pb and Zn masses of c. 480, 1200 and 1650 kg respectively around the perimeter of the site, in sediments at risk of erosion.

This contamination record only considers one of the 5000 landfills within the Environment Agency flood alert area. Further work is therefore required to gain a more robust insight into the national context of contamination from historical landfills (Chapter 6).

4.1. Introduction

Historically, landfills within the United Kingdom have had limited pollution prevention controls, creating the potential for significant leachate discharge to the environment. The processes of waste degradation and leachate migration from landfills have been extensively researched in the literature elsewhere (Eleazer *et al.*, 1997; Williams, 2005; Andrews *et al.*, 2012), however the extent to which historical coastal landfills may pose a hazard to the environment through contamination of their surrounding sediments and surface waters remains poorly understood (Njue *et al.*, 2012; Green *et al.*, 2014).

Traditionally, research on landfill contamination has focused principally on directly assessing waste composition (Burnley, 2007; Kiddee *et al.*, 2013) or leachate captured from the site (Baun *et al.*, 2004; Cataldo, 2012). This body of literature suggests that waste goes through acetogenic degradation shortly after being deposited (Williams, 2005), releasing a discrete spike in heavy metals. Within coastal sediments, it is likely that these metals will become associated with fine-grained fraction due to their high Cation Exchange Capacity (Du Laing *et al.*, 2009), or sorbed to various particulate substrates. This has resulted in the formulation of a conceptual site model, summarising the expected transfer and storage route for metal contamination from historical landfills under acetogenic degradation (Figure 4.1).

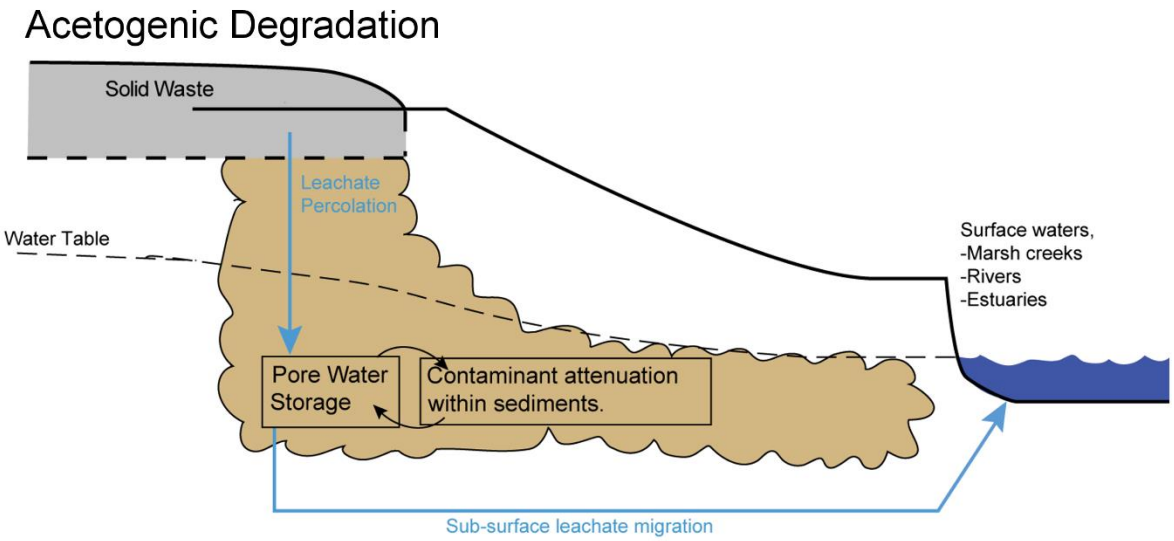

Figure 4.1: Conceptual model of leachate transfer under acetogenic waste degradation.

Consequently, sediments adjacent to historical landfill sites may represent significant contaminant sinks in the estuarine environment. Furthermore, as sediments are dynamic, they may ultimately evolve from a sink into a source as sediment erosion rates increase, physically releasing any stored metals to the estuarine water body with potential impacts on

water quality and eco-toxicological impacts for local biota (Figure 4.2), especially due to the vast number of coastal landfills within England and Wales (Cooper, 2012).

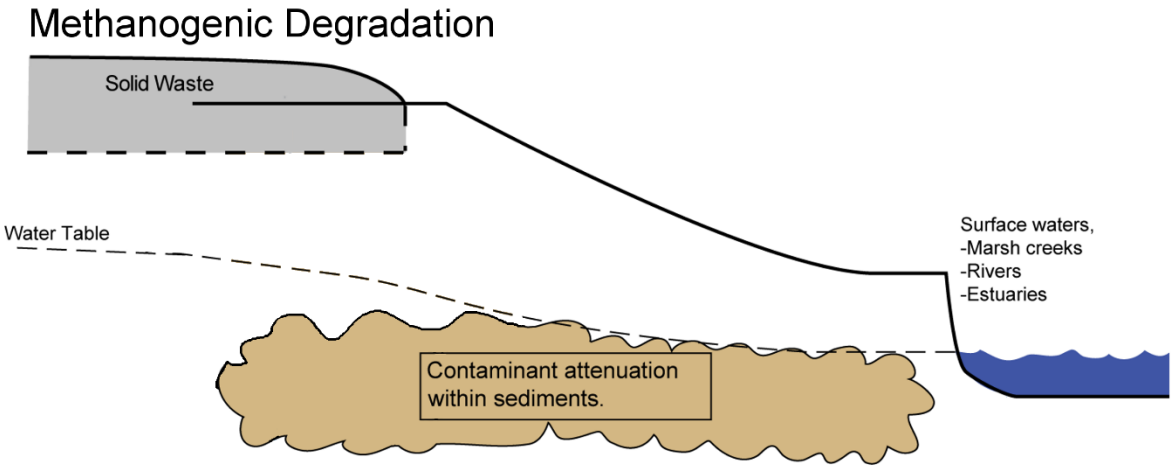

Figure 4.2: Sediment bound contamination storage under long-term methanogenic conditions.

This chapter presents an investigation into sediment contamination in a salt marsh adjacent to an historical landfill, in order to establish whether Newlands landfill has created a legacy source of contamination. This will be achieved by addressing the following research objectives:

Research Objective 1a: To assess the magnitude of metal concentrations within sediments and establish whether they pose an environmental threat.

Research Objective 1b: To examine the spatial distribution of contamination to support an investigation into the behaviour of metals.

Research Objective 2: To understand the potential pathway and behaviour of metals in the sediment.

4.2. Research Site

Newlands is an historic landfill site on Canvey Island, Essex, UK (TQ 81895 83719). This site was chosen as a representative landfill for this study due to: a) its coastal location; b) good site access; c) generic waste type; and d) the availability of waste disposal records from Essex County Council (Brown, 2012).

Newlands was opened as a civic amenity site in 1954 on reclaimed agricultural land, with plans to use the waste as a flood defence by raising the salt marsh level; a process known as 'landraise' (Gray, 1993). The site was constructed with no basal or side wall engineering, and received approximately 100 tonnes per day of household and non-hazardous commercial wastes (Caulmert Limited, 2011b). In 1978 approval was granted for the site to receive oil contaminated materials, as a designation for beach clean-up operations in Essex. In 1979, a council application was made to extend the landfill, to cover the majority of the north eastern tip of Canvey Island as well as extending out over the islands seawall. The extension was carried out in 1982, and involved raising the level of the landfill as well as installation of rock armouring and relocation of the public right of way. The site closed in 1989, after receiving approximately 1,000,000 m^3 waste (Caulmert Limited, 2011a) (Figure 4.3).

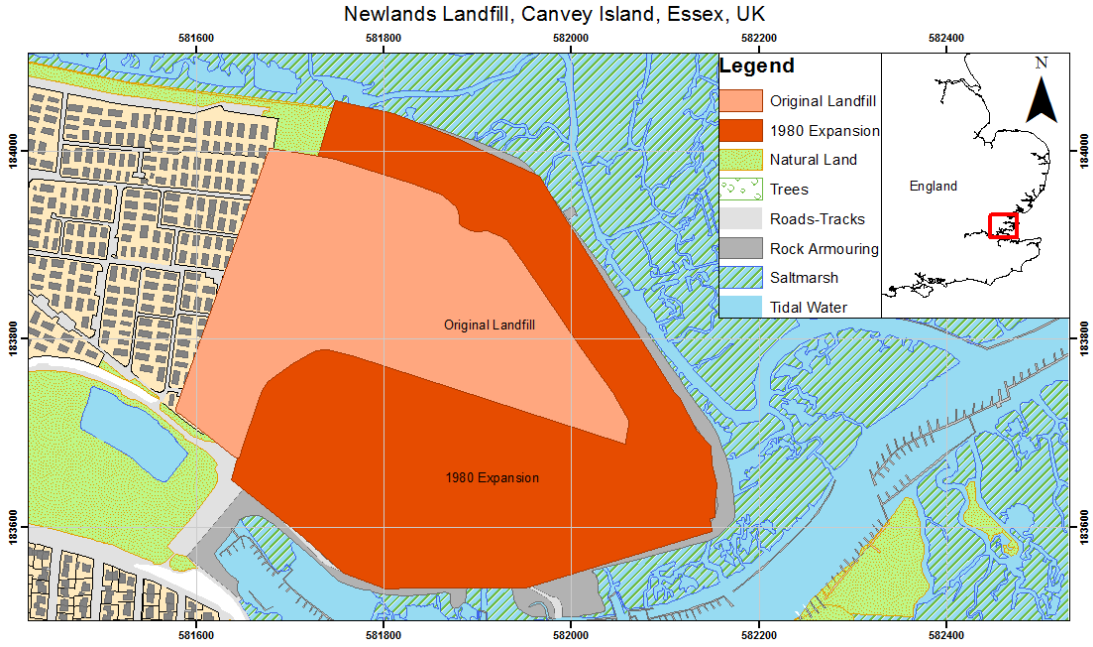

Figure 4.3: Newlands Landfill expansion shown on Canvey Island.

Newlands is currently being used as a council owned recreational park. The site is situated on the northern bank of the Thames Estuary and is adjacent to environmentally significant salt marshes which are nesting and breeding grounds for wildfowl and wading birds, and contain three rare species of flora; Lax-flowered sea-Lavender (*Limonium humile*), Golden Samphire (*Inula crithmoides*) and small Cord-grass (*Spartina maritima*) (Caulmert Limited, 2011b). The site is situated directly on sedimentary littoral marine sediments, overlying Ypresian (47.8-56 My) London Clay, a silty clay mudstone of marine origin (BGS, 2014), and presents no risk of groundwater migration to the chalk aquifer beneath (Caulmert Limited, 2011b) (Figure 4.4).

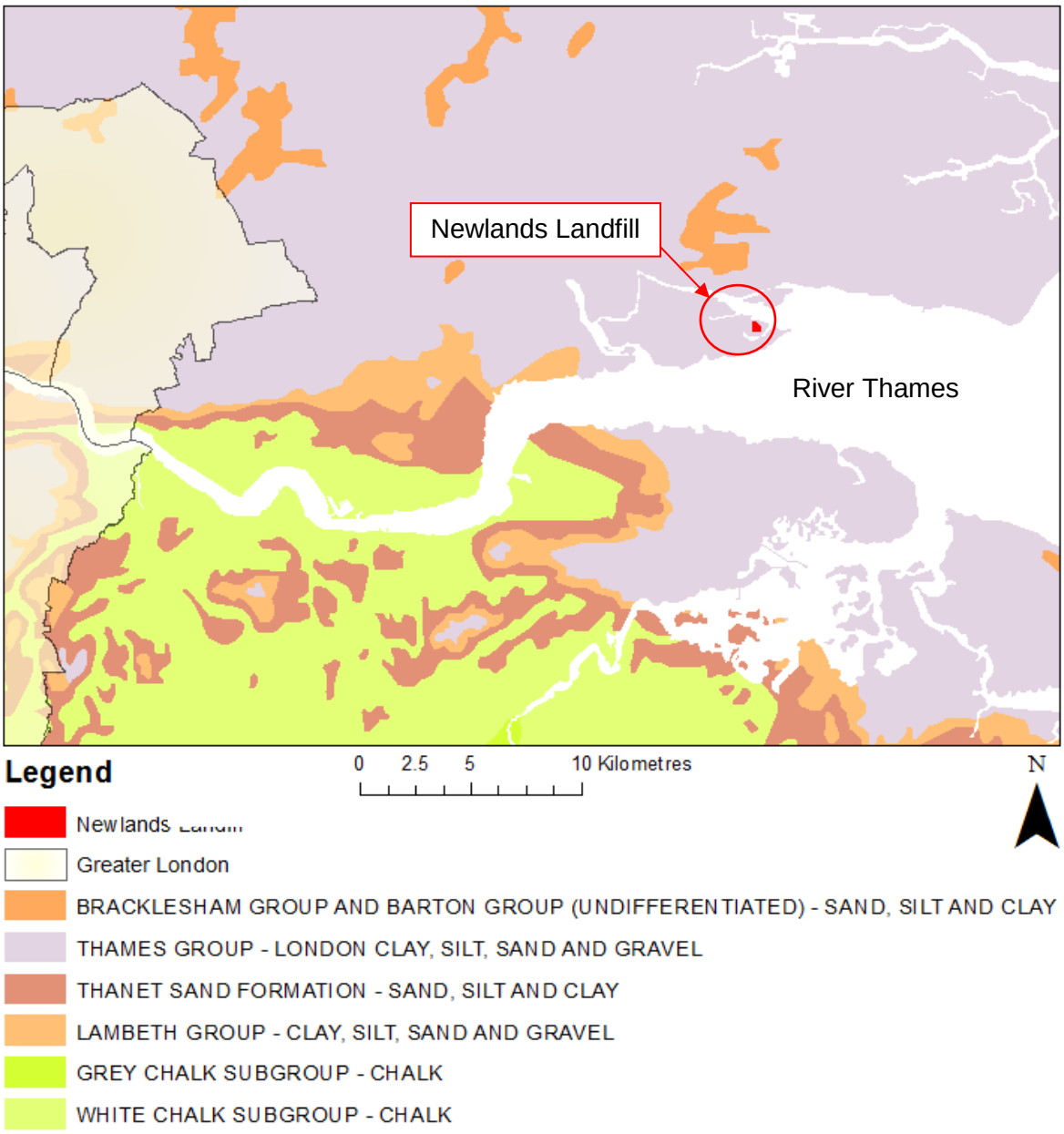

Figure 4.4: Bedrock Geology in the South East and Essex. Greater London and Newlands shown for reference (British Geological Survey, 2014).

4.3. Methods

4.3.1. Field Methodology

A site walkover was conducted to identify areas of potential failure within the landfill boundary. Surface samples were taken to evaluate whether there was any surface breakout from the site. In total, 43 surface grab samples were taken with a trowel every 50 m in triplicate along 12 radial transects perpendicular to the site boundary, avoiding the collection of excessive vegetation or surface detritus. All samples were immediately labelled, double bagged in polythene sample bags and refrigerated in field coolers and transported back to the laboratory for analysis.

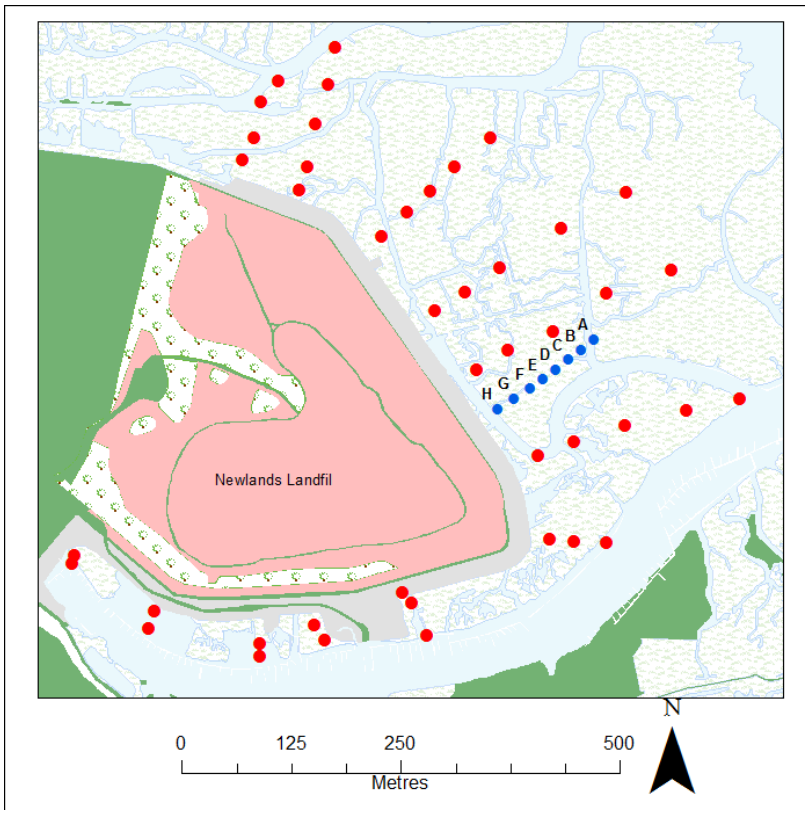

Figure 4.5. Newlands marsh sample locations. Red = surface samples, Blue = sediment cores.

Additionally, eight sediment cores were extracted at 10 m intervals along an easily accessible vegetated transect perpendicular to the site boundary (Figure 4.5) by pushing a 30 cm long, 10 cm diameter polycarbonate pipe into the sediment for the first 30 cm and using a Russian corer for deeper samples (Jowsey, 1966). Samples were extracted, wrapped in plastic wrap, labelled, returned to the laboratory and kept at -12° C until required. In order to avoid contamination, separate pipes were used for each core and equipment was cleaned between each use. Sediment compression was minimised by the use of the Russian corer (<5 %), and was measured in the field as the difference between coring depth

and extracted sample length. Table 4.1 shows information regarding core length, distance from the landfill edge and which parameters were measured.

Table 4.1: Sediment core location and analysed parameters description.

	Sediment Core							
	A	**B**	**C**	**D**	**E**	**F**	**G**	**H**
Distance from site edge (m)	100	80	60	50	40	30	20	10
Core length (cm)	300	440	240	220	240	640	200	220
Metals	✓	✓		✓	✓	✓	✓	✓
Mercury						✓		✓
LOI	✓	✓				✓		✓
pH	✓	✓	✓	✓	✓	✓	✓	✓
Grain Size				✓	✓		✓	
Radiometric Dating		✓			✓			✓

4.3.2. Laboratory Methodology

Sample Preparation

Sediment samples were cut from both frozen grab samples and cores after discarding the outer layers to ensure no cross contamination. Cores were cut at 5 cm intervals for the top 1 m, then 10 cm intervals at depths below this. Samples were then homogenised, and split, with a sub-sample used for pH, particle size and organic matter content while the other was freeze-dried for 24 hours for later metal analysis. Freeze drying was chosen as the method preserves chemical speciation (Quevauviller and Donard, 1991) whilst avoiding time consuming sediment grinding.

pH

A suspension of wet sediment and deionised water, at a ratio of 1:2.5, was shaken for 15 minutes prior to pH being measured with a VWR pH millivoltmeter. Analysis typically took three minutes and measurement was taken when readings had stabilised (Rowell, 1994). The pH probe was washed in deionised water and dried between readings. Individual samples were analysed in triplicate to quantify reproducibility, with a median %RSD of 0.2 (Equation 4.1).

Equation 4.1: Relative Standard Deviation (% RSD) calculation, where σ is standard deviation, and $\bar{x}$ is mean.

$$\%\mathrm{RSD} = \frac{\sigma}{\bar{x}} \times 100$$

LOI and Carbon Content

A test was undertaken to see whether percentage Loss on Ignition (LOI) could be used as a proxy for total carbon content. LOI was measured by placing 20 g ± 0.5 g of dried sediment in a furnace at 550 °C for four hours to combust organic matter. Samples were removed and weighed. For total carbon analysis, 1.5 mg ± 0.01 mg dried sediment was weighed into a tin capsule and analysed in a combustion column at around 1000 °C with blank samples and calibration standards (aspartic acid). A strong positive relationship between the methods was examined ($R = 0.847$ $p<0.01$) allowing LOI to be used as a proxy for Carbon content (Figure 4.6). Triplicate LOI samples measured a methodological reproducibility of 9% RSD.

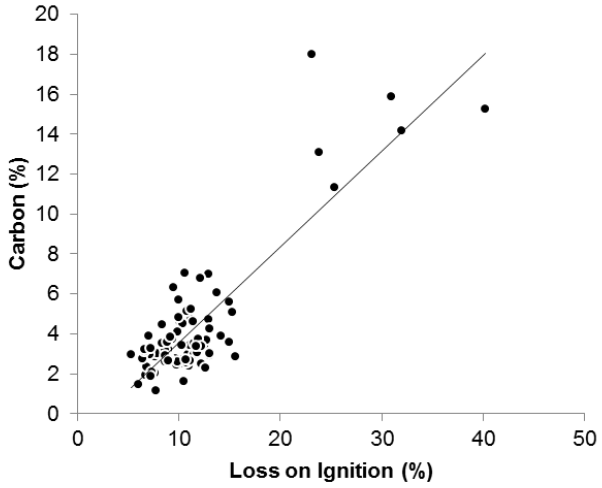

Figure 4.6: Relationship between Loss on Ignition (%) and Carbon content (%).

Sediment Grain Size

Volumetric particle size (<2 mm) was measured using a Beckmann laser diffraction granulometer. Samples were digested on a hotplate at 80 °C ± 5 °C with H_2O_2 to remove organic matter and subsequently disaggregated with Calgon (Sodium Hexametaphosphate and Sodium Carbonate) prior to analysis. One sample in every 10 was analysed in triplicate and a Certified Reference Material (Micrometrics Garnet Powder) was used to assess analytical precision (5.5 % RSD) and accuracy (Figure 4.7 and Table 4.2). All marsh surface samples were analysed for particle size, however, due to time constraints, only three sediment cores were measured (Cores D, E and G).

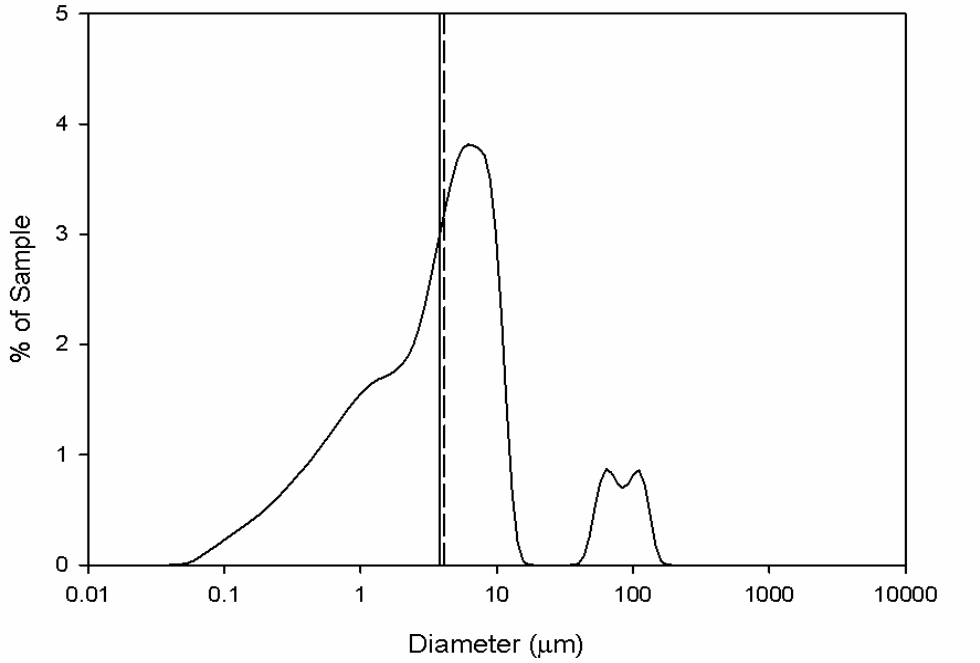

Figure 4.7: CRM recovery for particle size analysis showing particle size distribution. Dashed line is observed median (4.11 µm), solid line is certified median (3.77 µm).

Table 4.2: CRM values. Recovery shows the percentage to which the method was able to recover the certified value.

	Certified Value (µm)	Observed Value (µm)	Recovery (%)
Median	3.77	4.11	91.5
90%	6.68	7.85	85.1
10%	1.15	1.35	85.2

Metal Analysis

Metal concentrations were measured after sediment extraction. All samples were extracted on a hotplate with Aqua Regia (HNO_3:3HCl) a pseudo-total digestion, which provides an insight into potential environmental mobility, and is a well-established procedure for the quantification of sediment bound metals (Chen and Ma, 2001; Machado *et al.*, 2002; Rao *et al.*, 2008; Turner, 2013). The digestion involved placing 0.5 g ±0.01 g dry sediment into an acid washed Erlenmeyer flask, adding 12 ml of freshly prepared Aqua Regia and heating at 80 °C for four hours (Chen and Ma, 2001). Certified Reference Materials (LGC6137), sample triplicates and method blanks were also run to ensure methodological precision and accuracy (Table 4.3). Digested samples were then filtered through Whatman 540 (8 µm pores) quantitative filter paper, made up to 50 ml with deionised water in volumetric flasks and refrigerated at 4 °C until required.

Table 4.3: Analytical precision and accuracy for metals analysed by ICP-OES. Missing values indicate no certified concentration.

	Precision (RSD %)	Accuracy (%)
Al	2.40	
Ca	3.20	115
Co	3.06	101
Cr	1.09	86
Cu	0.90	111
Fe	3.10	113
Ga	2.38	
Hg	3.01	119
K	0.85	101
Li	0.70	107
Mg	2.90	112
Mn	1.03	104
Na	4.09	89
Ni	2.29	132
Pb	4.48	102
Sr	0.98	
V	0.69	90
Zn	1.01	98

Samples were analysed on a Varian Vista-Pro ICP OES (inductively coupled plasma optical emission spectrometry), with the exception of a small subset of samples analysed for Hg, which was performed on a Milestone Direct Mercury Analyser-80 at the Biotron Centre for Climate Change, University of Western Ontario, Canada. Mercury analysis required no pre-preparation, samples were weighed and inserted into the instrument.

The effects due to saline matrices within ICP-OES analysis are well understood (Ramsey and Thompson, 1986), therefore, calibration standards were matched to the ionic matrix

within the samples. Experimental work was carried out to measure the level of plasma suppression by testing analytical recovery of a range of reference materials with different matrices (fresh and saline). Plasma suppression was then observed, and salinity concentration accounted for within sample runs. All digested samples were analysed at full concentration for trace elements (Cd, Co, Cr, Cu, Ga, Li, Mn, Ni, Pb, Sr, V, Zn) and at 1:20 v/v dilution for major constituents (Al, Ca, Fe, K, Mg, and Na) to ensure they were within analytical range. ICP-OES operational conditions can be seen in Appendix 1.

A laboratory control standard (a sample with matched matrix and known concentration) was analysed every 10 samples to measure drift and maintain analytical accuracy. The limit of detection (LoD) was measured to ensure reported concentrations were not below detectable limit of the ICP-OES (outlined in Appendix 1). A summary of elemental LoD is shown in Table 4.4.

Table 4.4: Lowest reproducible concentration (mg kg $^{-1}$) for ICP-OES analysis.

Ag	Al	Ca	Cd	Co	Cr	Cu	Fe	Ga	K
2	500	500	8	4	2	4	500	2	500

Li	Mg	Mn	Na	Ni	Pb	Sn	Sr	Tl	V	Zn
4	500	4	1000	8	10	8	8	8	4	10

Prior to statistical analysis, data < LoD were replaced with a value of LoD/2 (Gochfeld *et al.*, 2005) and where the dataset contained > 25% of data < LoD, the whole set was discarded (Farnham *et al.*, 2002). As a result, all Ag and Cd data were omitted from subsequent analysis.

Radiometric Dating

Sedimentation rates were calculated through the measurement of both ^{210}Pb and ^{137}Cs within 17 salt marsh sediments, ranging from 0 to 30 cm within only cores B, E and H due to cost limitations. Measurement of ^{210}Pb to is a well-established method for calculating sedimentation rates of salt marsh sediment (Cundy *et al.*, 2002; Haslett *et al.*, 2003). ^{210}Pb ($T_{1/2}$ = 22.6 y) is a naturally occurring isotope, which is a member of the ^{226}Ra decay chain, originally derived from ^{238}U (Álvarez-Iglesias *et al.*, 2007). ^{210}Pb was measured in sediments through both, (a) $^{210}Pb_{supported}$, a product of natural *in-situ* ^{238}U degradation, continually produced within the sediment and in equilibrium with ^{226}Ra (Putyrskaya *et al.*, 2015) and (b) $^{210}Pb_{unupported}$ from the decay and deposition of atmospheric components (Dörr, 1994). $^{210}Pb_{unsupported}$ is determined by subtracting $^{210}Pb_{supported}$ from $^{210}Pb_{total}$ and can be used to calculate a measurement of sedimentation accurate to within the last 100-150 years (Álvarez-Iglesias *et al.*, 2007). Sedimentation and chronology is calculated by adopting a model to the data. The constant rate supply (CRS) model assumes that $^{210}Pb_{unsupported}$ concentrations are similar at each stage of accumulation (Appleby and Oldfield, 1978), whilst the constant initial concentration (CIC) model suggests a constant initial concentration regardless of accumulation rates (Krishnaswamy *et al.*, 1971).

Additionally, the anthropogenic radionuclide, ^{137}Cs, which is produced from nuclear weapons testing and nuclear plant accidents, is also commonly used as a worldwide soil erosion tracer (Bai *et al.*, 2011c). ^{137}Cs had a peak fallout in 1963, and due to the short term association with sediments allows it to be used as a tracer for sediments approximately 50 years old (Álvarez-Iglesias *et al.*, 2007). As ^{210}Pb and ^{137}Cs exist over different timescales, they are corroborated to independently validate sedimentation estimates (Baskaran and Naidu, 1995; Kim *et al.*, 1997; Simms *et al.*, 2008).

Samples were counted on a Canberra well-type ultra-low background HPGe gamma ray spectrometer at the University of Brighton to determine the activities of ^{137}Cs, ^{210}Pb and other gamma emitters. Spectra were analysed using the Genie 2000 system, and accumulated using a 16K channel integrated multichannel analyzer. Energy and efficiency calibrations were carried out using bentonite clay spiked with a mixed gamma-emitting radionuclide standard, QCYK8163, and checked against an IAEA marine sediment certified reference material (IAEA 135). Detection limits depend on radionuclide gamma energy, count time and sample mass, but were typically ca. 15 - 20 Bq/kg for ^{210}Pb, and 3 Bq/kg for ^{137}Cs, for a 150,000 second count time (Cundy, 2014).

4.3.3. Data Analysis

Data Pre-Treatment

Frequency distributions were computed to explore normality (Attrill, 1995) and the Kolmogorov-Smirnov test was used to examine whether the data fitted a normal distribution (Razali and Wah, 2011). The majority of data exhibited a non-normal frequency distribution, therefore parametric tests, such as Pearson correlations, could not be used without prior transformation of the data (Quinn and Keough, 2002). However, due to the varying level of skew across the dataset, no single transformation was appropriate to normalise the distribution. Instead, despite their reduced statistical power, non-parametric methods were used to analyse data correlations and relationships, chiefly Spearman's rank. This test ranks the variables separately and makes no assumptions about the distribution of the data (Quinn and Keough, 2002). Additionally, due to non-normal data distribution, median values were used in place of mean values within all summary statistics (Gibbs *et al.*, 2014) as mean values from environmental datasets could skew results.

Principal Component Analysis

Principal Component Analysis (PCA) was applied to data from each sediment core to explore whether any significant controls exist on distribution of metals within the salt marsh. Due to the non-normality exhibited by the data, PCA was used to calculate eigenvalues from a Spearman's rank correlation matrix of all variables (normalised metal ratios, pH, LOI) projecting them into fewer variables, or Principal Components (PCs) (Quinn and Keough, 2002), by combining the variables that contain inter-correlations and rejecting those without (Field, 2009). The extracted components reflect a combination of the original variables, via factor loadings. Factor scores are also produced, which show the relative loading (or coordinate) of the original sample on each PC. All analysis was undertaken using XLstat Version 2.01. Preliminary tests were undertaken to ensure all normalised data were suitable for analysis, namely the Kaiser-Meyer-Olkin measure of sampling adequacy (measuring the ratio of squared correlation and squared partial correlation between variables) and the Bartlett's test of sphericity (measurement of inter-correlation) (Table 4.5).

Table 4.5: Appropriateness testing for PCA variables.

Kaiser-Meyer-Olkin Measure of Sampling Adequacy		0.896
Bartlett's Test of Sphericity	Approx. Chi-Square	8546.653
	df	136
	Significance	0.000

Data rotation was used to maximise the loading that a single variable has on an individual factor. Orthogonal rotation retains the independent assumption of the factors, ensuring their

perpendicular offset in space (Field, 2009). As no correlation was assumed between factors, orthogonal varimax rotation was used. The factor loadings were then observed and interpreted based on their value. Only factors with eigenvalues > 1 were retained from each analysis, as a value of < 1 represent less variance within the original data (Tabachnick and Fidell, 2006). When interpreting PC loadings, values of > 0.6 were considered strong, however, values > 0.4 were also reported (Reid and Spencer, 2009).

Spatial Data Analysis

The spatial distribution of surface contaminants was predicted using Kriging. The first step involved deriving a variogram for each variable, which reveals the spatial correlation of the data (Figure 4.8). The variogram produced an expected nugget value (Critto *et al.*, 2003), which is the semivariance (γ) offset when h=0 (C_0) and a sill, the γ value where the model line flattens off; the point at which spatial dependence is no longer apparent (C_1). Minimum and maximum distance (h) values were also presented and their calculated range (a) is the slope of the model, or the distances over which there is spatial dependancy (Burrough and McDonnell, 1998).

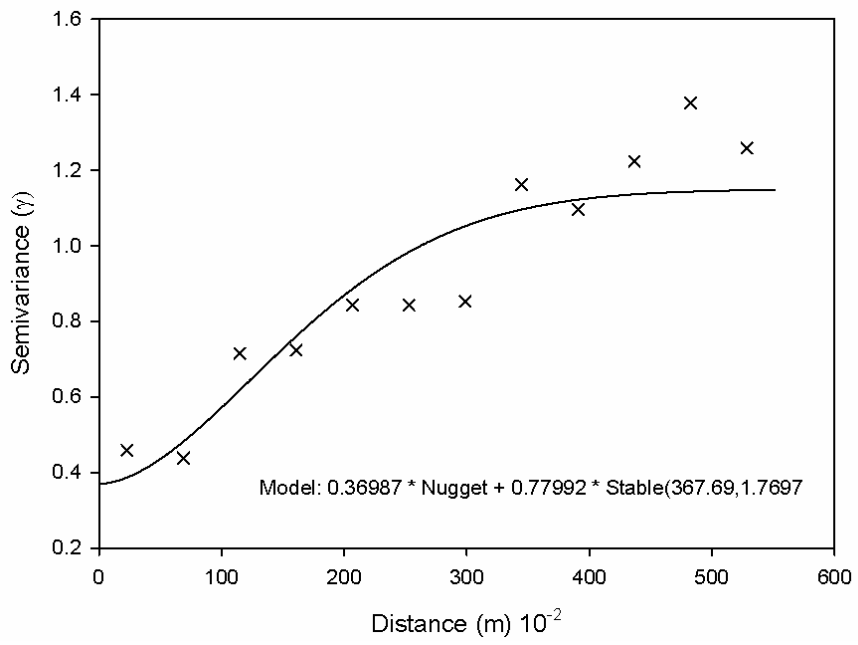

Figure 4.8: Variogram for Lead (Pb) surrounding Newlands Landfill.

Figure 4.7 shows an example variogram for Pb. The fitted model was 'stable', where C_o = 0.34, C_1 = 0.78 and a = 367.69-1.77. This model was then used to predict spatial distributions using the known values, weighted based on their spatial dependence, at original sample distances (Figure 4.9). The weighting values gave an unbiased predicted value, which resulted in low estimation errors due to the low influence of more distal points (Burrough and McDonnell, 1998).

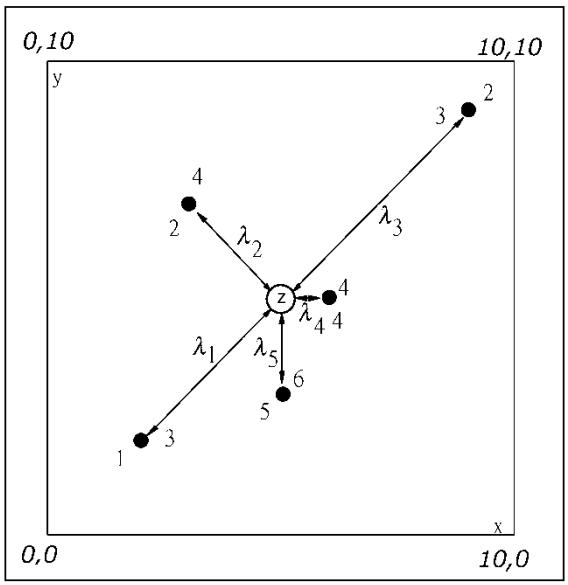

Figure 4.9: Prediction of 'z', showing weightings of different sampled sites λ_1, λ_2, λ_3, λ_4 and λ_5 (Burrough and McDonnell, 1998).

Data Normalisation

The prevalence of fine-grained material within a sample can magnify metal concentrations as the increased surface area of fine-grained particles providing a greater binding capacity for metals (Kersten and Smedes, 2002; Idris *et al.*, 2007; Szava-Kovats, 2008). In order to interpret data, the effect was compensated through the use of normalisation (Tam and Yao, 1998). As particle size data were not available for every sample, data were normalised geochemically. This approach involves normalising to a proxy element which is not impacted by anthropogenic activity, such as Al or Li, but which is also subject to the same grain-size dependent increase in sorption (Loring, 1991). This method has been used extensively (Din, 1992; Tam and Yao, 1998; Aloupi and Angelidis, 2001b; Liaghati *et al.*, 2004) across a range of normalising elements, such as Fe (Helz and Valette-Silver, 1992), Li (Loring, 1991) and Al (Din, 1992) and to identify the most suitable normalising element for this study the < 63 μm (silt and clay) sediment fraction (where available) was compared to Al, Fe and Li, concentrations (Table 4.6).

Table 4.6: Spearman's rank correlation coefficients for grain size in sediment core E and potential geochemical normalising elements (All significant to <0.001).

	Al	**Fe**	**Li**
<63μm	0.864	0.638	0.901

The strongest correlations were between Al and Li, and the < 63 μm fraction (R = 0.864 and 0.901 respectively) suggesting both as adequate proxies for grain size (Figure 4.10). However, the Aqua Regia extraction used in this study does not result in complete digestion of the alumino-silicate clay mineral lattice (Chen and Ma, 2001) and hence Li was used as the normalising element. All spatial metal data are presented as ratios of element/Li whereas summary tables remain presented as raw concentrations.

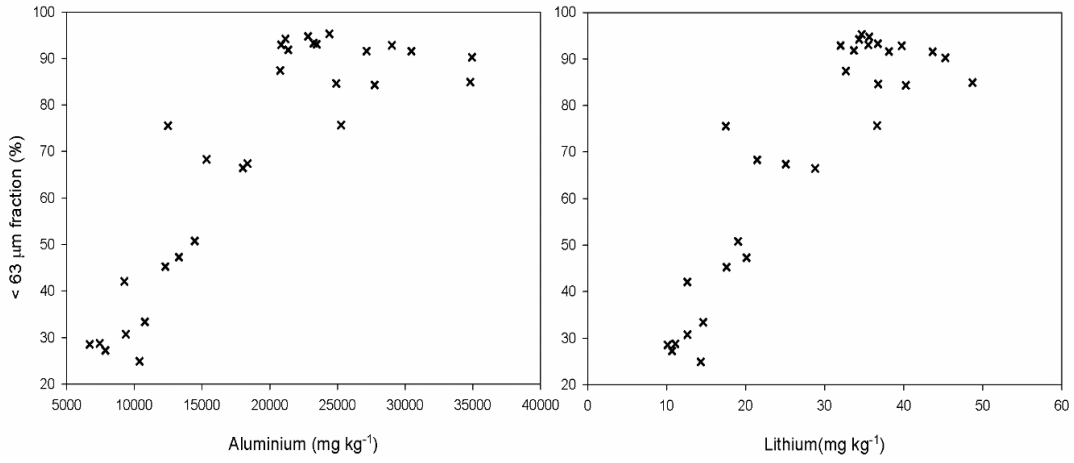

Figure 4.10: Scatterplots showing Al and Li correlations with measured grain size data.

4.4. Results

4.4.1. Marsh Surface Samples

Table 4.7 presents descriptive statistics for pH, %LOI and < 63 µm fraction for all surface samples.

Table 4.7: Descriptive statistics for marsh surface samples.

	< 63 µm fraction (%)	**%LOI**	**pH**
Median	97.37	10.6	7.85
Min	93	7	7.01
Max	100	16	9.20
Range	7	9	2.19
St Dev	1.713	2.125	0.434

Sediment Grain Size

The majority of marsh surface samples were classified as silty clay or clayey silt (Shepard, 1954) due to the predominance of mud-sized (<3.9 µm) and silt-sized (3.9-63 µm) sediment fractions (Figure 4.11).

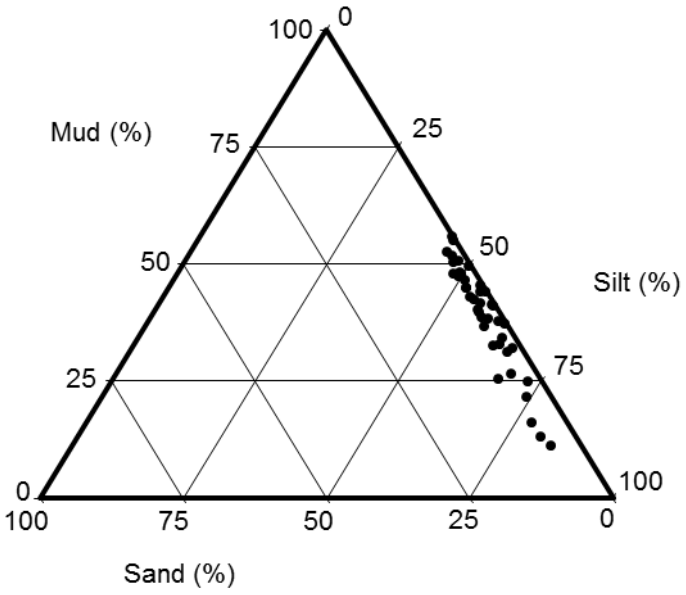

Figure 4.11: Ternary plot for all 43 surface sediment samples.

The data show little variation, with a range of only 7 %. Plotting the spatial distribution of the < 63 µm fraction shows very little trend across the marsh surface, with slightly higher concentrations of fine grained material South of the landfill boundary and at the North /North East (Figure 4.12).

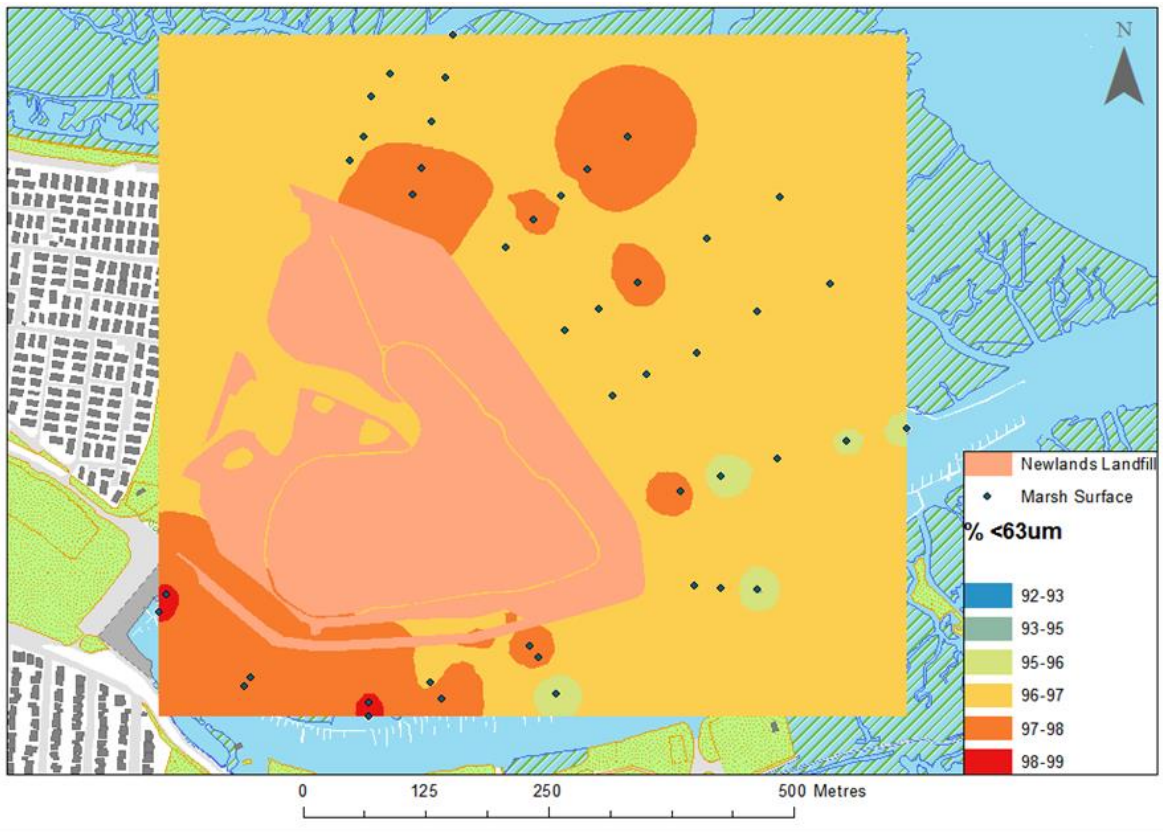

Figure 4.12: Predicted spatial distribution of sample < 63 µm in surface sediments.

Carbon Content

Percentage Carbon did not greatly vary across the surface of the marsh, with maximum and minimum values of 16 % and 7 % respectively, with a median value of 10 % and a %RSD of 9.3 (Table 4.7). Spatial distribution of Carbon shows very little variation across the surface of the salt marsh, with a slight enhancement within the North (Figure 4.13).

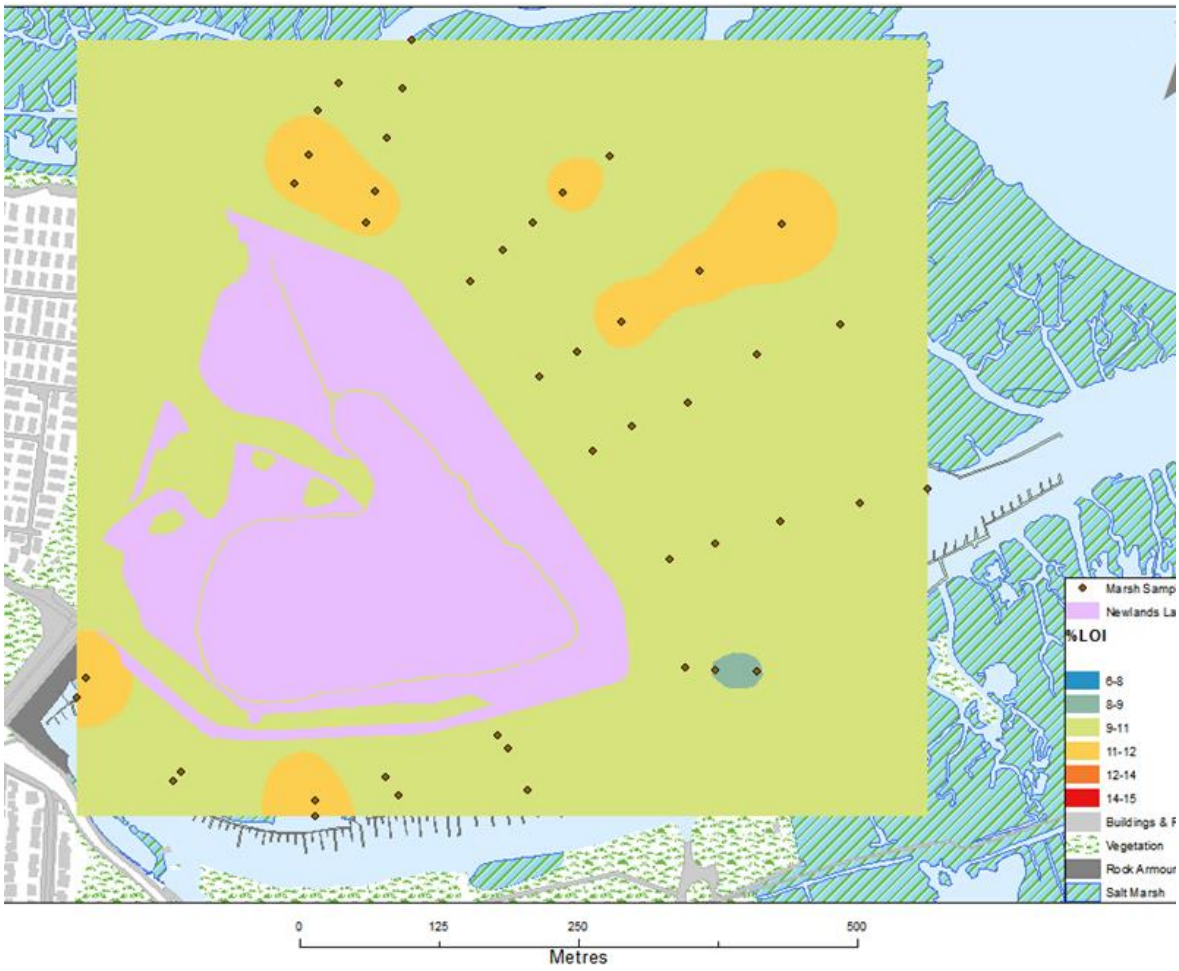

Figure 4.13: Predicted spatial distribution of Carbon across the salt marsh surface.

Reproducibility of measurements gave an average RSD value of 0.2 %. Spatially, pH shows a trend of higher values approximately 50 m from the North East boundary, reducing within distances over 200 m and generally lower values to the South of the site (Figure 4.14).

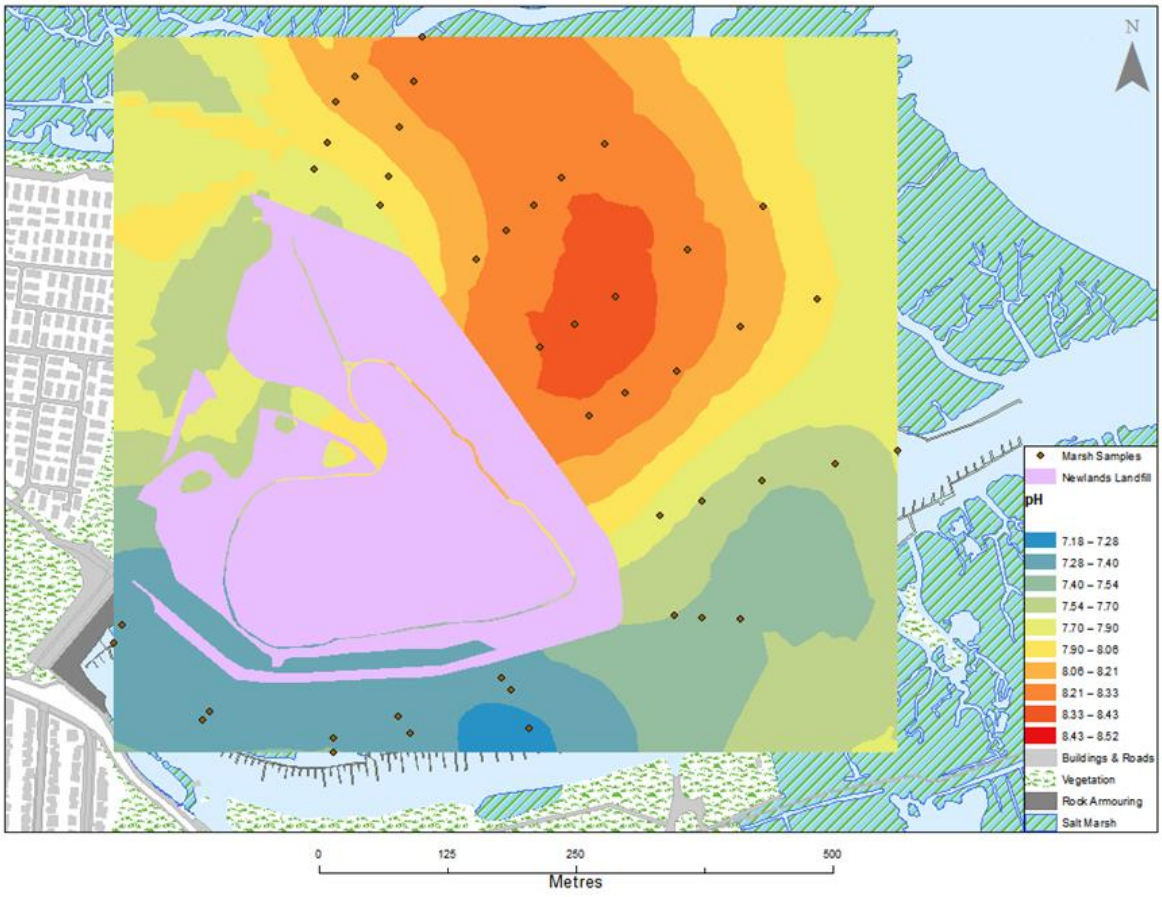

Figure 4.14: Predicted spatial distribution of sediment pH across the salt marsh surface.

Surface Metal Concentrations

Marsh surface sediment metal concentrations are given in Table 4.8 with a complete data set in Appendix 2.

Table 4.8: Descriptive statistics for marsh surface samples (mg kg^{-1}).

	Al	Ca	Co	Cr	Cu	Fe	K	Li	Mg	Mn	Na	Ni	Pb	Sr	Zn
Median	17985	35797	16	38	32	27225	3953	29	7064	248	9303	33	48	92	117
Min	10708	15342	12	22	15	17268	2416	16	4691	199	4684	21	29	53	68
Max	29288	55460	21	59	58	42058	5608	46	10029	356	14177	49	118	163	175
Range	18579	40117	9	37	43	24789	3193	29	5337	157	9492	28	89	110	108
St Dev	4805	7121	3	9	10	4951	804	7	1530	36	2109	5	17	23	22

Normalised metal ratios were plotted to visualise the spatial distribution of metals without influence from grain size. The ratios of Cr, Pb, Fe, K and Ni to Li all exhibit elevated levels at distances over 100 m at the North, East and South boundaries of the site (Cr and Pb shown in Figures 4.15 and 4.16), whilst Co, Cu, Sr and Mn ratios are only elevated within the sediments to the South of the site boundary, (Figure 4.17). The only element which did not show elevated levels to the South of the landfill was Mg (Figure 4.18).

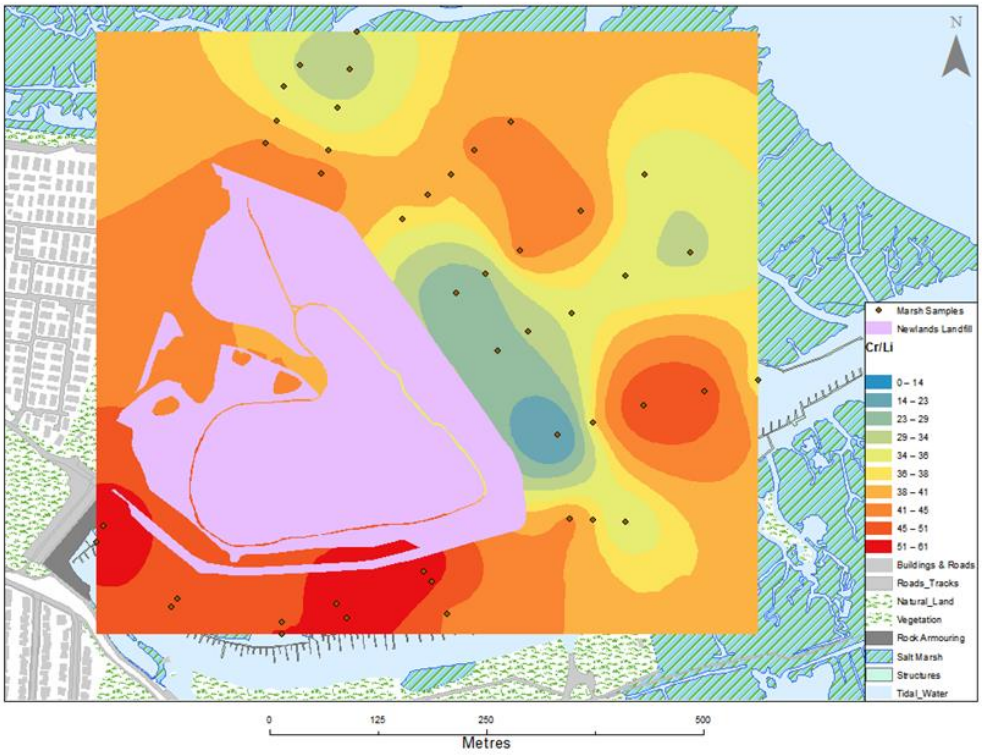

Figure 4.15: Predicted spatial distribution of Cr/Li around Newlands landfill.

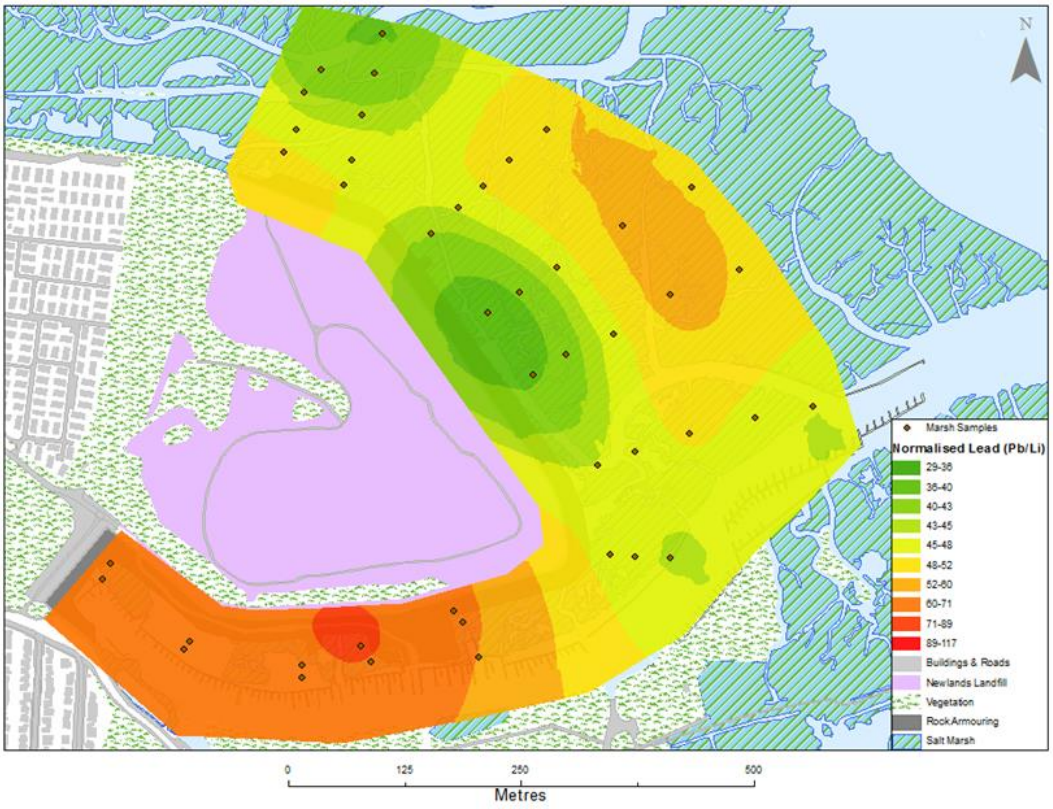

Figure 4.16: Predicted spatial distribution of Pb/Li around Newlands landfill.

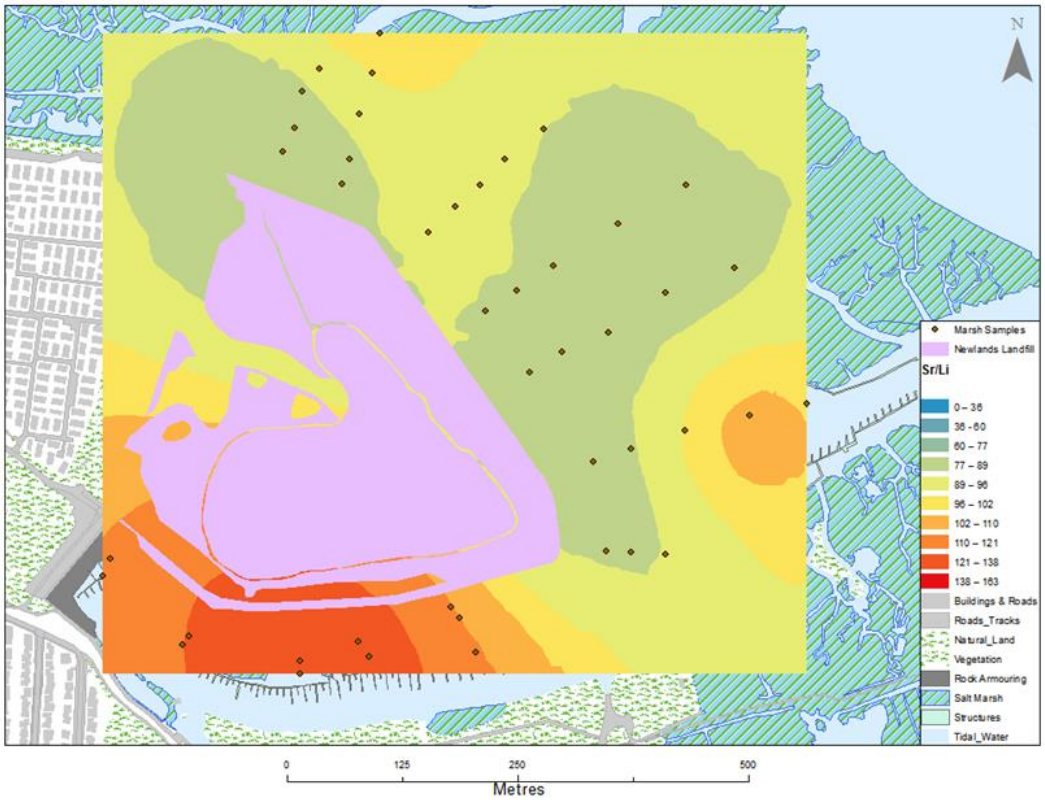

Figure 4.17: Predicted spatial distribution of Sr/Li around Newlands landfill.

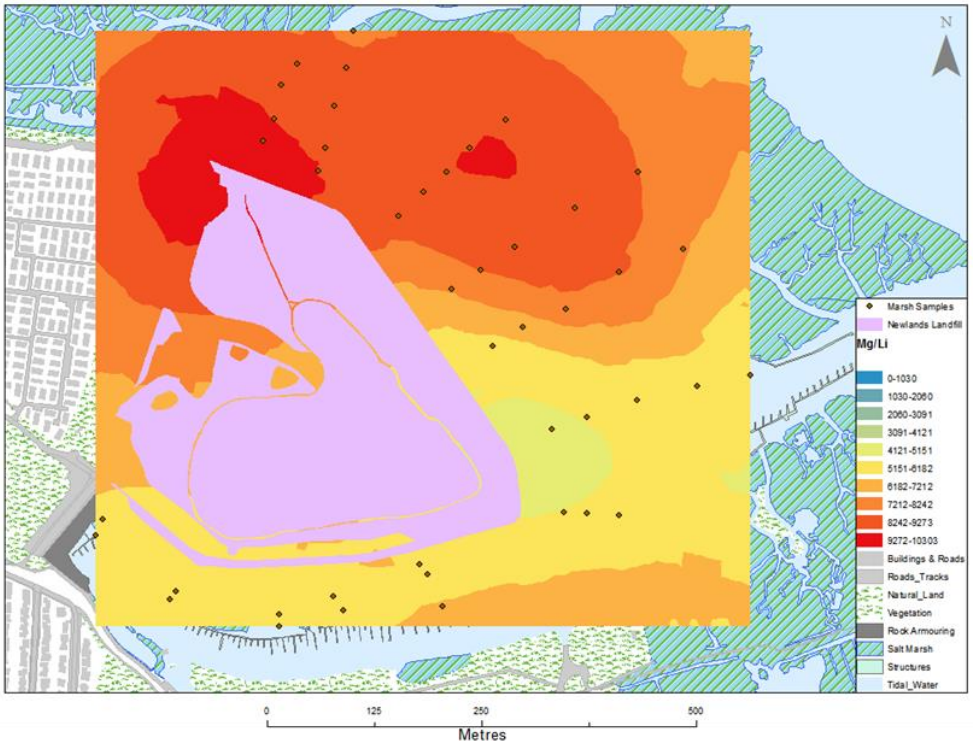

Figure 4.18: Predicted spatial distribution of Mg/Li around Newlands landfill.

Inter-Elemental Relationships

Inter-elemental relationships identify possible associations between different variables and indications of source/behaviour of metals and are given in Table 4.9. The data showed significant correlations between most variables, with Al, Cr, Cu, Fe K, Mn and Ni all showing strong correlations. Trace metals, such as Pb, Cr, Cu and Zn all show strong correlations to each other. However, the trace metal Zn shows strong correlations to the major element K. Mn is only correlated to Sr, whilst Mg, LOI and pH are not strongly correlated to any other variables. LOI and < 63 µm fraction show moderate correlation.

Table 4.9: Spearman's Rank correlation coefficient table for pH, LOI%, <63µm fraction and normalised metal ratios. Values shown are different from 0 with a significance level alpha=0.05. Values in bold show an R value > 0.7.

	LOI	pH	63um	Al	Ca	Co	Cr	Cu	Fe	K	Mg	Mn	Na	Ni	Pb	Sr	Zn
LOI			0.576	0.459			0.388	0.591	0.514	0.577	0.366		0.695	0.459	0.39		0.567
pH					-0.331	-0.682	-0.654	-0.345	-0.37	-0.359	0.606	-0.568		-0.492	-0.556	-0.503	-0.329
63um				0.467			0.385	**0.711**	0.461	0.554			0.354	0.432	0.419		0.633
Al						0.657	**0.914**	**0.756**	**0.854**	**0.934**		**0.71**	0.419	**0.802**	0.594	0.63	0.633
Ca						0.384					-0.435	0.534				0.65	
Co							**0.777**	0.375	0.602	0.5	-0.538	**0.782**		0.656	0.494	0.644	
Cr								**0.719**	**0.847**	**0.84**		**0.758**		**0.829**	**0.738**	0.617	0.61
Cu									**0.777**	**0.808**		0.374	0.421	**0.72**	**0.764**	0.379	**0.919**
Fe										**0.87**		0.654	0.402	**0.793**	0.587	0.589	0.633
K												0.587	0.596	**0.813**	0.542	0.512	**0.721**
Mg												-0.388	0.684			-0.397	
Mn														0.511	0.371	**0.87**	
Na														0.461			0.5
Ni															0.695	0.459	0.691
Pb																0.337	**0.765**
Sr																	
Zn																	

4.4.2. Sediment Core Samples

Table 4.10 shows a summary of all available LOI, pH and grain size data.

Table 4.10: Descriptive statistics for marsh surface samples.

	Core A			Core B			Core D			Core E	
	<63um (%)	**pH**	**LOI (%)**	**<63um (%)**	**pH**	**LOI (%)**	**<63um (%)**	**pH**	**LOI (%)**	**<63um (%)**	**pH**
Median		8.3	6.2		8.3	4.9	31.3	8.4		77.5	8.2
Max		8.9	14.2		8.7	15.0	63.9	8.8		98.9	8.6
Min		7.7	1.2		7.5	1.1	4.6	7.6		26.5	7.5

	Core F			Core G			Core H		
	<63um (%)	**pH**	**LOI (%)**	**<63um (%)**	**pH**	**LOI (%)**	**<63um (%)**	**pH**	**LOI (%)**
Median		8.5	5.1	73.2	8.0			8.7	9.1
Max		8.8	17.7	97.8	8.6			8.9	18.3
Min		7.5	2.9	12.6	7.6			7.9	4.7

Sediment Grain Size

Ternary plots for sediment cores D, E and G are shown in Figure 4.19. There is a clear trend within each core, showing a shift from clayey silt near the sediment surface to silty sand at depth. Figure 4.20 shows that grain size remains consistent in all cores in the top 70 cm, before coarsening with depth, with a marked increase in the percentage of sandy grains at 1 m. The sediment core nearest the landfill (core G) becomes sandier than the distal cores.

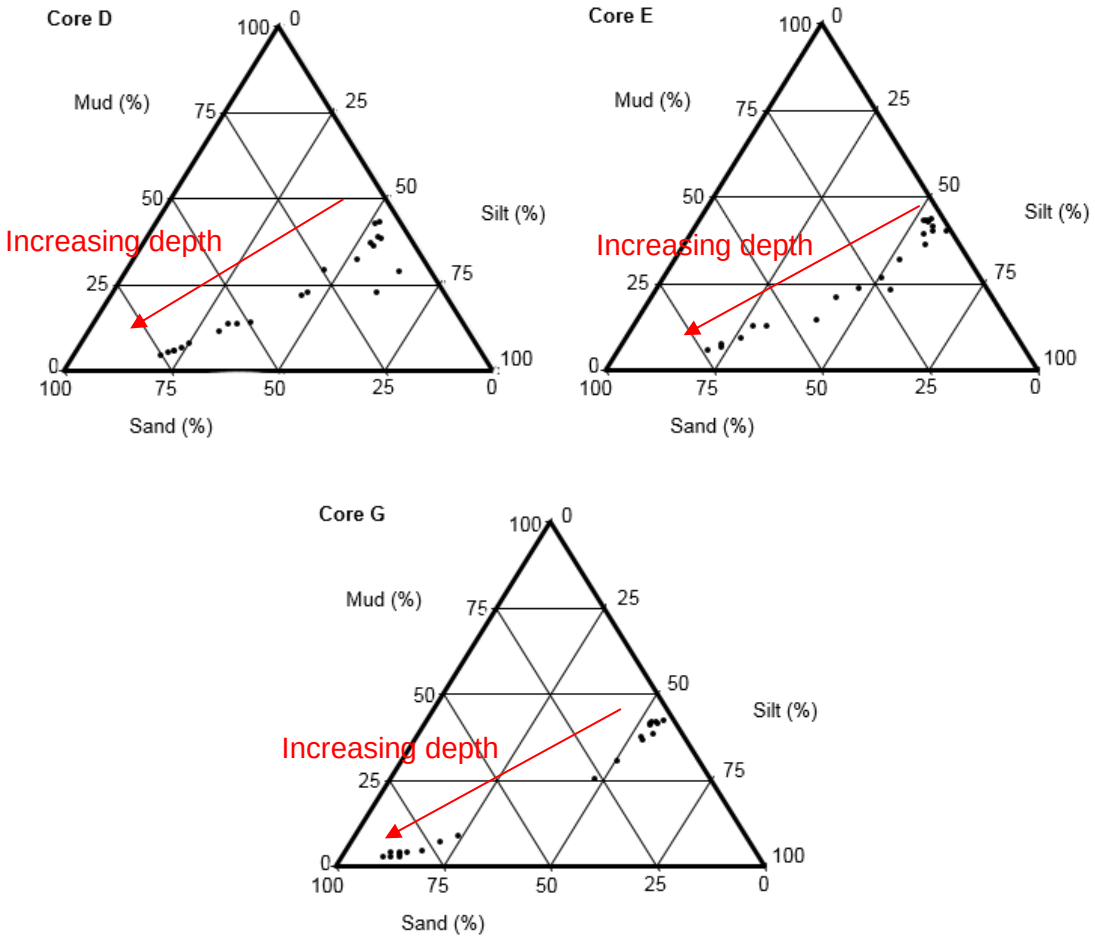

Figure 4.19: Ternary plots for cores D, E and G.

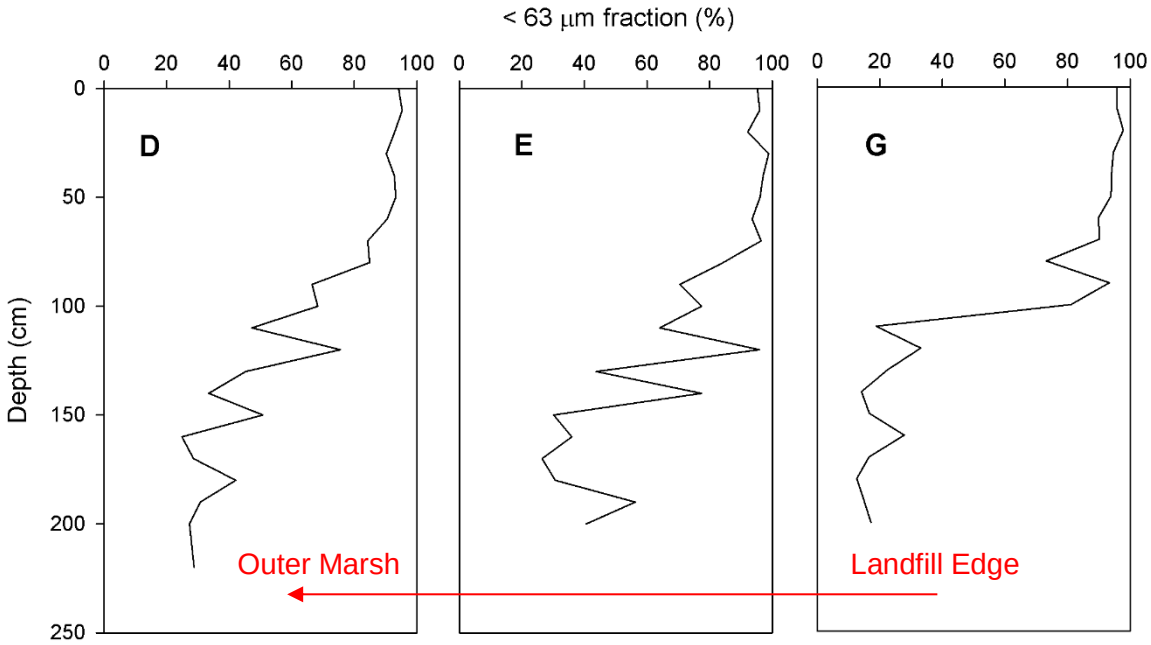

Figure 4.20: Grain size distribution with depth for sediment core D (furthest from the landfill boundary), E and G (closest to the landfill boundary).

Carbon Content

Carbon content percentages for sediment cores are shown below in Figure 4.21, with complete results within Appendix 3. All cores show a sharp initial decrease between 0 and 20 cm depth with a more gradual decrease to the base of the cores. With the exception of a small increase around 280 cm in core B, all values remain constant at depth. Median values are higher at the landfill edge (9.1 %) than in both cores within the middle (5 %) and outer marsh (4 %).

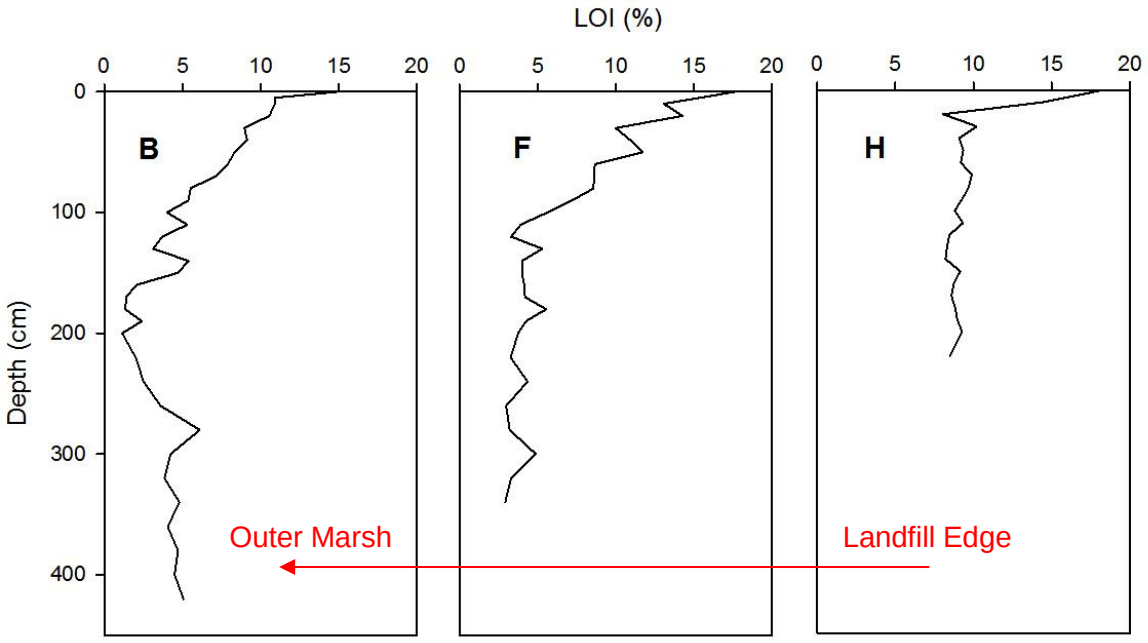

Figure 4.21: Carbon content within sediment cores. Core H is closest to the landfill core B is furthest away.

Sediment pH

The pH data for sediment cores is given in Figure 4.22, and ranged from 7.5 to 8.9. A complete dataset is shown in Appendix 4. pH was generally more alkaline than the surface samples and pH increased with depth in all cores (except A), from an average (median) of 7.7 within top 1 m, to 8.5 at depth. Median core pH shows no trend with distance from the landfill.

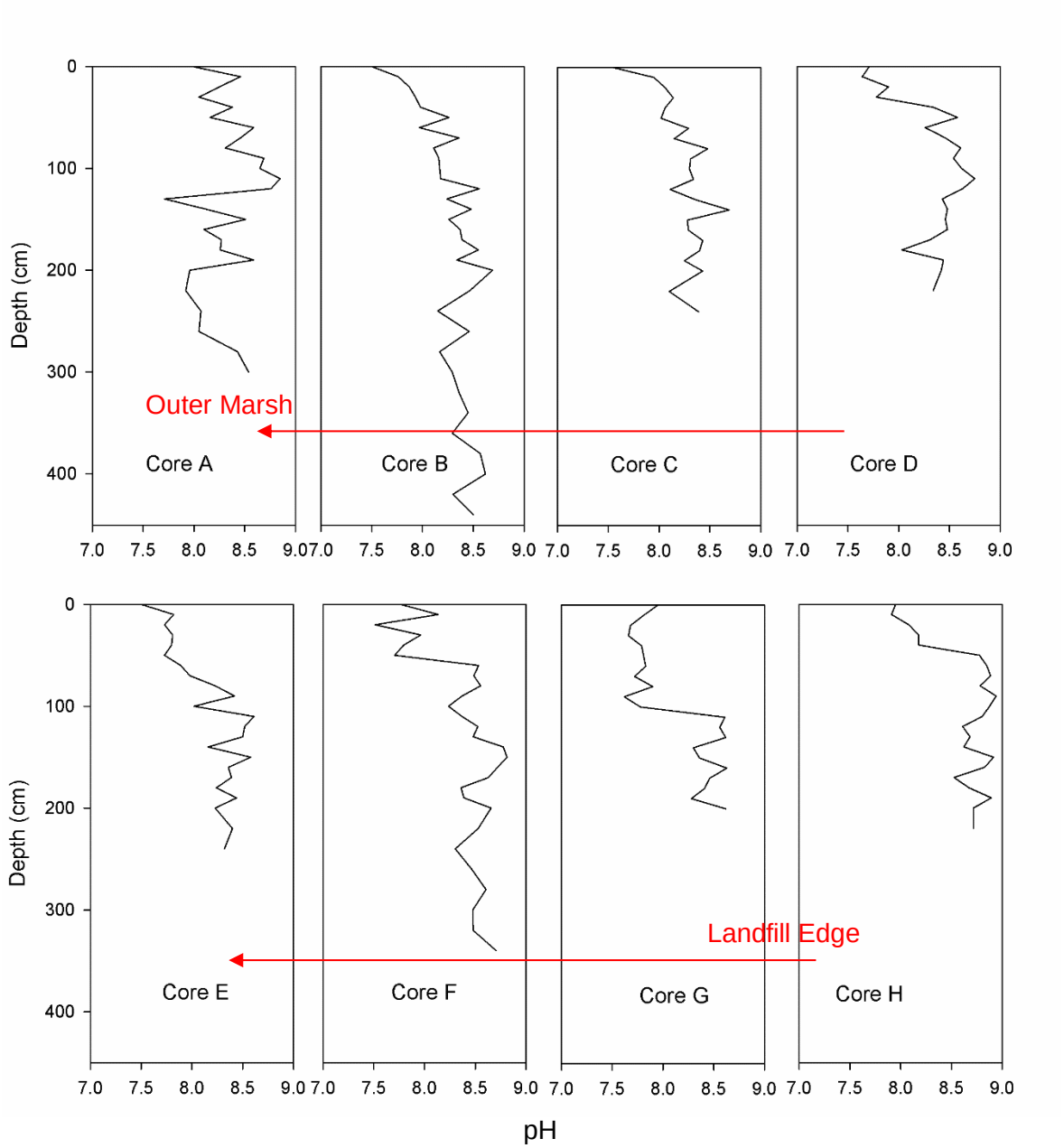

Figure 4.22: pH values for 8 sediment cores. Core A is furthest from the landfill and Core H is adjacent to the landfill boundary.

Sediment Core Metal Concentrations

Trace and major elements were measured for cores A, B, D, E, F, G and H. A summary of concentrations can be seen in Table 4.11, with complete datasets within Appendices 5a and 5b. Generally, major elements show little variability across the cores, such as Al (1.9 - 3 %), Fe, K, Mg and Na. However, Ca concentrations vary more between and within the cores (0.1 – 5 %). Cobalt shows low variability of median concentration across the cores (9-12 mg kg $^{-1}$), as does Cr (41-54 mg kg $^{-1}$), Li (31-38 mg kg $^{-1}$) and Ni (25-35 mg kg $^{-1}$). Trace metals usually associated with anthropogenic activity, such as Cu, Pb and Zn show higher variability. Mn, Sr and V show highly variable concentrations across the sediment cores, however, with all metals, there appears to be no trend either toward or away from the landfill.

Normalised Metal/Li Distributions

Normalised metal ratios were plotted to exclude grain size effects when observing distributions within the salt marsh. These will be used to discuss vertical distributions. Full results can be seen in Appendices 3 and 4. Aluminium (Al) and Magnesium (Mg) show little variation with depth in all cores, with only slight elevations at depth within cores E, F and G. However, Fe appears to show slightly more variable levels, with higher levels in the base of cores D, E, F and G and elevations in the subsurface, around 50 cm depth. Figure 4.23 illustrates an example of the limited variation in Al and Mg, and to a lesser extent Fe, within Core B.

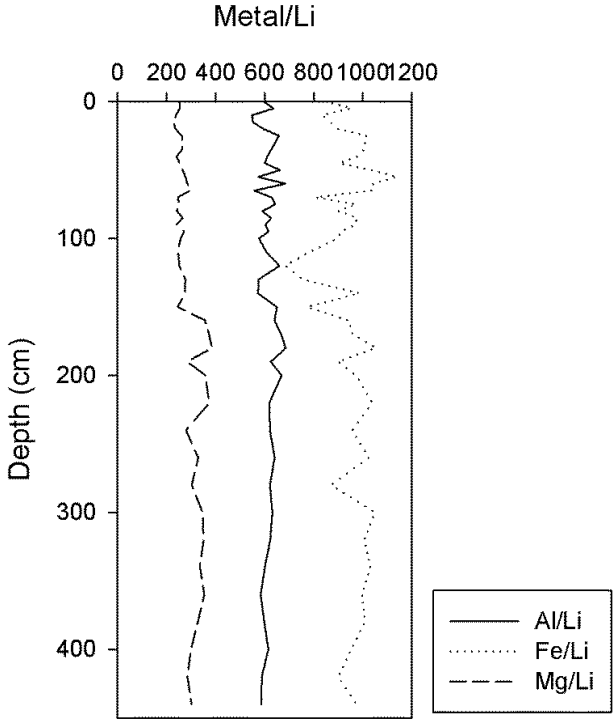

Figure 4.23: Normalised Al, Fe and Mg levels within core B as an example.

Calcium, K and Na show more variability. K is generally consistent with depth in all cores, with some cores showing slightly higher levels towards the base. Na data show high values at the very surface (0 – 5 cm) then increase at depths over 100 cm in cores B, D, E, F and G. Calcium shows a similar trend to K, however the higher levels at depth are even more pronounced, exceeding surface values (Figure 4.24). Sr data also show the same pattern, with elevations at both the surface and at depth (Appendix 6).

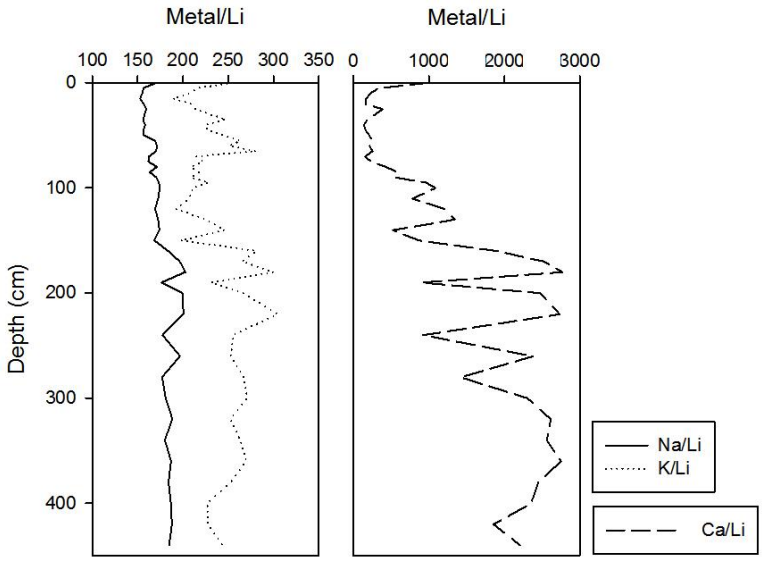

Figure 4.24: Normalised Ca, K and Na levels within core B as an example.

Generally, trace metals show more variability than the major elements with the exception of Co and V. Cobalt shows a consistent distribution, with slight subsurface enrichment within 30 cm depth within cores D, E and H. Vanadium shows similar distributions, with the exception of Core G, which shows elevated levels at depths over 150 cm (Appendix 6).

Chromium and Ni show similar spatial distributions. With the exception of Core A, all cores show enhanced levels within the first 50 cm, returning to surface levels at depths over 100 cm, with the exception of Core A, which shows elevated levels at the surface (Figure 4.25). Cores E and G show elevated levels at 200 cm, however, these single data points are likely to be non-representative. The distributions are similar to Mn; however, the magnitude of subsurface enhancements is much higher for Mn (Figure 4.26).

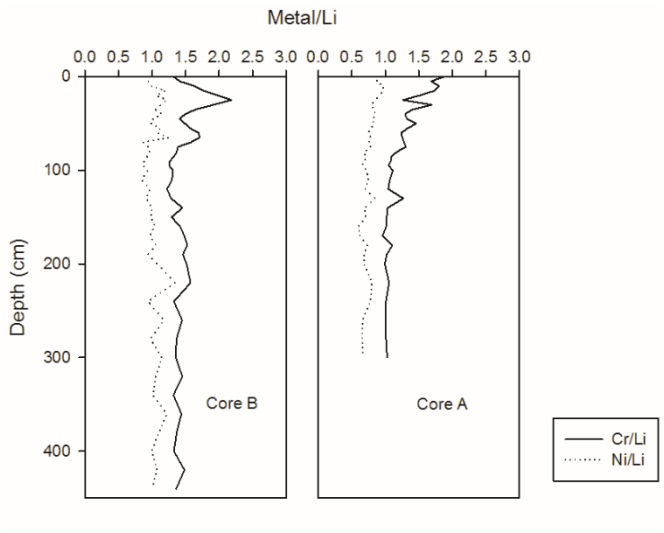

Figure 4.25: Normalised Cr and Ni in cores A and B.

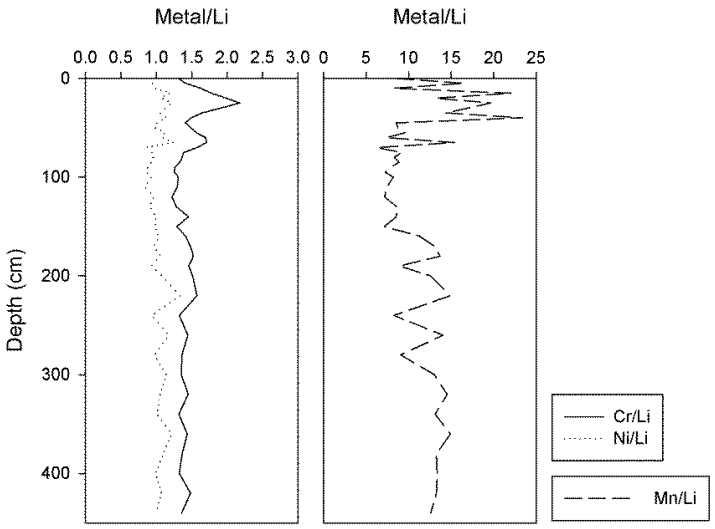

Figure 4.26: Normalised Cr, Ni and Mn levels within core B as an example.

Maximum Hg concentrations were higher in the core nearest the landfill than the distal core (Table 4.11 and Appendix 5b). The data were limited so trends could not be plotted across the whole site. Copper, Pb and Zn all show similar distributions, with subsurface enrichment within the top 100 cm (peaking c. 50 cm depth) then a return to surface levels at depths greater than 100 cm (Figure 4.27). Lead shows a much more varied and erratic distribution than Cu and Zn. Cores B to G show subsurface enrichments within the top 25 cm, and a reduction at depth. Core A shows an erratic, yet generally consistent signal with depth. Vertical profiles in core H, which is closest to the landfill, show a very different vertical distribution with subsurface elevation which is then sustained at depth. Zn shows a similar depositional signature to other trace metals, however, the record within core H is similar to that seen with Pb, with elevated levels throughout the length of the core (Figure 4.28).

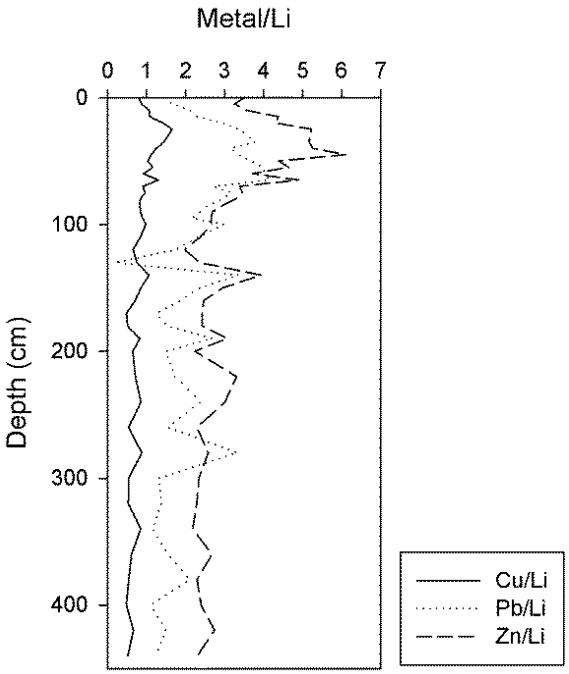

Figure 4.27: Normalised Cu, Pb and Zn levels within core B.

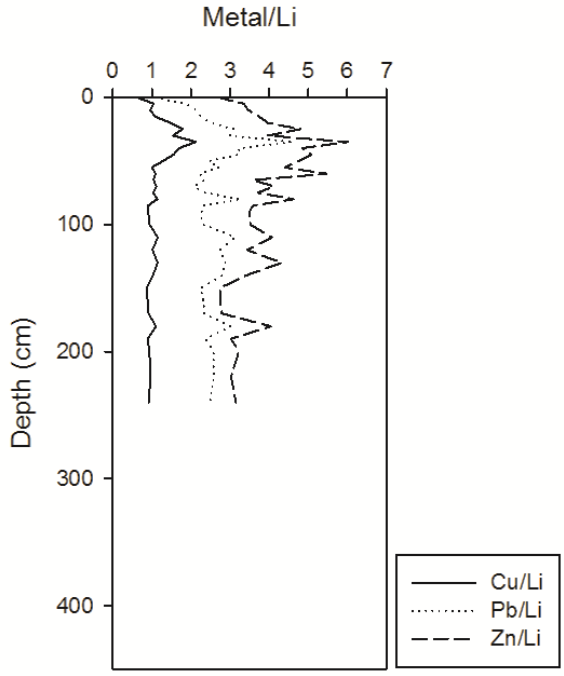

Figure 4.28: Normalised Cu, Pb and Zn levels within core H

.

Table 4.11: Median and range concentrations for major (%) and trace metals (mg kg $^{-1}$) from Newlands sediment cores.

	Core A		Core B		Core D		Core E		Core F		Core G		Core H	
	Median	Range	Median	Range	Median	Range	Median	Range	Median	Range	Median	Range	Median	Range
(%)														
Al	3	1.3-3.6	1.9	0.7-2.7	2.1	0.6-3.4	2.6	0.6-3.5	2.5	0.6-3.7	2.5	0.4-3.8	2.3	1.8-3.9
Ca	3	0.8-5.0	2.8	0.5-4.3	2.6	0.4-4.9	0.7	0.4-4.7	0.8	0.3-3.6	0.5	0.1-4.2	3.5	0.5-4.7
Fe	3.5	2.4-4.6	2.8	1.1-4.3	3.1	1.4-6.0	3.8	1.1-6.1	3	1.0-5.1	4.2	0.8-5.1	3	2.2-4.9
K	0.7	0.3-0.7	0.5	0.2-0.6	0.5	0.2-0.7	0.6	0.2-0.6	0.6	0.1-0.8	0.6	0.1-0.7	0.6	0.4-0.8
Mg	1.1	0.7-1.4	0.9	0.4-1.1	1	0.4-1.2	1.1	0.4-1.3	1	0.3-1.2	1	0.3-1.3	0.9	0.7-1.3
Na	1	0.5-3.5	0.7	0.3-1.0	0.7	0.3-1.1	0.9	0.3-1.1	0.7	0.2-1.1	0.8	0.2-1.3	0.8	0.6-1.2
(mg kg $^{-1}$)														
Co	10	5.1-14.9	12.5	6.2-20.8	9.8	4-17.6	11.7	4.9-25.6	12.6	7-24.4	12.5	3.2-19.4	9.2	7.1-16.4
Cr	52.2	23.5-82.3	43	17.7-82.3	41.3	12-72.4	52	14.6-80	43.7	6.5-88.5	54	9.1-86	46.5	36-90.6
Cu	37.6	15.9-73.6	29	6-62.5	23.4	5-54.9	31.2	5.1-66.3	22.8	3.7-68.5	31.7	3.6-67.1	36.3	28.8-68
Hg									0.8	0.1-2			1.3	0.6-1.6
Li	43.3	22.8-52.4	31.5	11.5-42.7	32.3	10.1-48.7	37.8	9.8-48.5	38.4	8.8-57.3	37.6	5.6-53.4	34.8	28.5-60.8
Mn	269.6	220.6-640.8	247.4	159.5-988.5	204.6	153.4-1016.1	252.6	161.6-1717.6	175	142.5-1349.1	336	124.7-1052.3	269.9	206.5-1066.5
Ni	32.9	15.2-42.3	29.4	12.4-48.3	29.5	9.6-45.2	35.6	9.7-68.8	25.6	2.6-57	37.3	7.7-48.8	29.6	24.6-54.2
Pb	94.6	37.8-204.7	76.1	16.4-154.1	53.6	10.4-149.7	85.6	11.3-187.5	55.3	4.2-169	78.2	7.8-155.2	88.7	65.9-132.1
Sr	79.6	49.5-123.6	71	49.6-132.1	65.3	49.4-114.7	57	38.6-126.5	55.1	30.6-123.3	56.8	33.7-96.4	89.4	43.1-168.6
V	90.3	48-99.2	72	31.4-102.6	74.5	26.6-99.2	84.6	31.4-106	82.6	21.7-118	89.6	21.5-111.3	71.4	60.3-110
Zn	119.1	54.3-262.3	90.1	28.2-259.9	85.5	29.3-193.1	127.4	33-260.7	97.8	22.1-204.8	113.2	27.1-180.7	134.2	87.8-202.4

Inter-Elemental Relationships

Spearman's rank correlation tables are shown in Tables 4.12 to 4.18. All cores show a strong correlation between Ca and Sr, with the lowest value being 0.82 in Core E. Additionally, within all cores, Na is strongly correlated to Mg, showing similar values to Ca and Sr correlations. Major elements, such as Fe, K, Mg and Mn show strong positive inter-correlations which vary in strength dependent on the core. For example, core A, furthest from the landfill boundary, shows no correlation between Fe and K, but exhibits a strong positive correlation between Fe – Mn and Mg – Na. Conversely, Core G, which is the second closest to the landfill boundary shows strong correlations between the majority of major elements.

Similarly, inter-elemental positive correlations exist within each core for trace metals, such as Cu, Cr, Pb and Zn. Some trace metals exhibit strong negative correlations with major elements, for example within core D, where Pb and Sr are correlated (R = -0.83). Cores E and G also show strong positive associations between major and trace metals, namely Fe with Zn (Core G) and Fe with Cr (Core E), however this is limited and is not prevalent through the data. pH shows a negative correlation with the majority of elements, however the correlation is rarely strong, except with Pb in Core F (R = -0.7). Within cores B, F and H, Carbon appears negatively correlated to most major and trace metals, except for Cu in Core B and Pb in Core F. Furthermore, Pb is not strongly correlated with any other elements in Core H, nor is Zn in Core F.

Table 4.12: Spearman's Rank correlation coefficient table for Sediment core A data. Values shown are different from 0 with a significance level alpha=0.05. Values in bold show an R value > 0.7.

	LOI	pH	Al/Li	Ca/Li	Co/Li	Cr/Li	Cu/Li	Fe/Li	K/Li	Mg/Li	Mn/Li	Na/Li	Ni/Li	Pb/Li	Sr/Li	V/Li	Zn/Li
LOI																	
pH																	
Al/Li								0.333									
Ca/Li						-0.681	-0.546		0.562		0.364		-0.594	-0.562	**0.934**	-0.419	-0.648
Co/Li						0.484	0.464	0.595		0.523	0.368		**0.738**	0.359		0.545	0.519
Cr/Li							**0.930**		-0.339				**0.865**	**0.789**	-0.646	**0.762**	**0.944**
Cu/Li										0.407		0.356	**0.848**	**0.762**	-0.526	**0.784**	**0.950**
Fe/Li										0.673	**0.810**	0.416	0.46			0.572	
K/Li										0.477		0.489			0.488		
Mg/Li											0.403	**0.792**	0.405			0.694	0.449
Mn/Li															0.477	0.367	
Na/Li														0.35		0.56	0.383
Ni/Li														0.616	-0.554	**0.711**	**0.849**
Pb/Li															-0.675	0.557	**0.816**
Sr/Li																-0.354	-0.647
V/Li																	**0.824**
Zn/Li																	

Table 4.13: Spearman's Rank correlation coefficient table for Sediment Core B data. Values shown are different from 0 with a significance level alpha=0.05. Values in bold show an R value > 0.7.

	LOI	pH	Al/Li	Ca/Li	Co/Li	Cr/Li	Cu/Li	Fe/Li	K/Li	Mg/Li	Mn/Li	Na/Li	Ni/Li	Pb/Li	Sr/Li	V/Li	Zn/Li
LOI		**-0.720**	-0.359	**-0.753**	-0.502		**0.702**		**-0.747**	**-0.714**		-0.379		0.47	-0.613	-0.661	0.627
pH			0.353	0.67	0.461		-0.675	0.369	0.685	0.66	0.386			-0.472	0.642	0.521	-0.601
Al/Li										0.323							
Ca/Li					0.544		**-0.848**		**0.912**	**0.816**		0.526		**-0.731**	**0.941**	0.577	**-0.756**
Co/Li							-0.444	0.412	0.508	0.608	0.633	0.588	**0.734**	-0.448	0.61	0.661	-0.442
Cr/Li							0.357	0.414			0.533		0.512	0.357	-0.345	0.411	0.564
Cu/Li									**-0.805**	-0.635		-0.339		**0.815**	-0.834	-0.431	**0.810**
Fe/Li									0.351	0.597	0.53	0.604	0.496			0.629	
K/Li										**0.854**		0.605		-0.581	**0.857**	0.691	-0.652
Mg/Li											0.402	**0.823**		-0.428	**0.718**	**0.786**	-0.478
Mn/Li												0.337	0.602			0.565	
Na/Li													0.433		0.475	0.661	
Ni/Li																0.598	
Pb/Li															**-0.774**		**0.752**
Sr/Li																0.502	**-0.785**
V/Li																	
Zn/Li																	

Table 4.14: Spearman's Rank correlation coefficient table for Sediment Core D data. Values shown are different from 0 with a significance level alpha=0.05. Values in bold show an R value > 0.7.

	LOI	pH	Al/Li	Ca/Li	Co/Li	Cr/Li	Cu/Li	Fe/Li	K/Li	Mg/Li	Mn/Li	Na/Li	Ni/Li	Pb/Li	Sr/Li	V/Li	Zn/Li
LOI																	
pH						-0.481		-0.535			-0.511	-0.471	-0.494				-0.696
Al/Li				0.362			-0.561	0.45		0.417	0.368			-0.428			
Ca/Li							**-0.852**	0.416	**0.970**	**0.843**		0.516	-0.379	**-0.828**	**0.881**	0.426	-0.393
Co/Li											0.377	0.598	**0.740**		0.376	0.447	
Cr/Li							0.441	0.482			0.5		0.446	0.43		0.628	**0.813**
Cu/Li									**-0.798**	-0.623			0.535	**0.909**	**-0.766**		0.644
Fe/Li									0.519	**0.741**	**0.812**	0.597			0.374	0.636	0.436
K/Li										**0.902**	0.364	0.581		**-0.784**	**0.863**	0.523	
Mg/Li											0.54	**0.756**		-0.641	**0.775**	0.639	
Mn/Li												0.442				0.495	0.479
Na/Li													0.434	-0.376	0.662	0.611	
Ni/Li														0.357			0.494
Pb/Li															**-0.83**		0.652
Sr/Li																	-0.426
V/Li																	0.419
Zn/Li																	

Table 4.15: Spearman's Rank correlation coefficient table for Sediment Core E data. Values shown are different from 0 with a significance level alpha=0.05. Values in bold show an R value > 0.7.

	LOI	pH	Al/Li	Ca/Li	Co/Li	Cr/Li	Cu/Li	Fe/Li	K/Li	Mg/Li	Mn/Li	Na/Li	Ni/Li	Pb/Li	Sr/Li	V/Li	Zn/Li
LOI																	
pH							-0.512		0.632		-0.475			-0.473			-0.479
Al/Li																	
Ca/Li					0.590		-0.392	0.546	0.616	**0.841**	0.351	**0.839**	0.386	-0.436	**0.819**	0.567	
Co/Li						**0.713**		0.625	0.611	0.595	**0.745**	0.669	**0.826**		**0.795**	**0.809**	
Cr/Li							0.346	**0.774**		0.504	**0.782**	0.619	**0.828**		0.487	0.566	**0.725**
Cu/Li									-0.574					**0.891**	-0.413		**0.760**
Fe/Li										**0.711**	0.685	**0.798**	0.628		0.513	0.58	0.47
K/Li										0.662		0.566	0.359	-0.554	**0.709**	**0.791**	
Mg/Li												**0.862**	0.481		0.652	0.695	
Mn/Li												0.514	**0.786**		0.548	0.384	0.674
Na/Li													0.627		**0.749**	0.607	
Ni/Li															0.613	0.601	0.571
Pb/Li															-0.473		0.654
Sr/Li																0.685	
V/Li																	
Zn/Li																	

Table 4.16: Spearman's Rank correlation coefficient table for Sediment Core F data. Values shown are different from 0 with a significance level alpha=0.05. Values in bold show an R value > 0.7.

	LOI	pH	Al/Li	Ca/Li	Co/Li	Cr/Li	Cu/Li	Fe/Li	K/Li	Mg/Li	Mn/Li	Na/Li	Ni/Li	Pb/Li	Sr/Li	V/Li	Zn/Li
LOI		-0.545		**-0.773**	**-0.746**	**0.83**	0.669	-0.420	**-0.794**	**-0.754**		-0.427	0.619	**0.731**	-0.673	-0.545	
pH				0.505	0.623	-0.645	-0.600		0.586	0.585				**-0.701**	0.463		-0.406
Al/Li										0.328						0.411	
Ca/Li					**0.762**	**-0.732**	-0.585	**0.707**	**0.826**	**0.849**	0.373	**0.709**	-0.333	**-0.753**	**0.944**	0.674	
Co/Li						**-0.758**	-0.607	**0.728**	**0.799**	**0.817**	0.489	**0.712**		-0.661	**0.779**	**0.762**	
Cr/Li							**0.902**	-0.423	**-0.915**	**-0.712**		-0.415	0.665	**0.911**	-0.65	-0.418	0.621
Cu/Li									**-0.796**	-0.6			0.612	**0.868**	-0.481		0.671
Fe/Li									0.559	0.661	0.684	**0.882**		-0.333	**0.804**	**0.867**	
K/Li										0.832		0.562	-0.622	**-0.846**	**0.733**	0.585	-0.467
Mg/Li												0.641	-0.39	-0.695	**0.772**	**0.733**	
Mn/Li												**0.743**			0.584	0.618	0.487
Na/Li														-0.373	**0.826**	**0.839**	
Ni/Li														0.61			0.654
Pb/Li															-0.663	-0.363	0.62
Sr/Li																**0.735**	
V/Li																	
Zn/Li																	

Table 4.17: Spearman's Rank correlation coefficient table for Sediment Core G data. Values shown are different from 0 with a significance level alpha=0.05. Values in bold show an R value > 0.7.

	LOI	pH	Al/Li	Ca/Li	Co/Li	Cr/Li	Cu/Li	Fe/Li	K/Li	Mg/Li	Mn/Li	Na/Li	Ni/Li	Pb/Li	Sr/Li	V/Li	Zn/Li
LOI																	
pH				0.665			-0.521		0.551	0.558				**-0.721**	0.664	0.473	
Al/Li							-0.59		0.387	0.406				-0.61			
Ca/Li					0.508			0.585	**0.833**	**0.863**	0.477	**0.773**	0.368	-0.516	**0.964**	0.597	0.493
Co/Li								0.358			0.486	0.471	0.608		0.605		0.435
Cr/Li							0.438	0.596	0.39	0.415	0.62	0.555				0.473	**0.885**
Cu/Li													0.472	**0.825**			
Fe/Li									**0.721**	**0.781**	0.667	**0.733**			0.525	**0.87**	**0.712**
K/Li										**0.938**	0.672	0.677		-0.504	**0.781**	**0.787**	0.604
Mg/Li											0.609	**0.718**		-0.478	**0.793**	**0.795**	0.600
Mn/Li												0.502			0.491	0.618	**0.760**
Na/Li													0.552		**0.746**	0.663	**0.746**
Ni/Li															0.451		0.546
Pb/Li															-0.487		
Sr/Li																0.581	0.493
V/Li																	0.635
Zn/Li																	

Table 4.18: Spearman's Rank correlation coefficient table for Sediment Core H data. Values shown are different from 0 with a significance level alpha=0.05. Values in bold show an R value > 0.7.

	LOI	pH	Al/Li	Ca/Li	Co/Li	Cr/Li	Cu/Li	Fe/Li	K/Li	Mg/Li	Mn/Li	Na/Li	Ni/Li	Pb/Li	Sr/Li	V/Li	Zn/Li
LOI																	
pH											-0.634		-0.466				
Al/Li				-0.374					-0.45			-0.424			-0.37		
Ca/Li						-0.611	-0.462		**0.842**				-0.354		**0.96**	-0.385	-0.392
Co/Li						0.691	0.606	0.663		0.635	0.683	0.487	**0.788**	0.468		**0.752**	0.381
Cr/Li							**0.799**	0.508	-0.356	0.553	0.571		**0.784**	0.551	-0.692	**0.887**	0.608
Cu/Li										0.487			0.593	0.621	-0.582	**0.738**	**0.852**
Fe/Li										0.69	**0.842**	0.644	**0.745**	0.365		0.62	
K/Li												0.413			**0.772**		
Mg/Li											0.465	**0.816**	0.628	0.674		**0.798**	0.355
Mn/Li												0.422	**0.757**			0.546	
Na/Li													0.451	0.489		0.498	
Ni/Li														0.387	-0.386	**0.797**	0.396
Pb/Li																0.640	0.511
Sr/Li																-0.489	-0.524
V/Li																	0.601
Zn/Li																	

Principal Component Analysis

Principal Component Analysis was carried out on normalised data for each core separately to determine whether factors controlling the variability of major and trace metals changed with distance from the landfill site. All cores, except A and D, extracted 3 Principal Components (PC's), with A and D extracting 4 and 2 respectively. Overall, similar components were extracted from each core, however, certain notable differences were observed. Table 4.19 shows significant factor loadings on each sediment core, after (Reid and Spencer, 2009).

Table 4.19: Principal Component Analysis factor loading tables for each sediment core. Significant (>0.6) loadings are shown in bold, weak loadings (<0.4) are in small text.

	Core A				Core B			Core D		
	PC1	PC2	PC3	PC4	PC1	PC2	PC3	PC1	PC2	PC3
LOI					**-0.819**	0.265	-0.222			
pH	-0.183	-0.358	0.308	0.487	**0.796**	-0.187	0.229	0.271	-0.745	0.074
Al/Li	0.232	0.181	-0.282	**0.775**	0.257	-0.003	**0.751**	0.475	-0.093	**0.617**
Ca/Li	**-0.642**	**0.648**	0.007	-0.194	**0.940**	-0.185	-0.021	**0.951**	-0.165	0.009
Co/Li	**0.680**	0.262	-0.240	0.167	**0.712**	0.401	-0.419	0.246	0.578	**-0.608**
Cr/Li	**0.927**	-0.213	-0.113	-0.112	-0.111	**0.820**	0.165	-0.104	**0.815**	0.364
Cu/Li	**0.916**	-0.071	-0.004	-0.218	**-0.847**	0.384	0.007	**-0.844**	0.457	-0.106
Fe/Li	0.443	**0.809**	-0.244	0.097	0.407	**0.684**	0.293	0.587	**0.650**	0.333
K/Li	-0.151	**0.649**	**0.645**	-0.068	**0.928**	-0.072	0.112	**0.960**	-0.040	0.020
Mg/Li	0.576	**0.636**	0.350	0.172	**0.897**	0.242	0.218	**0.921**	0.276	0.048
Mn/Li	0.237	**0.734**	-0.492	-0.141	0.358	**0.690**	-0.283	0.461	**0.638**	0.316
Na/Li	0.486	0.433	**0.612**	0.117	**0.653**	0.431	0.113	**0.642**	0.538	-0.396
Ni/Li	**0.919**	-0.022	-0.263	-0.082	0.261	**0.779**	-0.363	-0.198	**0.745**	-0.475
Pb/Li	**0.759**	-0.331	0.342	-0.211	**-0.689**	0.403	0.360	**-0.854**	0.381	0.108
Sr/Li	**-0.612**	**0.720**	-0.091	-0.153	**0.898**	-0.232	-0.257	**0.899**	-0.082	-0.368
V/Li	**0.873**	0.249	0.112	0.043	**0.740**	0.538	0.078	0.488	0.643	0.082
Zn/Li	**0.956**	-0.129	0.053	-0.100	**-0.735**	0.548	0.123	-0.322	**0.850**	0.271

	Core E			Core F		Core G			Core H		
	PC1	PC2	PC3	PC1	PC2	PC1	PC2	PC3	PC1	PC2	PC3
LOI				**-0.818**	0.306				0.064	-0.522	-0.192
pH	0.133	**-0.822**	-0.042	**0.668**	-0.470	0.446	**-0.683**	0.368	**-0.714**	0.146	0.441
Al/Li	-0.014	0.290	**0.831**	0.141	0.453	0.280	**-0.633**	-0.449	0.200	-0.562	-0.065
Ca/Li	**0.788**	-0.333	0.271	**0.901**	0.167	**0.886**	-0.234	0.284	-0.513	**0.786**	0.012
Co/Li	**0.902**	0.031	-0.280	**0.896**	0.201	0.558	0.219	0.519	**0.827**	0.188	-0.074
Cr/Li	**0.765**	0.526	-0.087	**-0.907**	0.356	0.545	**0.617**	-0.358	**0.928**	-0.170	0.151
Cu/Li	-0.140	**0.909**	-0.072	**-0.778**	0.468	-0.126	**0.894**	0.101	**0.780**	-0.135	0.515
Fe/Li	**0.799**	0.353	0.332	**0.693**	**0.617**	**0.827**	0.183	-0.327	**0.718**	0.344	-0.511
K/Li	**0.682**	**-0.602**	-0.131	**0.946**	-0.181	**0.915**	-0.214	-0.130	-0.335	**0.798**	0.311
Mg/Li	**0.829**	-0.196	0.398	**0.895**	0.111	**0.924**	-0.215	-0.139	**0.710**	**0.604**	0.097
Mn/Li	**0.684**	0.554	-0.130	0.327	**0.780**	**0.741**	0.226	-0.310	**0.721**	0.116	-0.595
Na/Li	**0.886**	0.000	0.260	**0.689**	**0.635**	**0.843**	0.272	0.155	0.435	**0.789**	-0.148
Ni/Li	**0.797**	0.400	-0.300	-0.509	**0.614**	0.427	0.542	0.551	**0.891**	0.079	-0.185
Pb/Li	-0.179	**0.857**	0.016	**-0.859**	0.360	-0.357	**0.858**	-0.063	0.586	0.453	0.458
Sr/Li	**0.866**	-0.276	-0.132	**0.857**	0.359	**0.864**	-0.183	0.389	-0.580	**0.723**	-0.155
V/Li	**0.832**	-0.240	-0.178	**0.716**	0.574	**0.834**	0.013	-0.265	**0.929**	0.129	0.169
Zn/Li	0.299	**0.863**	-0.098	-0.348	**0.829**	**0.767**	0.538	-0.165	0.554	-0.202	**0.741**

PC1 in cores B, D, E, F and G contain high loadings (>0.6) for major elements such as Ca, Fe, K, Mg and Na, with Core F also containing negative loadings for trace metals Pb and Cu. PC2 from these cores contains the majority of trace metals, such as Ni, Pb and Zn, with Cores B and F showing strong loading for major elements Fe and Mn. Cores A (furthest from the landfill) and H (closest to the landfill) show different factor loadings, with PC1 being dominated by high loadings of trace metals such as Co, Cr, Cu, Ni (and Pb in the case of A) whilst PC2 contains mainly major elements. PC3 in Core H contains only Zn whilst PC3 in Core A contains K and Na. PC3 within cores B, D and E and PC4 within core A contains exclusively Al.

Geochronological Data

^{137}Cs activity for cores B, E and H are shown in Figure 4.29.

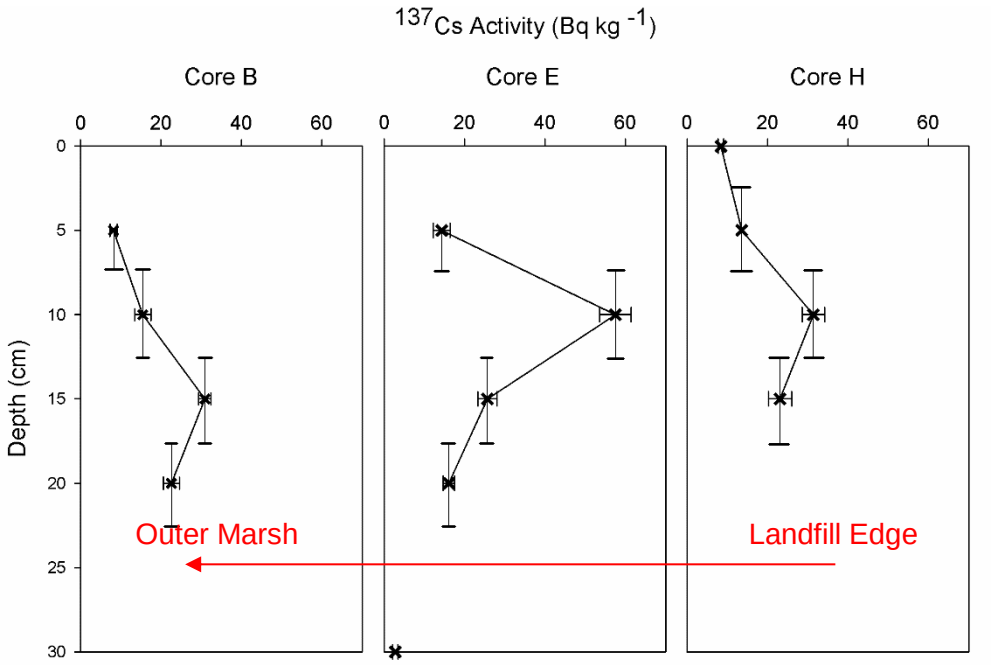

Figure 4.29: ^{137}Cs activity for sediment cores B, E and H.

All three plots show an increase in ^{137}Cs from ~ 5 cm to a peak within the top 15 cm. Core H (nearest the landfill) and Core E (in the centre of the marsh) measured a peak at 10 cm (31.4 and 57.5 Bq kg $^{-1}$ respectively). Within Core B, towards the outer marsh, the peak was at a deeper 15 cm (30.9 Bq kg $^{-1}$). In the absence of other peaks, this peak is likely to be consistent with the 1963 weapons fallout (Teasdale *et al.*, 2011), suggesting an assumed sedimentation rate of around 2 mm a $^{-1}$ (± 0.5 mm a $^{-1}$) at the site boundary and 3 mm a^{-1} (± 0.5 mm a $^{-1}$) within the outer marsh. All samples were collected on a flat salt marsh, allowing the peak depths to be directly cross-correlated. These rates are in good agreement with the 3.4 mm a $^{-1}$ sedimentation measured at Benfleet Creek, approximately 1 km further inland (van der Wal and Pye, 2004). The first appearance of ^{137}Cs was not measured due to the shallow nature of sampling. The broad nature of the peaks observed is likely due to the low resolution sampling, and as such, the data can only be applied indicatively.

Despite extremely long count times, ^{210}Pb data were mostly below detection limit, likely due to the limited supply of ^{210}Pb to the salt marsh (Cundy, 2014) and hence ^{210}Pb was not suitable for dating these sediments.

4.5. Discussion

4.5.1. Surface Metal Concentrations

In general, surface heavy metal concentrations reflect those of an active contemporary salt marsh. Copper and Pb concentrations are comparable to those found within the surface samples of the Mersey Estuary, however Zn is much lower (Harland *et al.*, 2000). Conversely, the samples from Newlands exhibit a much higher degree of contamination in comparison to lesser industrialised coasts, such as the Everglades National Park (Castro *et al.*, 2013).

In the absence of UK specific screening values (Environment Agency, 2004), concentrations were compared against NOAA marine sediment guidelines (Buchman, 2008), which provide an initial screening assessment of the potential for sediments to cause harm to native species. Table 4.20 shows that the maximum observed concentrations of Cr, Cu, Ni, Pb and Zn all exceed the threshold effect level (TEL). The TEL represents a concentration above which test sediment bioassays or benthic communities have shown to exhibit a detrimental effect as a direct result of the contaminant (Buchman, 2008). Furthermore, median concentrations for Cu, Ni and Pb exceed the threshold of concern, showing that the marsh surface exhibits a level of contamination which would fail initial risk screening. Irrespective of the source of contamination within the marsh, the data therefore suggest that concentrations exist at levels high enough to pose a concern as a threat to the health of the ecosystem.

Table 4.20: Surface sediment statistics and guideline values (Buchman, 2008).

	This Study			Sediment Guidelines		
	Median	**Min**	**Max**	**Threshold Effect**	**Probable Effect**	**Apparent Effect**
Co	16	12	21			10
Cr	38	22	59	52.3	160	62
Cu	32	15	58	19.7	108	390
Mn	248	199	356			260
Ni	33	21	49	15.9	42.8	110
Pb	48	29	118	30.2	112	400
Zn	117	68	175	124.4	271	410

4.5.2. Spatial Distribution of Surface Metals

Geochemically normalised data were used to predict spatial variability of key contaminants around the site. The spatial distribution of Cr, Pb, Fe, K and Ni is elevated in a radial pattern; to the North, East (over 100 m from the site boundary) and South of the site. Inter-elemental relationships show that these metals, with the exception of Pb are inter-related, suggesting that a proportion of the heavy metals are introduced into the system with major elements, i.e. via inundation with contaminated water during high tide, or in-wash of contaminated sediments to the surface. The enhanced levels of contamination to the north are possibly due to the sewage treatment works located with Benfleet Creek. The outfall from plants such as this have shown elevated concentrations within coastal sediments (Udayakumar *et al.*, 2014), leading to potential risks due to vegetation uptake (Sharma *et al.*, 2007).

Enhanced contaminant magnitudes to the East are likely to reflect present day water quality, as surface vegetation will reduce the amplitude of entering tides, dissipating wave energy (Möller *et al.*, 2014), depositing associated contamination. Higher levels of contamination to the south of the site were noticed within the previously mentioned elements as well as Co, Cu, Sr and Mn. This area is home to an active marina (Smallgains Marina), which in 2005 had a significant organic pollutant event (Environment Agency, 2015) and was likely to have utilised hazardous anti-fouling paints containing chemicals such as Pb and Cu (Rees *et al.*, 2014) as well as PCBs (Martin and Richards, 2010). The legacy of this contamination is likely to be reflected in the sediment record. On the whole, spatial plots do not show a decline in concentrations away from the site edge, as would be expected if the landfill was the principal source. Conversely, the majority of elements show concentrations increasing with distance from the site edge. It is unlikely, therefore that contamination is associated to the landfill.

Median LOI of 10% was within a similar range to other sites within the literature (Fitzgerald *et al.*, 2003), yet sediment pH showed variation (range of 7.18 – 8.52), reflective of diurnal inundation of saline water (Fergusson, 1990). pH is likely to fluctuate with tidal cycles (Portnoy and Valiela, 1997), however is not reflected in the data as all sampling took place at low tide.

Although surface samples show contamination at levels high enough to suggest an environmental concern, the mapped spatial distribution does not provide convincing evidence that the source of this is the landfill. The lack of extreme hotspots of contamination or an indicative concentration decline from the site edge twinned with the varied contamination inputs to the estuary (Attrill, 1995) does not allow point sources to be identified. Salt marsh surface samples are therefore inadequate for identifying any evidence

of contamination from either a landfill or contaminated leachate plume, as the spatial distribution is more likely to reflect a record of present day surface water quality (MacKenzie *et al.*, 1994).

4.5.3. Sediment Core Concentrations

It is complicated to compare sediment core concentrations to other sites, as various diagenetic processes, such as mixing or mobilisation may have redistributed metals within the sediment profile, therefore median concentrations for this study have been compared to sediment profiles from other estuaries (Table 4.21).

Table 4.21: Maximum sediment core concentrations from other industry impacted estuaries. (1) Li et al. (2000), (2) Benninger et al. (1979) (3) Veerasingam et al. (2015).

	Co	Cu	Mn	Ni	Pb	Zn
Pearl Estuary[1]	20.5	74.3		91	99	332
This Study (Thames)	26	74	1718	69	205	262
Long Island[2]		96	639		52	194
Mandovi[3]	29	58	1842		28	71

The maximum sediment core concentrations from Newlands exhibit similar concentrations to other estuarine sediments, such as the Pearl Estuary, China; an area dominated by rapid industrial expansion (Woods, 2009). The Thames sediments, however, contain much higher Pb concentrations. Lead and Zinc concentrations for the Thames are also higher than in the Mandovi, a river contaminated by ore transportation (Veerasingam *et al.*, 2015) and Long Island.

Median concentrations for the majority of cores exceed the threshold above which there is a potential for ecological harm, with the exception of Mn and Zn. This threshold is exceeded by the maximum concentrations for Co, Ni (except Core A), Pb and V. Median Hg concentration from cores F and H was 842 ng g^{-1} and 1258 ng g^{-1} respectively, both exceeding the PEL of 700 ng g^{-1} (Buchman, 2008). The PEL should however, only be used as a screening assessment; providing a rapid overview of the potential for harm. Nonetheless, the data suggest that, regardless of the contamination source, the majority of samples from within the salt marsh exhibit contamination above the TEL and PEL, and could therefore pose an environmental hazard. While of concern, this simple analysis of median concentrations does not give any indication of the contaminant source and a deeper examination of both inter-elemental relationships and the spatial distribution of contamination is needed to support such inferences.

Data from the cores generally appears to show more variability than surface concentrations. Major constituents such as Al, Fe, K, Mg and Na appear to be relatively consistent across the site, however Ca concentrations vary greatly, from 0.7 to 3 %, likely to reflect natural variation in abundances of calcitic shells and other detritus (Zwolsman *et al.*, 1993). All trace metals, with the exceptions of Co and Ni, show varying median concentrations across the site. This is likely a result of varying metal inputs to the sediments, whether atmospheric deposition (Tipping *et al.*, 2010) or surface inundation (Emmerson *et al.*, 2000). Despite this variation, none of the elements appear to show a trend along the sediment core transect, providing no evidence to suggest a source of contamination. Despite the source being unknown, it can still be concluded that metals are at similar concentrations to those found within other industrialised sediments, above a threshold of eco-toxicological concern.

4.5.4. Sediment Core Inter-Elemental Relationships

Inter-element correlations and PCA have frequently been used to provide information regarding the source and behaviour of metals in sediments (Rubio *et al.*, 2000; Yang *et al.*, 2014; Zhao *et al.*, 2014). Here, both correlations and PCA were performed on separate cores to determine whether factors controlling metal variability changed with increasing distance from the landfill. All Spearman's rank and PCA was undertaken using normalised sediment core data and Figure 4.5 may be referred back to as a reminder of the sample locations, with Core H nearest the site boundary and Core A at the distal margin.

The majority of samples from individual sediment cores exhibit significant correlations between both major and trace elements making the individual controls on variability within the site difficult to discern. Evidently, the interactions between elements of toxicological concern (e.g. Cu and Pb) with geochemical carriers, such as Al, Fe, Mn and LOI must be further examined in order to infer any controls on metal variability (Ruiz-Fernández *et al.*, 2001).

All cores, except A and B, demonstrate correlations between trace metals and Fe and Mn, suggesting that Fe/Mn oxyhydroxides are an important carrier phase for trace metals in these sediments. Their distribution may be controlled by the same diagenetic processes that control Fe and Mn (Guo *et al.*, 1997) and this is reflected in PCA scores, where Fe, Mn, Cr, Co, Na and Ni are strongly loaded in PC1 for most cores and is indicative of the influence of diagenetic processes on distribution of these elements (Table 4.19 and Figure 4.30). Metals such as Cr, Cu, Pb and Zn are strongly loaded onto PC2, suggesting an anthropogenic source. When PC1 and PC2 for Core E are plotted together (Figure 4.30), clear groupings of elements emerge. The clustering of Cu, Pb and Zn suggests a single source and behaviour, likely to be anthropogenic (Chatterjee *et al.*, 2007), whilst the clustering of Ca, K, Mg, V and Sr indicates a lithogenic source (Yang *et al.*, 2014), possibly with V and K associating with the Mg clay rich minerals. Chromium and Ni are also associated with both Fe and Mn, suggesting the distribution of the former is controlled by diagenetic behaviour (Zwolsman and van Eck, 1999).

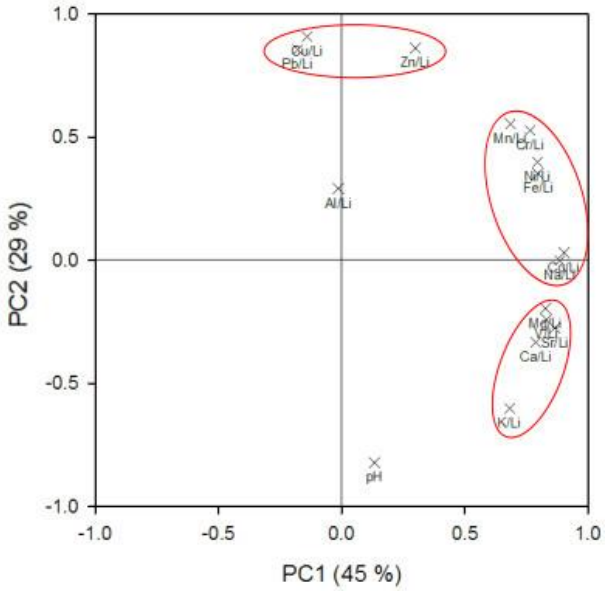

Figure 4.30: PCA loadings biplot for PC1 and PC2 from Core E.

On the whole, the distinction between trace metals and major elements is clear within both PCA and correlation tables. However, there are instances where major and trace elements show significant correlation, such as within Core D (Figure 4.31) where the strong loading of Fe and Mn may suggest trace metal remobilisation via diagenetic changes. Vanadium is also positively correlated to major elements indicating a natural source of V (Zenz, 1980).

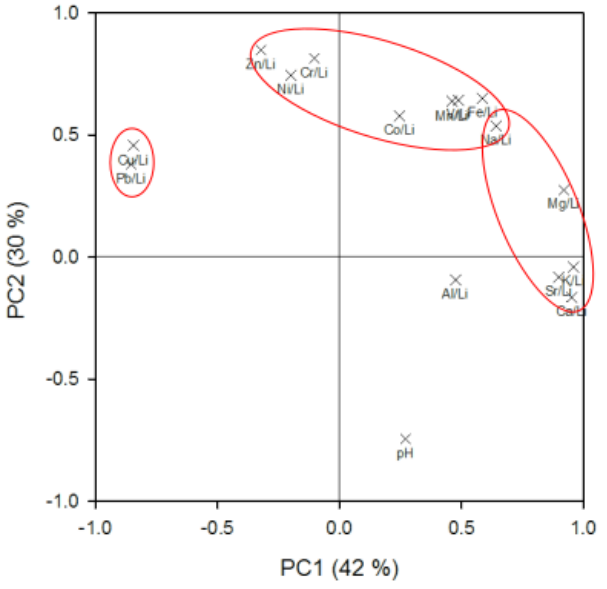

Figure 4.31: PCA loadings biplot for PC1 and PC2 from Core D.

In cores where data were available, LOI was strongly correlated with metals, such as Cu (Core B) (Figure 4.32) and Cr, Pb (Core F). Conversely, Core H shows no elements correlated to LOI, suggesting that organic matter was not a major substrate for particulate metals.

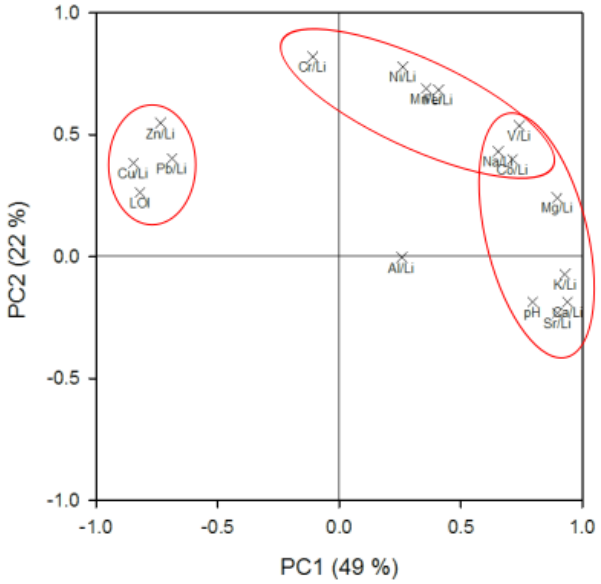

Figure 4.32: PCA loadings biplot for PC1 and PC2 from Core B.

Additionally, Al appears as a separate PC within each sediment core, and is not correlated to any other element. This may suggest the influence of grain size, and specifically the clay fraction. As all data have been normalised to take into account grain size, it is likely that no other elements will show correlations to a terrigenous indicator elements, such as Al (Ruiz-Fernández *et al.*, 2001).

Within Core H, closest to the landfill, PC1 is indicative of anthropogenic input whilst PC2 reflects natural inputs to the system (such as Ca and Na). However, PC3 contained strong loadings for Cu, Pb and Zn, separated from the other trace metals extracted within PC1 (Figure 4.33). This is possibly due to landfill plume contamination, and will be discussed further in Section 4.5.5.

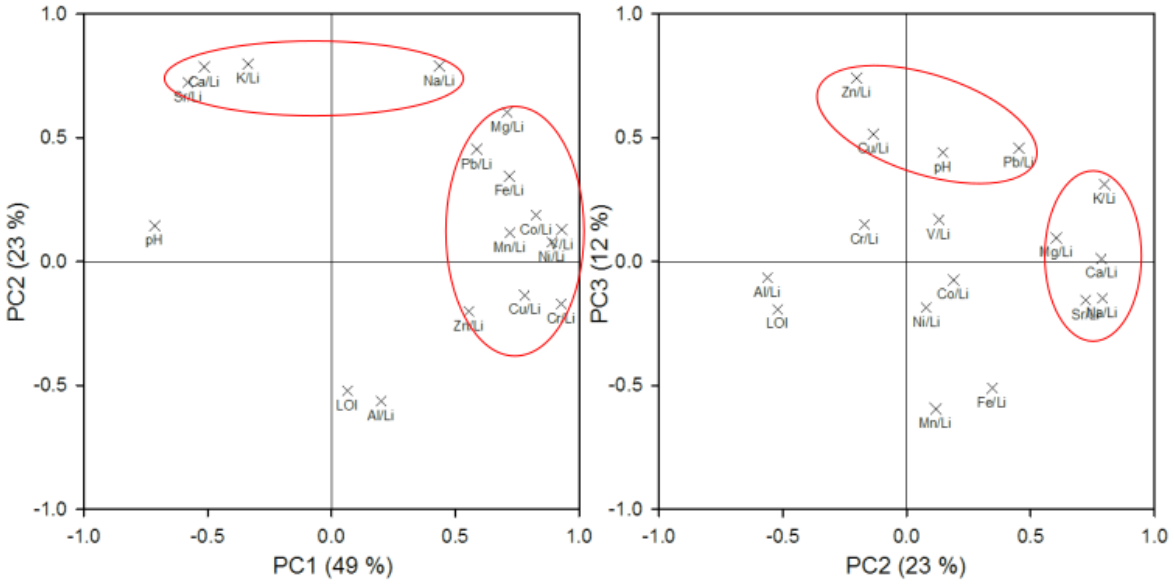

Figure 4.33: PCA loadings biplot for PC1:PC2 and PC2:PC3 from Core H.

The data show clear correlations between the majority of trace and major elements for the majority of cores. There are some associations between trace metals and redox elements (Fe and Mn), suggesting an alternative control. Overall it can be assumed that the majority of cores exhibit clear terrigenous and anthropogenic inputs. The separate association with Zn, Pb (and Cu to an extent) within Core H will be discussed in Section 4.5.5.

4.5.5. Spatial Trends within Sediment Cores across the Salt marsh

The vertical distribution of metal concentration in dated sediments can also be used to help explain the source and behaviour of contamination (Audry *et al.*, 2004; Spencer *et al.*, 2008; Parsons *et al.*, 2014). The inability to collect ^{210}Pb was likely a result of a lack of input to the salt marsh (Cundy, 2014). Nevertheless, the vertical profile of ^{137}Cs obtained allows reliable inferences about average sedimentation rates of the salt marsh. These data suggest indicative sedimentation rates of approximately 2 mm a $^{-1}$ (± 0.5 mm a $^{-1}$) at the site boundary, increasing to 3 mm a $^{-1}$ (± 0.5 mm a $^{-1}$) within the outer marsh, shown within Figure 4.34. Moreover, the vertical profiles reveal reasonably well defined peaks, however the lack of a distinct peak, such as those found within Russian (Jones *et al.*, 2015) or US (Baskaran *et al.*, 2014) sediments, may be indicative of post depositional vertical migration of ^{137}Cs (Ward *et al.*, 2014). Unfortunately, the lack of corroborating ^{210}Pb measurements implies that such inferences must be treated tentatively.

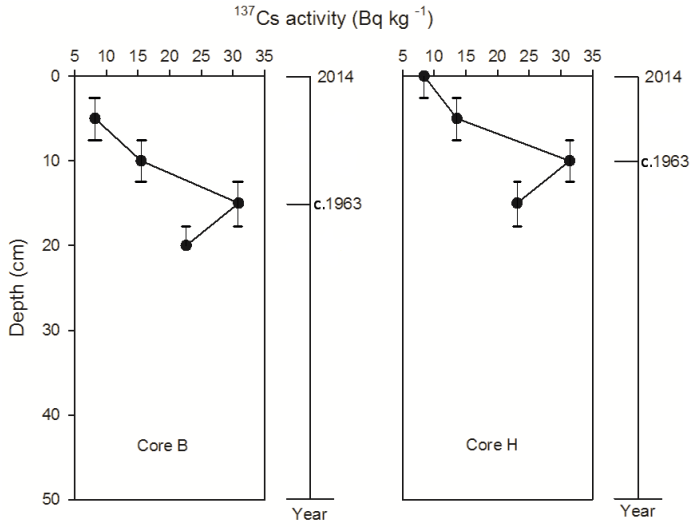

Figure 4.34: Salt marsh chronology, inferred from ^{137}Cs dating.

Heavy metal enrichment values (EF) were used to measure elevations in metal concentrations above the natural geochemical background (Equation 4.2). Many previous studies have utilised the standard shale concentrations to calculate enrichment (Çevik *et al.*, 2009; Kaushik *et al.*, 2009), however using a local reference element, such as local, low variability trace concentrations will be more representative of local enrichment (Loska *et al.*, 2004). EF was therefore calculated using the average concentration of the lowest 1 m of Core B, a 4 m core, showing consistent low concentrations at depth.

$$EF = \frac{\left(\frac{M_{sample}}{R_{sample}}\right)}{\left(\frac{M_{average}}{R_{average}}\right)}$$

Equation 4.2: Calculation of Enrichment Factor.

where M_{sample} is the concentration of the examined metal, R_{sample} was the concentration of the normalising metal in the sample, $M_{average}$ is the average concentration of the examined metal over the lowest 1 m of sediment within Core B (assumed local background concentration) and $R_{average}$ is the average concentration of the reference element over the lowest 1 m of sediment within Core B (Çevik *et al.*, 2009). The complete Enrichment Value dataset is shown in Appendix 7. The data show erroneous spikes within the core profiles, however, this is due to the inclusion of LoD/2 values where data were unavailable.

Major Elements (Al, Ca, Fe, K, Mg Na)

Al and Mg remain consistent with depth across all cores. This is likely to represent an association with the alumino-silicates and therefore show a clear association with the uniform mineralogy of the salt marsh (Zwolsman *et al.*, 1993). Observing the spatial distribution of Fe (and to a degree Mn) allows conclusions to be drawn about the redox conditions within the core. The diagenetic changes of Fe (and Mn) occur within sediments as a result of their redox sensitivity (Dong *et al.*, 2014). The main control on the distribution of Fe and Mn is their reduction, as a result of burial or flooding (Adriano, 2001). The Carbon content decrease shown in all sediment cores (Figure 4.21) reflects microbial activity. This utilises the available oxygen, subsequently reducing Fe^{3+} (to Fe^{2+}) and Mn^{4+} (to Mn^{2+}), increasing their solubility, resulting in mass movement or diffusion into more oxic sediments, where they are re-precipitated (Burdige, 1993). Therefore, the Fe enhancements shown in the subsurface of cores D, E, F and G are likely to be a result of diagenetic remobilisation. The enhancements of Mn within cores A, D, E and G occur at more shallow depths due to the preferential utilisation of Mn over Fe as an electron acceptor (Kalnejais *et al.*, 2015). These elevations are expected, as the secondary precipitations are reported widely in the literature (Canfield *et al.*, 1993; Thamdrup *et al.*, 1994; Müller *et al.*, 2002). Within cores D, E, F and G, both Fe and Mn increase in concentration at depths over 100 cm, which may be due to either local groundwater seepage or an historical benthic release of Mn^{2+} (Thamdrup, 2000).

Calcium shows a rapid decline from the high concentrations in the surface sediments, which may be due to the decalcification within oxic sediments as a result of the lowering of pH from organic matter breakdown (Spencer *et al.*, 2003). Ca distribution then shows a re-precipitation at depth, a process which is likely to be caused by secondary carbonate

mineral formation, following the increased alkalinity caused by sulphate reduction (Cundy *et al.*, 2003). This is supported by pH data; as lowest values were found nearer the surface. The magnitude of elevation is in keeping with previous work (Zwolsman *et al.*, 1993), however, re-precipitated concentrations are an order of magnitude higher, up to 30x larger than the surface value. The reason for this is unknown, as the low permeability of the approximately 100 m thick London Clay will separate the marsh sediments from the chalk aquifer beneath. There is also no evidence of calcitic deposits within local borehole logs (British Geological Survey, 1974). Sr distributions are similar to Ca, which is due to the similar chemical behaviour of the metals, as Sr is easily incorporated into the calcium carbonate fraction (Salomons, 1975; Robinson, 1980).

The distribution of Na and K differs across the cores. It is likely that surface enhancements in Na are a result of daily inundation of seawater into the environment (Kadiri *et al.*, 2011) as reflected in cores A, B, D, E and G. It is likely that these levels are stable in the short term, however seasonal variations were not measured as fieldwork was undertaken during one season at low tide.

The overview of the spatial trends of major elements show that distributions are in keeping with previous work (Finney and Huh, 1989; Fox *et al.*, 1999; Cundy *et al.*, 2003; Spencer *et al.*, 2003). The geochronological dating indicated that the sediments may have been subject to limited, yet not significant reworking, with the only major re-distribution process in the sediment column being associated with chemical diagenesis as a result of either redox controls (Fe and Mn), chemical changes (Ca and Sr), or daily influx of seawater (Na).

Trace Metals (Co, Cr, Cu, Hg, Ni, Pb, V, Zn)

The vertical concentration profile of Co and V is constant with depth within all cores, apart from a systematic enrichment at the base of core G, likely to be a relic of the normalisation process. Enrichment plots (Abrahim and Parker, 2008) (Figure 4.35) show little enrichment of Co, Ga or V within sediments, suggesting no significant enrichment from anthropogenic sources. This is in fitting with other research within the Thames, which has found Co and V to be found below levels of environmental concern (Attrill, 1995; O'Reilly Wiese *et al.*, 1997a; Pope and Langston, 2011).

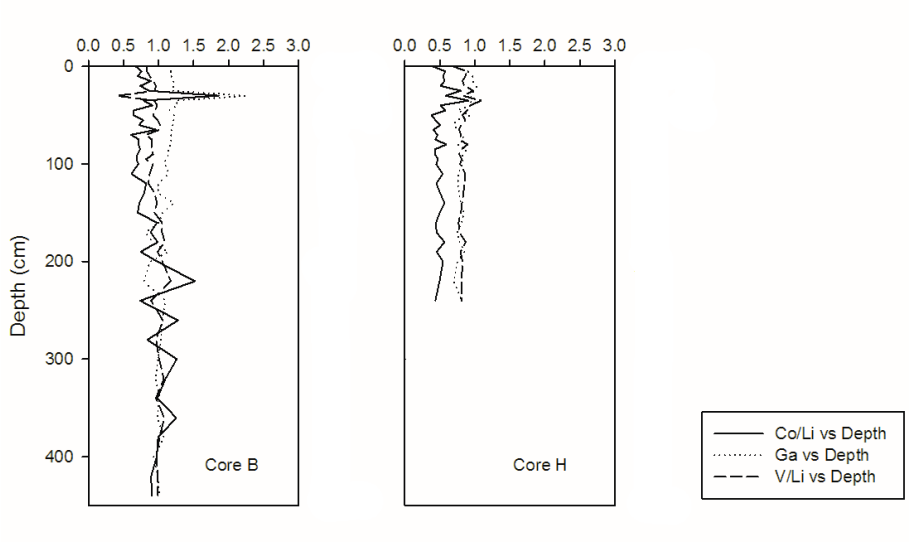

Figure 4.35: Enrichment Factors for Co, Ga and V.

Chromium, Cu and Ni exhibit similar down-core trends. Cores B, D, E, F, G and H all show enrichment approximately 20 cm below the surface. Salt marsh sediment cores have been extensively used to reconstruct historical contamination trends (Fletcher *et al.*, 1994; Fox *et al.*, 1999; Plater *et al.*, 1999; ElBishlawi *et al.*, 2013). Using the estimated sediment accumulation rate of c. 2 mm a^{-1}, this peak corresponds to the height of industrial revolution within the UK (late 1800's) and the decline at shallower depths represents the onset of discharge and emission regulations (Valette-Silver, 1993). Below this peak metal EFs are c.1 suggesting that these deep sediments which pre-date the onset of industrial activity within the UK are not influenced by anthropogenic inputs (Figure 4.36).

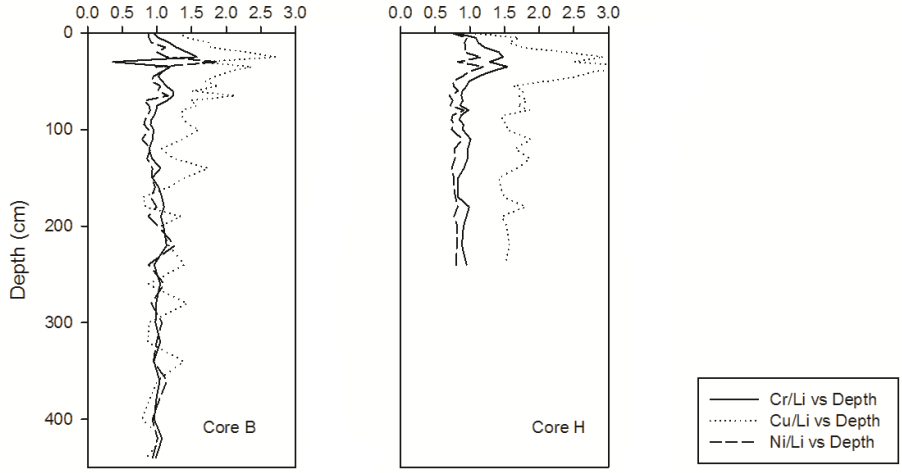

Figure 4.36: Enrichment Factors for Cr, Cu and Ni.

Vertical distributions of Pb and Zn appear to show the most information regarding landfill pollution within the salt marsh. Core A shows the same surface enrichment as with other elements, further suggesting that there has been a post-depositional change in the sediments. Zn concentrations throughout the remainder of the cores show the typical sub-surface peak (around 30 - 50 cm), with Cores B-G showing a reduction (to an enrichment value of around 1) at depths below this. A similar vertical distribution is also shown with Pb, however the signal shows a much higher sensitivity to small scale changes due to the much higher affinity of the Pb cations to bind to organic matter and fine grained material (Ackermann *et al.*, 1983). Core H, collected adjacent to the landfill, shows a distribution unlike the other cores. Both Pb and Zn demonstrate a peak at around 40-50 cm, corresponding to industrial contamination from the 19th Century (Rothwell *et al.*, 2007). However, Pb, and to a lesser extent, Zn, do not return to geochemical background levels at depth in the sediment core. Rather, even at a depth of 2.3 m, enrichment values for Pb and Zn are 2 and 1.7 respectively, indicating anthropogenic inputs of these metals (Figure 4.37). These values do not seem exceptionally high, in comparison to values of 10-15, which are commonplace within industry impacted sediments (Abrahim and Parker, 2008; Karageorgis *et al.*, 2009). This trend is also present within Hg data, in which Core H shows a subsurface elevation and which is sustained to the base of the core. These values are reflected within PCA loadings, which show Zn, and to a lesser extent, Pb and Cu, within a separate component (Table 4.19).

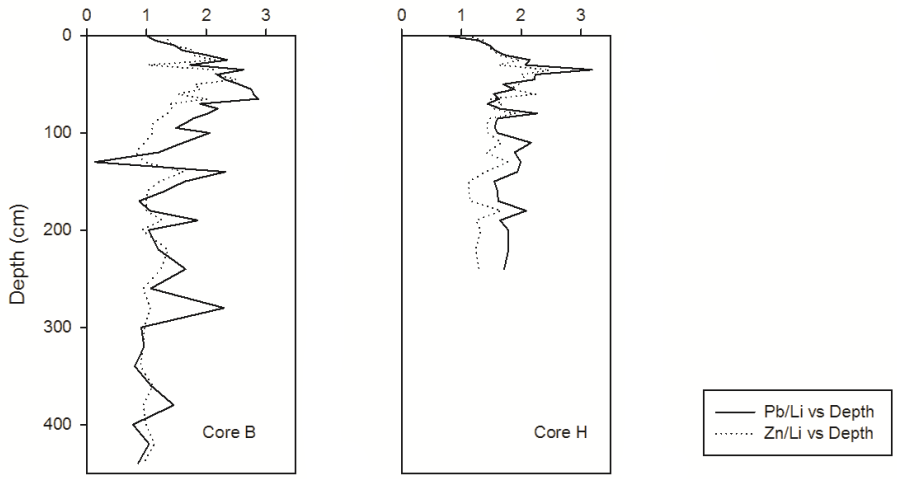

Figure 4.37: Enrichment Factors for Pb and Zn.

Assuming a linear sedimentation rate of c. 2 mm within core H, sediments below 50 cm were deposited at the beginning of the 19th Century, representing the onset of industrialisation in the UK (Rothwell *et al.*, 2007). Therefore, EFs > 1, which are indicative of concentrations elevated above natural anthropogenic background are unlikely to represent water/sediment quality in the estuary or atmospheric inputs at the time of deposition. Any contamination that occurs at depths greater than the onset of industrialisation must have been introduced to the environment at a later date and via a different pathway, such as the influx of contaminated leachate. Since the distribution of elements in all other cores show a typical decrease to a background level at depth, this infers that Core H, adjacent to the landfill must be subject to an additional source of pollution.

It is likely that Newlands landfills is currently undergoing methanogenic degradation as the age of the landfill (Williams, 2005), twinned with lack of contaminants within present day leachate samples (Caulmert Limited, 2011b). This would mean that any contamination that has been released from the waste was in a discrete pulse, as a function of the pH drop due to the production of acetic acid. It is likely that the Hg, Pb and Zn elevations shown at the base of core H reflect an area that was once a leachate attenuation zone, designed to attenuate and decrease concentrations of contaminants within leachates (Bjerg *et al.*, 2011). This distribution has been observed elsewhere, associated with groundwater pollution plumes within the immediate vicinity of an inland landfill (Bhalla *et al.*, 2011). It can therefore be concluded that metals flushed from the landfill under acidic conditions were carried within the sites leachates. This was due to the high affinity and stability of lead within the environment (Bai *et al.*, 2011b), combined with the buffering effect due to the rapid rise in pH as the sediments leave the site. Contaminants would therefore immediately sorb to sediments, giving rise to a proximal pattern of contamination that only spreads

approximately 20 m from the boundary of the landfill, in keeping with results from Bhalla *et al.* (2011). These patterns are therefore consistent with the conceptual site model presented earlier in Figure 4.2.

Although Pb and Zn concentrations surrounding the landfill are not severe compared to other areas of contaminated sediment (Grant and Middleton, 1990), there is potential for the mass present to act as a source to the surrounding environment. The fronting area of the site is approximately 1000 m, with a contamination present from approximately 1 to 2 m depth. Using an average bulk density of 0.54 g cm^{-3}, and average Cu, Pb and Zn concentrations of 32, 80 and 110 mg kg^{-1} respectively, the estimated contamination masses (Chen *et al.*, 2006) surrounding Newlands are 480 kg of Cu, 1200 kg of Pb and 1650 kg of Zn. Considering that the salt marsh is situated within the Environment Agencies flood alert area and is not currently undergoing any flood management, the consequences of erosion and redistribution of this 3330 kg of contamination should be considered within future flood/erosion planning.

4.6. Conclusion and Implications

Sediment analysis has shown contamination within surface samples at concentrations sufficient to cause ecological concern. Within estuarine sediments such as those at Newlands, it is common for the surface materials to reflect the current water quality (Spencer *et al.*, 2003), so that the presence of elevated levels of contamination is likely to indicate processes currently impacting the sediments. There is, however, no evidence that the source of this contamination is the historical landfill, as the spatial distribution of contamination revealed no trend associated with the landfill boundary, as would be expected from a point pollution source (Bhalla *et al.*, 2011). This surface contamination must, nonetheless, be treated with caution, as the site is environmentally significant as a nesting area for wildfowl and wading birds (Caulmert Limited, 2012).

The concentration record obtained from the sediment cores reveals a different pathway of contamination. The major elements and majority of the trace metals show a typical vertical profile, whether controlled by redox, chemical association, seawater influx or industrial contamination. There are, however, concentrations that must also be treated with care as they are above the TEL for environmental concern. These patterns suggest that the majority of contamination within the subsurface is not sourced from the landfill. However, the impacts of industrialisation have resulted in a large mass of sediment contamination which could itself, present an environmental risk under either physical or chemical alterations predicted under climate change, such as a mass erosion event from an increase in wave energy (Solomon *et al.*, 2007).

There is however a signal within the sediments proximal to the landfill that suggests an alternative pathway of contamination that may be attributed to rapidly attenuated leachate. Sediment Core H exhibited a contamination distribution which could not be explained by other processes, with elevated concentrations of Hg, Pb and Zn at depth. This suggests that the base of Core H represents an historical attenuation zone, through which leachates percolated, in order to reduce their contamination load. Core H was extracted at a distance of approximately 15-20 m from the site boundary. Assuming that the leachate attenuation zone is ubiquitous around the perimeter of a landfill, there exists the potential for a large yet contained, mass of contaminated sediments to be present within the coastal zone immediately adjacent to similar landfill sites, the redistribution of which may have an impact on biological life, the water environment, vegetation and human health.

Salt marshes, such as the one at Newlands, are home to a diverse range of species. Their protected, sheltered nature provides breeding grounds for fish and birds, whilst providing dense amounts of vegetation for both macro and micro faunal feeding (Gribsholt and

Kristensen, 2002). The release of metals into this ecosystem could potentially result in detrimental effects to local species, many of which are protected, through vegetation uptake (Windham *et al.*, 2003), which may hinder seedling germination (Williams, 1993), or mobilise contaminants to feeding birds. These contaminated sediments contain root matter, through which metals can be taken up into the plant and translocate to the shoots (Peng *et al.*, 2006), sometimes in greater concentrations than in surrounding sediment (Sauerbeck, 1991). This uptake could have deleterious effects on the local wildfowl and wading birds (Caulmert Limited, 2012), which graze on the vegetation, potentially leading to bioaccumulation (Chandra Sekhar *et al.*, 2004). This has previously been observed, with harvested plants situated on historic landfills exhibiting concentrations high enough to have a detrimental impact on grazing animals in a situation where soil is ingested through feeding (Green *et al.*, 2014).

Eroding sediments from a coastal landfill could release contaminants straight into drinking water, or areas used for the production of food. The main reason is the impact that landfills have on local groundwater (Kiddee *et al.*, 2013). Within unlined sites, leachates immediately percolate, directly impacting the chemistry of the adjacent groundwater (Christensen *et al.*, 2001). An example from the River Huaile, (the most populated in China) (Han *et al.*, 2014) shows that unlined landfills exhibit a major threat to groundwater quality, rendering it unsuitable for humans or agricultural use.

The magnitude, extent and consequences of contamination from Newlands has been addressed, however, this chapter has focused only on one site and in order to gain a more robust understanding of contaminant behaviour from historical landfills, further research is required to place this result into a regional context.

Chapter 5 Assessing the use of XRF for the *In-Situ* Determination of Contamination in Coastal Sediments

Abstract

Common laboratory geochemical analysis (such as ICP-OES) is capable of generating highly accurate data, yet it is extremely resource intensive. Within recent years, XRF has emerged as an effective non-destructive analytical technique for rapid analysis of metals in environmental media. However, one of the main limitations of *in-situ* XRF analysis is the reduction in accuracy as a result of sample moisture, an influence which has been overlooked in previous work. This chapter investigated whether XRF could be used *in-situ* to generate accurate and precise data within coastal sediments.

Certified Reference Materials were sequentially wetted and scanned with a Niton XL3t XRF, and were subsequently corrected for moisture content using an existing method. Additionally, 90 samples were measured *in-situ*, moisture corrected and compared to data from ICP-OES, using linear regression. Experiments were also carried out to ascertain whether moisture content could be measured *in-situ*, with the aim to omit laboratory moisture measurement.

Sample moisture exhibited a linear, deterministic effect on As, Cu, Fe, Pb, Sr and Zn, with moisture corrections accurate to within 20 %, increasing the number of elements that can be effectively measured by the correction method. XRF was also comparable to ICP for Fe, Pb, Sr and Zn, but underestimated concentrations of Cu and Mn. *In-situ* measurement of moisture content was not possible within the marsh sediments due to varying environmental conditions.

XRF was therefore considered suitable as a rapid screening tool for Fe, Pb, Sr and Zn. Despite sample moisture requiring laboratory measurement, the time and cost of generating quantitative data was greatly reduced.

5.1. Introduction

Landfill site managers and consultants have a duty of care to ensure compliance with legislation such as the Water Framework (2000/60/EC) and Waste Directives (2008/98/EC) in respect to contaminated land hazards. Chapter 4 highlighted the environmental hazard of an historical landfill to adjacent coastal sediments, emphasising the need to investigate contamination on a wider UK scale, and help understand the potential for environmental harm from historical landfills within the coastal zone. In recent years, consultancies and stake holders have shifted towards qualitative risk assessments (QLRA), which adopt broad scale, tiered approaches in order to identify contaminated sites through hazard quotients, prioritising them for individual site assessment (Figure 5.1) (Weeks and Comber, 2005). The advantage of such qualitative assessments is that sites can be rapidly classified as showing 'no risk', allowing them to be omitted from further assessment, saving time and money. Sites classified as presenting a risk are then advanced through the assessment, with increased data requirements, resulting in a more intensive, yet more relevant exercise (Energy Institute, 2013).

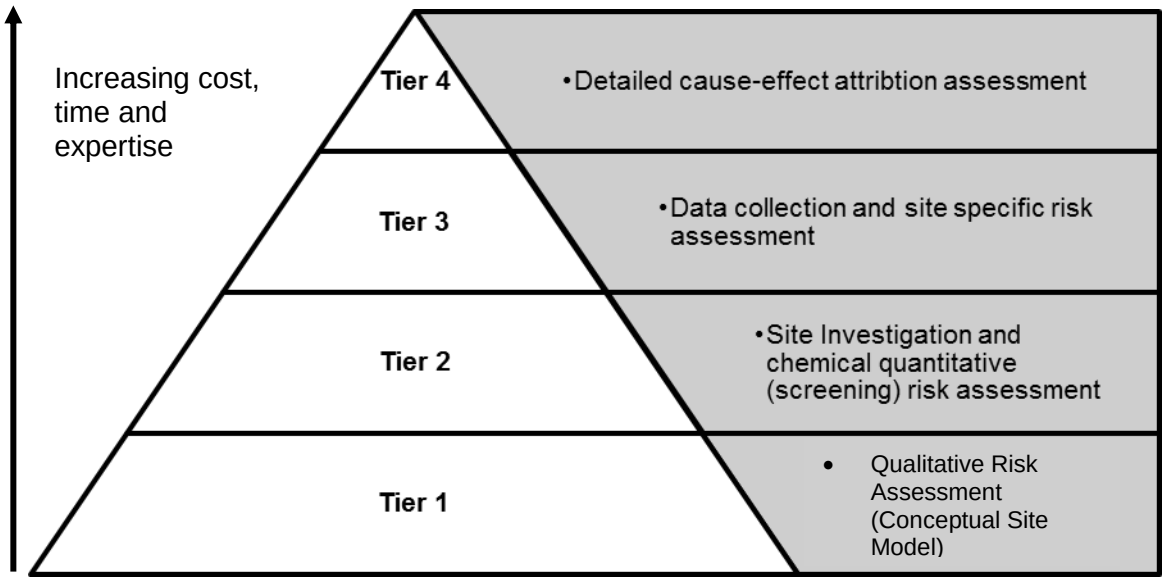

Figure 5.1: Tiered risk assessment methodology. From The Energy Institute (2013).

Quantifying sediment contamination requires detailed field campaigns with sample collection and extensive laboratory preparation (drying, grinding, sieving and acid digestion (e.g. Chen and Ma (2001)) followed by analytical quantification typically using either ICP-OES (Remon *et al.*, 2005), ICP-MS (Whiteley and Pearce, 2003), or AAS (Rothwell *et al.*, 2007). These geochemical techniques have significant benefits, with detection limits down to parts per trillion (ppt) and high measurement precision (Perkin Elmer, 2011), however they are costly, may be limited by reagent strength (Weindorf *et al.*, 2013) and require

significant, intensive laboratory time and resources (Carr *et al.*, 2008). Matrix effects are also prominent with geochemical techniques such as ICP-OES, particularly in saline coastal sediments, dominated by easily ionisable elements (Morishige, 2008), adding extra troubleshooting time to analysis (Olesik, 1991). These time consuming methods introduce a bottleneck into QLRA's, as large amounts of planning and resources are required to collect robust empirical data (Hu *et al.*, 2014). There is therefore scope for a more immediate, rapid method for quantifying contamination in coastal sites.

Portable X-ray Fluorescence (XRF) is an emerging non-destructive technique used in environmental settings for the rapid assessment of metals (Chenhall *et al.*, 1992; Stallard *et al.*, 1995; Mortimer and Rae, 2000; Zhu *et al.*, 2011; Rodríguez-Germade *et al.*, 2014). It operates based on the photoelectric effect, where atoms fluoresce at different energies once excited by absorbed X-rays generated by an X-ray tube. Radiation is emitted from an analyser and is absorbed by the test sample, dislodging an electron and creating a vacancy within the innermost shell of an atom, which is immediately filled by an electron from an outer shell. This cascading of higher energy, outer shell electrons creates an energy surplus which is subsequently emitted, known as X-ray fluorescence (US-EPA, 2007). The fluorescence emission spectrum consists of a multitude of electron shell peaks, occurring at wavelengths characteristic of each element. Concentration can therefore be calculated from the intensity of specific X-rays (Kalnicky and Singhvi, 2001).

Previous work has shown XRF as an accurate method for the determination of metals within a range of media, such as contaminated soils (Hürkamp, 2009; Towett *et al.*, 2013; Hu *et al.*, 2014), sediments (Weltje and Tjallingii, 2008; Hennekam and de Lange, 2012), rocks (Potts *et al.*, 1995; Revenko, 2002) and cultural artefacts (Ferretti, 2014; Hinds *et al.*, 2014). Analysis is commonly undertaken in a laboratory on prepared, pressed sample pellets (Cook *et al.*, 1997) in order to achieve the same levels of analytical accuracy as conventional geochemical analysis using ICP OES and ICP MS (Radu and Diamond, 2009; Peinado *et al.*, 2010), reducing the benefit of rapid assessment. The overall lack of *in-situ* applications is due to the high degree of uncertainty that arises from the analysis of wet sediment, as sample moisture scatters fluorescent X-rays (Ge *et al.*, 2005), lowering the X-ray intensity compared to dried samples, resulting in under-estimation of elemental concentration and hence poor analytical accuracy when compared to certified reference materials (Tjallingii *et al.*, 2007). The degree to which moisture content reduces accuracy has been previously underestimated (Parsons *et al.*, 2013) with some studies omitting data correction (Bernick *et al.*, 1995; Kirtay *et al.*, 1998; Carr *et al.*, 2008; Liu *et al.*, 2013; Weindorf *et al.*, 2013). Moisture content corrections have, however, been proposed in the literature, though they have been limited to either single elements, such as Pb (Shuttleworth

et al., 2014), a narrow (0 - 20%) range of sample moisture contents (Ge *et al.*, 2005), or have required complex detection of scattered X-rays (Kido *et al.*, 2006; Bastos, 2012).

This chapter focuses on the application of portable XRF for the *in-situ* determination of a suite of metals within coastal sediments as a rapid screening tool. These sediments are characterised by high and variable moisture contents (e.g. (Kadiri *et al.*, 2011)) which are likely to vary over both short-term temporal and small spatial scales as a result of both tidal cycles (Silvestri *et al.*, 2005) and limited horizontal pore water fluxes (Nuttle, 1988). There is a linear, proportional relationship between X-ray attenuation and moisture content (Ge *et al.*, 2005) and therefore a correction should be possible for all metals, providing X-ray scattering does not prevent accurate analysis (Ge *et al.*, 2005) and sample moisture can be measured in the field. Therefore, an investigation is required to demonstrate the accuracy of an *in-situ* correction that takes into account the potentially large range in moisture contents of coastal sediment and is applicable for a wide range of elements.

In-situ analysis therefore depends on the ability to accurately measure sample moisture. Gravimetric determination of moisture content is well established (ISO Standard, 1993), using oven drying methods to measure mass losses (Suchkova *et al.*, 2010). This method provides limited advantages to the speed of analysis as samples still need to be returned to the laboratory. Conversely, volumetric moisture content measurements via Time Domain Reflectometry or Theta Probe measurements produce data rapidly, requiring little calibration (Noborio, 2001). These volumetric methods, such as theta probe analysis, have limitations, as signals can be easily attenuated within brackish or saline coastal sediments due to ionic conductivity (Miller, 1999), particle texture, temperature and density (Kargas and Kerkides, 2008). Therefore, there is a requirement to establish whether these rapid methods are 'good enough' to use alongside XRF, as the application of an *in-situ* correction for moisture content would provide site users with immediate access to data, maximising analytical coverage (Kalnicky and Singhvi, 2001), providing field scale elemental analysis (Parsons *et al.*, 2013), with minimal redundant sampling and analysis time.

The main research aim of this chapter is to assess whether *in-situ* XRF can be used to generate rapid, accurate and precise sediment contamination data within coastal sediments suitable for onsite investigations commonly undertaken within QRLAs. This will be achieved by addressing the following research objectives:

Research Objective 1: To examine the influence of moisture content on X-ray suppression and determine a moisture correction factor that can be applied to field wet *in-situ* sediment samples.

Research Objective 2*:* To undertake and examine the accuracy of *in-situ* sample moisture measurements.

Research Objective 3*:* To determine whether moisture corrected *in-situ* XRF analysis provides analytically accurate data for a range of metals, in comparison to *ex-situ* ICP-OES analysis.

5.2. Methodology

5.2.1. Influence of Sample Moisture on X-Ray Suppression

Samples were analysed by XRF using a Niton XL3t analyser theoretically capable of detecting elements from Cl to U (Thermo Scientific, 2011). To assess initially which metals could be accurately and precisely detected by the XRF unit, 3 x 1 g dried and ground Certified Reference Materials (CRM's) (TILL4, PACS2 and LOAM7004) were placed into a 0.5 cm diameter disc and analysed in replicate (n = 5) using the soil Standard Operating Procedure (SOP) and an analysis time of 60 seconds. This small mass was used as the majority of XRF fluorescence signal is contained within the first few µm of sample (Ferretti, 2014). Due to the prevalence of non-normally distributed data within environmental datasets (Chapter 4), median concentrations were used to measure recovery as a measurement of analytical accuracy (Equation 5.1), with precision calculated using percentage Relative Standard Deviation (RSD%). This operational procedure was used for all XRF analyses.

Equation 5.1: Calculation of elemental recovery (R %), where O_c is the observed concentration (mg kg $^{-1}$) and C_c is the certified concentration (mg kg $^{-1}$).

$$\mathrm{R\%} = \left(\frac{\mathrm{O_c}}{\mathrm{C_c}}\right) \mathrm{x}\ 100$$

PACS2 (marine sediment from Esquimalt Harbour, British Columbia, Canada) was then used to examine the effect of moisture content on X-ray suppression. The wide range of moisture contents used reflects the high variability of moisture in coastal sediments. Incremental measures of de-ionised water were added to dry sediment samples prior to analysis to achieve the following representative dry weight moisture contents (Windham *et al.*, 2001; Crooks *et al.*, 2002); 0, 10, 15, 20, 25, 30, 40, 50, 60, 65, 70, 80 and 90 %DW.

The measured metal concentration at each moisture level was then plotted and correlations visually observed. An existing moisture correction (Equation 5.2) previously used to correct Pb measurements within peatlands was applied to all elements (Shuttleworth *et al,* 2014).

Equation 5.2: Moisture correction equation, where C_c and C_f are corrected and non-corrected concentrations, respectively, m_w is wet sample mass and m_d is dry sample mass. From Shuttleworth et al. (2014).

$$\mathrm{C_c} = \frac{\mathrm{C_f} \,.\, \mathrm{m_w}}{\mathrm{m_d}}$$

After correction for moisture, recovery values (Equation 5.1) were calculated to determine whether accurate data could be produced using XRF on samples with varying moisture. This comparison was undertaken on all metals that showed accurate recovery within dry sediments (0% moisture) (Section 5.3.1).

5.2.2. Measuring Field Sample Moisture

To examine the accuracy of *in-situ* sample moisture measurements and in particular, to determine whether field methods could be used to predict accurate laboratory methods (O'Kelly, 2004), theta probe conductivity sample moisture (Volumetric) was compared to oven drying moisture (Gravimetric). Volumetric moisture content is defined as the ratio of water volume in a sample to the total volume of the sample (Equation 5.3) whilst gravimetric moisture content is calculated by the wet mass divided by the dry mass of sample (Equation 5.4).

Equation 5.3: Calculation of Volumetric moisture content Θ_v, where V_w is volume of sample water and V_s is total sample volume.

$$\Theta_v = \frac{V_w}{V_s}$$

Equation 5.4: Calculation of gravimetric moisture content Θ_g, where M_w is wet mass of sample and M_s is dry mass.

$$\Theta_g = \frac{M_w}{M_s}$$

In order to directly compare volumetric and gravimetric measurements, representative literature bulk density values for similar salt marsh sediments (Tempest *et al.*, 2014) were used to convert volumetric data (Equation 5.5). Volumetric moisture content (Θ_v) was measured within 115 samples *in-situ* (Section 5.2.3) using a Delta instruments ML2 Theta Probe. Immediately after field measurement, samples were returned to the laboratory, where gravimetric moisture content (Jensen *et al.*, 2015) was measured by placing a sample of known mass in an oven at 105°C for 24 hours, after Suchkova *et al.* (2010). The correlation between gravimetric sample moisture (Θ_g) and Θ_v was analysed, and the accuracy/feasibility of field measurements was determined from the strength of the relationship.

Equation 5.5: Converting Θ_v to Θ_g, where ρ_w is bulk density of water (=1 at 20 ^oC) and ρ_s is sample bulk density.

$$\Theta_g = \Theta_v \times \left(\frac{\rho_w}{\rho_s}\right)$$

5.2.3. Comparison of metal data from in-situ XRF and ex-situ ICP analysis

To compare *in-situ* and *ex-situ* data, two 2 m sediment cores were extracted within 0.5 m of each other from Newlands salt marsh within the Thames Estuary, UK (Figure 5.2). One core was analysed *in-situ* at 5 cm increments, using XRF (Niton XL3t, Soil SOP, analysis 60 seconds). Samples were returned to the laboratory where moisture content was calculated via oven drying (see Section 5.4.3 for justification). The moisture correction factor (Equation 5.2) was subsequently applied to generate moisture corrected *in-situ* XRF data.

The other core was returned to the laboratory, sliced at 5 cm increments, freeze dried and ground. These samples were then digested using Aqua Regia (HNO_3:3HCl) on a hotplate for 4 hours with subsequent ICP-OES analysis (Chen and Ma, 2001). Analytical accuracy was assessed via CRM (LGC6137) analysis (average recovery ~90 %) and triplicate samples ensured analytical precision (% RSD).

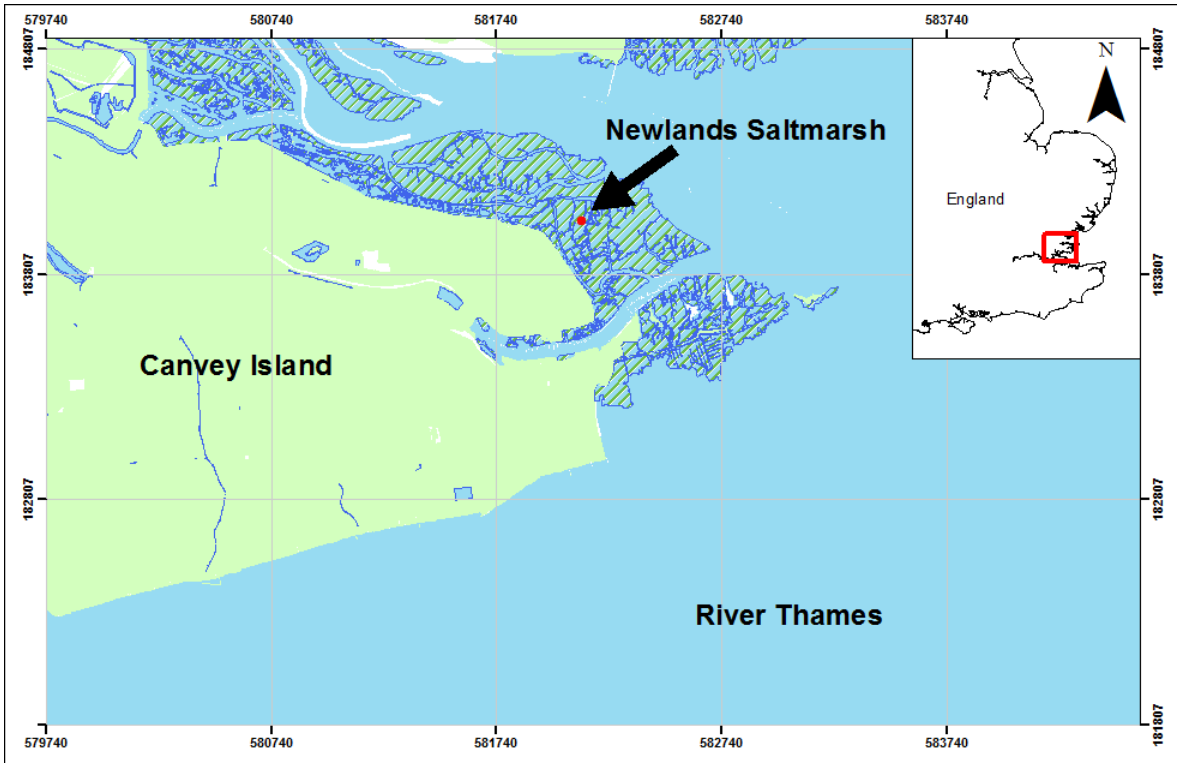

Figure 5.2: Location of Newlands Salt marsh within the Thames Estuary.

In order to compare the relationship between the datasets, moisture corrected *in-situ* data generated by XRF were compared to data from *ex-situ* ICP analysis by using a method derived from Kilbride *et al.* (2006), looking at model attributes from linear regression analysis (Figure 5.3). The data were logged prior to analysis, in order to satisfy the assumption of normally distributed residuals for linear regression analysis (Shuttleworth *et al.*, 2014). Normality was confirmed using the Kolmogorov-Smirnov test and any remaining non-normal residuals were then transformed, and analysis repeated. R^2 values for the

relationship were analysed and placed into categories of either ≥ 0.85, ≥ 0.7 or ≤ 0.7. If the R^2 was ≤ 0.7 then the relationship was weak and *in-situ* measurements could only be considered to generate qualitative estimations of data.

The next step of interpretation was to observe the RSD values to determine the precision of *in-situ* measurements. These were then classified into 3 categories, ≤ 10 %, ≤ 20 % and > 20 %. Elements with an RSD of > 20 % was immediately classified as Qualitative whilst an RSD of ≤ 20 % would result in a Quantitative relationship. At this point, elements would only remain unclassified if they had an R^2 of ≥ 0.85 and an RSD of ≤ 10 %. The c value (y-intercept) of the equation was subsequently tested to equal 0 at a 95% confidence level. Failing this resulted in a quantitative relationship. The final test was to see whether the gradient, m, was equal to 1 at 95% confidence level. Satisfying this test resulted in a definitive predictor relationship (y = x) whilst failing the test resulted in quantitative data (y = mx). Table 5.1 outlines the data quality criteria.

Table 5.1: Relationship quality comparison criteria. Adapted from Kilbride et al. (2006).

Relationship Quality	**Statistical Requirement**
Definitive	R^2 = 0.85 - 1.00 RSD < 10 % Relationship is statistically similar, *y=x* is accepted.
Quantitative	R^2 = 0.70 - 1.00 RSD < 20 % Relationship is statistically different, *y=mx* or *y=mx+c*.
Qualitative	R^2 < 0.70 RSD > 20 % Relationship is statistically different.

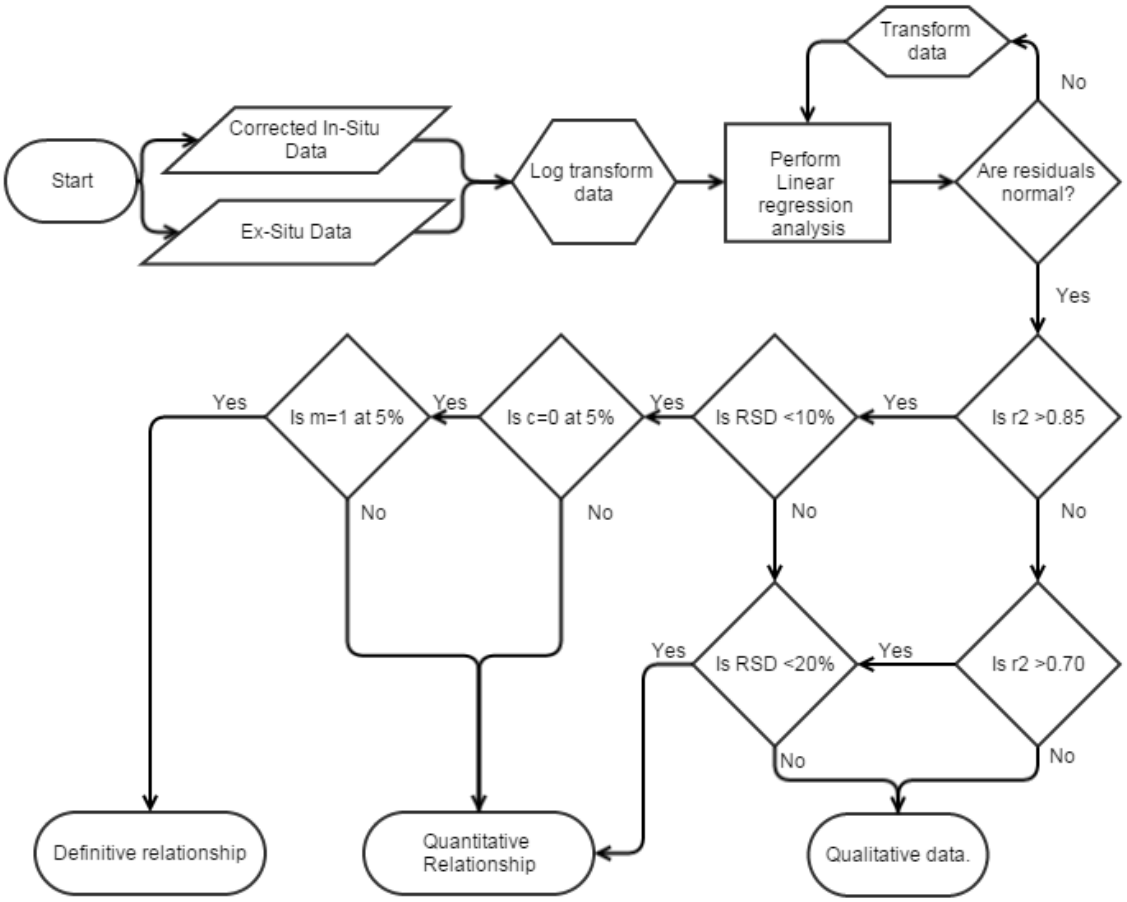

Figure 5.3: Methodological workflow for assessing the relationship between in-situ and ex-situ methods. Derived from Shuttleworth et al. (2014).

5.3. Results

5.3.1. Ex-situ metal analysis by XRF in dry sediments

Elemental recovery and RSD% values (n = 5) from initial laboratory XRF analysis on dry sediments are presented within Table 5.2.

Table 5.2: Atomic number (Z), recovery (%) and RSD% of CRM sediments determined through XRF, n.a. represents no certified concentration and <dl is below detection limit.

Z	Element	TILL4		LOAM7004		PACS2	
		Recovery %	RSD %	Recovery %	RSD %	Recovery %	RSD %
33	As	**99**	3.62	**105**	9.34	**115**	9.78
56	Ba	**111**	4.36	**n.a.**		**n.a.**	
20	Ca	**n.a.**		**n.a.**		**66**	0.33
27	Co	**<dl**		**118**	71.87	**<dl**	
24	Cr	**34**	12.46	**60**	2.82	**54**	6.00
29	Cu	**81**	6.29	**81**	3.09	**82**	2.59
26	Fe	**82**	0.40	**n.a.**		**90**	0.36
19	K	**n.a.**		**n.a.**		**69**	0.30
25	Mn	**93**	4.49	**83**	3.09	**73**	2.61
42	Mo	**123**	6.41	**n.a.**		**160**	12.62
28	Ni	**76**		**<dl**		**<dl**	
82	Pb	**101**	5.51	**104**	2.47	**99**	2.10
37	Rb	**99**	1.67	**n.a.**		**n.a.**	
38	Sr	**111**	1.08	**n.a.**		**103**	0.51
22	Ti	**71**	6.24	**n.a.**		**65**	0.77
23	V	**92**	11.01	**95**	5.08	**70**	3.56
30	Zn	**96**	6.31	**98**	1.30	**103**	1.92
40	Zr	**116**	0.72	**n.a.**		**n.a.**	

Accuracy, measured as Recovery %, for As, Ba, Cu, Fe, Mn, Pb, Rb, Sr, V, Zn and Zr were within 20 % of the certified values and in agreement with Hu *et al.* (2014), although certified values for Ba, Rb and Zr were only available for one CRM. Precision was generally within 10 % RSD for these elements. Therefore, XRF is a suitable analytical tool for the measurement of As, Cu, Fe, Mn, Pb, Sr, V and Zn and these metals will be investigated further in this study.

Data quality was poor for Ca, Co, Cr, Mo, Ni and S (low recovery and/or high variability (%RSD) between CRMs). Although recovery for Co was within 20 % for LOAM7004, high variability (>70 RSD%) suggests the concentration is at/below the analytical detection limit (US-EPA, 2007). Cr and Ti were below detection within all samples. Therefore, these metals will not be considered further in this study.

5.3.2. Influence of Sample Moisture on X-Ray Suppression

The effect of moisture content on elemental recovery for PACS2 CRM is shown in Table 5.3 (metal concentrations are given in Appendix 8). Scatterplots of concentration (mg kg^{-1}) against moisture content (%) are given in Figure 5.4.

Table 5.3: PACS-2 recovery (%) at different levels of moisture content.

		Moisture Content (%DW)												
		0	**10**	**15**	**20**	**25**	**30**	**40**	**50**	**60**	**70**	**75**	**85**	**90**
Recovery (%)	**As**	115	90	97	95	96	70	78	49	60	54	64	73	62
	Cu	82	67	71	68	63	59	51	47	47	40	40	47	39
	Fe	90	71	78	73	69	64	55	49	49	46	46	50	45
	Mn	73	51	57	51	49	41	32	39	26	33	21	20	17
	Pb	99	80	86	81	97	72	63	64	60	54	53	54	53
	Sr	103	81	89	84	80	74	68	66	56	62	55	56	51
	V	68	57	65	58	63	51	69	67	64	63	63	58	61
	Zn	103	80	85	81	75	71	62	66	52	60	55	58	51

All elements, except V, show a reduction in recovery with increasing moisture content, with V showing approximately 60 % recovery at all moisture contents. Cu and Mn show the lowest recovery at 90 % MC; 39 % and 17 % respectively. Arsenic (As) shows large variability within the dataset, potentially due to the certified concentration (26.2 mg kg^{-1}) approaching the XRF detection limit of 12 mg kg^{-1} (NITON, 2010).

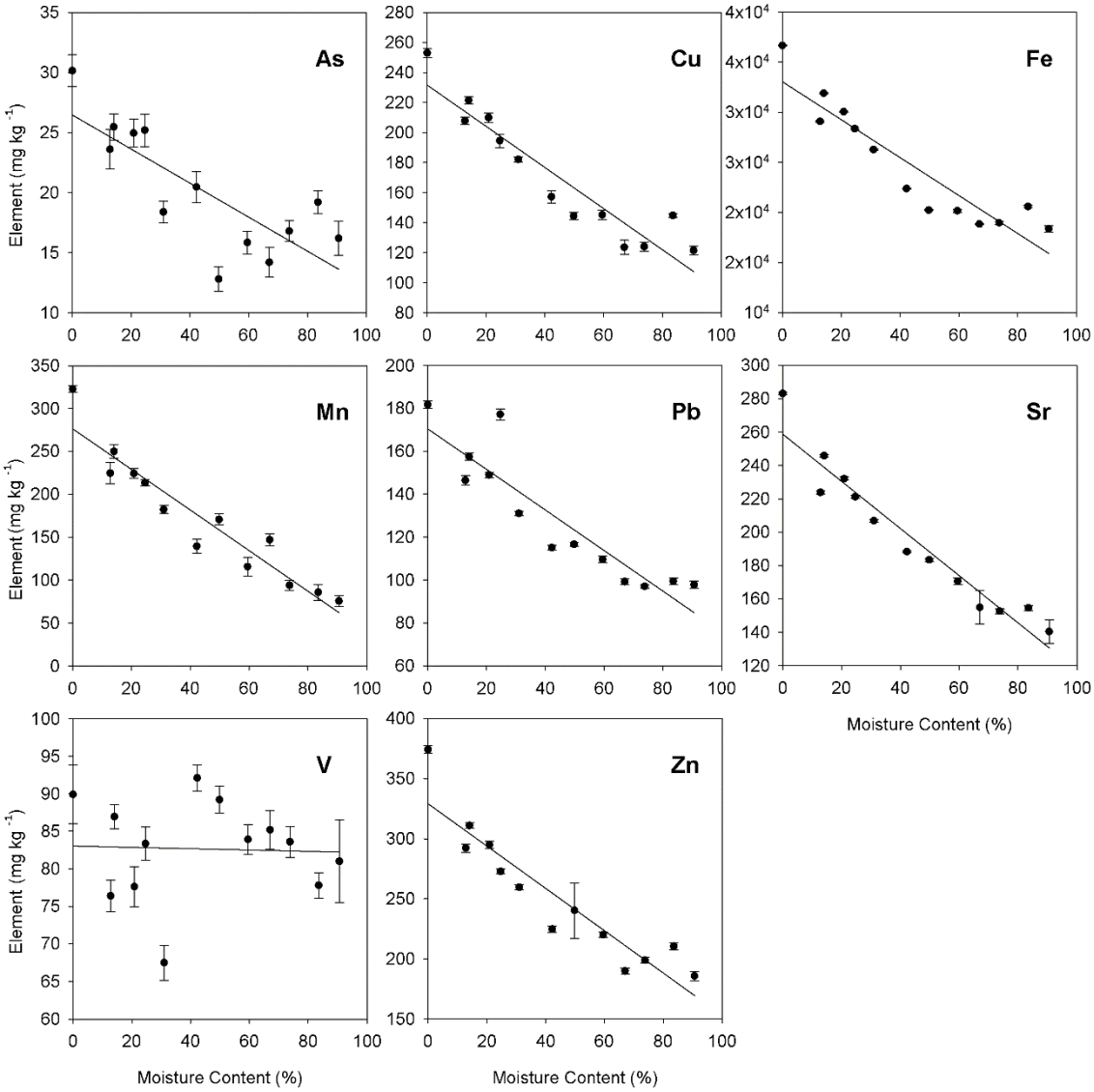

Figure 5.4: Relationship between moisture content and concentration (mg kg $^{-1}$) for each element. Error bars show standard error.

Moisture corrections used in the literature (Shuttleworth *et al.*, 2014) make an assumption that X-ray suppression is directly related to moisture content with a ratio of 1:1. This is shown in the scatterplots, as all elements (with exception of V) showed a similar slope. Data were then converted for moisture content (Equation 5.2) and recovery values analysed. Average recovery values (%) after moisture correction are shown in Table 5.4. Detailed correction analysis tables are shown in Appendix 9.

Table 5.4: Average recovery values (%) for moisture corrected data.

Element	Moisture corrected recovery (%)
As	107
Cu	76
Fe	83
Mn	52
Pb	97
Sr	98
Zn	95

Application of the moisture correction was able to generate accurate data for As, Pb, Sr, Zn and to lesser extent Cu and Fe across a range of 0-90 % moisture. The recovery of 52 % for Mn is outside the acceptable accuracy level (100 ± 20 %) (Hu *et al.*, 2014).

5.3.3. Measuring Field Sample Moisture

Table 5.5 shows a comparison between moisture content derived from *in-situ* theta probe measurements (volumetric), and from oven drying (gravimetric). In order to allow direct comparison, volumetric data from the theta probe have also been converted to gravimetric data using literature sediment bulk density values (Tempest *et al.*, 2014). The correlation between gravimetric theta probe and oven dried data can be seen in Figure 5.5.

Table 5.5: Soil moisture (%) method comparison statistics (n =115).

	Theta (Volumetric)	Theta (Gravimetric)	Oven (Gravimetric)
Mean	31.0	92.1	68.9
Standard Error	0.2	2.4	2.6
Median	31.7	95.6	61.9
Standard Deviation	2.8	25.5	27.7
Range	16.4	113.5	110.2
Minimum	19.6	44.2	27.9
Maximum	36.0	157.6	138.1

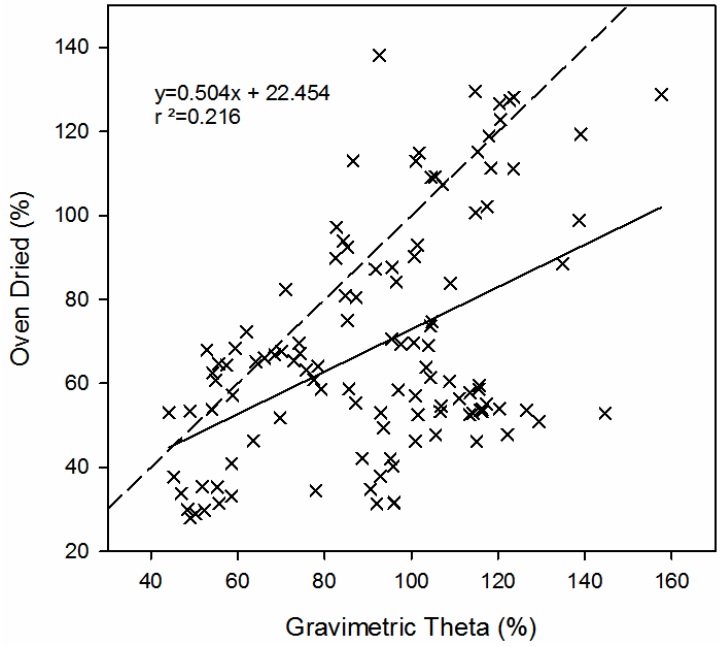

Figure 5.5: Relationship between Gravimetric Theta Probe and oven drying soil moisture measurements. Dashed line represents 1:1 relationship.

Gravimetric theta probe measurements over represent the moisture content with a mean value of 92.1 %, compared to the 68.9 % mean after oven drying. However, the poor correlation between the two methods (Figure 5.5), suggests the over recovery is not systematic and that there is an external factor influencing moisture content data, rendering theta probe measurements unreliable for the *in-situ* measurement of soil moisture contents. Due to the lack of correlation, moisture content will be measured using gravimetric methods for the remainder of this chapter.

5.3.4. Comparison of metal data from in-situ XRF and ex-situ ICP analysis

Table 5.6 shows descriptive statistics for metal concentration data derived from moisture corrected (gravimetric) *in-situ* XRF analysis and from *ex-situ* ICP-OES analysis from the salt marsh sediments collected from the Newlands site. Data are presented for Cu, Fe, Mn, Pb, Sr and Zn as these were the only metals accurately recoverable for moisture content and above LoD. Results of a Mann-Whitney U test, to examine significant differences in median concentrations derived from XRF and ICP are given in Table 5.7. Figure 5.6 shows scatterplots of the data used to undertake linear regression analysis, whilst Table 5.8 shows the model attributes from the regression analysis; R^2, %RSD, m, c and Kolmogorov-Smirnov test results. Residuals from all variables (Cu, Fe, Mn, Pb, Sr and Zn) showed normal distributions and were therefore suitable for analysis (Kilbride *et al.*, 2006).

Table 5.6: Descriptive statistics (mg kg^{-1}) for ICP and moisture corrected XRF data.

		Cu	**Fe**	**Mn**	**Pb**	**Sr**	**Zn**
		(mg kg^{-1})	(mg kg^{-1})	(mg kg^{-1})	(mg kg^{-1})	(mg kg^{-1})	(mg kg^{-1})
Corrected XRF	Median	41	25537	189	100	111	89
	Max	65	34826	361	269	150	220
	Min	27	15604	114	40	68	36
	Range	38	19223	247	230	82	184
ICP-OES	Median	38	35496	270	95	80	119
	Max	74	46448	641	205	124	262
	Min	16	24942	221	38	49	54
	Range	58	21505	420	167	74	208

Table 5.7: Mann-Whitney U test results for the difference between median in-situ and ex-situ concentrations. Significance level = 5 % (n = 36).

	U	***p***
Cu	632.000	0.239
Fe	61.500	< 0.001
Mn	109.500	< 0.001
Pb	659.000	0.906
Sr	1081.500	< 0.001
Zn	398.000	0.06

Median Zn concentrations derived from XRF and ICP were not significantly different (*U* = 398, *p* = 0.06) and showed the strongest correlations (R^2 0.90) and an RSD of 9.7 %. The model was subsequently tested to see whether it satisfied c = 0 and m = 0 at 95 % confidence and the results *t* 0.00 and *t* 0.00 respectively show that the relationship is definitive, and can therefore be considered as y=x. Therefore, moisture corrected *in-situ* XRF can be used to determine accurate Zn concentrations.

Fe shows a significant difference between median concentrations (*U* = 61.5, *p* = <0.001). However, the two methods exhibited a strong positive correlation (R^2 0.79) and RSD of 1.60 %, with c and m both equalling 0, resulting in a definitive data quality.

Median values of XRF and ICP data for Cu and Pb were not significantly different (*U* = 623*, p* = 0.24 and *U* = 659, *p* = 0.90 respectively), showing differences of c. 5 mg kg^{-1}. The relationship between corrected *in-situ* and *ex-situ* values for Cu is not strong (R^2 0.30) and therefore, *in-situ* XRF Cu data are qualitative. Lead showed an extremely high correlation between corrected *in-situ* and *ex-situ* data (R^2 0.89) and a low RSD (7.8 %) and was tested further to see whether the relationship was definitive. However, the intercept with the y axis ('c') was not statistically similar to 0 (*t* 0.25) and therefore *in-situ* XRF data are quantitative.

Median Sr concentrations were significantly different in ICP and XRF data (*U* = 1081, *p*= <0.001), however the relationship exhibited a strong correlation (R^2 0.70) and low RSD (3.63 %) resulting in the XRF data quality to be considered quantitative. Similarly, median Mn concentration showed a significant difference (*U* = 109.5, *p* = <0.001) and a weak correlation between the methods (R^2 0.61), resulting in XRF being able to only measure data to a qualitative level.

Table 5.8: Linear regression attributes and method decisions from the relationship between log moisture corrected XRF and ICP-OES data (t-test at 95 % confidence level). Yes/No indicates whether the t-statistic meets the requirement to a 95 % confidence level.

	Normal?	R^2	RSD (%)	c (*y-intercept*)	m (*gradient*)	Data Quality
Cu	Yes	0.307	6.08	0.06 No	0.00 Yes	Qualitative
Fe	Yes	0.797	1.60	0.00 Yes	0.00 Yes	Definitive
Mn	Yes	0.611	5.01	0.01 Yes	0.00 Yes	Qualitative
Pb	Yes	0.897	7.83	0.25 No	0.00 Yes	Quantitative
Sr	Yes	0.702	3.63	0.01 Yes	0.00 Yes	Quantitative
Zn	Yes	0.904	9.78	0.00 Yes	0.00 Yes	Definitive

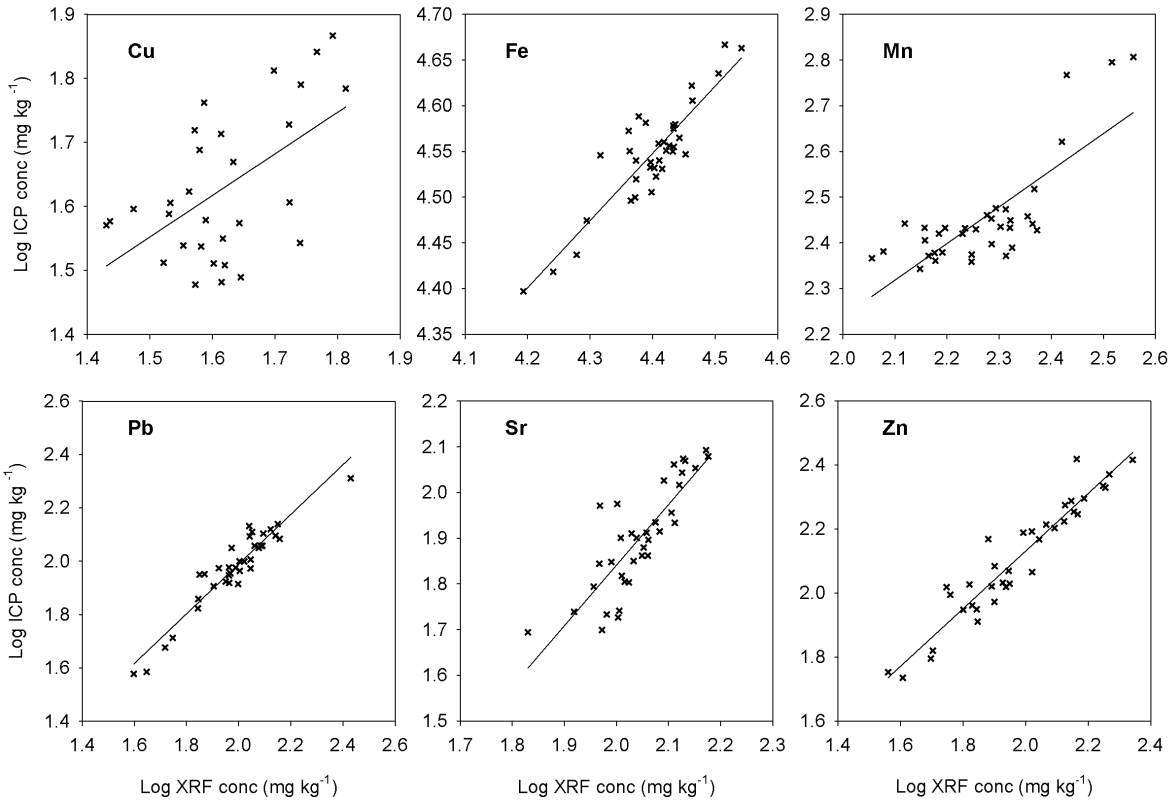

Figure 5.6: Relationship between XRF and ICP datasets. Lines represent the linear regression equation.

5.4. Discussion

5.4.1. Ex-situ metal analysis by XRF on dry sediments

In this study, As, Ba, Fe, Pb, Rb, Sr, Zn and Zr were accurately and precisely analysed by XRF within dry sediments, in keeping with previous studies (Clark *et al.*, 1999; Kalnicky and Singhvi, 2001; Kilbride *et al.*, 2006; Bastos, 2012; Hu *et al.*, 2014; Shand and Wendler, 2014). Copper, Mn and V (within PACS2), however, show slightly lower recovery and this is likely to be due to their lower atomic number (Z = 29, 25 and 23 respectively) (Bastos, 2012). Additionally, Ca, K, S and Ti (Z = 20, 19, 16 and 22, respectively) were recovered poorly, however reduced analytical accuracy of these elements has been previously documented (Kregsamer *et al.*, 1999). These elements have a lower photoelectric absorption coefficient, which, when twinned with absorption of primary and florescent radiation by the sample matrix (Van Dyck and Van Grieken, 1980), reduces the intensity and increases scattering of characteristic emitted X-rays (Giauque *et al.*, 1979).

Certified concentrations of Cr, Co, Mo and Ni were below detection in the CRM's (Table 5.9) and therefore data quality could not be readily assessed. However, certified concentrations for these elements were at magnitudes that are similar to those expected within UK coastal sediments (Bryan and Langston, 1992) and, therefore, it is unlikely that XRF can be used to analyse Cr, Co, Mo and Ni in estuarine sediments unless they are known to have been specifically contaminated by these metals.

Table 5.9: Operational LoD (mg kg $^{-1}$) calculations for XRF. Based on 100-600 second count time of SiO_2 samples. Bold values represent CRM concentrations exceeding the LoD.(US-EPA, 2007).

Chemical	LoD (mg kg $^{-1}$)	TILL4	PACS2	LOAM7004
Antimony (Sb)	40	1		
Arsenic (As)	40	**111**	26	**49.6**
Barium (Ba)	20	**395**		
Chromium (Cr)	150	53	91	82.2
Cobalt (Co)	60	8		20
Copper (Cu)	50	**237**	**310**	**183**
Iron (Fe)	60	**39700**	**40900**	
Lead (Pb)	20	**50**	**183**	**93.4**
Manganese (Mn)	70	**490**	**440**	**869**
Molybdenum (Mo)	10	**16**	5	
Nickel (Ni)	50	17		
Rubidium (Rb)	10	**161**		
Strontium (Sr)	10	**109**	**276**	
Thorium (Th)	10	**17.4**		
Vanadium (V)	50	**67**	**133**	**126**
Zinc (Zn)	50	**70**	**364**	**227**
Zirconium (Zr)	10	**385**		

5.4.2. Influence of Sample Moisture on X-Ray Suppression

Arsenic, Cu, Fe, Mn, Pb, Sr and Zn all show similar X-ray suppression with increasing sample moisture (Figure 5.4). X-ray suppression can also be caused by increased matrix absorption as a result of varying particle size (Clark *et al.*, 1999) and sample surface roughness (IAEA, 2005). However, in these sediments, particle size and sample roughness were consistent and therefore unlikely to have had a significant impact on X-ray suppression and hence metal recovery. In addition, the strong linear relationship suggests that the X-ray suppression is solely a result of moisture content. Arsenic showed a weaker relationship with increased moisture content (R = 0.632), as the certified concentration was lower than the detection limit (Table 5.9).

Data were adjusted for moisture content using a method applied to Pb suppression in peatlands (Shuttleworth *et al.*, 2014) and the correction yielded accurate concentrations for As, Fe, Sr and Zn, in addition to Pb. Therefore, the correction is applicable across both a broader range of metals and a wider range of moisture contents than previously suggested (0 – 30 %).

In order to test further whether a more accurate method existed for measuring the dependence of elemental recovery on sediment moisture, linear regression analysis was used to predict accuracy losses with increasing moisture. Table 5.10 shows that there are no additional advantages in undertaking regression corrections, with the exception of As, inferring that the correction suggested by Shuttleworth *et al.* (2014) is suitable for this range of metals.

Table 5.10: Comparison between the correction proposed by Shuttleworth et al (2014) and correction using regression analysis.

Element	Shuttleworth *et al* (2014)	Regression Correction
As	107	101
Cu	76	75
Fe	83	81
Mn	52	63
Pb	97	96
Sr	98	93
Zn	95	90

Conversely, X-ray suppression did not respond similarly with moisture content for all elements. Recovery of V was poor (68 %) within dry sediment which is consistent with previous work (Revenko, 2002). However, recovery was not dependent on moisture content, which showed highly variable data. As mentioned in Section 5.4.1, light elements

such as V (Z = 23), have lower mass energy-absorption coefficients, resulting in lower energy levels emitted after X-ray exposure (Hubbell, 1982). Assuming the wavelength of the analysis X-ray is uniform, the mass attenuation coefficient of water remains constant (Hubbell and Seltzer, 2004), however an increased concentration of moisture in the sample will be able to absorb more emitted energy, resulting in a weaker signal being recorded within the XRF detector. In the case of V, the majority of the XRF signal is being attenuated and scattered by the water, resulting in inaccurate readings. This was also the case with Cu data, as the concentration of moisture increases, the sample becomes effectively diluted with respect to moisture content (Lemiere *et al.*, 2014). As moisture is added the X-ray suppression appears linear, suggesting that Cu could be measured qualitatively, or for screening purposes in the field (Lemiere *et al.*, 2014), with quantitative analysis requiring laboratory sample preparation.

These data provide evidence for the significant impact that sample moisture has on analytical accuracy and that detection limits quoted by XRF manufacturers are clearly operational, based on both the element and sample moisture content. Yet, numerous studies have conducted *in-situ* measurements and either omitted moisture correction (Kirtay *et al.*, 1998; Carr *et al.*, 2008; Weindorf *et al.*, 2013) or mentioned limitations, but not undertaken any moisture correction (Bernick *et al.*, 1995; Liu *et al.*, 2013), significantly limiting the accuracy of their data.

Figure 5.7 illustrates the consequences of not correcting for moisture content, using Pb data in the Newlands core as an example. The red line represents *in-situ* XRF Pb concentrations, whereas the black line represents corrected data, which can be up to 300 mg kg^{-1} higher. The grey area shows the potential concentration range if sample moisture is not measured, but assumed based on a range of sensible field values. This demonstrates that omitting to measure accurately and correct for field soil moisture, can lead to the under-estimation of metal concentrations by up to four times. The consequences of this may be the oversight of contamination hotspots, or underestimating concentrations that would otherwise be above a threshold of environmental concern. This is particularly concerning where studies are dealing with the identification of metal contamination e.g. (Kirtay *et al.*, 1998; Carr *et al.*, 2008; Weindorf *et al.*, 2013).

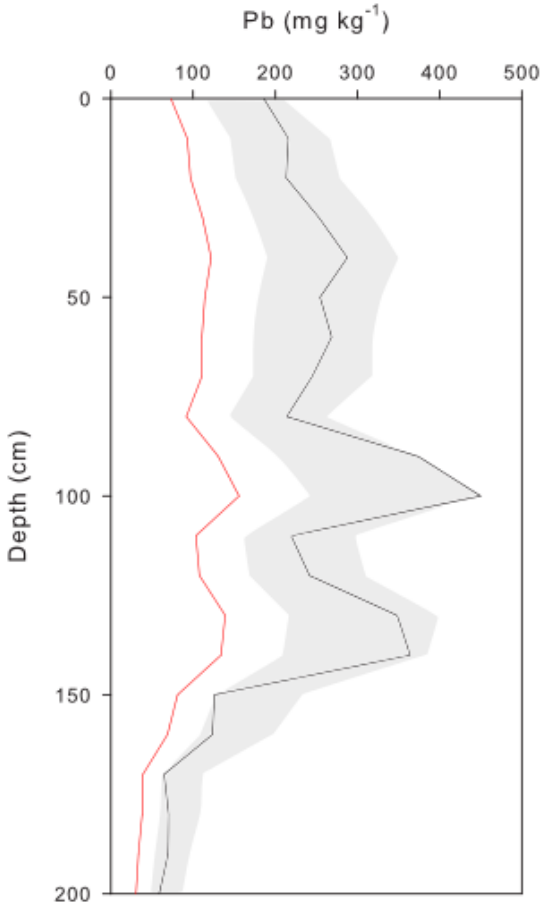

Figure 5.7: XRF In-situ Pb concentrations (red) and corrected Pb concentrations (black) with the grey area showing corrected measurements based on moisture content ranges.

5.4.3. Measuring Field Sample Moisture

Neither volumetric nor gravimetric (corrected using bulk density) moisture content data derived from theta probe measurements accurately replicated soil moisture derived from oven drying, a method known to accurately measure moisture content (O'Kelly, 2004). This suggested that an external factor was introducing noise into the data.

The theta probe measures standing wave impedance between an array of sensor rods, measuring water content due to its vastly differing dielectric permittivity (ε) from surrounding soil/sediment (Miller, 1999). However, there are parameters which can impact the electrical response, and therefore accuracy of the unit; including soil/sediment texture, structure, grain size, soluble salts, water content, temperature, density and measurement frequency (Topp *et al.*, 1980; Kargas and Kerkides, 2008). pH and grain size data, previously collected for this salt marsh (Chapter 4, Section 4.4.2) showed no correlation with theta probe measurements (r_s = -0.108, p = 0.164 and r_s = 0.585, p = <0.0001 respectively) signifying no impact as a result of texture/grain size. The effects of salinity on theta probe measurements are complex, often with conflicting findings (Kelleners *et al.*, 2004; Schmutz and Namikas, 2011). In the absence of pore water chemistry data, the effect due to salinity/presence of soluble salts could not be measured, therefore the factor introducing error to the data is unknown. Calibrations exist to try and account for the effects due to salinity within dielectric moisture sensors (Miller, 1999; Inoue *et al.*, 2008), though if the pore water chemistry is unknown, a calibration would not improve the accuracy of results and therefore it is difficult to accurately interpret data.

In conclusion, it is not possible to measure accurately the moisture content of saline, coastal sediments using a theta probe. There was no systematic error within the correlation between data derived from the theta probe and oven drying, and hence the method cannot be calibrated. Accurate measurements of soil moisture must therefore be undertaken within the laboratory. This introduces an extra step in the acquisition of high quality quantitative *in-situ* XRF data, however this analytical work is significantly less time consuming and requires fewer resources and stringent quality control than conventional geochemical analysis.

5.4.4. Comparison of metal data from in-situ XRF and ex-situ ICP analysis

The only elements measured with both moisture corrected *in-situ* and *ex-situ* methods were Cu, Fe, Mn, Pb, Sr and Zn. Differences in median values of Cu, Pb and Zn have been shown in previous work which compares ICP analysis after Aqua Regia digestion (AR) to XRF data (Radu and Diamond, 2009), whilst Cd and As appear to show a similar concentration (Kilbride *et al.*, 2006). The reason for this is that metals analysed by ICP-OES are first extracted by an acid, in this case Aqua Regia (AR). AR extracts a functionally defined, 'biologically available' fraction, measuring the maximum potential solubility of contaminants under extreme environmental regimes (Rao *et al.*, 2008). Unlike stronger Hydrofluoric Acid (HF) digestions (Sastre *et al.*, 2002), AR extractions cannot digest contaminants bound to the aluminosilicate phase, resulting in a 'pseudo total' metal concentration (Relić *et al.*, 2011). In contrast, these metals will be detected by XRF, as metal atoms fluoresce when excited by X-rays (Kalnicky and Singhvi, 2001), regardless of mineralogy or speciation. Studies comparing XRF with data from either HF (Böning *et al.*, 2007; Towett *et al.*, 2013; Hu *et al.*, 2014) or $HClO_4$ digests (Argyraki *et al.*, 1997) have found close agreement of data, as these reagents were able to digest contaminants bound to the silicate fraction.

Conversely, median concentrations for Fe and Mn were higher for ICP measurements than XRF. Both Fe and Mn can re-precipitate within oxic sediments as either oxides or carbonates (Farmer and Lovell, 1984), however several studies have found Fe and Mn bound mainly to the lattice/mineral phase (Licheng and Guijiu, 1996; Usero *et al.*, 1998; Spencer *et al.*, 2003) which, within an AR extract, should not be available. There are three possible explanations why ICP concentrations were higher, either; (1) the XRF is overestimating concentrations, which contradicts the accurate CRM data (Table 5.2); (2) there was analytical interference, over estimating Fe and Mn concentrations, or; (3) the significant difference represents the natural variability of analysing adjacent, yet not identical, sediments. Additionally, significant differences in median Sr concentrations were not explainable by the different extractions. Strontium is an alkali Earth metal that readily binds to carbonates (in place of calcium) or weakly sorbs to clay minerals (Lerouge *et al.*, 2010), easily extracted from soils or sediments using relatively weak acids (Oughton *et al.*, 1993; Shan and Chen, 1993; Davidson *et al.*, 2005). It would therefore be expected that the AR extraction would be able to accurately recover all Sr within a sample, however the XRF, which showed accurate measurement of Sr (103 %, Table 5.2) suggested a 30 mg kg^{-1} over estimation. It is likely that this is due to the AR extraction inefficiently attacking the Sr within the carbonate phase, as the XRF showed accurate data recovery.

Statistical criteria from linear regressions show that moisture corrected *in-situ* XRF data are able to accurately predict Fe and Zn to a definitive level, whilst Pb and Sr concentrations are comparable to a quantitative level. Copper showed a poor relationship between ICP and XRF data, with large residuals and a qualitative relationship at best. This is due to the median Cu concentration (38 mg kg $^{-1}$) being below the LoD for XRF (50 mg kg $^{-1}$). These concentrations are within an expected range for estuarine sediments not directly impacted from industrial activities (Bryan and Langston, 1992), suggesting that *ex-situ* analysis, such as ICP-OES, with a lower LoD of 4 mg kg $^{-1}$ is more suitable for Cu analysis at lower concentrations. *In-situ* analysis may be suitable in heavily contaminated sediments, such as mining sites where Cu concentrations may exceed 2000 mg kg $^{-1}$ (Hutchinson and Whitby, 1974). Likewise, *in-situ* XRF only provided qualitative Mn data. Although the concentrations are all above the theoretical LoD of 70 mg kg $^{-1}$, the attenuation of the X-rays from lighter elements with lower mass energy absorption coefficients introduces large amounts of error during analysis within such saturated sediment (Hubbell, 1982). This error is therefore propagated during correction, resulting in statistically significant differences within the datasets.

In-situ XRF analysis presents a powerful, rapid method for analysis of a limited suite of major and trace metals (Fe, Pb, Sr, and Zn) commonly analysed to assess contamination (Pelfrêne *et al.*, 2011) or supporting analysis, such as geochemical normalisation to Fe (Aloupi and Angelidis, 2001a). It showed an advantage over *ex-situ* methods as extensive field campaigns and laboratory work (acid digestion, filtering, sample preparation, creation of calibration standards) was not needed. As *in-situ* methods do not require calibration, they are deemed suitable for exploratory site investigations or QLRA's, rapidly obtaining indicative concentration data, where the distribution and magnitude of contamination is unknown. There are limitations of XRF analysis, as laboratory moisture content measurements are required to make the data quantitative and the suite of elements is limited, excluding elements such as As, Cd, Cr, Cu and Ni which are common indicators of anthropogenic activity (Guo *et al.*, 1997; Machado *et al.*, 2002; Tavakoly Sany *et al.*, 2013; Udayakumar *et al.*, 2014; Zhuang and Gao, 2014).

5.5. Conclusion

In-situ XRF is a powerful analytical tool, showing great potential to identify and accurately measure a large suite of heavy metals within dry sediments (As, Ba, Fe, Pb, Rb, Sr, Zn and Zr). Moisture content has a significant effect on XRF data accuracy, however, a simple correction, previously only validated for use on Pb within peatlands, can be applied to produce accurate data for As, Cu, Fe, Pb, Sr and Zn across a broad range of moisture contents. The magnitude of the impact due to moisture is significant enough that the omission of moisture content correction has shown to underestimate metal concentrations (up to hundreds of mg kg^{-1}), a factor that users and practitioners need to be aware of when undertaking analysis.

Measurement of moisture content *in-situ* would provide immediate access to high quality quantitative data, however, the measurement of sample moisture within the coastal zone is not straightforward. Therefore, moisture content must be derived *ex-situ* following conventional oven heating, an additional inclusion to the laboratory method that introduces an extra step into analysis, but does not vastly reduce the advantage of such a rapid field analysis technique.

In-situ XRF analysis exhibited major limitations with both the measurement of elements around analytical detection limit as well as elements with low atomic numbers. Elemental detection, especially when moisture was present, was poor at values near the detection limit (e.g. Cu), whilst the absorption and scattering of low energy signals from light elements ($Z = < 26$) resulted in analysis of Li, Mg, K, Ca and V being unavailable, meaning that additional analysis, such as the observation of mineral components (Lovrenčić Mikelić *et al.*, 2013), was unobtainable.

When directly compared, *in-situ* data were not significantly different to *ex-situ* data for Cu, Pb and Zn, however, there were significant differences for Fe, Mn and Sr, possibly due to inaccuracies with the acid digestion or analytical interferences. Additionally, Cu was poorly recovered within the dry sediment scans, as well as only predicting concentrations to a qualitative level once moisture was added. This was, however, due to the concentrations being around the LoD, suggesting that analysis would be available in areas with higher magnitude contamination, such as ores or mine impacted sediments (Higueras *et al.*, 2012; Escárate *et al.*, 2015). Although *in-situ* analysis of Mn was only qualitative in comparison to *ex-situ* data due to low levels in tested sediments, *in-situ* methods could potentially replace *ex-situ* methods for initial testing for QRLA's, providing accurate initial screening data, whilst removing a great deal of time and cost to analysis, providing useful information to inform further, more in depth, analysis.

If quantitative data is needed for a rapid risk assessment, then *in-situ* analysis is able to measure metals (Fe, Pb, Sr, and Zn) over large sample moistures (0 – 90 %), providing analytical advantages in both time and cost. Sampling campaigns can be undertaken with immediate access to screening level data, influencing on-site sampling decisions, leading to efficient elemental mapping at field level (Parsons *et al.*, 2013). Sample moisture must be measured in the laboratory, however, this step can be undertaken after field analysis, and is much more controllable/reproducible than conventional analytical laboratory work, which requires specialist training, dedicated space and resources. Despite the extra requirement, *in-situ* analysis still requires fewer resources and negates the need for potentially hazardous laboratory work, whilst still producing accurate data (Fe, Pb, Sr and Zn) and will therefore be used as the analysis method throughout the rest of the thesis.

Chapter 6 Broad Scale Assessment of Landfill Contamination in South East England.

Abstract

Chapter 4 provided evidence that during acetogenic waste degradation, Newlands historic landfill, Essex, UK released a metal rich leachate plume, resulting in metal accumulation at depth in surrounding sediments. The site therefore has the potential to release sediments with 60 mg kg $^{-1}$ Pb and 100 mg kg $^{-1}$ Zn to the surrounding environment. There are c. 5000 landfills within UK flood alert area which may present a source of diffuse contamination, highlighting an urgency to estimate risk on regional and national scales. Therefore, this chapter investigates whether findings at Newlands are representative of other historic landfills.

Eight historic landfill sites were selected for investigation using GIS and freely available Environment Agency geospatial data. Five sites had received a combination of Industrial, Commercial and Household (hazardous) waste, whilst three sites containing only inert waste were chosen as a control. At each site, 2 m sediment cores adjacent to the landfill site boundary were analysed *in-situ* for Fe, Mn, Pb and Zn using XRF, to determine whether there was evidence of subsurface metal enrichment and hence diffuse pollution from the historic landfill. Data were recorded and examined *in-situ* and used to inform subsequent sampling and data collection. At least one core was taken at each site as far as possible from the landfill site boundary, as a control.

Proximal to hazardous landfill sites, enrichment values at depth for Pb and Zn were significantly higher than distal, control cores. There was no discernible change in enrichment values at the inert sites. This suggests that historical landfill sites with similar waste types are likely to have released metal rich leachates to surrounding sediments during acetogenic waste degradation, and now provide a secondary source of diffuse contamination in the coastal zone. Based on these findings, historic hazardous landfills within the Thames have the potential to release a contaminant mass of 706 t, an order of magnitude higher than the annual Port of London dredging activity.

6.1. Introduction

Chapter 4 provided evidence of sediment metal enrichment at depths of 1.5 – 2 m which were interpreted as attenuation of metal contaminated leachate in sediments surrounding Newlands historic landfill, Essex. Despite the landfill ceasing operations over 20 years ago, and subsequently being repurposed as a public country park, a significant contamination legacy exists within the surrounding coastal sediment, extending approximately 15 m from the landfill boundary. The leachate has generated an estimated contamination mass of 3330 kg Cu, Pb and Zn, and well as containing Cu, Hg, Pb and Zn concentrations that exceed the threshold (TEL) of ecological concern (Buchman, 2008). This provides evidence of both the historic release of metal rich leachate during acetogenic waste degradation and attenuation within the fine-grained salt marsh sediments surrounding the site.

Publically available Environment Agency data show that there are approximately 20000 historic landfills within England and Wales (Cooper, 2012), a quarter of which are situated within the coastal zone and predicted to be at risk of flooding within the next 50 years. There is therefore potential for a much larger scale environmental problem across the UK. These historic landfills could be a significant source of diffuse pollution in the coastal zone, especially considering the predicted effects of climate change within the coming decades (IPCC, 2013). UK climate predictions indicate an increase in temperatures and precipitation, increased frequency and magnitude of weather extremes (Lowe *et al.*, 2001) as well as sea level rise (Jenkins, 2008), resulting in the landward migration and erosion of salt marshes (Hughes, 2004). The latter two effects are of critical importance when considering coastal contamination as these historic landfill sites are situated on low lying land, near densely populated centres (Environment Agency, 2010a), and hence require immediate management from the risks of inundation, flooding and erosion.

The United Kingdom is one of the leading industrialised nations in adapting to climate change, developing legislative and regulative policies for coastal planning, with numerous existing frameworks (Carina, 2010). One of the main programmes set to manage the coastline are Shoreline Management Plans. These are semi-economic frameworks, assessing the coastal process, local requirements, environmental considerations, planning issues and future land use around the coast (DEFRA, 2006). There are 4 main compliance policies available to shoreline managers through the framework (Table 6.1), requiring a thorough investigation at each site to ensure the correct policy is applied. Unidentified and unquantified contamination from historic coastal landfills could have significant consequences within the coastal zone especially in areas where managed realignment or no active intervention is adopted, as landward migration of the coast would erode sediment,

physically and chemically redistributing contamination (Sheahan, 2006). There is therefore an urgent need to investigate and quantify the extent and magnitude of this 'hidden' contamination from historic landfills already present within the coastal zone in the UK, as landowners and managers are responsible for managing the risks posed by the release of waste / environmental damage as a result of their landfills, and may be required to undertake remedial action under part IIa of the Environmental Protection Act (Cooper, 2012).

Table 6.1: SMP policies available to shoreline managers (DEFRA, 2006).

Hold the existing defence line	**Maintenance or upgrading the standard of protection.**
Advance the existing defence line	Building of new structures on the seaward side of original defences.
Managed realignment	Allowing the movement of the shoreline, with managed control to limit movement
No active intervention	No investment in coastal defence.

Chapter 5 outlined a method for a rapid, screening level assessment of a common suite of metals (Fe, Mn, Pb, and Zn) within coastal sediments which provides cost effective *in-situ* screening level data, with little post processing required to obtain robust quantitative readings. This method will now be applied to a wider scale assessment, to investigate contamination surrounding other historic landfill sites in the South East. The aim of the assessment is to indicate whether historic contaminant release from the Newlands landfill and resultant contamination of surrounding sediments is representative of other sites in SE England and hence, whether historic landfills present a significant problem in the southeast and more widely within the whole UK. This will be achieved by addressing the following research objectives.

Research Objective 1: To identify potentially hazardous historical landfill sites using publicly available secondary data.

Research Objective 2: To use *in-situ* XRF as a rapid screening tool to identify the presence and extent of sub-surface contaminated sediments indicative of a legacy leachate plume and attenuation within surrounding coastal sediments.

Research Objective 3: To provide a recommended 'next step' for the assessment of risk from historical landfills.

6.2. Methodology

6.2.1. Site Selection Workflow

A GIS based method was adopted to identify suitable sites within South East England that may have historically released contaminated leachate, resulting in the contamination of surrounding sediment. In order to identify potentially hazardous sites, the Environment Agency Geostore (Environment Agency, 2014), a repository containing a range of environmental data from the Canal and River Trust, DEFRA, English Heritage, The Forestry Commission and Natural England, was used to identify sites with attributes similar to Newlands historic landfill (Chapter 4). The criteria for the selection of potential landfill sites were; a waste age over 20 years old, sites situated within the EA flood alert area, adjacent to fine grained sediment and constructed without basal or side-wall engineering. Subsequently, boundary shapefiles of superficial and bedrock geology, landfill location, age and waste type and extent of salt marsh sediments were downloaded. All geospatial analysis was carried out using ArcGIS 10.2.

To reduce processing demand all datasets were clipped to include only the coastal/ estuarine areas of the main river reaches draining the South East coast; the Blackwater, Crouch, Roach, Thames, Medway and Swale estuaries (Figure 6.1).

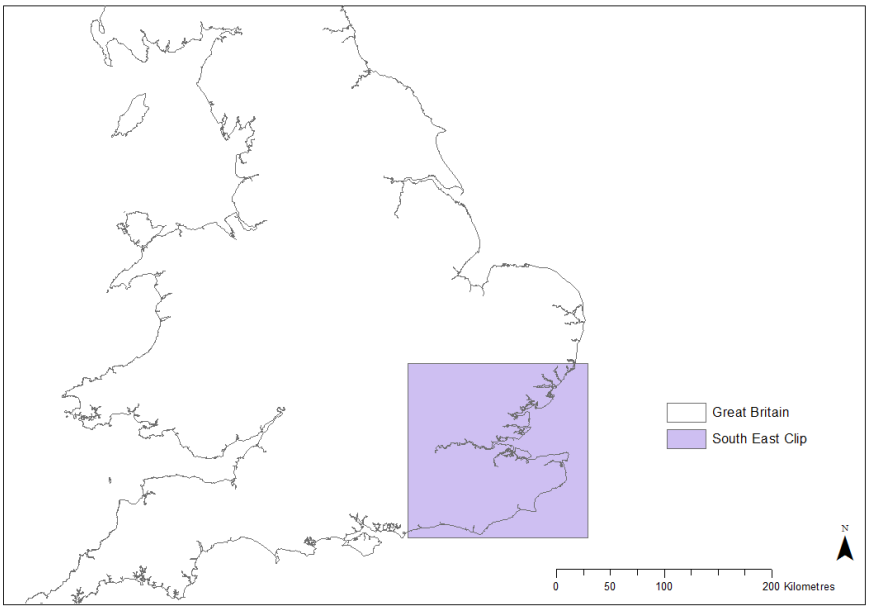

Figure 6.1: Study location (polygon) for site selection methodology (Environment Agency, 2012).

The landfill dataset initially contained records for c. 20000 sites. As the efficiency of contaminant attenuation is dependent on sediment characteristics (Christensen *et al.*, 2001; Bjerg *et al.*, 2011), only historical landfills that intersected fine-grained sediments, such as salt marshes were considered for analysis. A 100 m buffer zone was added to each salt

marsh polygon to help identify suitable areas (Figure 6.2), highlighting 163 historical landfill sites that intersected salt marshes (Figure 6.3).

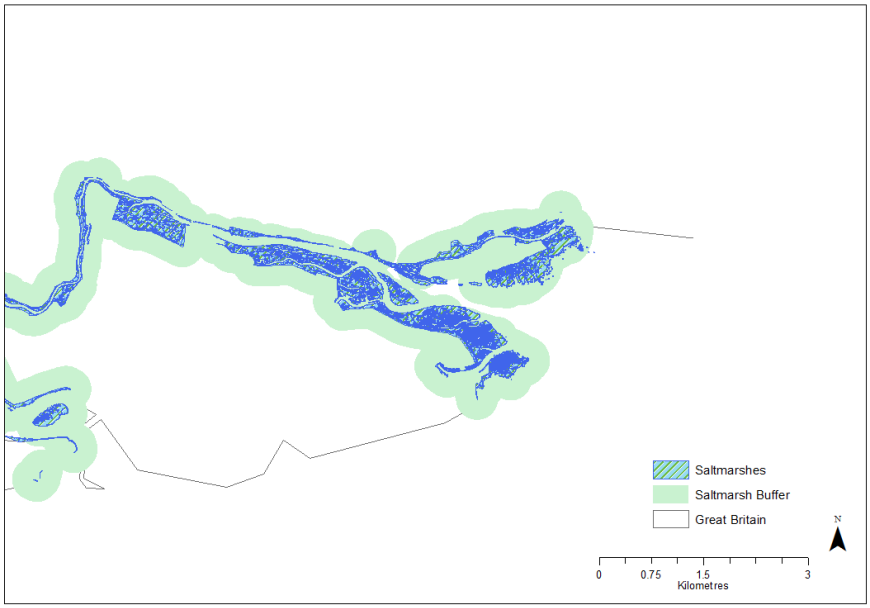

Figure 6.2: Salt marsh polygons with 100 m buffer zone added (Environment Agency, 2012).

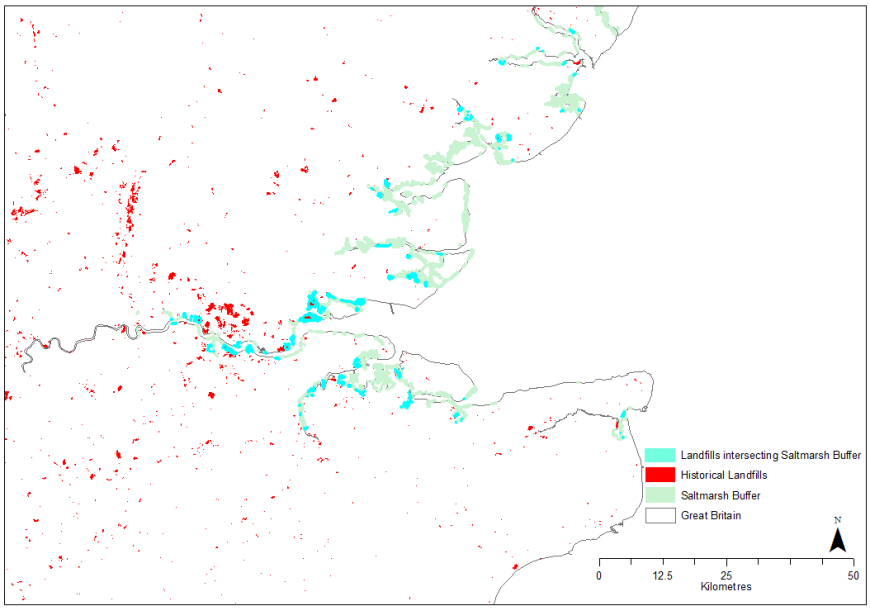

Figure 6.3: Selection of historical landfills (turquoise) that intersect salt marsh locations (green). Red sites indicate historic landfills that do not intersect marsh sediments (Environment Agency, 2012).

Of the 163 sites that intersected salt marshes, further classifications were undertaken based on waste age and waste type. As waste degradation is dependent on time, care was taken to ensure that selected sites were at least 20 years old (Figure 6.4), where the waste is likely to have concluded acetogenic degradation and will be undergoing methanogenic

degradation, and the peak flow of contaminated leachates will have ceased (Njue *et al.*, 2012). At this stage, 44 sites were identified that matched Newlands in terms of waste age, proximity to coastal sediments and location within the estuarine environment (Figure 6.5).

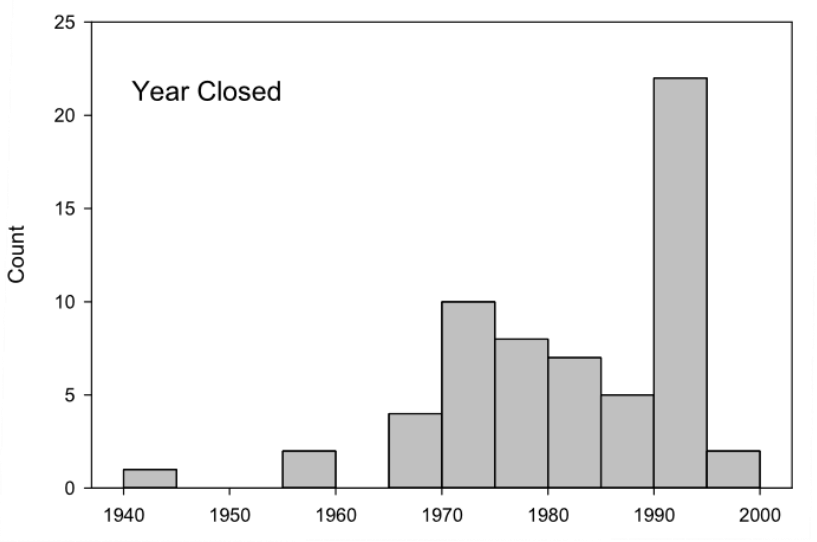

Figure 6.4: Dates of last waste disposal histogram for landfills within South East England.

28 of the identified sites contained exclusively or a combination of industrial, commercial and household waste, similar to Newlands, whilst, 16 sites were identified that exclusively received inert waste. These inert sites were selected as a control as, by definition, inert waste does not undergo any physical, chemical or biological transformation, does not dissolve, burn or biodegrade in a way which would result in environmental pollution or harm to human health, or endanger surface or groundwater (Environment Agency, 2010b) and therefore, contamination should not have been released.

Of these, eight sites were chosen at random, five sites containing industrial, commercial, household waste and three inert sites (Table 6.2). All site records were manually checked and confirmed as far as possible due to the inherent lack of confidence in historical landfill data (Cooper, 2012).

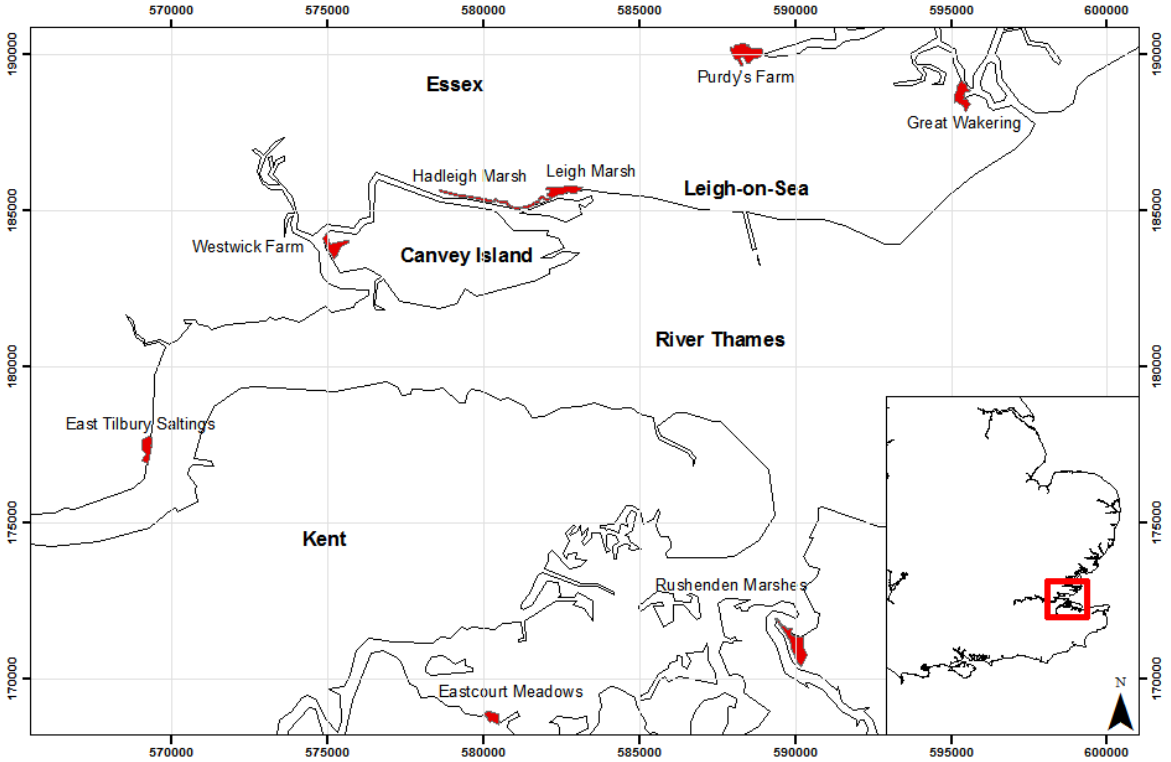

Figure 6.5: Historical landfills situated on salt marsh sediments within the South East.

Table 6.2: Site details for eight selected sites. Ind = Industrial waste, Com = Commercial waste, Hou = Household waste.

Site Name	Date Opened	Date Closed	River Catchment	Waste Type
Great Wakering	1977	1990	Roach	Ind Com Hou
Purdy's Farm	1950	1976	Roach	Ind Hou
Hadleigh Marsh	1979	1985	Thames	Com Hou
Leigh Marshes	1955	1967	Thames	Ind Com Hou
Westwick Farm	1935	1972	Thames	Ind Com Hou
Eastcourt Meadows	1950	1977	Medway	Inert
Rushenden	c. 1960	c. 1990	Medway	Inert
East Tilbury Saltings	1988	1993	Thames	Inert

6.2.2. Site Description

Site areas, together with sample locations are presented in Section 6.2.3.

Great Wakering is a 260000 m^2 municipal waste site situated on the Middleway on the River Roach. The site operated from 1977 to 1990s, receiving industrial, commercial and household waste and prior to landfilling was a major deposition area for the local brickworks within the peak of the industrial revolution (Furness, 2014). The site is currently used as a private boatyard.

Purdy's Farm, also situated on the River Roach, is a 414000 m^2 industrial and household landfill situated 2 km east of Southend Airport. The site opened in 1950 and closed in the late 1970's before being home to a private commercial wharf.

Hadleigh Marsh comprises a 4 km long, 250000 m^2 bund seawall, constructed in 1979 as a coastal flood defence (HALCROW, 2012). Records state household and commercial wastes were used to create the 2.5 m high seawall. Current land use comprises of agricultural land as well as Hadleigh Country Park.

The adjacent site, Leigh Marsh is the oldest landfill selected, with historical mapping suggesting its operational period was between 1930 and 1970 (HALCROW, 2012). The site is 250000 m^2 and comprises of industrial, commercial and household waste, some of which is visible on the land surface. Previous work has highlighted the risks associated with these two sites, mainly limited by uncertainties regarding the waste type and extent (HALCROW, 2012). Both of these sites are situated on Hadleigh Ray, a coastal creek within the Thames estuary.

Westwick Farm is situated on the West side of Canvey Island, on the Thames estuary. It originally opened in 1935, and eventually closed in 1972 having received industrial, commercial and household waste. The site has an area of 230000 m^2 and is situated adjacent to Pitsea Landfill, a currently operational, licensed landfill.

Eastcourt Meadows is situated on the River Medway, on an old grazing site 2 km North East of Rochester. The site was council reclaimed in 1950 for use as a municipal rubbish tip. The site is the smallest to be examined, with an area of 128000 m^2. Receiving only inert waste, the site remained in operation until 1977, before being converted into Riverside Country Park.

Rushenden Marshes is the largest site, at 416000 m^2. However, not much information is known about the site apart from it is comprised entirely of inert waste. There are proposals

for dredging disposals on the site, however the progress/status of these plans is currently unknown.

East Tilbury Saltings sits on the foreshore of Coalhouse Fort, within the Thames estuary. The site is the newest of all sites, opened in 1988. The site has an area of 193000 m^2 and contains only inert waste.

6.2.3. Field and Laboratory Methods

Previous work uncovered contamination enrichment at depth, in sediments proximal to the landfill boundary, representing attenuated metals from historical leachate flow. In order to assess whether this attenuation zone existed at the other sites, a minimum of three 2 m deep sediment cores were extracted from each of the eight sites, using a 5 cm diameter Russian corer (Jowsey, 1966). An initial core was extracted as close as possible to the landfill site boundary (within 15 m with the exception of Westwick Farm), which was then immediately wrapped in plastic wrap, labelled and screened *in-situ*, through the wrapping, using the XRF analytical protocols outlined in Chapter 5. The *in-situ* data were then used to inform site sampling decisions. This was done through observation of Pb and Zn, metals indicative of anthropogenic inputs. The data were measured qualitatively (Chapter 5) in the field and plotted *in-situ* on a field portable laptop. If metal concentrations showed no enrichment relative to background at depth, then it was assumed that there was no evidence for historic contamination and no further sampling was carried out.

However, if metal sediment concentrations remained elevated relative to the background concentration at depth, subsequent cores were extracted, at approximately 5 m intervals from the landfill edge (where site access allowed), and the process repeated until no enrichment at depth was identified (Figure 6.6). Hence, the extent of the leachate plume could be identified. Finally, a distal core was extracted from as far as practically possible on the salt marsh from the site boundary to supply local geochemical background data. Table 6.3 and Figures 6.7 to 6.14 outline sampling details.

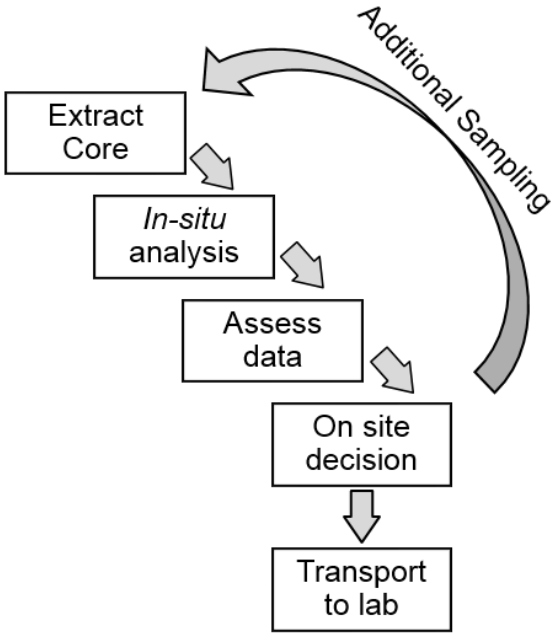

Figure 6.6: Fieldwork flow-chart.

Table 6.3: Sediment core sample information and in-situ observations.

Site	Distances from site boundary	Information
Hazardous		
Great Wakering	10, 15, 20 m	Brick fragments from historical brickworks at depth resulted in incomplete 15 and 20 m sediment cores (1 and 1.5 m respectively).
Purdy's Farm	5, 10, 35 m	
Hadleigh Marsh	5, 45, 65 m	Samples extracted from a sheltered salt marsh area of the 4 km seawall
Leigh Marsh	10, 15, 40 m	
Westwick Farm	25, 25, 60 m	GIS data inaccurate, resulting in the smallest distance from the site boundary being 25 m, large scale rock armouring present.
Inert		
Eastcourt Meadows	15, 15, 30 m	Only one complete core could be extracted from the site boundary due to rocks and shell fragments.
Rushenden Marshes	15, 15, 20 m	Like Eastcourt Meadows, shelly fragments within samples prevented complete cores being extracted.
East Tilbury Saltings	10, 15, 20 m	

Sediment cores were returned to the laboratory where moisture content was measured in order to generate quantitative data for a suite of common metals (Fe, Mn, Pb and Zn) (Chapter 5; Section 5.2.1). The moisture correction method is outlined in Chapter 5, Section 5.2.2.

No Mn data above LoD were recorded at Eastcourt Meadows hence no data was presented.

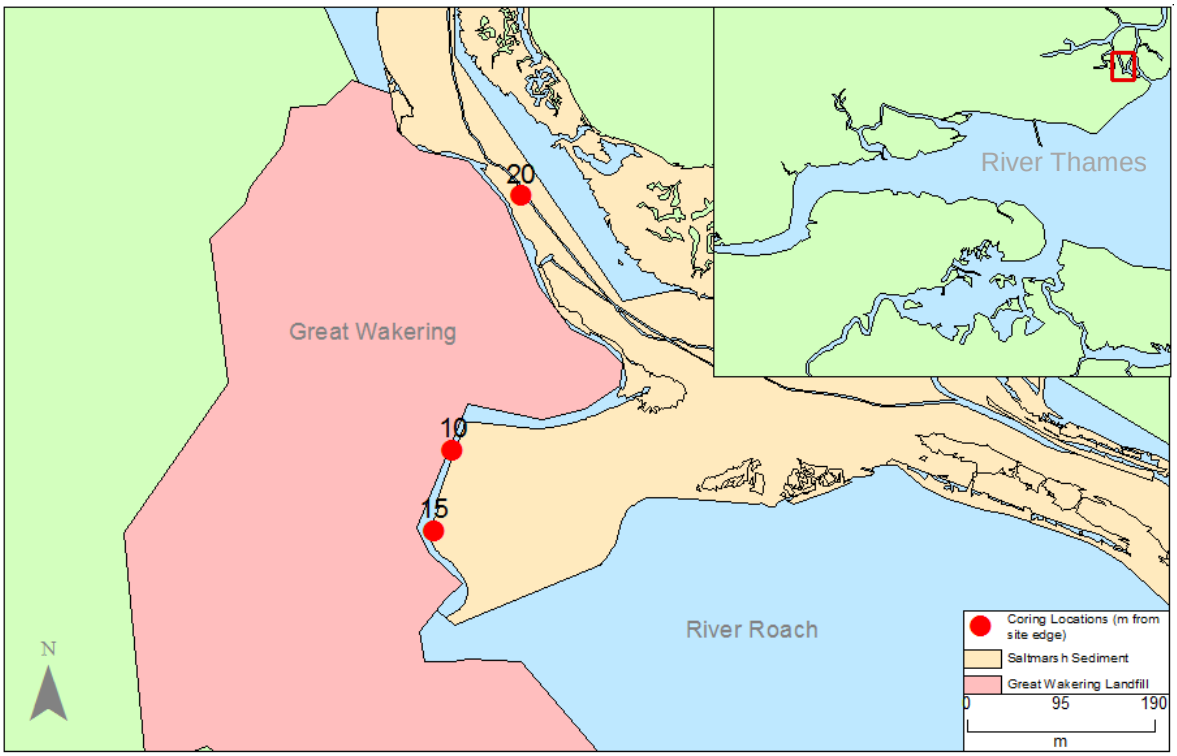

Figure 6.7: Coring locations at Great Wakering. Numbers represent distance from the site edge (in metres).

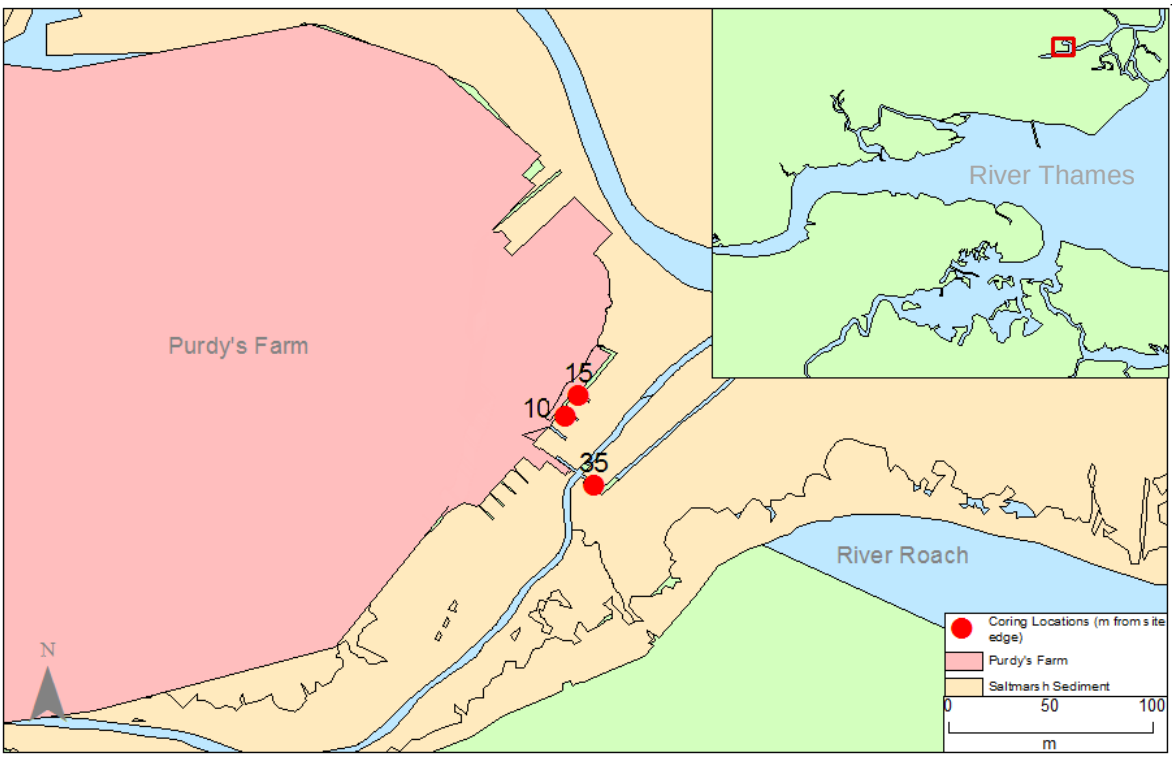

Figure 6.8: Coring locations at Purdy's Farm. Numbers represent distance from the site edge (in metres).

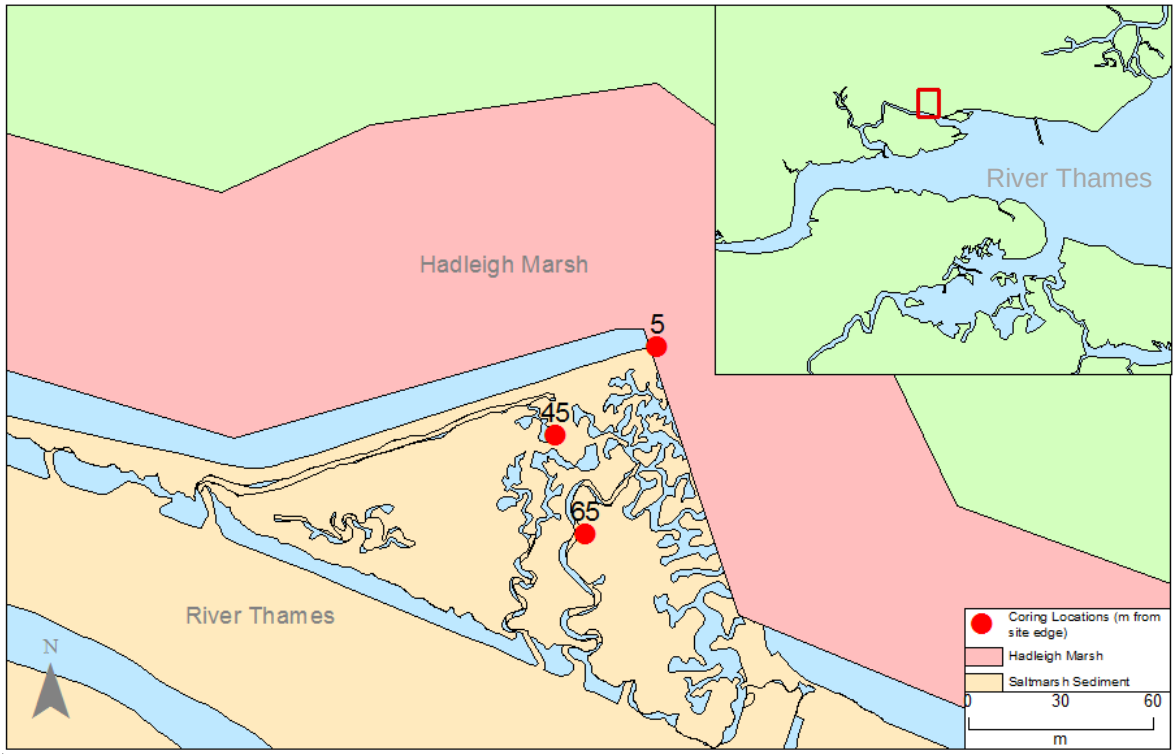

Figure 6.9: Coring locations at Hadleigh Marsh. Numbers represent distance from the site edge (in metres).

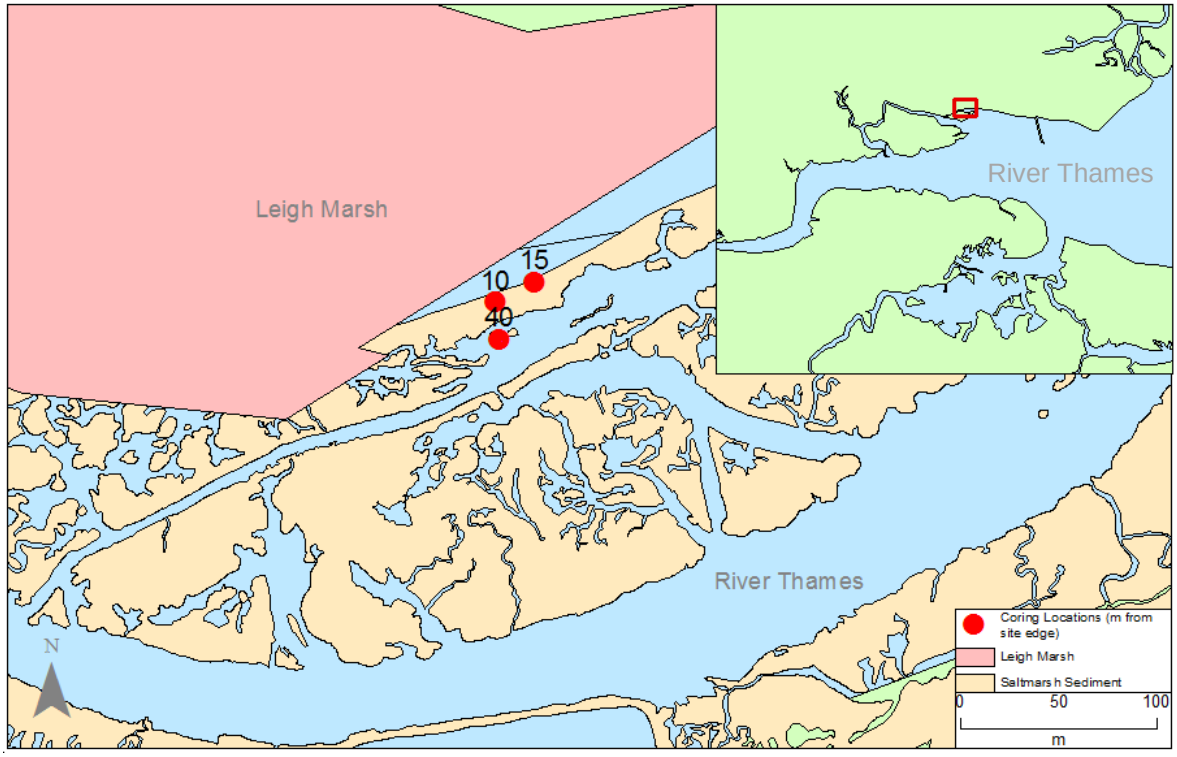

Figure 6.10: Coring locations at Leigh Marsh. Numbers represent distance from the site edge (in metres).

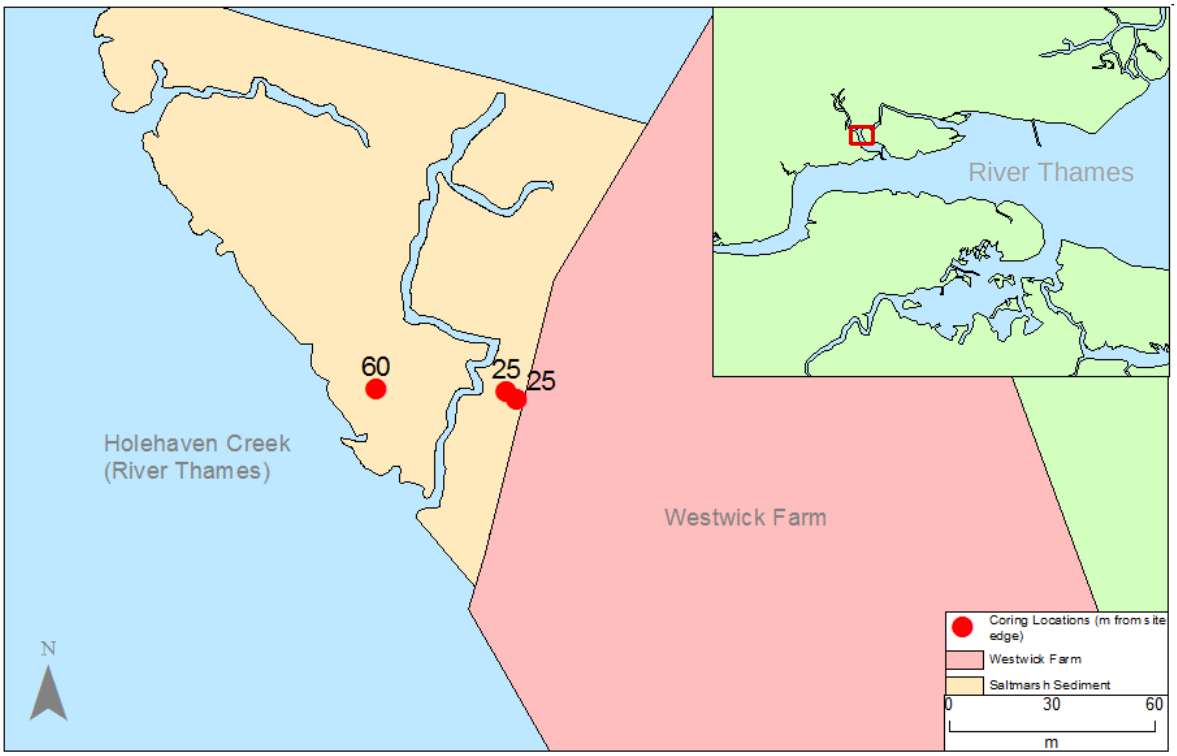

Figure 6.11: Coring locations at Westwick Farm. Numbers represent distance from the site edge (in metres).

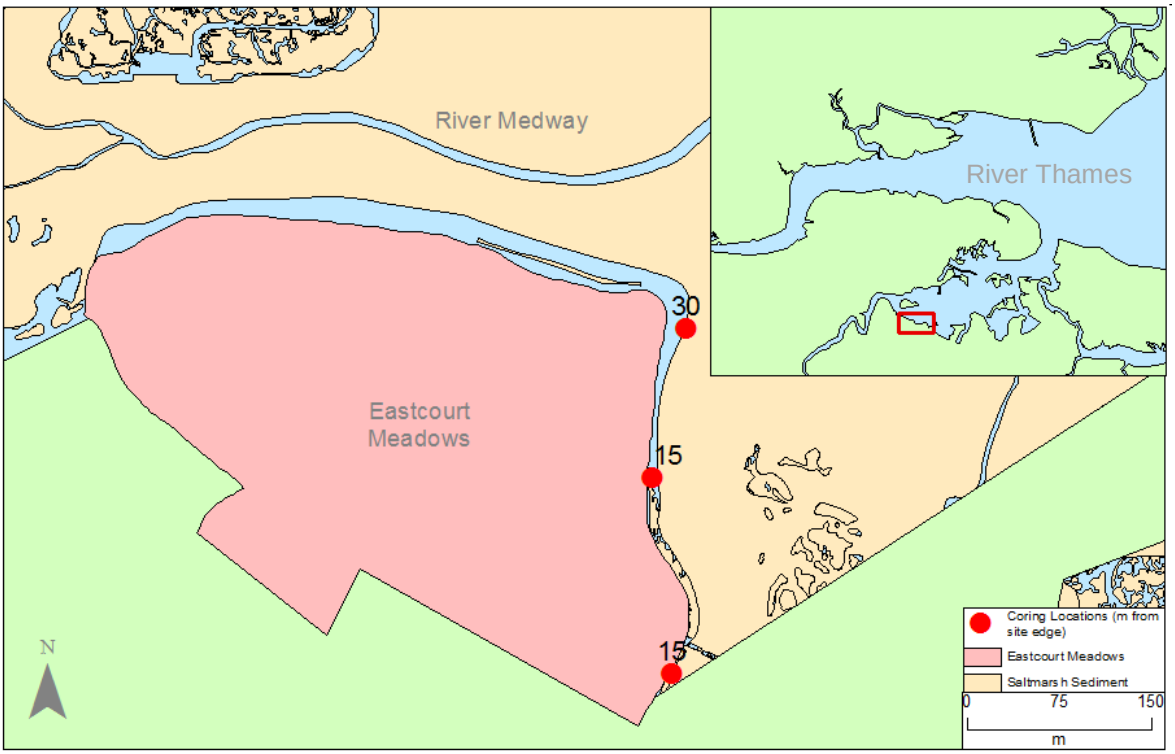

Figure 6.12: Coring locations at Eastcourt meadows. Numbers represent distance from the site edge (in metres).

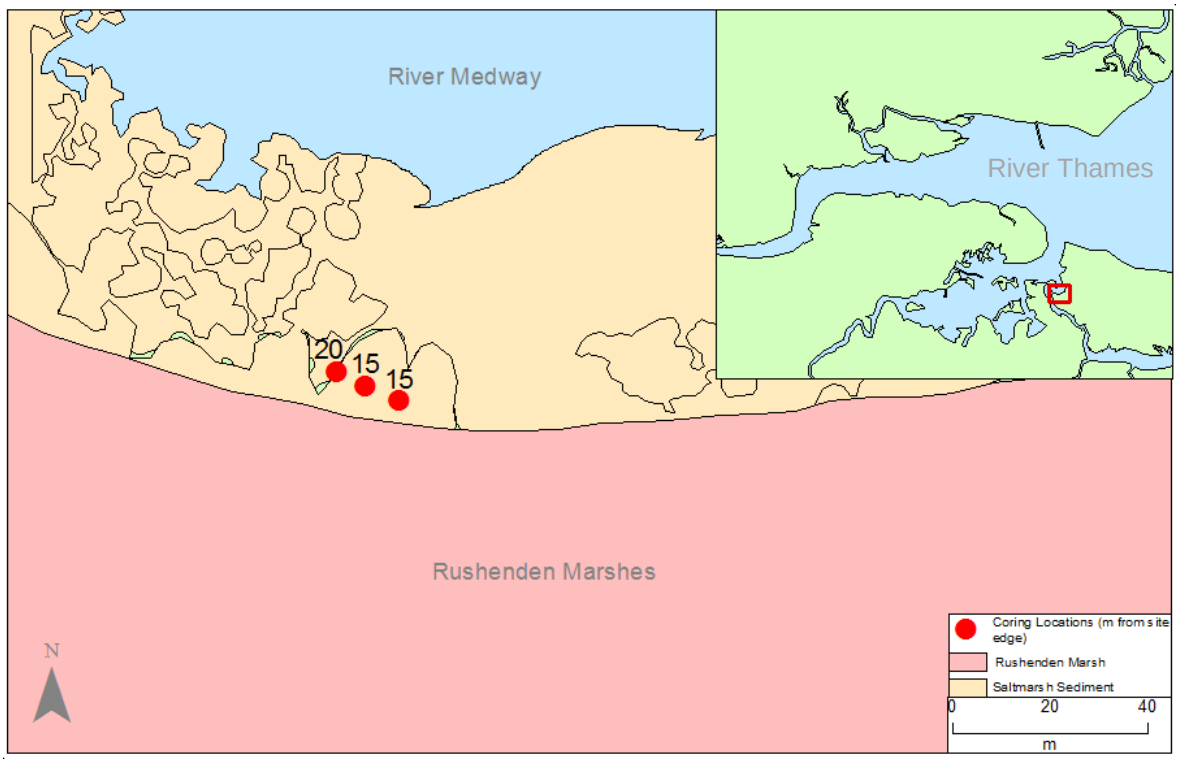

Figure 6.13: Coring locations at Rushenden Marshes. Numbers represent distance from the site edge (in metres).

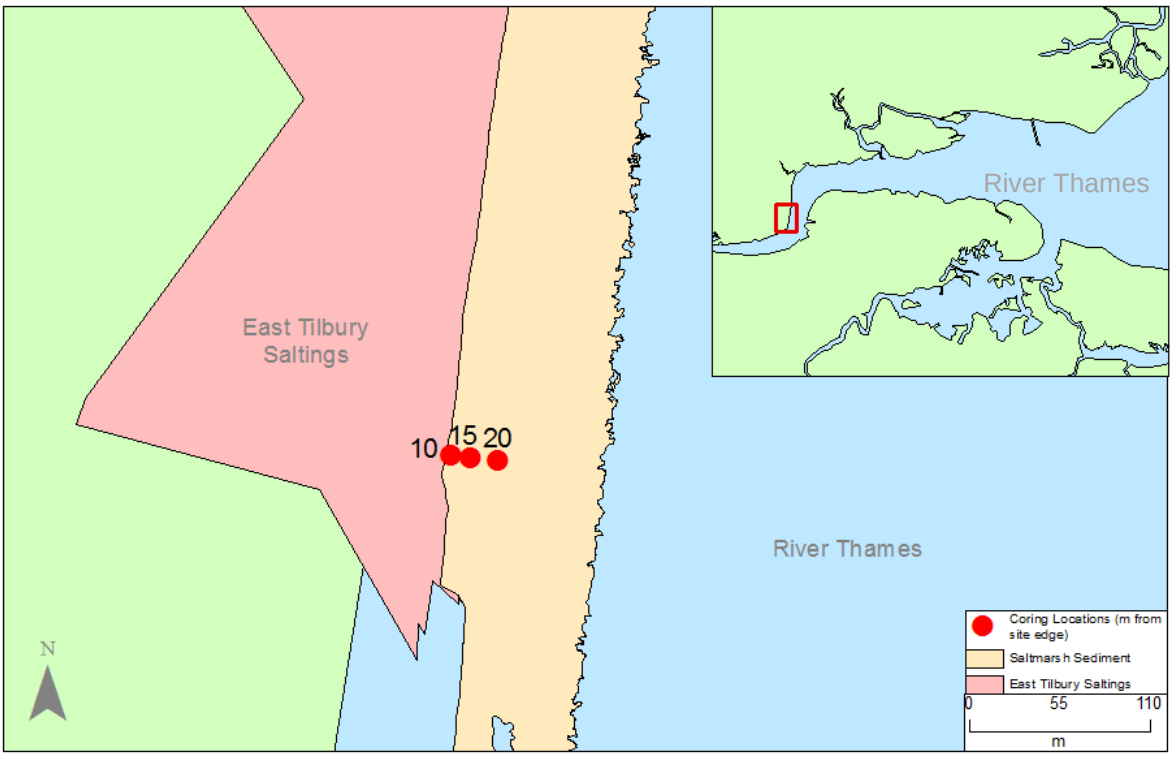

Figure 6.14: Coring locations at East Tilbury Saltings. Numbers represent distance from the site edge (in metres).

6.3. Results

6.3.1. In-situ and Ex-Situ Metal Concentrations

An overview of both qualitative *in-situ* and quantitative *ex-situ* (moisture corrected) sediment metal concentrations are given in Table 6.4.

Table 6.4: Median and range in-situ and moisture corrected concentrations for sediment core heavy metals (mg kg^{-1}). Key to site names: GW Great Wakering, PF Purdy's Farm, HM Hadleigh Marsh, LM Leigh Marsh, WF Westwick Farm, EM Eastcourt Meadows, RM Rushenden Marshes, ET East Tilbury Saltings.

	***In-situ* concentration (mg kg $^{-1}$)**					**Moisture corrected concentration (mg kg $^{-1}$)**				
	Fe (%)	**Mn**	**Pb**	**Sr**	**Zn**	**Fe (%)**	**Mn**	**Pb**	**Sr**	**Zn**
GW	1.7	113	25	76	56	2.6	183	49	138	95
n=48	(0.9-3.5)	(64-249)	(11-68)	(57-93)	(38-130)	(1.8-5.1)	(127-358)	(17-109)	(82-257)	(55-199)
PF	1.5	97	31	63	69	3.0	170	64	108	122
n=62	(0.9-2.8)	(52-163)	(9-117)	(37-130)	(38-201)	(1.2-4.8)	(91-273)	(11-181)	(53-277)	(47-495)
HM	1.3	96	34	53	62	1.7	117	41	67	75
n=63	(0.4-2.6)	(65-286)	(9-127)	(33-93)	(30-164)	(0.5-3.0)	(73-372)	(12-142)	(38-110)	(36-207)
LM	1.3	103	31	74	62	1.6	126	37	89	70
n=63	(0.9-2.0)	(56-171)	(9-303)	(42-100)	(22-310)	(1.1-2.6)	(74-202)	(11-384)	(54-132)	(29-403)
WF	1.1	88	36	60	54	1.5	123	53	80	72
n=63	(0.7-1.8)	(61-168)	(10-251)	(37-89)	(43-145)	(0.7-2.5)	(78-228)	(12-335)	(39-137)	(37-282)
EM	1.2		18	54	46	2.7		34	105	89
n=32	(0.9-1.7)		(8-69)	(26-97)	(29-111)	(1.5-5.9)		(17-152)	(80-213)	(48-251)
RM	1.6	138	14	57	47	3.1	196	26	103	86
n=53	(0.4-3.4)	(66-498)	(5-57)	(29-371)	(20-63)	(1.4-9.2)	(109-756)	(11-186)	(74-623)	(42-207)
ET	1.3	155	41	83	70	2.9	333	96	175	159
n=63	(0.3-2.8)	(55-438)	(8-165)	(24-128)	(35-154)	(1.6-4.7)	(130-635)	(14-271)	(90-297)	(59-419)

In-situ concentrations for each element show lower median values within each site, further clarifying the impact of moisture content on XRF measurement accuracy (Figure 6.15). However, these *in-situ* data provided indicative information on metal concentrations within the sediment cores, informing the sampling strategy, demonstrated within Figure 6.16, which shows both *in-situ* and moisture corrected data illustrating Pb elevations at depth within a sediment core.

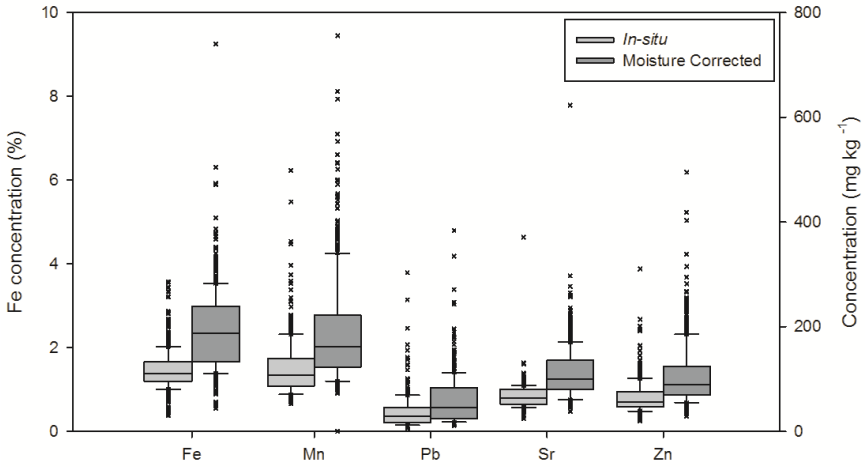

Figure 6.15: In-situ and moisture corrected concentrations. In-situ measurements show systematic underestimation of all elements (Mn was not measured at Eastcourt Meadows).

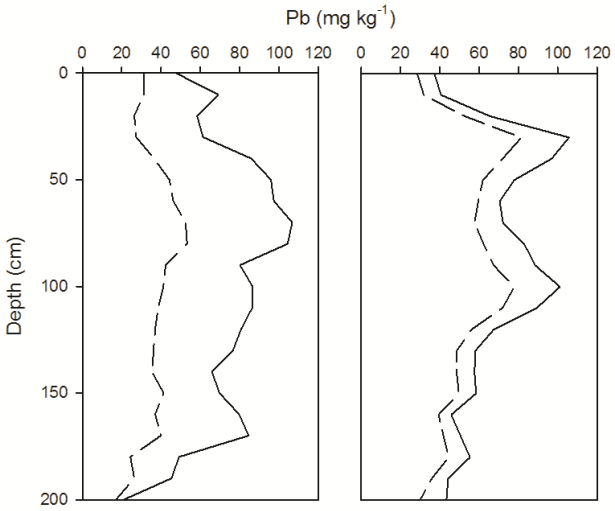

Figure 6.16: Examples of In-situ (dashed) and moisture corrected (solid line) concentrations from Purdy's Farm (left) and Leigh Marsh (right) used to inform on-site sampling decisions.

Within moisture corrected data, median Fe concentrations were lowest at Hadleigh Marsh, Leigh Marsh and Westwick Farm. Median Mn concentrations were also lowest at these sites, although there was much less variability in the magnitude of the concentrations. Likewise, the site with the highest Fe concentration (RM) also corresponded to the highest Mn concentration. Median Pb concentrations were relatively uniform throughout the sites, however East Tilbury showed a higher median concentration and Leigh Marsh showed the highest maximum concentration. Sr concentrations were similar with the exception of Hadleigh Marsh, Leigh Marsh and Westwick farm, which showed lower concentrations. Zinc and Pb showed similar patterns, with East Tilbury recording the highest median concentration for both metals, however, the highest concentrations were recorded at Purdy's Farm and Leigh Marsh for Zn and Pb respectively.

6.3.2. Vertical Metal Distributions (Moisture Corrected Data)

Vertical profiles are shown in Figures 6.17 to 6.24.

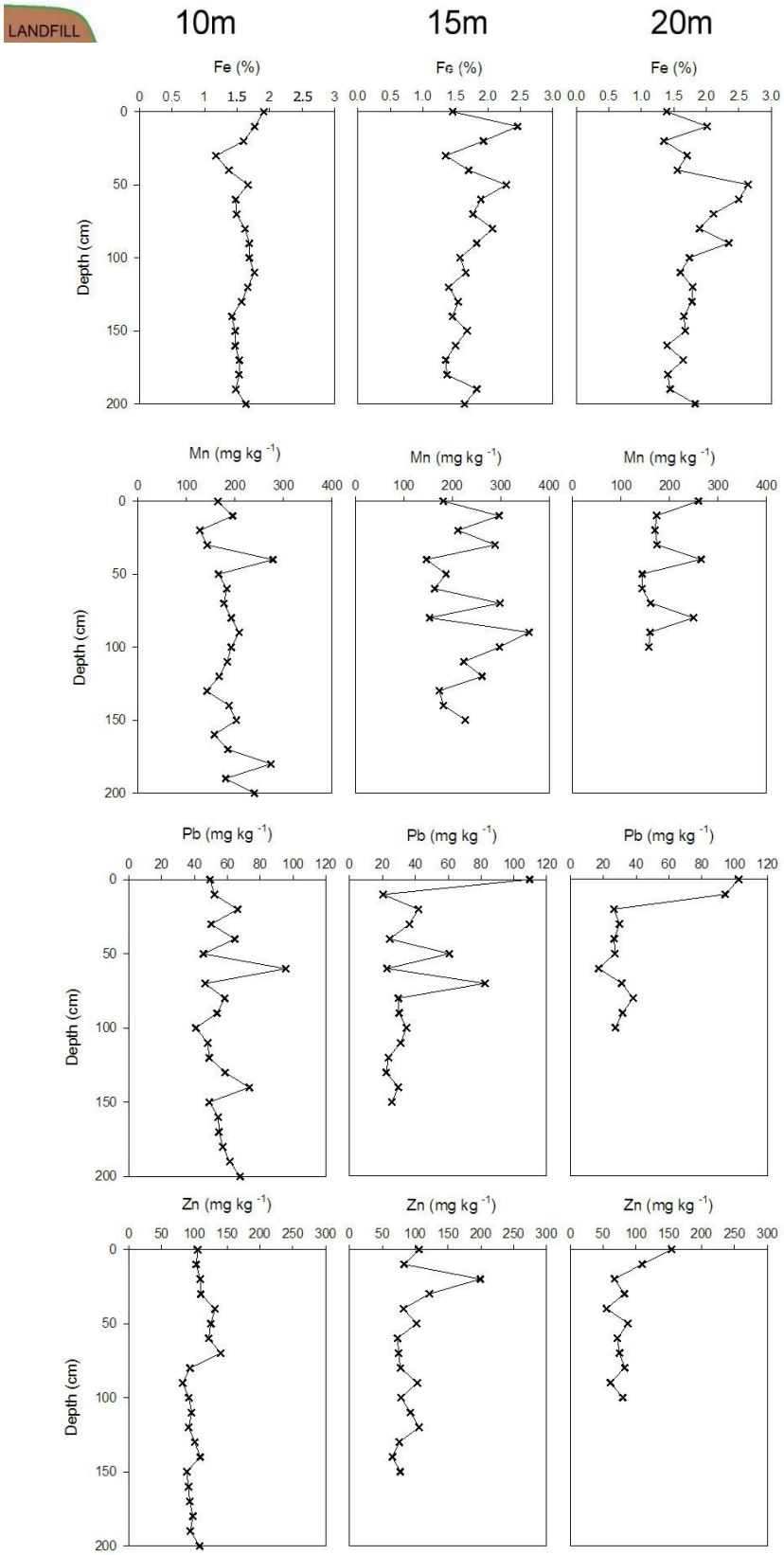

Figure 6.17: Quantitative Fe, Mn Pb and Zn concentrations (mg kg $^{-1}$) from Great Wakering (Industrial, Commercial, Household waste).

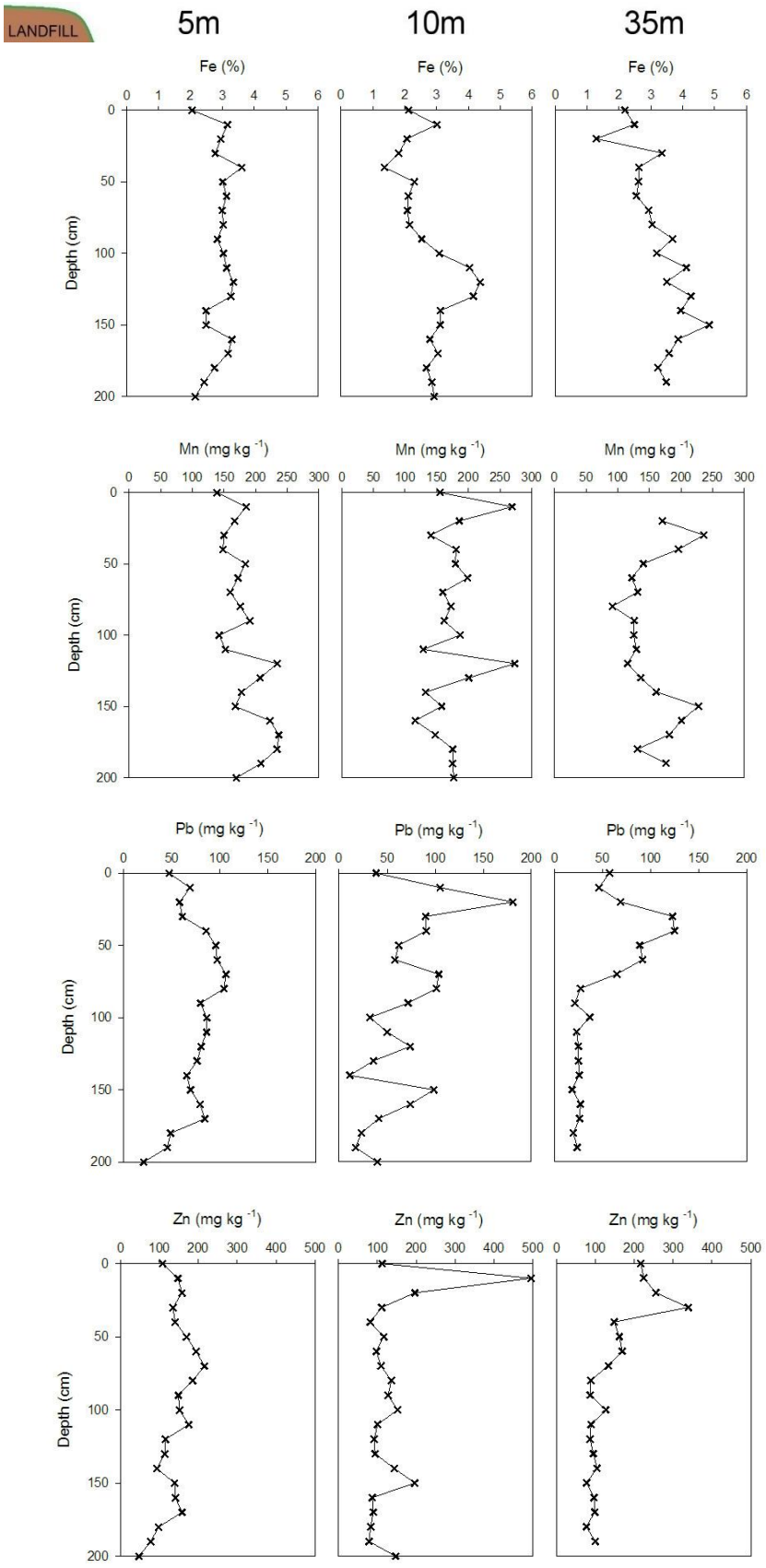

Figure 6.18: Quantitative Fe, Mn, Pb and Zn concentrations (mg kg $^{-1}$) from Purdy's Farm (Industrial and Household waste).

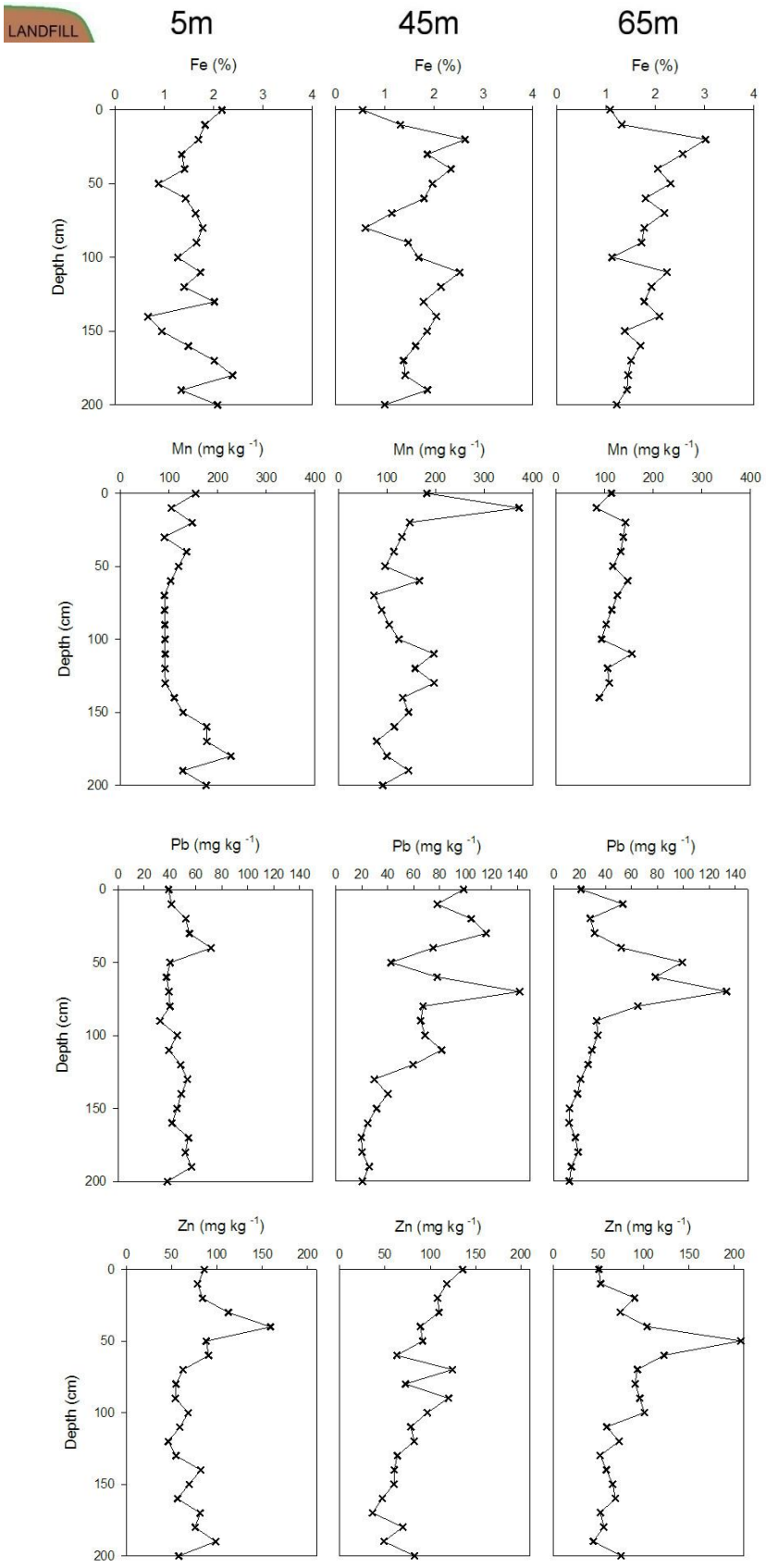

Figure 6.19: Quantitative Fe, Mn, Pb and Zn concentrations (mg kg $^{-1}$) from Hadleigh Marsh (Commercial and Household waste).

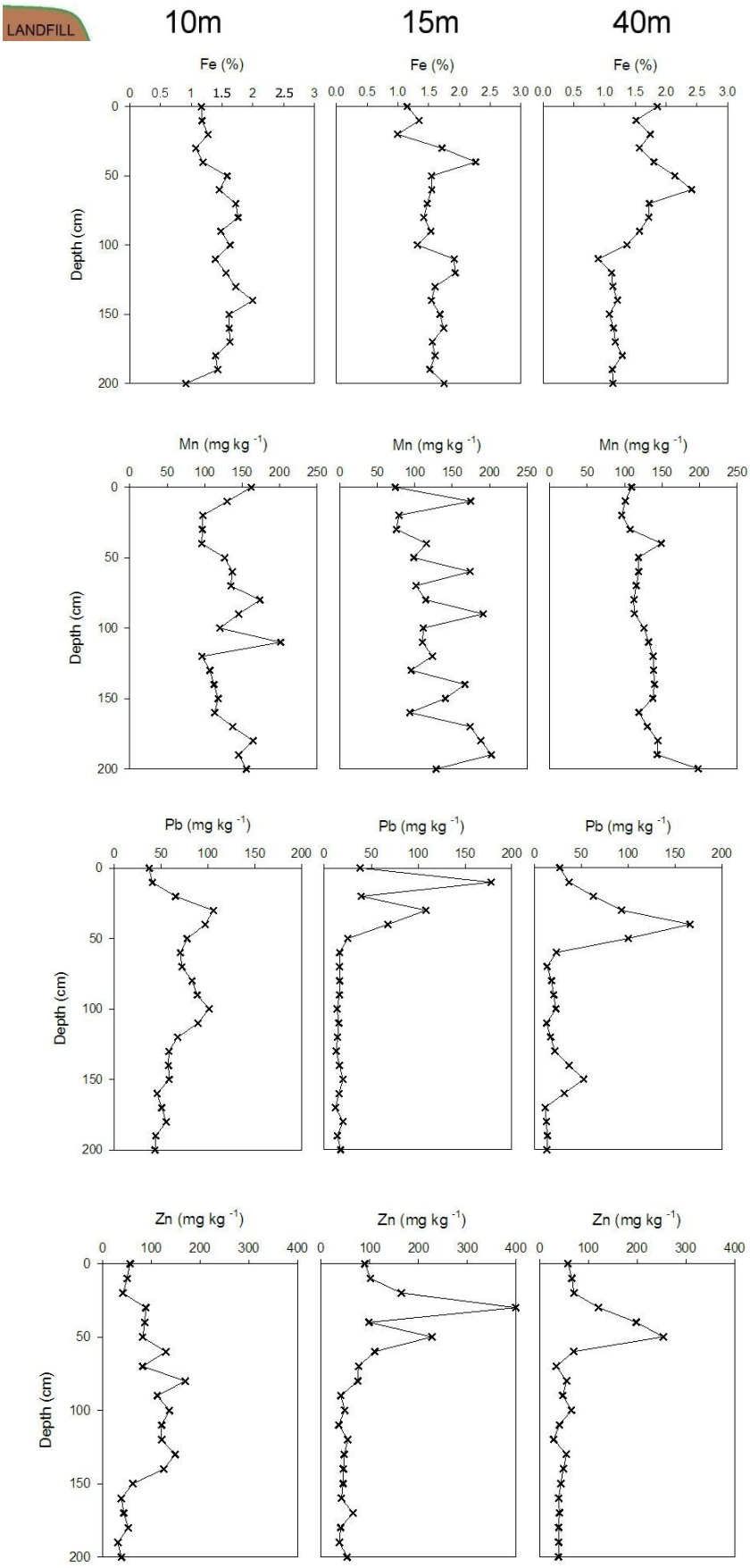

Figure 6.20: Quantitative Fe, Mn, Pb and Zn concentrations (mg kg $^{-1}$) from Leigh Marsh (Industrial, Commercial, Household waste).

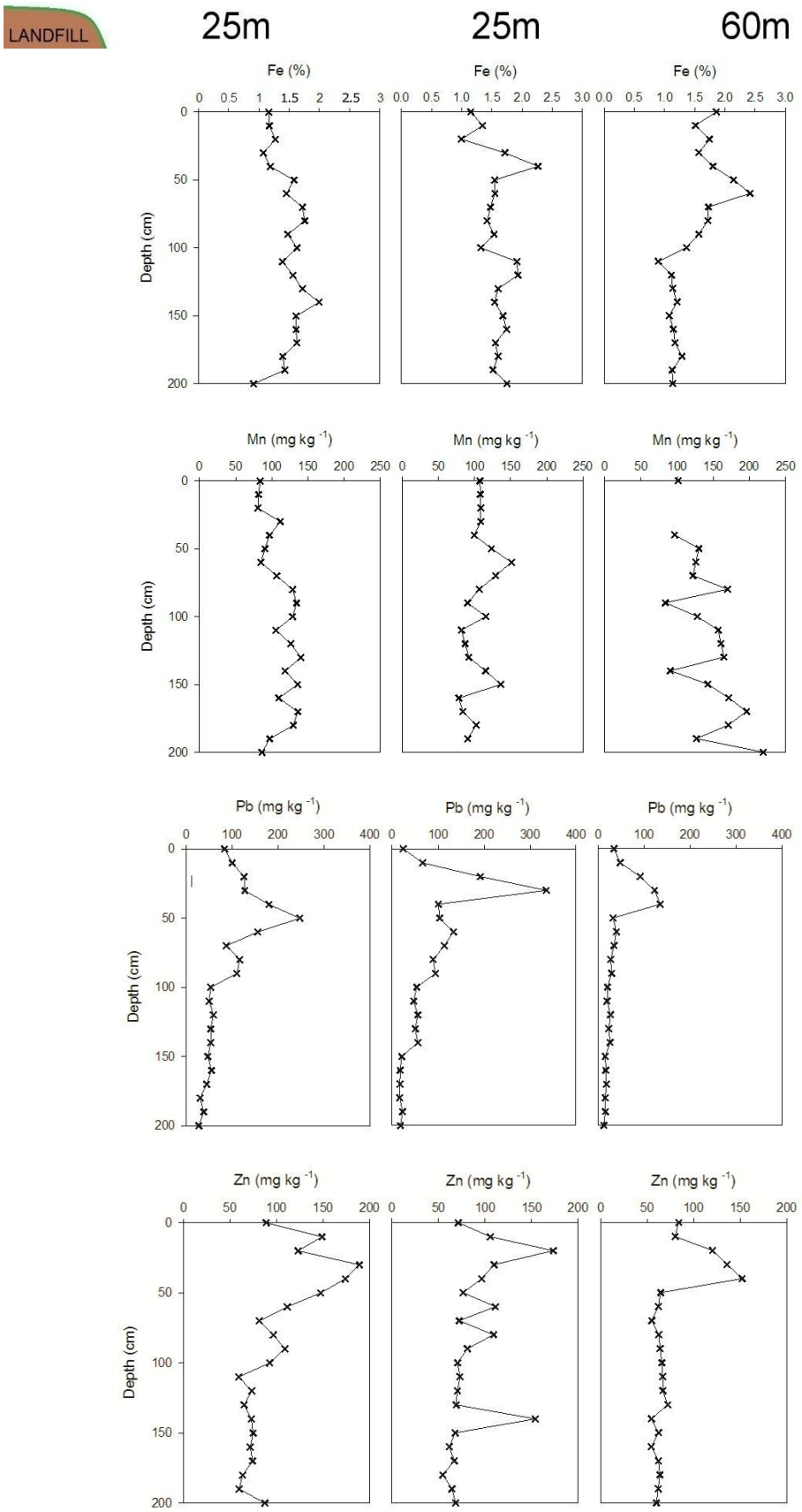

Figure 6.21: Quantitative Fe, Mn, Pb and Zn concentrations (mg kg $^{-1}$) from Westwick Farm (Industrial, Commercial, Household waste).

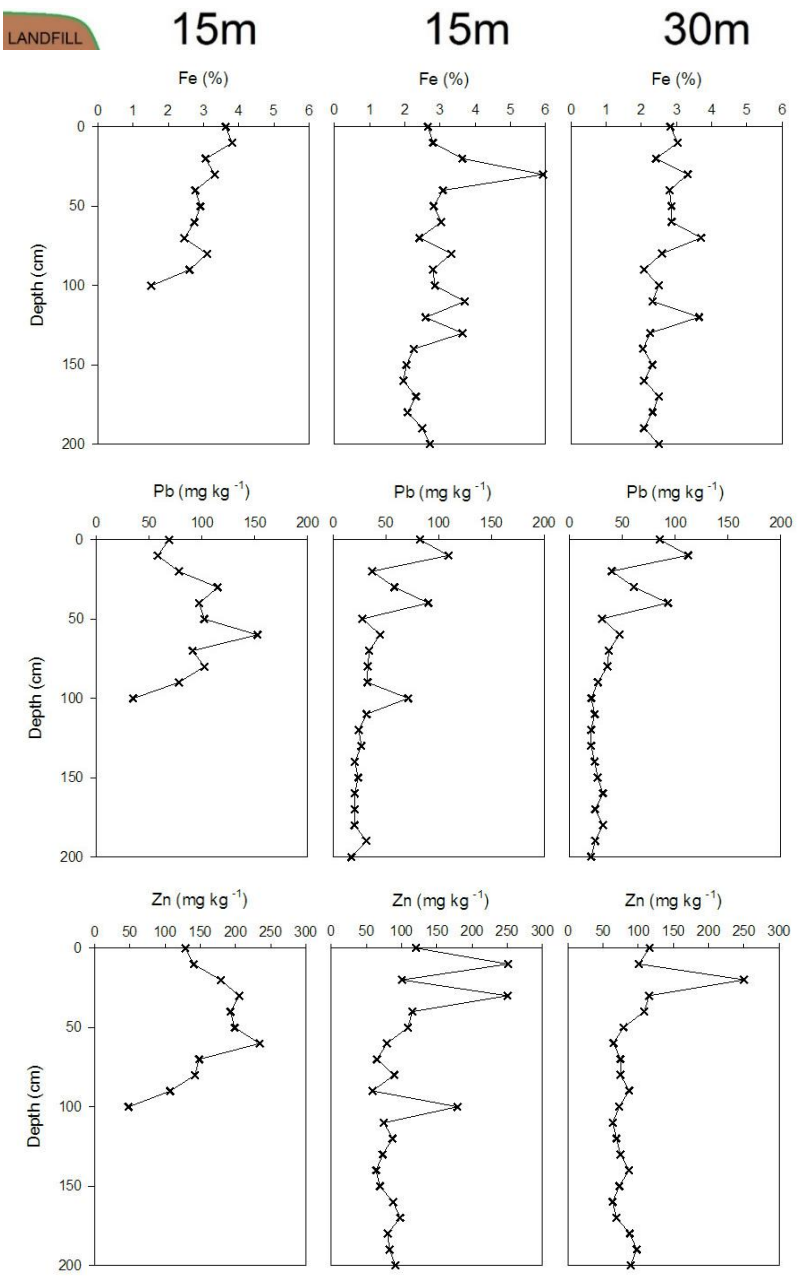

Figure 6.22: Quantitative Fe, Pb and Zn concentrations (mg kg $^{-1}$) from Eastcourt meadows (Inert waste).

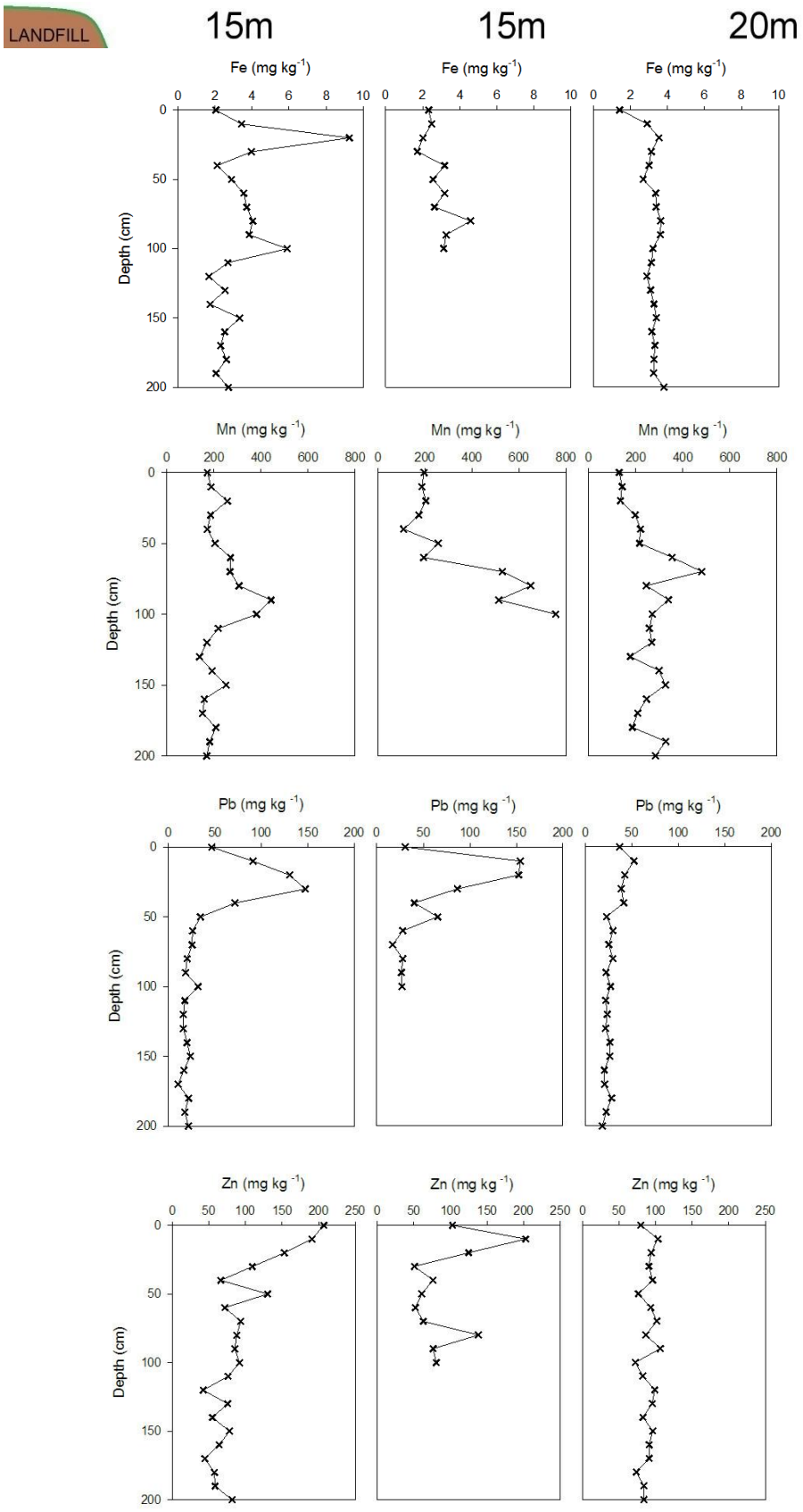

Figure 6.23: Quantitative Fe, Mn Pb and Zn concentrations (mg kg $^{-1}$) from Rushenden Marshes (Inert waste).

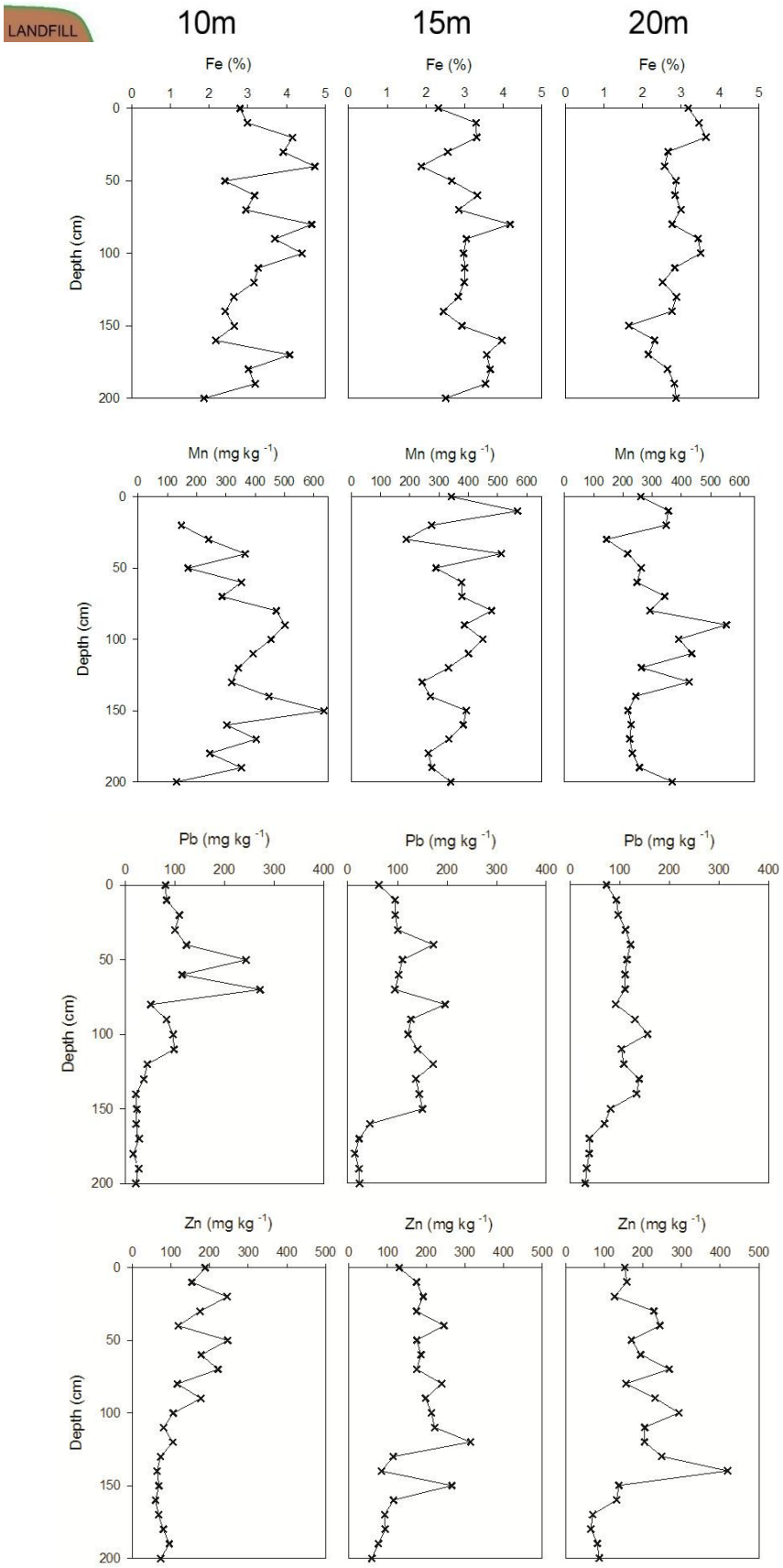

Figure 6.24: Quantitative Fe, Mn, Pb and Zn concentrations (mg kg $^{-1}$) from East Tilbury Saltings (Inert waste).

Hazardous Landfills: Industrial, Commercial and Household Waste

Great Wakering

Fe and Mn concentrations vary both with depth and between cores but do not show any consistent trends. Both Pb and Zn concentrations are elevated in the upper 15 cm of cores collected at 15 and 20 m, whilst Pb shows a steady increase with depth (> 100 cm) in the core collected nearest the landfill boundary (10 m). This trends is not observed within the 15 m cores.

Purdy's Farm

Fe and Mn concentrations are highly variable, yet Fe shows a general increase at 10 and 35 m. Pb shows broad peaks (between 30 and 70 cm) at 35 m, yet shows a decrease at depth to c. 20 mg kg^{-1}, whereas the cores at 5 and 10 m distance show higher concentrations at depth. Zn concentrations show sharp peaks (10-30 cm) in the most distal cores (10 and 35 m) and slow low concentrations at depth.

Hadleigh Marsh

Fe concentrations are highly variable, showing increases at 30 and 120 cm in the distal cores (45 and 65 m), whilst the 5 m core shows no trend with depth. There are no consistent trends with Mn, as the close (5 m) and distal (65 m) cores show consistent concentrations whilst the 45 m core shows elevated levels in the near surface (< 20 cm). Pb shows a trend at 45 and 65 m, with concentration elevations from c. 20 cm to 100 cm depth. Below this, concentrations are low (c. 20 mg kg^{-1}). At 5m, there is a little peak (40 cm depth), however concentrations at the base are higher (c. 60 mg kg^{-1}). Zn concentrations show little trend, with the 5 and 65 m cores showing subsurface peaks <50 cm depth, whilst at 45 m, there is a general decrease with depth.

Leigh Marsh

Fe concentrations show subsurface (< 50 cm) fluctuations in all cores and consistency at depth (1.5-2 %). Mn within all cores show a general trend of increasing concentration with depth, with slightly erratic measurements within the 15 m core. At 15 and 40 m, Pb shows a sharp peak (> 150 mg kg^{-1}) before returning to a low concentration at depth. At 10 m, the Pb peak is much broader, resulting in elevated concentrations to the base of the core. Zn shows a similar trend to Pb, however the elevations at depth in the 10 m core only extend to 150 cm depth.

Westwick Farm

Fe and Mn concentrations show a consistent trend, however, at 60 m, there is slight subsurface (c. 50 cm) enhancement and Mn increases with depth. Pb shows a subsurface

peak in all cores (c. 50 cm) reducing to lower concentrations with depth. Zn shows much broader subsurface peaks, with all cores reaching a flat, low concentration below 110 cm.

Inert Landfills

Eastcourt Meadows

Fe concentrations at 15 and 30 m show a general consistency, however one of the 15 m core showing reduction with depth. Pb concentrations at 15 and 30 m show a general trend of reduction with depth, which is also shown within the Zn data, albeit with higher magnitude subsurface peaks (250 mg kg^{-1}).

Rushenden Marshes

Fe concentrations show little trend, with the 20 m core showing an increase over the top 50 cm and then stable with depth. The close cores show an erratic distribution throughout. Mn within all cores shows a slight increase with depth, however, one of the 15 m cores remains constant. At 15 m, both cores show sharp Pb peaks and a reduction at depth. The 20 m core shows consistent concentrations with depth. At 20 m, Zn remains constant, however the 15 m cores show reductions from high surface /sub surface concentrations below 50 cm.

East Tilbury Saltings

All cores show erratic Fe concentrations, indicating no trend. This is also shown in the Mn data, with only the 10 m core showing increased concentrations at the base of the core. At 15 and 20 m, Pb shows consistent concentrations, with a slight elevation c. 100 cm depth. There is a distinct peak at 50 cm in the closest core (10 m). Zn shows slight increases with depth in the 15 and 20 m cores, however the 10 m core shows little trend, with low concentrations at the base.

In all sediment cores at potentially hazardous sites, Fe and Mn show variable trends with both distance from the site and depth, however consistent patterns cannot be easily distinguished. Pb and Zn concentrations generally show broad or sharp peaks in the upper sediment layers (10-50 cm). At Great Wakering, Purdy's Farm, Hadleigh Marsh and Leigh Marsh, Pb concentrations decrease in the cores collected closest to the landfill boundary. This can also be observed for Zn at Hadleigh Marsh and to a lesser extent Leigh Marsh. The site which does not show this pattern is Westwick Farm, however, due to site access, the nearest core was collected at 25 m from the site boundary. Inert sites, however, showed a contrasting pattern. Although Fe and Mn were similarly variable across the sites, Pb and Zn concentrations all decreased with depth and did not show the elevations at depth evident at Great Wakering, Purdy's Farm, Hadleigh Marsh and Leigh Marsh.

6.4. Discussion

6.4.1. Metal Distributions

Fe and Mn showed both low variability (e.g. Eastcourt Meadows), and largely fluctuating concentrations, with distance from the landfill boundary and depth (Purdy's Farm and Hadleigh Marsh). The fluctuations are likely a result of diagenetic remobilisation within the sediment column, resulting in the subsurface (c. 120 cm) elevations of Mn at Purdy's Farm and Fe at Hadleigh Marsh and Leigh Marsh (c. 100 cm). This is due to the precipitation of (hydr)oxides in the upper oxic layers of the sediment (Van Cappellen and Wang, 1996). This was also evident at inert sites, with Rushenden Marshes showing elevated Fe concentrations within near surface sediments. Fe and Mn distributions at East Tilbury Saltings showed no trend either with distance or depth, suggesting the sediment has been disturbed, possibly through bioturbation (Burdige, 1993). No sedimentation rates were calculated; therefore, any disturbance or erosional episodes are unknown.

The distribution of elevated trace metal concentrations provide the most valuable information regarding impacts due to human activity. With the exception of East Tilbury Saltings, all sites show subsurface (< 50 cm depth) peaks of Pb and Zn. The elevations are likely a record of historic industrial sediment inputs (Fox *et al.*, 1999), with the peaks corresponding to the onset of heavy industrial activity in the 19th Century (Valette-Silver, 1993). The peaks occur at different depths at different sites, and in the absence of sedimentation data, a sensible average sedimentation rate was assumed at around 0.2 cm^{-1} a^{-1} (Table 6.5). Although this must be used with caution as sedimentation is highly variable even within a site, this value would result in peaks corresponding to periods of high levels of industrial activity, suggesting industrial discharges as the source (Table 6.6). East Tilbury Saltings did not show any clear peaks, further suggesting either erosion or bioturbation of sediments.

Table 6.5: Sedimentation rates for local study sites. (1) Spencer et al. (2003), (2) O'Reilly Wiese et al. (1997b), (3) Sheldon (1968).

Catchment	Accumulation Rate	Method
Medway$_1$	0.23 cm^{-1} a^{-1}	^{210}Pb and ^{137}Cs
Thames$_2$	0.20 cm^{-1} a^{-1}	Sounding Survey
Roach$_3$	0.20 cm^{-1} a^{-1}	Subsidence proxy

Table 6.6: Approximate peak depth from each landfill site.

Site	Depth of Peak
Great Wakering	25 cm
Purdy's Farm	25 - 40 cm
Hadleigh Marsh	40 - 50 cm
Leigh Marsh	50 cm
Westwick Farm	50 cm
Eastcourt Meadows	25 cm
Rushenden Marshes	25 cm
East Tilbury Saltings	n/a

Within a number of cores, such as the distal cores at Great Wakering, Purdy's Farm, Hadleigh Marsh, Leigh Marsh, and all three cores at Westwick Farm, Eastcourt Meadows and Rushenden Marshes, concentrations below the industrial peak reduce with depth, reaching an assumed geochemical background level between approximately 70 and 100 cm depth. It is likely that this plateau represents sediments deposited around 1600, a period of low global industrial activity (Renberg *et al.*, 2001). This concentration reduction is common place within sediment contamination analysis (Grousset *et al.*, 1999; Miller *et al.*, 2014; Allan *et al.*, 2015) and was also evident within the distal cores at Newlands (Chapter 4, Section 4.5.5).

At Great Wakering, Purdy's Farm, Hadleigh Marsh and Leigh Marsh, all sites where potentially hazardous waste was deposited, Pb, and to a lesser extent, Zn concentrations within the core most proximal to the landfill boundary do not show the same characteristic decrease with depth. This is also reflective of the findings within Chapter 4, where Pb and Zn concentrations at depth exclusively within the core closest to the landfill boundary represented enrichment of the landfill. Zn concentrations are likely to be less pronounced than Pb at depth as Zn has a weaker binding force and is more diagenetically reactive than Pb, resulting in more post depositional mobility within the environment (Néel *et al.*, 2007). Conversely, Westwick Farm showed little enrichment at depth within any of the cores. Limited site access due to a newly constructed seawall resulted in the nearest core being collected at 25 m from the site boundary. It is likely that the nearest core was therefore situated beyond the spatial extent of the landfill leachate plume (Bhalla *et al.*, 2011).

6.4.2. Enrichment Factors

Enrichment factors (EF's) for the anthropogenic metals Pb and Zn were subsequently calculated using the same method as Chapter 4 (Section 4.5.5). The broad sub-surface Pb and Zn peaks, associated with the onset of heavy industrial inputs (Vane *et al.*, 2011) occur within most sediment cores between c. 0 and 50 cm depth. The sediment deposited below these peaks represent geochemical background concentrations and will have not received contamination from atmospheric or fluvial inputs. Using local sedimentation rates (Table 6.5) any sediment older than 1600, or below 50, 42 and 42 cm for the Medway, Thames and Roach respectively, that contains elevated concentrations must have been impacted by an alternative source and were therefore the focus for enrichment calculations.

For enrichment calculations, using a reference concentration from sediments that are mineralogically, texturally and chemically similar is advantageous, therefore the average concentration from the basal 1 m of each reference (distal) core from each site was used as a background concentration (Abrahim and Parker, 2008), with the exception of Great Wakering, where lowest concentrations in 15 m core were assumed to reflect geochemical background. Enrichment values could then be compared quantitatively (Table 6.7) to assess the anthropogenic contamination present within each sediment core. Table 6.8 shows average enrichment values for the core sections across the eight sites.

Table 6.7: Enrichment value contamination indicators. From Sakan (2009).

Enrichment Level	
< 1	No Enrichment
< 3	Minor
3-5	Moderate
5–10	Moderately Severe
10–25	Severe
25–50	Very Severe
> 50	Extremely Severe

Table 6.8: Median enrichment values for sediment cores from all eight sites (range values shown in brackets).

Site	Pb (Nearest)	Pb (Distal)	Zn (Nearest)	Zn (Distal)
Hazardous				
Great Wakering	2.6 (1.8-4.3)	1.2 (0.8-1.8)	1.7 (1.3-2.1)	2.1 (0.9-1.4)
Purdy's Farm	4.0 (1.4-5.2)	1.0 (0.6-5.3)	1.9 (0.8-2.7)	1.0 (0.6-2.5)
Hadleigh Marsh	0.8 (0.6-2.2)	1.3 (0.7-6.2)	0.8 (0.5-2.4)	1.0 (0.6-2.2)
Leigh Marsh	4.0 (2.6-5.9)	0.9 (0.7-1.4)	2.3 (1.4-3.2)	1.0 (0.7-1.3)
Westwick Farm	4.5 (2.9-21)	2.1 (0-3.2)	1.9 (1.5-4)	2.0 (1.1-3.1)
Inert (control)				
Eastcourt Meadows	0.9 (0.6-2.3)	1.1 (0.5-1.5)	1.0 (0.6-1.8)	0.9 (0.6-1.4)
Rushenden Marshes	0.9 (0.6-1.6)	1.0 (0.7-1.2)	1.0 (0.6-1.3)	1.1 (0.9-1.4)
East Tilbury Saltings	1.6 (0.7-12.8)	4.8 (1.4-6.3)	1.1 (0.6-3.9)	2.6 (0.9-5.8)

Enrichment values for Pb and Zn vary greatly between both site and with distance from the landfill site edge. The highest EF's for Pb were at Leigh Marsh and Purdy's Farm, all from cores nearest the site boundary, whilst the highest values for Zn were at Westwick Farm in the nearest core, and East Tilbury Saltings in the most distal core. A number of enrichment values greater than 5 would classify a number of sites as moderately to severely enriched, however the majority of sites only present minor to moderate enrichment (Sakan, 2009), still potentially hazardous to the environment.

With the exception of Hadleigh Marsh, hazardous sites show higher average enrichment values nearest the site edge compared to the distal cores. Conversely, inert sites show similar values at both the site edge and distal cores, suggesting that the presence of hazardous waste influences sediment contamination surrounding those sites.

Using the non-parametric Mann-Whitney U test, EF values from the core closest to the site edge were statistically compared to the distal core. Non-parametric testing was used due to the prevalence of non-normal data throughout the dataset. The test compared median values against the null hypothesis that multiple groups are statistically similar. Table 6.9 shows the results Mann-Whitney U test of difference.

There was no significant difference in Pb enrichment values between the nearest and the distal cores at inert sites Eastcourt Meadows and Rushenden Marshes (p >0.05), with significant differences present at every other site. Zinc enrichment values showed a slightly different distribution. As well as Eastcourt Meadows and Rushenden Marshes, Hadleigh Marsh and Westwick Farm also showed no significant difference between the nearest and distal cores (p >0.05).

Table 6.9: Testing differences between enrichment values nearest the landfill and the reference core (Mann Whitney-U). H = hazardous, I = inert site.

Site	Pb	Zn
Great Wakering [H]	U = 95, p = 0.001	U = 95, p = 0.001
Purdy's Farm [H]	U = 222, p = 0.000	U = 204, p = 0.004
Hadleigh Marsh [H]	U = 52, p = 0.004	U = 90, p = 0.158
Leigh Marsh [H]	U = 256, p = <0.0001	U = 256, p = <0.0001
Westwick Farm [H]	U = 254, p = <0.0001	U = 138, p = 0.720
Eastcourt Meadows [I]	U = 102, p = 0.678	U = 113, p = 1.000
Rushenden Marshes [I]	U = 95, p = 0.481	U = 76, p = 0.135
East Tilbury Saltings [I]	U = 57, p = 0.008	U = 50, p = 0.003

It is clear that there is a difference in the enrichment between sites that contain inert and potentially hazardous waste. However, compared to other industrially impacted areas (Table 6.10), average sediment concentrations and enrichment factors from all sites are relatively low. This suggests that the contamination potential from this legacy secondary source of pollution is not the major issue for aquatic habitats, however, the number of sites evident within the South East may result in a significant amount of contamination that may potentially be released as a result of climate change.

Table 6.10: Comparative Enrichment Values from other studies. (1) Hamdoun et al. (2015), (2) Chen et al. (2007), (3) Grant and Middleton (1990).

Area	Element	Average Pb Concentration (mg kg^{-1})	Average Enrichment	Classification
English Channel [(1)]	Pb	67	14	Severe
Kaohsiung, Taiwan [(2)]	Pb	55	8	Moderately Severe
This Study	Pb	50	2.9	Minor
Humber Estuary [(3)]	Pb	127	5.8	Moderately Severe

6.4.3. Wider implications and Further Risk Assessment

Environment Agency data suggest a conservative estimate of 20000 unlicensed landfills within England and Wales (Cooper, 2012). Of these 20000 sites, approximately 4000 contain non-inert waste and are located within the Environment Agency Flood Alert Area. The results of this study indicate that sites containing a combination of commercial, household and industrial waste have historically released leachates resulting in contamination of surrounding sediment and that this is likely to be the same for other sites with similar physical and chemical attributes within the UK. The average metal concentrations within the enrichment zones at depth was 60 mg kg^{-1} Pb and 100 mg kg^{-1} Zn. This legacy sediment contamination, hypothesised to be from landfills, is above the threshold effect level for potential to cause ecological harm and if released would be in exceedance of CEFAS action level 1 (CEFAS, 2012), which is used as part of a weight of evidence assessment for dredging material.

This estimation suggests that although the sediment concentration is not severely high, the presence of 50 sites within the Thames estuary and 4000 around the UK coast predicted to flood within the next 50 years (Environment Agency, 2014) suggests that released contamination due to a catastrophic flood event would be at a magnitude of concern. This highlights the extent of the legacy contamination held within our vulnerable coastal sediments, which at present is not formally classified as contaminated land under part IIa of the Environmental Protection Act and as such is not considered within Environmental Impact Assessments (DCLG, 2015).

Risk Estimation

The classification of risk does not only consider the effects of an identified hazard, but also estimates the probability of that hazard occurring (Lim *et al.*, 2008). For example, within the context of contamination release from landfills, there will be little/no risk if there is no direct connection between the contamination and environmental receptors. It is the formulation and identification of source, pathway and receptor links that forms the cornerstone of environmental risk assessment. The following section proposes a method for classifying the significance of risk from contamination from historic coastal landfills within the UK and presents a risk evaluation for Newlands Landfill, Essex, UK.

These methods are also applicable for risk assessment on a broader national scale, however, to maintain a level of computational and labour feasibility, a tiered, probabilistic approach is required. Such methods are adopted as an industry standard in order to efficiently manage project resources. Approaches such as the DEFRA and EA Management of Land Contamination (DEFRA and Environment Agency, 2004) or Greenleaves III (DEFRA, 2011a) guidelines outline methods for identifying and mitigating risk in ways compliant with UK regulations such as Part IIa of the Environmental Protection Act (1990) or the Habitats Directive (92/43/EEC).

Chapters 4 and 6 concluded that there is contaminated sediment (60 mg kg^{-1} Pb, 100 mg kg^{-1} Zn) within a 15 m limit of the site edge as well as likely to be contaminated with other trace metals and organic contaminants (Schwarzbauer *et al.*, 2002). The initial step in risk assessment would be the characterisation of the site, through the development of a Conceptual Site Model (Table 6.11).

Table 6.11: Example CSM data for Newlands landfill, Essex, UK.

SPR	Hazard Information
Source	Contaminated sediment within the EA flood alert area. Pb = ~100 mg kg^{-1}, Zn = ~ 100 mg kg^{-1}, Hg = ~ 1200 ng g^{-1}.
Pathway	Erosion and redistribution of sediment located within the EA Flood Alert Area (1 in 50 return period).
Receptors	Environmental Receptors - Sediments form RAMSAR site, SSSI, SPA, MCZ. - Adjacent waters are shellfish areas. Human Health Receptors - Leisure users, dog walkers etc. - Unlikely that the water will be used for swimming.

The consequences, or severity of the hazards have to be measured. The data from Chapter 4 suggest that Newlands landfill could impose a negative effect on surrounding sediments, with concentrations of Pb and Zn of ~100 mg kg^{-1}, and Hg of 1200 ng g^{-1}. Utilising the NOAA sediment reference tables (Buchman, 2008), both Pb and Zn exceed threshold levels, classified as medium severity, whilst Hg exceeds the apparent effect threshold, classifying the contamination as high severity. If this data were not available, the figures would be assumed based on research into the waste type (Section 6.1.1.) and other site specific data.

In order to define the significance of the risk, an assessment of the likelihood of the identified hazard occurring, or in this case the erosion and redistribution of sediment-associated contaminants from Newlands, must be undertaken (NIGLQ, 2011). The IPCC reported an average rise in sea levels of 1.8 ± 0.5 mm $year^{-1}$ throughout the 20th Century (IPCC, 2007). This trend is set to continue, with an increased storm energy (Jenkins, 2008) being responsible for a predicted 0.4 m rise by 2100 (Raper and Braithwaite, 2006), further exacerbated by subsidence within the South East (Shennan, 1989). This rise in sea level is likely to result in 'coastal squeeze' with salt marshes migrating landwards, resulting in their erosion (Hughes, 2004), chemical changes in contaminant mobility as a result of the saline intrusion (Speelmans *et al.*, 2007) or sediment oxidation (Neuhold, 2013).

Although, there is no single method for defining or classifying likelihood (Table 6.12), they all have a common aim to define the frequency under which a consequence is likely to occur (DEFRA, 2011a). As Newlands landfill is located within the Environment Agency 1 in 50 year return period flood zone, there is a 50 % chance that the sediments will be flooded and disturbed within the next 25 years. Using the IPCC table (Table 6.12), a 50 % chance is classified as 'More likely than not'. It is important to note that this stage of the assessment is extremely dependent on timescale, as the likelihood of flooding within the next 50 years increases the probability to 'virtually certain'. This illustrates how undertaking risk assessments on different timescales can significantly alter the outcome.

Table 6.12: A comparison of 'Likelihood of consequence occurring' tables from different sources, Defence Estates (2007) and IPCC (2007).

Defence Estates (2007)		**IPCC (2007)**	
Certain	100%	Virtually Certain	>99% probability
Almost Certain	95-99%	Almost Certain	>95% probability
Likely / Probable	55-94%	Very Likely	>90% probability
		Likely	>66% probability
Possible	45-54%	More likely than not	>50% probability
		About as likely as not	33-60% probability
Unlikely	5-44%	Unlikely	<33% probability
		Very Unlikely	<10% probability
Nil Chance	0-4%	Extremely Unlikely	<5% probability
		Exceptionally Unlikely	<1% probability

Once consequences have been defined and a site-based evaluation of the probability of exposure occurring, risk can be estimated. The risk is a function of both the consequence and likelihood (Table 6.13), and is calculated for all identified contaminants, scenarios and timescales that have been flagged as potential to present a threat. At Newlands landfill, over a 25-year time scale, the risk is medium/high, due to the likely chance of erosion and the moderate/severe contamination. Alternatively, over the next 50 years, the risk is high, as the likelihood becomes certain, whilst the consequences remain moderate. This shows how risk is flexible, and a multitude of risk values exist. Various methods are available to categorise and rank these risk scores, such as adopting Analytical Hierarchy Processes to rank site risk based on spatial attributes such as soil permeability, land use and protected areas (Aydi *et al.*, 2013). Additionally, methods have been adopted which measure and rank 'impact factors' from dependent variables, such as exposure routes and toxicity of pollutants (Li *et al.*, 2012).

Table 6.13: An example of an aggregated risk significance table, based on consequence and likelihood categories. From Rudland (2001).

		Likelihood of Consequence Occurring					
		Very Likely / Certain	**Likely**	**Unlikely**	**Very Unlikely**	**Extremely Unlikely**	**No Pollutant Linkage**
Potential Consequence	**Severe**	Very High	Very High	High	Medium	Low	None
	Moderate	High	High	Medium	Low	Very Low	
	Mild	Medium	Medium	Low	Very Low	Trivial	
	Negligible	Low	Very Low	Very Low	Trivial	Trivial	

If this approach was to be used on a national scale, an informed risk threshold would be chosen, and any sites/scenarios that present a risk greater than this would be advanced to the next tier of assessment. There are certain drawbacks with this method, namely the bias influence that similar risk assessors can have if undertaking the method with different expertise, and that outcomes may contradict the initial conceptual model. There are also a multitude of limitations at this point in the method, which may introduce a level of epistemic uncertainty to any calculated risk. It is therefore a requirement that the data are scrutinised at this point by the risk assessor (DEFRA, 2011a).

Sites that have been identified as presenting a risk to their identified receptors above the chosen threshold, would be investigated, with all other sites and scenarios disregarded. At this point, site-specific data collection would be required in order to further assess the magnitude of risk. The aim at this stage would be to evaluate the specific current condition of high risk sites, monitoring and analysing receptors at site level and evaluating options for raising the quality of the site to a level required by current legislation. Common collected data types are shown in Table 6.14, which would also form the basis of an advanced level of assessment.

Detailed cause-effect attribution modelling is the most resource intensive step of the assessment in terms of both time and cost. Usually focusing on ecosystems, multiple lines of evidence would be drawn together to evaluate the presence and effect of a hazard (Energy Institute, 2013). This stage of assessment will only usually be undertaken if great losses are at stake, or if the level of risk is severe, however, detailed analysis will commonly lead to a clearer outcome as to the available options for remediation.

Table 6.14: Examples of data collection requirements for a site-specific risk assessment. From the Energy Institute (2013).

Element	Data Requirements	Example Methods
Source	- Partitioning into pore water - Bioavailability	- Pore-water sampling
Fate and Transport Pathway	- Flux of contaminant from sediment to water column - Bioavailability - Erosional areas	- Seepage meters - Aquatic organism testing - Photography
Exposure Pathway	- Waterway use patterns - Food chain routes of exposure.	- Exposure survey - Trophic level survey
Receptor	- Types of human receptors - Specific aquatic organisms.	- Land use survey - Bioassays

6.4.4. Application of GIS and in-situ XRF for rapid screening of coastal landfill contamination.

The ability to obtain quantitative data using XRF, as shown in both Chapter 5 and previous studies (Radu and Diamond, 2009; Weindorf *et al.*, 2013), can rapidly generate large amounts of site specific contamination data. However, as the majority of contaminated land investigations depend on time intensive site selection and characterisation, the efficiency and overall applicability of such a rapid method diminishes. The site selection method adopted within this study was undertaken with set objectives, to use secondary data in order to rapidly select sites based on the findings from a previous study (Chapter 4). The contamination extent shown at Newlands, was conceptualised (Figure 6.27), allowing sites to be chosen based on these findings. This allowed sites to be disregarded that were not valid based on either location or waste age. Adopting a GIS method permitted large volumes of spatial data from various sources to be managed and analysed (Şener *et al.*, 2006; Nas *et al.*, 2010), allowing rapid analysis of otherwise time-consuming methods (Zamorano *et al.*, 2008). As all of the data were freely available through the Environment Agency data store, the method showed effectiveness as a cost effective site selection tool.

The combination of the GIS based site selection methodology with XRF site analysis allowed rapid contamination screening to be undertaken. The ability to observe screening level data *in-situ* permitted a rapid understanding of the contamination distribution, informing the field campaign to be undertaken with efficiency. This method was shown to be successful at both rapidly identifying and prioritising sites presenting the most hazard, a task which is critically important considering the vast number of sites within the UK which need to be investigated, with finite time and monetary resources.

6.5. Conclusion

This chapter has presented a novel method for the classification of contamination across the broad scale, using both a site selection based on a previous intensive site investigation and *in-situ* analytical methods. The work has outlined the efficiency with which broad scale field investigations can be planned and the speed of data collection and processing. In addition, the XRF method (introduced in Chapter 5), provided rapid data acquisition, allowing data to be scrutinised, and *in-situ* decisions to be made. The ability to analyse a standard suite of heavy metals such as Pb and Zn, whilst also obtaining redox sensitive elements Fe and Mn allowed a thorough understanding of the contamination at each site.

There were, however, limitations of undertaking broad scale analysis in this way, as the XRF methodology is quite restricted in terms of which elements can be accurately measured and limits of detection, potentially overlooking other contaminants of concern. However, the method is effective for use as a rapid way of identifying sites and their contamination status, to further inform more conventional geochemical analysis campaigns.

This study has demonstrated that historic landfill sites containing industrial, commercial and household waste within the South East present a legacy of contamination and a diffuse source of pollution that has not been previously identified or quantified, despite these sites being closed for up to 30 years. Although levels of enrichment are relatively low, the erosion and subsequent redistribution of contamination from historic landfills within England and Wales could potentially release contaminated sediments to the estuarine environment under future climate change scenarios. This requires consideration within both coastal management and Shoreline Management Plans, and the environmental impact assessment of historic coastal landfills.

Chapter 7 Summary and Further Research

This research has identified and quantified metals present within coastal sediments in South East England, identifying for the first time, that historical landfills have left a legacy of contamination in the coastal zone. Landfilling has been the primary, low cost method for waste disposal for many years (Hübner, 2010), and as a result there are over 5000 historical landfill sites within the 1 in 50 year flood zone in the UK (Environment Agency, 2014). This study examined nine of these sites in South East England and determined that unlined historical landfills receiving industrial, commercial and household waste had contaminated adjacent salt marsh sediments with a suite of metals. These sediments are now secondary sources of contamination and have the potential to present an environmental hazard under current climate change scenarios. Although not examined in this study, this suggests that some historical landfills in the UK with similar physical and chemical attributes in similar environments, may have contaminated adjacent fine-grained sediments and this presents a significant, yet currently unidentified and unquantified source of diffuse pollution in the coastal and estuarine environment. In order to adequately manage these historical landfills and the coastal zone under future scenarios of climate change there is now a need to assess the extent of this contamination and the potential risks associated sediment erosion and re-working. This chapter provides a brief overview of all research objectives, synthesizing the empirical findings and suggesting where further work is warranted.

7.1. Overview of Research Aims and Objectives

Aim: To establish whether Newlands Landfill has created a legacy source of contamination (Chapter 4)

This research was undertaken to establish whether historical coastal landfills had contaminated surrounding sediments, presenting a hazard to the surroundings. Newlands Landfill was chosen based on waste age, as metals are released in leachate during acetogenic degradation soon after initial deposition (Williams, 2005), and due to its proximity to fine-grained coastal sediments which would have aided natural attenuation. Surface samples were collected to establish whether there was any evidence of surface leachate breakout, whilst sediment cores were collected to investigate contamination within the attenuation zone adjacent to the landfill. Sediment metal concentration data, together with physicochemical parameters (pH, LOI, grain size) were measured.

To assess the magnitude of metals within sediments and establish whether they pose an environmental threat.

Both surface sediments and sediment cores collected from the adjacent salt marsh were compared to data from other industry impacted estuaries, and marine sediment quality guidelines. Trace metal concentrations within surface samples were comparable to other industrially impacted estuaries (e.g. Mersey), and maximum concentrations of Cr, Cu, Mn, Ni and Pb exceeded the Probable Effect Level (PEL), suggesting that the sediments may present an environmental threat to local ecology (Buchman, 2008).

Metals at depth in sediment core samples were within a similar range to other industrialised estuaries e.g. the Pearl Estuary, China, with median Co, Hg, Ni, Pb and Zn concentrations exceeding the marine sediment PEL, with the median Hg concentration of 1258 ng g^{-1} exceeding the 700 ng g^{-1} PEL. Consequently, there may be a potential threat to the local ecosystem from contamination present within salt marsh sediments adjacent to Newlands landfill.

To understand the spatial distribution, potential source and behaviour of metals in the sediment.

Spatial distribution mapping showed that surface contamination was not a result of the adjacent landfill. Trends did not show a typical decline from the landfill edge, suggesting that the source of contamination was likely a combination of current and historical point sources, such as the proximal marina, sewage treatment works and atmospheric deposition, or a reflection of present day surface water quality, due to the depositional nature of salt marshes. Observing the spatial pattern of surface contamination in this way, justified investigating the behaviour and distribution of metals within the sediment cores in attempt to identify landfill contamination.

PCA, inter-elemental correlations and down core profiles were used to investigate the controls and behaviour of metals within the salt marsh sediment cores. Major elements, Al and Mg showed little variation with either depth or distance from the landfill edge, suggesting uniform mineralogy across the site, whilst Na and K were likely present within sediments due to influx of saline water / mineral elements. Vertical variations in Ca, Fe and Mn were due to post depositional diagenesis. The trace metals Co, Ga and V, were correlated with major elements (from PCA) suggesting their input was from a mineralogical source. The metals Cr, Cu, Ni, Pb and Zn exhibited sub-surface enrichment (< 50 cm depth), likely due to industrial activity. However, Pb and Zn concentrations were enriched (EF> 2) at depth (> 100 cm) in pre-industrial sediments within the core closet to the site boundary, suggesting metal rich leachates from the adjacent landfill as the source of contamination. Although the enrichment levels were not as high as surface samples, the landfill has produced a

previously undiscovered contamination load of approximately 1200 kg Pb and 1650 kg of Zn within the coastal zone.

Aim: To assess whether in-situ XRF analysis can be used to generate rapid, accurate and precise sediment contamination data within coastal sediments suitable for onsite investigations (Chapter 5).

Sample moisture results in X-ray suppression resulting in underestimations of concentration within wet samples and hence this may be problematic for its *in-situ* application in coastal and wetland environments where moisture content is high and variable. Therefore, laboratory and field assessments were undertaken to provide a method for the generation of accurate field XRF data. The effect of moisture content on data accuracy was investigated using certified laboratory samples and the moisture correction method was validated using field samples taken from Newlands salt marsh. These samples were analysed *in-situ* prior to *ex-situ* laboratory analysis and moisture content correction in order to compare the data.

To examine the influence of moisture content on X-Ray suppression and determine a moisture correction factor that can be applied to field wet in-situ sediment samples.

Arsenic, Cu, Fe, Mn, Pb, Sr and Zn all showed a similar, linear X-ray suppression response to increasing sample moisture. XRF moisture content corrections have been demonstrated previously for single elements (Shuttleworth *et al.*, 2014) or over narrow moisture content ranges (Ge *et al.*, 2005). However, this research demonstrates that using corrections based on gravitational moisture content, accurate elemental recoveries can be achieved for As, Fe, Pb, Sr and Zn, for moisture contents between 0 and 90 %. This expanded range of both recoverable elements and moisture contents suggests that the method could be applied to a wider range of scenarios.

To examine the accuracy of in-situ sample moisture measurements.

As XRF methods can generate accurate *in-situ* data if sample moisture is known, there is a great advantage in being able to also measure sample moisture *in-situ.* Theta probe measurements were taken in the field and compared to gravitational (oven drying) results within the laboratory. There was no correlation between theta probe and gravitational oven drying data due to varying pore water salinity and/or sediment texture/shape and/or temperature in the field. Therefore, in the absence of suitable methods for *in-situ* moisture content measurement, analysis requires the use of oven drying to provide accurate data. Despite the requirement of laboratory based moisture content measurement, XRF analysis still provides the advantage of reduced analytical complexity, resource cost and risk of contamination with only having to undertake oven drying within the laboratory.

To determine whether moisture corrected in-situ XRF analysis provides analytically accurate data for a range of metals, in comparison to ex-situ ICP-OES analysis.

To determine whether moisture corrected *in-situ* XRF analysis provides analytically accurate data XRF data were compared to data derived from Aqua Regia extraction and ICP-OES analysis. The relationships for Fe and Zn were definitive, however the relationships for Pb and Sr were only quantitative probably due to the different sediment fractions measured by each method or analytical interferences within the ICP-OES. Nevertheless, *in-situ* XRF analysis, with ex-situ sample moisture measurement can be used effectively in salt marsh sediments for the measurement of Fe, Pb, Sr and Zn and was adopted for use within the broad scale study.

Aim: To investigate whether historic contaminant release from Newlands landfill and resultant contamination of surrounding sediments is representative of other sites in SE England (Chapter 6).

Chapter 4 identified that the natural attenuation of metal rich leachates by fine-grained salt marsh sediments has left a legacy of contamination in sub-surface sediments adjacent to Newlands historical landfill. To investigate whether this a wider regional issue, and whether Newlands is representative of other landfill sites, a broad scale investigation was undertaken. Historical landfills were selected using GIS based criteria, and sediment cores extracted and analysed *in-situ* using XRF before being returned to the laboratory for the analysis of moisture content.

To identify potentially hazardous historical landfill sites using publicly available secondary data.

The contamination profiles from landfills containing only inert wastes were different from sites containing a combination of either commercial, industrial or household (hazardous) wastes. A comparison between the downcore enrichment profiles proximal and distal to the site boundary revealed no significant differences adjacent to inert sites. This suggested that the waste was the source of contamination within salt marshes adjacent to hazardous landfills. The magnitude of contamination within the eight sites investigated suggests that the contamination load present within coastal sediments as a result of the 50 historic landfills within the Thames estuary is an order of magnitude higher than the annual contamination load released by Port of London dredging operations. The contamination already present within coastal sediments indicates a requirement to include the effects of predicted sediment erosion and redistribution within coastal management plans.

To use in-situ XRF as a rapid screening tool to identify the presence and extent of sub-surface contaminated sediments indicative of a legacy leachate plume and attenuation within surrounding coastal sediments.

The use of GIS in site selection, and the use of freely available site data allowed site selection and characterisation to be undertaken within one field day. A conceptual site model was developed and eight sites were chosen based on attributes such as proximity to salt marshes, location in the coastal zone and waste age. Using *in-situ* XRF data were rapidly obtained and accurately screened to establish the presence of hazards at each site.

To provide a recommended 'next step' for the management of risk from historical landfills within South East England.

There are 5000 historical landfills within Flood Alert Areas in the UK, this research suggests that these landfills may all present a source of diffuse pollution in the coastal zone requiring a framework for the assessment of risk. A number of key methods were proposed to undertake a risk assessment for landfills by adopting a tiered approach: (i) assessment of the likelihood of the hazard occurring, through the classification of probabilities; (ii) evaluating risk using an aggregation table for consequence and likelihood and (iii) requirements for data collection for further work on sites whose risk has been identified as significant. The section concluded that the contamination load at Newlands Landfill (examined in Chapter 4) exhibits a medium risk to the surrounding environment within the next 25 years, extending to a high risk over the next 50 years.

7.2. Direction of Further Research

The three main research chapters within this thesis have identified potential sources of coastal contamination across the UK, and assessed the risks based on waste type, age and location, however, the research has also highlighted areas for future research.

National Risk Assessment Framework

Chapter 6 outlined a method by which publically available spatial data could be used to rapidly identify hazardous landfill sites through classification based on an existing conceptual model. The flexibility of using commercially available data could allow the formation of an online mapping service, available to local authorities and stakeholders to map and classify sites based on their attributes, with the addition of being able to add local receptor data, such as SSSI details or protection orders. A distributed system of this kind, would provide stakeholders with a more accurate method for assessing hazard consequences for risk assessment, allowing sites to be prioritised especially when considering the additional stressors that coastal contamination may add to ensuring compliance with policy such as the Water Framework Directive or Shoreline Management Plans. Additionally, a distributed risk assessment framework could allow expansion beyond the South East, further informing the extent of risk on a national scale. However, to undertake an informed national risk assessment, more robust investigations of the various landfill types and settings across the UK will be required in order to better parameterise a national risk model.

For example, this research focused exclusively on fine-grained, estuarine sediments, which are widely recognised as sinks for metals in the environment (Cundy *et al.*, 2003). However, many historical landfill sites exist within differing geological and hydrological conditions, which will influence the attenuation capacity of the surrounding sediments and final fate of metal contaminants. Observing the effects of leachate attenuation within either different hydrological regimes or sites situated on terrestrial, coarser sediment will allow a more informed estimation of the mass of contamination present within our environment.

Chapter 6 concluded that sites containing a combination of commercial, household and industrial waste exhibited significantly higher contamination enrichment than inert sites. Environment Agency data show that out of the approximately 5000 sites that are located within the Flood Alert Area, 260 sites contain exclusively industrial waste, 107 commercial and 273 household waste (Environment Agency, 2012). Whether these sites will present different waste compositions and hence different metal magnitudes is currently unknown and could be investigated in order to further establish how specific waste type influences environmental contamination.

Additionally, landfills do not only exist within reasonably sheltered marsh environments, there are instances of waste sites that are currently eroding, with waste either entering the environment during catastrophic events and being actively eroded due to tidal flooding (Jones, 2008; Pope *et al.*, 2011). In order to have a greater understanding of the threat posed by these landfills, the ease by which they may erode, or fail, needs to be understood. Coastal evolution modelling is readily undertaken (de Winter *et al.*, 2015), yet, there are no current attempts to quantify the threat as a result of waste erosion.

Sediment bound contamination speciation

The quantity of sediment bound contamination from landfills has been estimated within this thesis, however in order to estimate a more accurate potential for ecological damage within a risk assessment, metal speciation could be measured. In the environment, metals are present in many forms and associated with numerous fractions, which, due to their varying binding strength, directly influence metal ecotoxicity and mobility (Quevauviller, 1998). Consequently, undertaking a single step extraction, such as the one performed in this study generated rapid, accurate concentrations for a suite of elements (Tokalioğlu *et al.*, 2003), but provided no indication of metal bioavailability (Ashrafi *et al.*, 2015).

An assessment of this kind would not only present information on the current form and therefore bioavailability of metals, but the ability to easily assess the likelihood for which metals will be released as a result of changing conditions, such as sediment oxidation or reworking.

Investigating Alternative Contamination Types

This thesis focused exclusively on metal contamination released from landfills during acetogenic waste degradation. Previous work (Hansen *et al.*, 1997; Weber *et al.*, 2011) has noted that Persistent Organic Pollutants (POP's), such as Polychlorinated Biphenyls (PCBs), polybrominated diphenyl ethers (PBDEs) and organochlorine pesticides (e.g. DDT) (Jones and de Voogt, 1999) have been found within sediment in the vicinity of closed landfills, either from leachate transfer or waste erosion. Additionally, waste degradation produces high levels of ammonia within leachate (Osada *et al.*, 2011), which, together with the persistence and high risk of organic contaminants (Herbert *et al.*, 2006) may summate to a much greater issue than solely the metal attenuated within sediments. An investigation would therefore be undertaken of the presence of POP's and organic contaminants such as ammonia within the attenuation zone identified around landfills.

7.3. Conclusion

This thesis has adopted novel field techniques, laboratory investigation and experimentation as well as geospatial methods to uncover a previously unquantified source of contamination within the coastal zone of the UK. Despite historic landfills being designed around the basis of natural attenuation, data have illustrated that these landfills are a contamination source, creating a contamination legacy within UK coastal sediments at risk of erosion.

Although this work has outlined a new contamination source, it has also generated scope for additional research in order to understand holistically the lasting legacy of the waste deposited around our coastline.

Reference List

Abrahim, G. & Parker, R. (2008). Assessment of heavy metal enrichment factors and the degree of contamination in marine sediments from Tamaki Estuary, Auckland, New Zealand. *Environmental Monitoring and Assessment,* **136**, 227-238.

Ackermann, F., Bergmann, H. & Schleichert, U. (1983). Monitoring of heavy metals in coastal and estuarine sediments - a question of grain-size: <20 µm versus <60 µm. *Environmental Technology Letters,* **4**, 317-328.

Adriano, D. C. (2001). *Trace elements in terrestrial environments: biogeochemistry, bioavailability, and risks of metals*, Springer. 867 pp.

Allan, M., Fagel, N., Van Rampelbergh, M., Baldini, J., Riotte, J., Cheng, H., Edwards, R. L., Gillikin, D., Quinif, Y. & Verheyden, S. (2015). Lead concentrations and isotope ratios in speleothems as proxies for atmospheric metal pollution since the industrial revolution. *Chemical Geology,* **401**, 140-150.

Allen, J. R. L. (2000). Morphodynamics of Holocene Salt Marshes: A Review Sketch from the Atlantic and Southern North Sea coasts of Europe. *Quaternary Science Reviews,* **19**, 1155-1231.

Aloupi, M. & Angelidis, M. O. (2001a). Geochemistry of Natural and Anthropogenic Metals in the Coastal Sediments of the Island of Lesvos, Aegean Sea. *Environmental Pollution,* **113**, 211-219.

Aloupi, M. & Angelidis, M. O. (2001b). Normalization to lithium for the assessment of metal contamination in coastal sediment cores from the Aegean Sea, Greece. *Marine Environmental Research,* **52**, 1-12.

Álvarez-Iglesias, P., Quintana, B., Rubio, B. & Pérez-Arlucea, M. (2007). Sedimentation rates and trace metal input history in intertidal sediments from San Simón Bay (Ría de Vigo, NW Spain) derived from ^{210}Pb and ^{137}Cs chronology. *Journal of Environmental Radioactivity,* **98**, 229-250.

Anderson, L. G., Hall, P. O. J., Iverfeldt, A., Rutgers van der Loejf, M. M., Sundby, B. & Westerlund, S. F. G. (1986). Benthic respiration measured by total carbonate production. *Limnology and Oceanography,* **31**, 319-329.

Andrews, W. J., Masoner, J. R. & Cozzarelli, I. M. (2012). Emerging Contaminants at a Closed and an Operating Landfill in Oklahoma. *Ground Water Monitoring & Remediation,* **32**, 120-130.

Apitz, S. E. (2012). Conceptualizing the role of sediment in sustaining ecosystem services: Sediment-ecosystem regional assessment (SEcoRA). *Science of The Total Environment,* **415**, 9-30.

Appleby, P. G. & Oldfield, F. (1978). The Calculation of ^{210}Pb dates assuming a constant rate of supply of unsupported ^{210}Pb to the sediment. *Catena,* **5**, 1-8.

Araújo, F. G., Williams, W. P. & Bailey, R. G. (2000). Fish assemblages as indicators of water quality in the Middle Thames Estuary, England (1980–1989). *Estuaries,* **23**, 305-317.

Argyraki, A., H. Ramsey, M. & J. Potts, P. (1997). Evaluation of Portable X-ray Fluorescence Instrumentation for in situ Measurements of Lead on Contaminated Land. *Analyst,* **122**, 743-749.

Ashrafi, M., Mohamad, S., Yusoff, I. & Shahul Hamid, F. (2015). Immobilization of Pb, Cd, and Zn in a contaminated soil using eggshell and banana stem amendments: metal leachability and a sequential extraction study. *Environmental Science and Pollution Research,* **22**, 223-230.

Attrill, M. J. (1998). *A Rehabilitated Estuarine Ecosystem: The environment and ecology of the Thames Estuary*, Springer. 1st Edition. 272 pp.

Attrill, M. J., Thomes, R. M., (1995). Heavy Metal Concentrations in Sediment from the Thames Estuary, UK. *Marine Pollution Bulletin,* **30**, 742-744.

Audry, S., Schäfer, J., Blanc, G. & Jouanneau, J.-M. (2004). Fifty-year sedimentary record of heavy metal pollution (Cd, Zn, Cu, Pb) in the Lot River reservoirs (France). *Environmental Pollution,* **132**, 413-426.

Aydi, A., Zairi, M. & Dhia, H. (2013). Minimization of environmental risk of landfill site using fuzzy logic, analytical hierarchy process, and weighted linear combination methodology in a geographic information system environment. *Environmental Earth Sciences,* **68**, 1375-1389.

Bagchi, A. (1987). Natural attenuation mechanisms of landfill leachate and effects of various factors on the mechanisms. *Waste Management & Research,* **5**, 453-463.

Bagchi, A. (1994). *Design, Construction and Monitoring of Landfills,* New York; Chichester, Wiley. 2nd Edition. 361 pp.

Bai, J., Huang, L., Yan, D., Wang, Q., Gao, H., Xiao, R. & Huang, C. (2011a). Contamination characteristics of heavy metals in wetland soils along a tidal ditch of the Yellow River Estuary, China. *Stochastic Environmental Research and Risk Assessment,* **25**, 671-676.

Bai, J., Xiao, R., Cui, B., Zhang, K., Wang, Q., Liu, X., Gao, H. & Huang, L. (2011b). Assessment of heavy metal pollution in wetland soils from the young and old reclaimed regions in the Pearl River Estuary, South China. *Environmental Pollution,* **159**, 817-824.

Bai, X., Zhang, X. & Wang, S. (2011c). The application of caesium-137 measurements to estimate recent sedimentation rates in a typical karst depression of Guizhou Plateau, China. *Chinese Journal of Geochemistry,* **30**, 84-92.

Baird, C. (2012). *Environmental Chemistry*, W. H. Freeman. 5th Edition. 650 pp.

Baskaran, M. & Naidu, A. S. (1995). 210Pb-derived chronology and the fluxes of 210Pb and 137Cs isotopes into continental shelf sediments, East Chukchi Sea, Alaskan Arctic. *Geochimica et Cosmochimica Acta,* **59**, 4435-4448.

Baskaran, M., Nix, J., Kuyper, C. & Karunakara, N. (2014). Problems with the dating of sediment core using excess 210Pb in a freshwater system impacted by large scale watershed changes. *Journal of Environmental Radioactivity,* **138**, 355-363.

Bastos, R. O., Melquiades, F. L., BIasi, G. E. V., (2012). Correction for the Effect of Soil Moisture on in situ XRF Analysis using Low-Energy Background. *X-Ray Spectrometry,* **41**, 304-307.

Baucom, K. & Ruhl, C. H. (2013). CCP Landfill Leachate Generation and Leachate Management. *2013 World of Coal Ash Conference - April 22-25, 2013 in Lexington, KY*.

Baun, A., Ledin, A., Reitzel, L. A., Bjerg, P. L. & Christensen, T. H. (2004). Xenobiotic organic compounds in leachates from ten Danish MSW landfills—chemical analysis and toxicity tests. *Water Research,* **38**, 3845-3858.

Bear, J. & Verruijt, A. (1987). *Modeling groundwater flow and pollution : with computer programs for sample cases*, Reidel. 414 pp.

Ben Salem, Z., Capelli, N., Laffray, X., Elise, G., Ayadi, H. & Aleya, L. (2014). Seasonal variation of heavy metals in water, sediment and roach tissues in a landfill draining system pond (Etueffont, France). *Ecological Engineering,* **69**, 25-37.

Benninger, L. K., Aller, R. C., Cochran, J. K. & Turekian, K. K. (1979). Effects of biological sediment mixing on the 210Pb chronology and trace metal distribution in a Long Island Sound sediment core. *Earth and Planetary Science Letters,* **43**, 241-259.

Bernick, M. B., Kalnicky, D. J., Prince, G. & Singhvi, R. (1995). Results of field-portable X-ray fluorescence analysis of metal contaminants in soil and sediment. *Journal of Hazardous Materials,* **43**, 101-110.

Bevan, K. J. (2004). *Rainfall-Runoff Modelling: The Primer*, Wiley-Blackwell. 372 pp.

BGS. 2014. *The BGS Lexicon of Names Rock Units, London Clay* [Online]. NERC,. Available: http://www.bgs.ac.uk/lexicon/lexicon.cfm?pub=LC [Accessed 13th August 2014].

Bhalla, G., Kumar, A. & Bansal, A. (2011). Assessment of Groundwater Pollution near Municipal Solid Waste Landfill. *Asian Journal of Water, Environment and Pollution,* **8**, 41-51.

Billon, G., Ouddane, B., Laureyns, J. & Boughriet, A. (2001). Chemistry of metal sulfides in anoxic sediments. *Physical Chemistry Chemical Physics,* **3**, 3586-3592.

Bjerg, P. L., Tuxen, N., Reitzel, L. A., Albrechtsen, H.-J. & Kjeldsen, P. (2011). Natural Attenuation Processes in Landfill Leachate Plumes at Three Danish Sites. *Ground Water,* **49**, 688-705.

Böning, P., Bard, E. & Rose, J. (2007). Toward direct, micron-scale XRF elemental maps and quantitative profiles of wet marine sediments. *Geochemistry, Geophysics, Geosystems,* **8**.

Boyes, S. J. & Allen, J. H. (2007). Topographic monitoring of a middle estuary mudflat, Humber estuary, UK–Anthropogenic impacts and natural variation. *Marine Pollution Bulletin,* **55**, 543-554.

British Geological Survey (1974). Essex River Authority Borehole Record. *Smallgains Creek, Canvey Island,* **BGS ID: 16087826**.

Bromhead, E. N. & Ibsen, M.-L. (2006). A review of Landsliding and Coastal Erosion Damage to historic fortifications in South East England. *Landslides,* **3**, 341-347.

Brown, A. 2012. *RE: Newlands Landfill and Site Access. Andrew Brown, Landfill Restoration Manager, Essex County Council.*

Brun, A. & Engesgaard, P. (2002). Modelling of transport and biogeochemical processes in pollution plumes: literature review and model development. *Journal of Hydrology,* **256**, 211-227.

Bryan, G. W. (1971). The Effects of Heavy Metals (other than Mercury) on Marine and Estuarine Organisms. *Proceedings of the Royal Society of London,* **177**, 389-410.

Bryan, G. W. & Langston, W. J. (1992). Bioavailability, accumulation and effects of heavy metals in sediments with special reference to United Kingdom estuaries: a review. *Environmental Pollution,* **76**, 89-131.

Buchman, M. F. (2008). NOAA Screening Quick Reference Tables, NOAA OR&R Report 08-1. Office of Response and Restoration Division, National Oceanic and Atmospheric Administration. *Seattle WA*, 34pp.

Burdige, D. J. (1993). The biogeochemistry of manganese and iron reduction in marine sediments. *Earth-Science Reviews,* **35**, 249-284.

Burnley, S. J. (2007). A review of municipal solid waste composition in the United Kingdom. *Waste Management,* **27**, 1274-1285.

Burrough, P. A. & McDonnell, R. A. (1998). *Principles of Geographic Information Systems,* Oxford, Oxford Universtiy Press,. 352 pp.

Burton, J. G. A. (2002). Sediment quality criteria in use around the world. *Limnology,* **3**, 65-76.

Butt, T. E. & Oduyemi, K. O. K. (2003). A holistic approach to Concentration Assessment of hazards in the risk assessment of landfill leachate. *Environment International,* **28**, 597-608.

Calmano, W., Hong, J. & Förstner, U. (1993). Binding and Mobilization of Heavy Metals in Contaminated Sediments Affected by pH and Redox Potential. *Water Science and Technology* **28**, 223-235.

Canfield, D. E., Thamdrup, B. & Hansen, J. W. (1993). The anaerobic degradation of organic matter in Danish coastal sediments: iron reduction, manganese reduction, and sulfate reduction. *Geochimica et Cosmochimica Acta,* **57**, 3867-3883.

CAPCOA (1990). *Suggested Control Measure for Landfill Gas Emissions*, California Air Pollution Control Officers Association, California Air Resources Board, Stationary Source Division, Sacremento, CA, USA. 23 pp.

Carina, E., Keskitalo, H., 2010. Chapter 3: Climate Change Adaptation in the United Kingdom: England and South-East England. *In:* Brännlund, L. (ed.) *Developing Adaptation Policy and Practice in Europe: Multi-level Governance of Climate Change.* Springer. 376 pp.

Carr, R., Zhang, C., Moles, N. & Harder, M. (2008). Identification and mapping of heavy metal pollution in soils of a sports ground in Galway City, Ireland, using a portable XRF analyser and GIS. *Environmental Geochemistry and Health,* **30**, 45-52.

Casado-Martinez, M. C., Smith, B. D. & Rainbow, P. S. (2012). Assessing metal bioaccumulation from estuarine sediments: comparative experimental results for the polychaete Arenicola marina. *Journal of Soils and Sediments,* **13**, 429-440.

Cassiani, G., Fusi, N., Susanni, D. & Deiana, R. (2008). Vertical radar profiling for the assessment of landfill capping effectiveness. *Near surface geophysics,* **6**, 133-142.

Castro, J. E., Fernandez, A. M., Gonzalez-Caccia, V. & Gardinali, P. R. (2013). Concentration of trace metals in sediments and soils from protected lands in south Florida: background levels and risk evaluation. *Environ Monit Assess,* **185**, 6311-6332.

Cataldo, F. (2012). Multielement analysis of a municipal landfill leachate with total reflection X-ray fluorescence (TXRF). A comparison with ICP-OES analytical results. *Journal of Radioanalytical and Nuclear Chemistry,* **293**, 119-126.

Caulmert Limited (2011a). Hadleigh Sea Wall Landfill Site. *Essex County Council, Annual Monitoring Report*, 28pp.

Caulmert Limited (2011b). *Newlands Landfill, Annual Monitoring Report,* Bangor, Caulmert Limited. 30 pp.

Caulmert Limited (2012). *Newlands Landfill, Annual Monitoring Report,* Bangor, Caulmert Limited. 28 pp.

CCME (2002). Canadian Sediment Quality Guidelines for the Protection of Aquatic Life. *Canadian Council of Ministers of the Environment*

CDOIF (2013). Environmental Risk Tolerability for COMAH Establishments: GUIDELINE. *Chemical and Downstream Oil Industries Forum* 88pp.

CEFAS. 2012. *Use of Action Levels in Dredged Material Assessments* [Online]. DEFRA. Available: http://www.cefas.defra.gov.uk/media/562541/cefas%20action%20levels.pdf [Accessed July 2015].

Çevik, F., Göksu, M., Derici, O. & Fındık, Ö. (2009). An assessment of metal pollution in surface sediments of Seyhan dam by using enrichment factor, geoaccumulation index and statistical analyses. *Environmental Monitoring and Assessment,* **152**, 309-317.

Chandra Sekhar, K., Chary, N. S., Kamala, C. T., Suman Raj, D. S. & Sreenivasa Rao, A. (2004). Fractionation studies and bioaccumulation of sediment-bound heavy metals in Kolleru lake by edible fish. *Environment International,* **29**, 1001-1008.

Chapman, P. M. & Wang, F. (2001). Assessing sediment contamination in estuaries. *Environmental Toxicology and Chemistry,* **20**, 3-22.

Chatterjee, M., Silva Filho, E. V., Sarkar, S. K., Sella, S. M., Bhattacharya, A., Satpathy, K. K., Prasad, M. V. R., Chakraborty, S. & Bhattacharya, B. D. (2007). Distribution and possible source of trace elements in the sediment cores of a tropical macrotidal estuary and their ecotoxicological significance. *Environment International,* **33**, 346-356.

Chen, C.-W., Kao, C.-M., Chen, C.-F. & Dong, C.-D. (2007). Distribution and accumulation of heavy metals in the sediments of Kaohsiung Harbor, Taiwan. *Chemosphere,* **66**, 1431-1440.

Chen, M. & Ma, L. Q. (2001). Comparison of three aqua regia digestion methods for twenty Florida soils. *Soil Science Society of America Journal,* **65**, 491-499.

Chen, S.-J., Luo, X.-J., Mai, B.-X., Sheng, G.-Y., Fu, J.-M. & Zeng, E. Y. (2006). Distribution and Mass Inventories of Polycyclic Aromatic Hydrocarbons and Organochlorine Pesticides in Sediments of the Pearl River Estuary and the Northern South China Sea. *Environmental Science & Technology,* **40**, 709-714.

Chenhall, B. E., Yassini, I. & Jones, B. G. (1992). Heavy metal concentrations in lagoonal saltmarsh species, Illawarra region, southeastern Australia. *Science of The Total Environment,* **125**, 203-225.

Christensen, T. H., Kjeldsen, P., Bjerg, P. L., Jensen, D. L., Christensen, J. B., Baun, A., Albrechtsen, H.-J. & Heron, G. (2001). Biogeochemistry of landfill leachate plumes. *Applied Geochemistry,* **16**, 659-718.

Clark, R. B., Frid, C., Attrill M., (2001). *Marine Pollution*, Oxford Science Publications. 5th Edition. 237 pp.

Clark, S., Menrath, W., Chen, M., Roda, S. & Succop, P. (1999). Use of a field portable X-Ray fluorescence analyzer to determine the concentration of lead and other metals in soil samples. *Annals of agricultural and environmental medicine : AAEM,* **6**, 27-32.

Cochran, J. K., Hirschberg, D. J., Wang, J. & Dere, C. (1998). Atmospheric Deposition of Metals to Coastal Waters (Long Island Sound, New York U.S.A.): Evidence from Saltmarsh Deposits. *Estuarine, Coastal and Shelf Science,* **46**, 503-522.

Constantino, C., Scrimshaw, M., Comber, S. & Churchley, J. (2011). An evaluation of biotic ligand models predicting acute copper toxicity to Daphnia magna in wastewater effluent. *Environmental Toxicology and Chemistry,* **30**, 852-860.

Cook, J. M., Gardner, M. J., Griffiths, A. H., Jessep, M. A., Ravenscroft, J. E. & Yates, R. (1997). The comparability of sample digestion techniques for the determination of metals in sediments. *Marine Pollution Bulletin,* **34**, 637-644.

Cooper, H. J., Cooper, T., Burd, F., (2001). 25 Years of salt marsh erosion in Essex: Implications for coastal defence and nature conservation. *Journal of Coastal Conservation,* **7**, 31-40.

Cooper, N., Bower, G., Tyson, R., Flikweert, J., Rayner, S., Hallas, A., (2012). Guidance on the Management of Landfill Sites and Land Contamination on Eroding or Low-Lying Coastlines (C718). *London, CIRIA*.

Council Directive (92/43/EEC). on the Conservation of natural habitats and of wild fauna and flora. *Official Journal of the European Communities*.

Council Directive (2000/60/EC). of the European Parliament and the Council establishing a framework for Community action in the field of Water Policy. *Official Jounral of the European Communities*.

Council Directive (2008/98/EC). Waste Framework Directive 2011. *Official Journal of the European Union*.

Council Directive (2008/105/EC). Directive 2008/105/EC of the European Parliament and of the Council of 16 December 2008 on environmental quality standards in the field of water policy, amending and subsequently repealing Council Directives 82/176/EEC, 83/513/EEC, 84/156/EEC, 84/491/EEC, 86/280/EEC and amending Directive 2000/60/EC of the European Parliament and of the Council. *Official Journal of the European Union*.

Council Directive (2013/39/EU). amending Directives 2000/60/EC and 2008/105/EC as regards priority substances in the field of water policy. *Official Journal of the European Union*.

Craft, C., Clough, J., Ehman, J., Joye, S., Park, R., Pennings, S., Guo, H. & Machmuller, M. (2009). Forecasting the effects of accelerated sea-level rise on tidal marsh ecosystem services. *Frontiers in Ecology and the Environment,* **7**, 73-78.

Critto, A., Carlon, C. & Marcomini, A. (2003). Characterization of contaminated soil and groundwater surrounding an illegal landfill (S. Giuliano, Venice, Italy) by principal component analysis and kriging. *Environmental Pollution,* **122**, 235-244.

Crommentuijn, T., Polder, M., van de Plassche, E., (1997). Maximum Permissible Concentrations and Negligible Concentrations for Metals, Taking Background

Concentrations into Account. *National Institution of Public Health and the Environment. Bilthoven, The Netherlands. RIVM Report 601501 001*.

Crooks, S., Schutten, J., Sheern, G. D., Pye, K. & Davy, A. J. (2002). Drainage and Elevation as Factors in the Restoration of Salt Marsh in Britain. *Restoration Ecology,* **10**, 591-602.

Cundy, A., Long, A., Hill, C., Spencer, C. & Croudace, I. (2002). Sedimentary response of Pagham Harbour, southern England to barrier breaching in AD 1910. *Geomorphology,* **46**, 163-176.

Cundy, A. B. 2014. *RE: Gamma Spectroscopy Methodology. Professor Andrew Cundy, University of Brighton.*

Cundy, A. B., Croudace, I. W., Cearreta, A. & Irabien, M. (2003). Reconstructing historical trends in metal input in heavily-disturbed, contaminated estuaries: studies from Bilbao, Southampton Water and Sicily. *Applied Geochemistry,* **18**, 311-325.

Cundy, A. B., Hopkinson, L., Lafite, R., Spencer, K., Taylor, J. A., Ouddane, B., Heppell, C. M., Carey, P. J., Charman, R., Shell, D. & Ullyott, S. (2005). Heavy metal distribution and accumulation in two Spartina sp.-dominated macrotidal salt marshes from the Seine estuary (France) and the Medway estuary (UK). *Applied Geochemistry,* **20**, 1195-1208.

Davidson, C. M., Gibson, M. D., Hamilton, E., MacGillivray, B. H., Reglinski, J. & Rezabal, E. (2005). The long-term environmental behaviour of strontium and barium released from former mine workings in the granites of the Sunart region of Scotland, UK. *Chemosphere,* **58**, 793-798.

Davies, S. (2012). Demise of landfill. *Engineering & Technology,* **6**, 42-45.

Dawson, R., Hall, J., Bates, P. & Nicholls, R. (2005). Quantified analysis of the probability of flooding in the Thames estuary under imaginable worst-case sea level rise scenarios. *Water Resources Development,* **21**, 577-591.

DCLG. 2015. *Considering and determining planning applications that have been subject to an Environmental Impact Assessment* [Online]. Paragraph: 057: Reference ID: 4-057-20140306. Available: http://bit.ly/1Iu9TNt [Accessed 28th June 2015].

de Polo, A. & Scrimshaw, M. D. (2012). Challenges for the development of a biotic ligand model predicting copper toxicity in estuaries and seas. *Environmental Toxicology and Chemistry,* **31**, 230-238.

de Winter, R. C., Gongriep, F. & Ruessink, B. G. (2015). Observations and modeling of alongshore variability in dune erosion at Egmond aan Zee, the Netherlands. *Coastal Engineering,* **99**, 167-175.

DEFRA (2006). *Shoreline Management Plan Guidance. Volume 1: Aims and Requirements,* London, Department for Environmental, Food and Rural Affairs. 54 pp.

DEFRA (2011a). Green Leaves III: Guidelines for Environmental Risk Assessment and Management. *Department for Environment, Food and Rural Affairs. Cranfield University.*, 84pp.

DEFRA (2011b). Guidance for Environmental Risk Assessment and Management, Green Leaves III. *Department of Environment, Food and Rural Affairs*, 82pp.

DEFRA (2011c). Guidance on Applying the Waste Hierarchy under the Waste Regulations 2011. *Department for Environment, Food and Rural Affairs*.

DEFRA & Environment Agency (2004). Model Procedures For The Management of Land Contamination. *Research and Development Publication CLR 11*.

Dhanakumar, S., Rutharvvel Murthy, K., Solaraj, G., Mohanraj, R., (2013). Heavy-Metal Fractionation in Surface Sediments of the Cauvery River Estuarine Region, Southeastern Coast of India. *Archives of Environmental Contamination and Toxicology,* **65**, 14-23.

Din, Z. B. (1992). Use of aluminium to normalize heavy-metal data from estuarine and coastal sediments of Straits of Melaka. *Marine Pollution Bulletin,* **24**, 484-491.

Dong, C., Zhang, W., Ma, H., Feng, H., Lu, H., Dong, Y. & Yu, L. (2014). A magnetic record of heavy metal pollution in the Yangtze River subaqueous delta. *Science of The Total Environment,* **476–477**, 368-377.

Dörr, H., Mangini, A,m Schmitz, W., Weber, F., Münnich, K. O., 1994. Stable Lead and ^{210}Pb in German Lake Sedimentsa nd Soils: A Tracer for Anthropogenic Lead Emission. *In:* Vernet, J. P. (ed.) *Heavy Metals in the Environment.* 2nd ed. Amsterdam, The Netherlands: Elsevier. 13 pp.

Driscoll, C. T., Mason, R. P., Chan, H. M., Jacob, D. J. & Pirrone, N. (2013). Mercury as a Global Pollutant: Sources, Pathways, and Effects. *Environmental Science & Technology,* **47**, 4967-4983.

Du Laing, G., Bogaert, N., Tack, F. M. G., Verloo, M. G. & Hendrickx, F. (2002). Heavy metal contents (Cd, Cu, Zn) in spiders (Pirata piraticus) living in intertidal sediments of the river Scheldt estuary (Belgium) as affected by substrate characteristics. *Science of The Total Environment,* **289**, 71-81.

Du Laing, G., Rinklebe, J., Vandecasteele, B., Meers, E. & Tack, F. (2009). Trace metal behaviour in estuarine and riverine floodplain soils and sediments: A review. *Science of The Total Environment,* **407**, 3972-3985.

El-Fadel, M., Bou-Zeid, E., Chahine, W. & Alayli, B. (2002). Temporal variation of leachate quality from pre-sorted and baled municipal solid waste with high organic and moisture content. *Waste Management,* **22**, 269-282.

ElBishlawi, H., Shin, J. Y. & Jaffe, P. R. (2013). Trace metal dynamics in the sediments of a constructed and natural urban tidal marsh: The role of iron, sulfide, and organic complexation. *Ecological Engineering,* **58**, 133-141.

Eleazer, W. E., Odle, W. S., Wang, Y.-S. & Barlaz, M. A. (1997). Biodegradability of Municipal Solid Waste Components in Laboratory-Scale Landfills. *Environmental Science & Technology,* **31**, 911-917.

Emmerson, R. H. C., Birkett, J. W., Scrimshaw, M. & Lester, J. N. (2000). Solid phase partitioning of metals in managed retreat soils: field changes over the first year of tidal inundation. *Science of The Total Environment,* **254**, 75-92.

Energy Institute (2013). Guidance on Characterising, Assessing and Managing Risks associated with Potentiallly Contaminated Sediments. *Arcadis*.

Environment Agency (2004). Soil Screening Values for the use in UK Ecological Risk Assessment. *Environment Agency, Air, Land and Water Group.*

Environment Agency (2010a). Thames Estuary 2100 (TE2100), Plan Consultation Document. *Action Plan Zone 7*.

Environment Agency (2010b). *Waste Acceptance at Landfils, Guidane on waste acceptance procedures and criteria,* Bristol, Environment Agency. 46 pp.

Environment Agency (2012). Whats in your Backyard? [Online] URL available at: http://www.environment-agency.gov.uk/homeandleisure/37793.aspx. *Accessed 20th October 2013*.

Environment Agency. 2014. *Environment Agency Geostore Online Data* [Online]. Available: http://www.geostore.com/environment-agency/ [Accessed December 20th 2014].

Environment Agency. 2015. *Interactive Maps - Pollution Incidents* [Online]. Castle Point, No 360804, 17th Nov 2005. Available: http://bit.ly/1EvDzDN [Accessed 1st May 2015].

Environmental Protection Act (1990). Part IIa. London: The Stationary Office: HMSO.

Erses, A. S., Onay, T. T. & Yenigun, O. (2008). Comparison of aerobic and anaerobic degradation of municipal solid waste in bioreactor landfills. *Bioresource Technology,* **99**, 5418-5426.

Escárate, P., Hein, R., Durán, M. & Ramaciotti, P. (2015). X-ray fluorescence spectroscopy for accurate copper estimation. *Minerals Engineering,* **71**, 13-15.

Farmer, J. G. & Lovell, M. A. (1984). Massive diagenetic enhancement of manganese in Loch Lomond sediments. *Environmental Technology Letters,* **5**, 257-262.

Farnham, I. M., Singh, A. K., Stetzenbach, K. J. & Johannesson, K. H. (2002). Treatment of nondetects in multivariate analysis of groundwater geochemistry data. *Chemometrics and Intelligent Laboratory Systems,* **60**, 265-281.

Fergusson, J. (1990). *The Heavy Elements: Chemistry, Environmental Impact and Health Effects,* Oxford, Pergamom Press. 614 pp.

Ferretti, M. (2014). The investigation of ancient metal artefacts by portable X-ray fluorescence devices. *Journal of Analytical Atomic Spectrometry,* **29**, 1753-1766.

Field, A. (2009). *Discovering statistics using SPSS*, Sage Publications Limited. 856 pp.

Field, C. D. (1995). Impact of Expected Climate Change on Mangroves. *Hydrobiologia,* **295**, 75-81.

Finney, B. P. & Huh, C. A. (1989). History of metal pollution in the Southern California Bight: an update. *Environmental Science & Technology,* **23**, 294-303.

Fitzgerald, E. J., Caffrey, J. M., Nesaratnam, S. T. & McLoughlin, P. (2003). Copper and lead concentrations in salt marsh plants on the Suir Estuary, Ireland. *Environmental Pollution,* **123**, 67-74.

Fletcher, C. A., Bubb, J. M. & Lester, J. N. (1994). Magnitude and distribution of anthropogenic contaminants in salt marsh sediments of the Essex coast, UK. II. Selected metals and metalloids. *The Science of the Total Environment,* **155**, 47-59.

Fox, W., Johnson, M., Jones, S., Leah, R. & Copplestone, D. (1999). The use of sediment cores from stable and developing salt marshes to reconstruct historical contamination profiles in the Mersey Estuary, UK. *Marine Environmental Research,* **47**, 311-329.

Furness, L. (2014). Personal Communication. *Sutton Boat Yard*.

Ge, L., Lai, W. & Lin, Y. (2005). Influence of and correction for moisture in rocks, soils and sediments on in situ XRF analysis. *X-Ray Spectrometry,* **34**, 28-34.

Gedan, K. B., Silliman, B. R. & Bertness, M. D. (2009). Centuries of Human-Driven Change in Salt Marsh Ecosystems. *Annual Review of Marine Science,* **1**, 117-141.

Giauque, R. D., Garrett, R. B. & Goda, L. Y. (1979). Determination of trace elements in light element matrices by x-ray fluorescence spectrometry with incoherent scattered radiation as an internal standard. *Analytical Chemistry,* **51**, 511-516.

Gibbs, H. M., Gurnell, A. M., Heppell, C. M. & Spencer, K. L. (2014). The role of vegetation in the retention of fine sediment and associated metal contaminants in London's rivers. *Earth Surface Processes and Landforms,* **39**, 1115-1127.

Giblin, A. E., Luther Iii, G. W. & Valiela, I. (1986). Trace metal solubility in salt marsh sediments contaminated with sewage sludge. *Estuarine, Coastal and Shelf Science,* **23**, 477-498.

Go, J., Lampert, D. J., Stegemann, J. A. & Reible, D. D. (2009). Predicting contaminant fate and transport in sediment caps: Mathematical modelling approaches. *Applied Geochemistry,* **24**, 1347-1353.

Gochfeld, M., Burger, J. & Vyas, V. (2005). Statistical analysis of data sets with values below detection limits. *Consortium for Risk Evaluation with Stakeholder Participation,* **3**.

Gooddy, D. C., Macdonald, D. M. J., Lapworth, D. J., Bennett, S. A. & Griffiths, K. J. (2014). Nitrogen sources, transport and processing in peri-urban floodplains. *Science of The Total Environment,* **494–495**, 28-38.

Grant, A. & Middleton, R. (1990). As Assessment of Metal Contamination of Sediments in the Humber Estuary, U.K. *Estuarine, Coastal and Shelf Science,* **31**, 71-85.

Gray, J. M. (1993). Quaternary geology and waste disposal in South Norfolk, England. *Quaternary Science Reviews,* **12**, 899-912.

Great Britain (1990). Environmental Protection Act. *Part IIa,* **London: The Stationary Office**.

Great Britain (1991). The Water Resources Act. **London: The Stationary Office**.

Great Britain (2003). The Water Environment (WFD) Regulations. **London: The Stationary Office**.

Green, I., Boughey, K. & Diaz, A. (2014). Potentially Toxic Metals in Historic Landfill Sites: Implications for Grazing Animals. *Water, Air, & Soil Pollution,* **225**, 1-12.

Gribsholt, B. & Kristensen, E. (2002). Effects of bioturbation and plant roots on salt marsh biogeochemistry: a mesocosm study. *Marine Ecology Progress Series,* **241**, 71-87.

Grousset, F. E., Jouanneau, J.-M., Castaing, P., Lavaux, G. & Latouche, C. (1999). A 70 year record of contamiantion from Industrial Activity along the Garonne River and its Tributaries (SW France). *Estuarine, Coastal and Shelf Science,* **48**, 401-414.

Guo, T., DeLaune, R. D. & Patrick Jr, W. H. (1997). The influence of sediment redox chemistry on chemically active forms of arsenic, cadmium, chromium, and zinc in estuarine sediment. *Environment International,* **23**, 305-316.

HALCROW (2012). Contamination Risk Assessment Report, Two Tree Island and Hadleigh Marshes Contamination Study. *Environment Agency*.

Hamdoun, H., Van-Veen, E., Basset, B., Lemoine, M., Coggan, J., Leleyter, L. & Baraud, F. (2015). Characterization of harbor sediments from the English Channel: assessment of heavy metal enrichment, biological effect and mobility. *Marine Pollution Bulletin,* **90**, 273-280.

Han, D., Tong, X., Currell, M. J., Cao, G., Jin, M. & Tong, C. (2014). Evaluation of the impact of an uncontrolled landfill on surrounding groundwater quality, Zhoukou, China. *Journal of Geochemical Exploration,* **136**, 24-39.

Hansen, L. G., Green, D., Cochran, J., Vermette, S. & Bush, B. (1997). Chlorobiphenyl (PCB) composition of extracts of subsurface soil, superficial dust and air from a contaminated landfill. *Fresenius' Journal of Analytical Chemistry,* **357**, 442-448.

Harino, H., O'Hara, S., Burt, G., Chesman, B., Pope, N. & Langston, W. (2003). Organotin compounds in Mersey and Thames Estuaries a decade after UK TBT legislation. *Journal of the Marine Biological Association of the United Kingdom,* **83**, 11-22.

Harland, B. J., Taylor, D. & Wither, A. (2000). The distribution of mercury and other trace metals in the sediments of the Mersey Estuary over 25 years 1974–1998. *Science of The Total Environment,* **253**, 45-62.

Haslett, S., Cundy, A., Davies, C., Powell, E. & Croudace, I. (2003). Salt marsh sedimentation over the past c. 120 years along the west Cotentin coast of Normandy (France): relationship to sea-level rise and sediment supply. *Journal of coastal research,* **19**, 609-620.

He, R. & Shen, D.-s. (2006). Nitrogen removal in the bioreactor landfill system with intermittent aeration at the top of landfilled waste. *Journal of Hazardous Materials,* **136**, 784-790.

Helz, G. R. & Valette-Silver, N. (1992). Beryllium-10 in Chesapeake Bay sediments: An indicator of sediment provenance. *Estuarine, Coastal and Shelf Science,* **34**, 459-469.

Hennekam, R. & de Lange, G. (2012). X-ray fluorescence core scanning of wet marine sediments: methods to improve quality and reproducibility of high-resolution paleoenvironmental records. *Limnol. Oceanogr. Methods,* **10**, 991-1003.

Henry, H. A. L. & Jefferies, R. L. (2003). Plant amino acid uptake, soluble N turnover and microbial N capture in soils of a grazed Arctic salt marsh. *Journal of Ecology,* **91**, 627-636.

Herbert, P., Silva, A. L., João, M. J., Santos, L. & Alves, A. (2006). Determination of semi-volatile priority pollutants in landfill leachates and sediments using microwave-

assisted headspace solid-phase microextraction. *Analytical and Bioanalytical Chemistry,* **386**, 324-331.

Higueras, P., Oyarzun, R., Iraizoz, J. M., Lorenzo, S., Esbrí, J. M. & Martínez-Coronado, A. (2012). Low-cost geochemical surveys for environmental studies in developing countries: Testing a field portable XRF instrument under quasi-realistic conditions. *Journal of Geochemical Exploration,* **113**, 3-12.

Hinds, M. W., Bevan, G. & Burgess, R. W. (2014). The non-destructive determination of Pt in ancient Roman gold coins by XRF spectrometry. *Journal of Analytical Atomic Spectrometry,* **29**, 1799-1805.

Hopkin, S. P. (1989). *Ecophysiology of metals in terrestrial invertebrates,* London & New York, Elsevier Applied Science. 366 pp.

Hopwood, M. J., Statham, P. J., Skrabal, S. A. & Willey, J. D. (2014). Dissolved iron(II) ligands in river and estuarine water. *Marine Chemistry,* **173**, 173-182.

Hu, W., Huang, B., Weindorf, D. & Chen, Y. (2014). Metals Analysis of Agricultural Soils via Portable X-ray Fluorescence Spectrometry. *Bulletin of Environmental Contamination and Toxicology,* **92**, 420-426.

Hubbell, J. H. (1982). Photon Mass Attenuation and Energy-Absorption Coefficients from 1 keV to 20 MeV. *International Journal of Applied Radiation and Isotopes,* **33**, 22.

Hubbell, J. M. & Seltzer, S. M. (2004). Tables of X-Ray Mass Attenuation Coefficients and Mass Energy-Absorption Coefficients from 1 keV to 20 MeV for Elements Z = 1 to 92 and 48 Additional Substances of Dosimetric Interest. *NIST Standard Reference Database 126,* **Gaithersburg, MD**.

Hübner, R., Astin, K. B., Herbert, R. J. H., (2010). Dispersal and Mobility of Metal Contamination Across a Salt Marsh from Coastal Landfill SItes using Ammonium Nitrate Extractions as an Indicator. *Journal of Environmental Monitoring,* **12**, 740-747.

Hughes, R. (2004). Climate change and loss of saltmarshes: consequences for birds. *Ibis,* **146**, 21-28.

Hung, M.-L., Wu, S.-Y., Chen, Y.-C., Shih, H.-C., Yu, Y.-H. & Ma, H.-w. (2009). The Health Risk Assessment of Pb and Cr leachated from fly ash monolith landfill. *Journal of Hazardous Materials,* **172**, 316-323.

Hürkamp, K., Raab, T., Völkel, J., (2009). Two and three-dimensional quantification of lead contamination in alluvial soils of a historic mining area using field portable X-ray fluorescence (FPXRF) analysis. *Geomorphology,* **110**, 28-36.

Hutchinson, T. C. & Whitby, L. M. (1974). Heavy-metal Pollution in the Sudbury Mining and Smelting Region of Canada, I. Soil and Vegetation Contamination by Nickel, Copper, and Other Metals. *Environmental Conservation,* **1**, 123-132.

IAEA (2005). In Situ Applications of X ray Flourescence Techniques: Final Report of a coordinated Research Project. *International Atomic Energy Agency,* **IAEA-TECDOC-1456**.

Idris, A. M., Eltayeb, M. A. H., Potgieter-Vermaak, S. S., Van Grieken, R. & Potgieter, J. H. (2007). Assessment of heavy metals pollution in Sudanese harbours along the Red Sea Coast. *Microchemical Journal,* **87**, 104-112.

Inoue, M., Ould Ahmed, B. A., Saito, T., Irshad, M. & Uzoma, K. C. (2008). Comparison of three dielectric moisture sensors for measurement of water in saline sandy soil. *Soil Use and Management,* **24**, 156-162.

IPCC 2007. *Summary for Policymakers,* [Solomon, S., D. Qin, M. Manning, Z. Chen, M. Marquis, K.B. Averyt, M. Tignor and H. L. Miller (eds.)]. Cambridge University Press, Cambridge, United Kingdom and New York, NY, USA. 20 pp.

IPCC 2013. *Climate Change 2013: The Physical Science Basis. Contribution of Working Group I to the Fifth Assessment Report of the Intergovernmental Panel on Climate Change,* [Stocker, T. F., D. Qin, G.-K. Plattner, M. Tignor, S.K. Allen, J. Boschung, A. Nauels, Y. Xia, V. Bex & Midgley., P. M. (eds.)]. Cambridge, United Kingdom and New York, NY, USA: Cambridge University Press. 1535 pp.

ISO Standard (1993). ISO 11465. Soil quality -- Determination of dry matter and water content on a mass basis -- Gravimetric method. *ICS: 13.080.20 Stage: 90.20 (2015-01-15)*.

Järup, L. (2003). Hazards of heavy metal contamination. *British Medical Bulletin,* **68**, 167-182.

Jenkins, G. J., Perry, M. C., Prior, M. J., (2008). The climate of the United Kingdom and recent trends. *Met Office Hadley Centre, Exeter, UK.*

Jensen, D. K., Tuller, M., de Jonge, L. W., Arthur, E. & Moldrup, P. (2015). A New Two-Stage Approach to predicting the soil water characteristic from saturation to oven-dryness. *Journal of Hydrology,* **521**, 498-507.

John, D. A. & Leventhal, J. S. 1995. Chapter 2: Bioavailability of Metals. *In:* Du Bray, E. A. (ed.) *Preliminary compilation of descriptive geoenvironmental mineral deposit models.* Denver, Colorado, USA: United States Geological Survey. pp.

Johnson, C. A., Kaeppeli, M., Brandenberger, S., Ulrich, A. & Baumann, W. (1999). Hydrological and geochemical factors affecting leachate composition in municipal solid waste incinerator bottom ash: Part II. The geochemistry of leachate from Landfill Lostorf, Switzerland. *Journal of Contaminant Hydrology,* **40**, 239-259.

Jones, B. (2008). Lyme Regis Landslip Pictures. *[online], available: http://www.thedailynovel.com/?p=636 [accessed 16th March 2012]*.

Jones, K. C. & de Voogt, P. (1999). Persistent organic pollutants (POPs): state of the science. *Environmental Pollution,* **100**, 209-221.

Jones, V. J., Rose, N. L., Self, A. E., Solovieva, N. & Yang, H. (2015). Evidence of global pollution and recent environmental change in Kamchatka, Russia. *Global and Planetary Change*.

Jørgensen, B. & Kasten, S. 2006. Sulfur Cycling and Methane Oxidation. *In:* Schulz, H. & Zabel, M. (eds.) *Marine Geochemistry.* Springer Berlin Heidelberg. 271-309 pp.

Jowsey, P. C. (1966). An Improved Peat Sampler. *New Phytologist,* **65**, 245-248.

Jürgens, M. D., Chaemfa, C., Hughes, D., Johnson, A. C. & Jones, K. C. (2015). PCB and organochlorine pesticide burden in eels in the lower Thames River (UK). *Chemosphere,* **118**, 103-111.

Kadiri, M., Spencer, K. L., Heppell, C. M. & Fletcher, P. (2011). Sediment characteristics of a restored saltmarsh and mudflat in a managed realignment scheme in Southeast England. *Hydrobiologia,* **672**, 79-89.

Kalman, J., Smith, B. D., Bury, N. R. & Rainbow, P. S. (2014). Biodynamic modelling of the bioaccumulation of trace metals (Ag, As and Zn) by an infaunal estuarine invertebrate, the clam Scrobicularia plana. *Aquatic Toxicology,* **154**, 121-130.

Kalnejais, L. H., Martin, W. R. & Bothner, M. H. (2015). Porewater dynamics of silver, lead and copper in coastal sediments and implications for benthic metal fluxes. *Science of The Total Environment,* **517**, 178-194.

Kalnicky, D. J. & Singhvi, R. (2001). Field portable XRF analysis of environmental samples. *Journal of Hazardous Materials,* **83**, 93-122.

Karageorgis, A., Katsanevakis, S. & Kaberi, H. (2009). Use of Enrichment Factors for the Assessment of Heavy Metal Contamination in the Sediments of Koumoundourou Lake, Greece. *Water, Air, and Soil Pollution,* **204**, 243-258.

Kargas, G. & Kerkides, P. (2008). Water content determination in mineral and organic porous media by ML2 theta probe. *Irrigation and Drainage,* **57**, 435-449.

Kaushik, A., Kansal, A., Santosh, Meena, Kumari, S. & Kaushik, C. P. (2009). Heavy metal contamination of river Yamuna, Haryana, India: Assessment by Metal Enrichment Factor of the Sediments. *Journal of Hazardous Materials,* **164**, 265-270.

Kelleners, T. J., Soppe, R. W. O., Ayars, J. E. & Skaggs, T. H. (2004). Calibration of Capacitance Probe Sensors in a Saline Silty Clay Soil. *Soil Science Society of America Journal,* **68**, 770-778.

Kennish, M. J. (2002). Environmental threats and environmental futures of estuaries. *Environmental Conservation,* **29**, 78-107.

Kersten, M. & Smedes, F. (2002). Normalization procedures for sediment contaminants in spatial and temporal trend monitoring. *Journal of Environmental Monitoring,* **4**, 109-115.

Kiddee, P., Naidu, R. & Wong, M. H. (2013). Metals and polybrominated diphenyl ethers leaching from electronic waste in simulated landfills. *Journal of Hazardous Materials,* **252–253**, 243-249.

Kido, Y., Koshikawa, T. & Tada, R. (2006). Rapid and quantitative major element analysis method for wet fine-grained sediments using an XRF microscanner. *Marine Geology,* **229**, 209-225.

Kilbride, C., Poole, J. & Hutchings, T. R. (2006). A comparison of Cu, Pb, As, Cd, Zn, Fe, Ni and Mn determined by acid extraction/ICP–OES and ex situ field portable X-ray fluorescence analyses. *Environmental Pollution,* **143**, 16-23.

Kim, G., Hussain, N., Chureh, T. M. & Carey, W. L. (1997). The fallout isotope ^{207}Bi in a Delaware salt marsh: a comparison with ^{210}Pb and ^{137}Cs as a geochronological tool. *Science of The Total Environment,* **196**, 31-41.

Kirtay, V. J., Kellum, J. H. & Apitz, S. E. (1998). Field-portable X-ray Fluorescence Spectrometry for metals in marine sediments: Results from multiple sites. *Water Science and Technology,* **37**, 141-148.

Kjeldsen, P., Barlaz, M. A., Rooker, A. P., Baun, A., Ledin, A. & Christensen, T. H. (2002). Present and long-term composition of MSW landfill leachate: a review. *Critical Reviews in Environmental Science and Technology,* **32**, 297-336.

Kostka, J., Roychoudhury, A. & Van Cappellen, P. (2002). Rates and controls of anaerobic microbial respiration across spatial and temporal gradients in saltmarsh sediments. *Biogeochemistry,* **60**, 49-76.

Kregsamer, P., Streli, C., Wobrauschek, P., Gatterbauer, H., Pianetta, P., Palmetshofer, L. & Brehm, L. L. (1999). Synchrotron radiation-excited glancing incidence xrf for depth profile and thin-film analysis of light elements. *X-Ray Spectrometry,* **28**, 292-296.

Krishnaswamy, S., Lal, D., Martin, J. M. & Meybeck, M. (1971). Geochronology of lake sediments. *Earth and Planetary Science Letters,* **11**, 407-414.

Kulikowska, D. & Klimiuk, E. (2008). The effect of landfill age on municipal leachate composition. *Bioresource Technology,* **99**, 5981-5985.

Lambeck, K. (1991). Glacial rebound and sea-level change in the British Isles. *Terra Nova,* **3**, 379-389.

Landfill Directive (1999/31/EC). of 26th April 1999 on the landfilling of waste. *Official Journal of the European Communities*.

Lavery, S. & Donovan, B. (2005). Flood risk management in the Thames Estuary looking ahead 100 years. *Philosophical Transactions of the Royal Society A: Mathematical, Physical and Engineering Sciences,* **363**, 1455-1474.

Lavoie, R. A., Jardine, T. D., Chumchal, M. M., Kidd, K. A. & Campbell, L. M. (2013). Biomagnification of Mercury in Aquatic Food Webs: A Worldwide Meta-Analysis. *Environmental Science & Technology,* **47**, 13385-13394.

Lee, P.-k., Kang, M.-J., Choi, S.-H. & Touray, J.-C. (2005). Sulfide oxidation and the natural attenuation of arsenic and trace metals in the waste rocks of the abandoned Seobo tungsten mine, Korea. *Applied Geochemistry,* **20**, 1687-1703.

Lemiere, B., Laperche, V., Haouche, L. & Auger, P. (2014). Portable XRF and wet materials: application to dredged contaminated sediments from waterways. *Geochemistry: Exploration, Environment, Analysis,* **14**, 257-264.

Lerouge, C., Gaucher, E. C., Tournassat, C., Negrel, P., Crouzet, C., Guerrot, C., Gautier, A., Michel, P., Vinsot, A. & Buschaert, S. (2010). Strontium distribution and origins in a natural clayey formation (Callovian-Oxfordian, Paris Basin, France): A new sequential extraction procedure. *Geochimica et Cosmochimica Acta,* **74**, 2926-2942.

Li, X., Wai, O. W. H., Li, Y. S., Coles, B. J., Ramsey, M. H. & Thornton, I. (2000). Heavy metal distribution in sediment profiles of the Pearl River estuary, South China. *Applied Geochemistry,* **15**, 567-581.

Li, Y., Li, J., Chen, S. & Diao, W. (2012). Establishing indices for groundwater contamination risk assessment in the vicinity of hazardous waste landfills in China. *Environmental Pollution,* **165**, 77-90.

Liaghati, T., Preda, M. & Cox, M. (2004). Heavy metal distribution and controlling factors within coastal plain sediments, Bells Creek catchment, southeast Queensland, Australia. *Environment International,* **29**, 935-948.

Licheng, Z. & Guijiu, Z. (1996). The species and geochemical characteristics of heavy metals in the sediments of Kangjiaxi River in the Shuikoushan Mine Area, China. *Applied Geochemistry,* **11**, 217-222.

Lim, H.-S., Lee, J.-S., Chon, H.-T. & Sager, M. (2008). Heavy metal contamination and health risk assessment in the vicinity of the abandoned Songcheon Au–Ag mine in Korea. *Journal of Geochemical Exploration,* **96**, 223-230.

Lion, L. W., Altmann, R. S. & Leckie, J. O. (1982). Trace-metal adsorption characteristics of estuarine particulate matter: evaluation of contributions of iron/manganese oxide and organic surface coatings. *Environmental Science & Technology,* **16**, 660-666.

Liu, X., Colman, S., Brown, E., Minor, E. & Li, H. (2013). Estimation of carbonate, total organic carbon, and biogenic silica content by FTIR and XRF techniques in lacustrine sediments. *Journal of Paleolimnology,* **50**, 387-398.

Lopez, A., Pagano, M., Volpe, A. & Di Pinto, A. C. (2004). Fenton's pre-treatment of mature landfill leachate. *Chemosphere,* **54**, 1005-1010.

Lord III, C. J. & Church, T. M. (1983). The geochemistry of salt marshes: Sedimentary ion diffusion, sulfate reduction, and pyritization. *Geochimica et Cosmochimica Acta,* **47**, 1381-1391.

Loring, D. H. (1991). Normalization of heavy-metal data from estuarine and coastal sediments. *Journal of Marine Science,* **48**, 101-115.

Loska, K., Wiechuła, D. & Korus, I. (2004). Metal contamination of farming soils affected by industry. *Environment International,* **30**, 159-165.

Louriño-Cabana, B., Lesven, L., Charriau, A., Billon, G., Ouddane, B. & Boughriet, A. (2011). Potential risks of metal toxicity in contaminated sediments of Deûle river in Northern France. *Journal of Hazardous Materials,* **186**, 2129-2137.

Lovrenčić Mikelić, I., Oreščanin, V. & Barišić, D. (2013). Distribution and origin of major, minor, and trace elements in sediments and sedimentary rocks of the Kaštela Bay (Croatia) coastal area. *Journal of Geochemical Exploration,* **128**, 1-13.

Lowe, J. A., Gregory, J. M. & Flather, R. A. (2001). Changes in the occurrence of storm surges around the United Kingdom under a future climate scenario using a dynamic storm surge model driven by the Hadley Centre climate models. *Climate Dynamics,* **18**, 179-188.

Luoma, S. N. & Rainbow, P. S. (2008). *Metal Contamination in Aquatic Environments: Science and Lateral Management*, Cambridge University Press. 573 pp.

Luther III, G. W. & Church, T. M. (1988). Seasonal cycling of sulfur and iron in porewaters of a Delaware salt marsh. *Marine Chemistry,* **23**, 295-309.

Machado, W., Moscatelli, M., Rezende, L. G. & Lacerda, L. D. (2002). Mercury, zinc, and copper accumulation in mangrove sediments surrounding a large landfill in southeast Brazil. *Environmental Pollution,* **120**, 455-461.

MacKenzie, A., Scott, R., Allan, R., Ben Shaban, Y., Cook, G. & Pulford, I. (1994). Sediment radionuclide profiles: implications for mechanisms of Sellafield waste dispersal in the Irish Sea. *Journal of Environmental Radioactivity,* **23**, 39-69.

Martin, M., E., & Richards, M. J. (2010). PCB And Heavy Metal Soil Remediation, Former Boat Yard, South Dartmouth, Massachusetts. *Proceedings of the Annual International Conference on Soils, Sediments, Water and Energy,* **14**, 9.

Mayer, L. M., Chen, Z., Findlay, R. H., Fang, J., Sampson, S., Self, R. F. L., Jumars, P. A., Quetél, C. & Donard, O. F. X. (1996). Bioavailability of Sedimentary Contaminants Subject to Deposit-Feeder Digestion. *Environmental Science & Technology,* **30**, 2641-2645.

McCarthy, J. F. & Zachara, J. M. (1989). Subsurface transport of contaminants. *Environmental Science & Technology,* **23**, 496-502.

McIntosh, A. D., Fryer, R. J., Webster, L. & Cundy, A. B. (2012). Long-term fate of polycyclic aromatic hydrocarbons (PAH) in sediments from Loch Leven after closure of an aluminium smelter. *Journal of Environmental Monitoring,* **14**, 1335-1344.

Michalak, A. M. & Kitanidis, P. K. Year. Application of Bayesian inference methods to inverse modeling for contaminant source identification at Gloucester Landfill, Canada. *In:* Hassanizadeh, S. M., Schotting, R. J., Gray, W. G. & Pinder, G. F., eds. XIVth International Conference on Computational Methods in Water Resources, 2002 Delft, The Netherlands. Elsevier.

Mil-Homens, M., Costa, A. M., Fonseca, S., Trancoso, M. A., Lopes, C., Serrano, R. & Sousa, R. (2013). Characterization of Heavy-Metal Contamination in Surface Sediments of the Minho River Estuary by way of Factor Analysis. *Archives of Environmental Contamination and Toxicology,* **64**, 617-631.

Miller, H., Croudace, I. W., Bull, J. M., Cotterill, C. J., Dix, J. K. & Taylor, R. N. (2014). A 500 year sediment lake record of anthropogenic and natural inputs to Windermere (English Lake District) using Double-spike Lead Isotopes, Radiochronology and Sediment microanalysis. *Environmental Science and Technology,* **48**.

Miller, J. D., Gaskin, G. L., (1999). ThetaProbe ML2X. Principles of Operation and Application. *MLURI Technical Note (2nd Edition)*.

Millward, G. E., Kitts, H. J., Ebdon, L., Allen, J. I. & Morris, A. W. (1997). Arsenic in the Thames Plume, UK. *Marine Environmental Research,* **44**, 51-67.

Möller, I., Kudella, M., Rupprecht, F., Spencer, T., Paul, M., van Wesenbeeck, B. K., Wolters, G., Jensen, K., Bouma, T. J., Miranda-Lange, M. & Schimmels, S. (2014). Wave attenuation over coastal salt marshes under storm surge conditions. *Nature Geoscience,* **7**, 727-731.

Morishige, Y., Kimura, A., (2008). Ionization Interference in Inductively Coupled Plasma-Optical Emission Spectroscopy. *SEI Technical Review,* **66**.

Morris, J. W. F., Vasuki, N. C., Baker, J. A. & Pendleton, C. H. (2003). Findings from long-term monitoring studies at MSW landfill facilities with leachate recirculation. *Waste Management,* **23**, 653-666.

Morritt, D., Stefanoudis, P. V., Pearce, D., Crimmen, O. A. & Clark, P. F. (2014). Plastic in the Thames: A river runs through it. *Marine Pollution Bulletin,* **78**, 196-200.

Mortimer, R. J. G. & Rae, J. E. (2000). Metal Speciation (Cu, Zn, Pb, Cd) and Organic Matter in Oxic to Suboxic Salt Marsh Sediments, Severn Estuary, Southwest Britain. *Marine Pollution Bulletin,* **40**, 377-386.

Mouser, P. J., Rizzo, D. M., Röling, W. F. M. & van Breukelen, B. M. (2005). A Multivariate Statistical Approach to Spatial Representation of Groundwater Contamination using Hydrochemistry and Microbial Community Profiles. *Environmental Science & Technology,* **39**, 7551-7559.

Müller, B., Granina, L., Schaller, T., Ulrich, A. & Wehrli, B. (2002). P, As, Sb, Mo, and other elements in sedimentary Fe/Mn layers of Lake Baikal. *Environmental science & technology,* **36**, 411-420.

Nas, B., Cay, T., Iscan, F. & Berktay, A. (2010). Selection of MSW landfill site for Konya, Turkey using GIS and multi-criteria evaluation. *Environmental monitoring and assessment,* **160**, 491-500.

Natural England. 2014. *Special Areas of Conservation* [Online]. Available: http://www.naturalengland.org.uk/ourwork/conservation/designations/sac/ [Accessed 7th August 2014].

Néel, C., Soubrand-Colin, M., Piquet-Pissaloux, A. & Bril, H. (2007). Mobility and bioavailability of Cr, Cu, Ni, Pb and Zn in a basaltic grassland: Comparison of selective extractions with quantitative approaches at different scales. *Applied Geochemistry,* **22**, 724-735.

Neuhold, C. (2013). Identifying flood-prone landfills at different spatial scales. *Natural hazards,* **68**, 1425-1440.

NIGLQ (2011). Qualitative Risk Assessment for Land Contamination, including Radioactive Contamination. *Industry Guidance; Nuclear Industry Group for Land Quality*.

NITON. 2010. *Portable XRF Analysers Detection Limits* [Online]. NITON. Available: http://www.niton.com/en/forum/archive/lists/forum-archive/element-detection-limits- [Accessed 12th December 2014].

Njue, C., Cundy, A., Smith, M., Green, I. & Tomlinson, N. (2012). Assessing the impact of historical coastal landfill sites on sensitive ecosystems: A case study from Dorset, Southern England. *Estuarine, Coastal and Shelf Science,* **114**, 166-174.

Noborio, K. (2001). Measurement of soil water content and electrical conductivity by time domain reflectometry: a review. *Computers and Electronics in Agriculture,* **31**, 213-237.

Nuttle, W. K. (1988). The extent of lateral water movement in the sediments of a New England Salt Marsh. *Water Resources Research,* **24**, 2077-2085.

O'Reilly Wiese, S. B., Bubb, J. M. & Lester, J. N. (1995). The significance of sediment metal concentrations in two eroding Essex salt marshes. *Marine Pollution Bulletin,* **30**, 190-199.

O'Reilly Wiese, S. B., Emmerson, R. H. C., MacLeod, C. L. & Lester, J. N. (1997a). Trends in the solid phase partitioning of metals in the Thames Estuary sediments during recent decades. *Estuaries,* **20**, 494-503.

O'Reilly Wiese, S. B., MacLeod, C. L. & Lester, J. N. (1997b). A recent history of metal accumulation in the sediments of the Thames Estuary, United Kingdom. *Estuaries,* **20**, 483-493.

O'Kelly, B. C. (2004). Accurate Determination of Moisture Content of Organic Soils Using the Oven Drying Method. *Drying Technology,* **22**, 1767-1776.

Olaniran, A. O., Balgobind, A. & Pillay, B. (2013). Bioavailability of Heavy Metals in Soil: Impact on Microbial Biodegradation of Organic Compounds and Possible Improvement Strategies. *International Journal of Molecular Science,* **14**, 31.

Olesik, J. W. (1991). Elemental Analysis Using ICP-OES and ICP/MS. *Analytical Chemistry,* **63**, 12A-21A.

Onay, T. T. & Pohland, F. G. (1998). In situ nitrogen management in controlled bioreactor landfills. *Water Research,* **32**, 1383-1392.

Osada, T., Nemoto, K., Nakanishi, H., Hatano, A., Shoji, R., Naruoka, T. & Yamada, M. (2011). Analysis of Ammonia Toxicity in Landfill Leachates. *ISRN Toxicology,* **2011**, 6.

OSPAR (2001). OSPAR Recommendation 2001/1 for the Management of Produced Water from Offshore Installations. 14.

Oughton, D. H., Salbu, B., Brand, T. L., Day, J. P. & Aarkrog, A. (1993). Under-determination of strontium-90 in soils containing particles of irradiated uranium oxide fuel. *Analyst,* **118**, 1101-1105.

Paller, M. H. & Knox, A. S. (2013). Bioavailability of Metals in Contaminated Sediments. *Web of Conferences,* **1**.

Pan, K. & Wang, W.-X. (2012). Trace metal contamination in estuarine and coastal environments in China. *Science of The Total Environment,* **421–422**, 3-16.

Pande, A. & Nayak, G. N. (2013). Understanding distribution and abundance of metals with space and time in estuarine mudflat sedimentary environment. *Environmental Earth Sciences,* **70**, 2561-2575.

Paquin, P. R., Gorsuch, J. W., Apte, S., Batley, G. E., Bowles, K. C., Campbell, P. G. C., Delos, C. G., Di Toro, D. M., Dwyer, R. L., Galvez, F., Gensemer, R. W., Goss, G. G., Hogstrand, C., Janssen, C. R., McGeer, J. C., Naddy, R. B., Playle, R. C.,

Santore, R. C., Schneider, U., Stubblefield, W. A., Wood, C. M. & Wu, K. B. (2002). The biotic ligand model: a historical overview. *Comparative Biochemistry and Physiology Part C: Toxicology & Pharmacology,* **133**, 3-35.

Pardu, J., Patrick Jr, W. H. & Herbert, A. (1995). Changes in metal speciation following alteration of sediment redox status. *Metal Contaminated Aquatic Sediments*, 169-185.

Parsons, C., Margui Grabulosa, E., Pili, E., Floor, G. H., Roman-Ross, G. & Charlet, L. (2013). Quantification of trace arsenic in soils by field-portable X-ray fluorescence spectrometry: considerations for sample preparation and measurement conditions. *J Hazard Mater,* **262**, 1213-22.

Parsons, M. J., Long, D. T., Giesy, J. P. & Kannan, K. (2014). Inferring Sources for Mercury to Inland Lakes Using Sediment Chronologies of Polycyclic Aromatic Hydrocarbons. *Environmental Science: Processes and Impacts,* **16**, 2018-2116.

Peinado, F. M., Ruano, S. M., González, M. G. B. & Molina, C. E. (2010). A rapid field procedure for screening trace elements in polluted soil using portable X-ray fluorescence (PXRF). *Geoderma,* **159**, 76-82.

Pelfrêne, A., Waterlot, C., Mazzuca, M., Nisse, C., Bidar, G. & Douay, F. (2011). Assessing Cd, Pb, Zn human bioaccessibility in smelter-contaminated agricultural topsoils (northern France). *Environmental Geochemistry and Health,* **33**, 477-493.

Peng, K., Li, X., Luo, C. & Shen, Z. (2006). Vegetation Composition and Heavy Metal Uptake by Wild Plants at Three Contaminated Sites in Xiangxi Area, China. *Journal of Environmental Science and Health, Part A,* **41**, 65-76.

Perkin Elmer. 2011. The 30-Minute Guide to ICP-MS. *ICP-Mass Spectrometry Technical Note* [Online]. Available: http://www.perkinelmer.co.uk/PDFs/Downloads/tch_icpmsthirtyminuteguide.pdf [Accessed 4th April 2014].

Plater, A. J., Ridgway, J., Appleby, P. G., Berry, A. & Wright, M. R. (1999). Historical Contaminant Fluxes in the Tees Estuary, UK: Geochemical, Magnetic and Radionuclide Evidence. *Marine Pollution Bulletin,* **37**, 343-360.

Pohland, F. G., Gould, J. P. & Ghosh, S. B. (1985). Management of Hazardous Wastes by Landfill Codisposal with Municipal Refuse. *Hazardous Waste and Hazardous Materials,* **2**, 143-158.

Pope, N., O'Hara, S., Imamura, M., Hutchinson, T. & Langston, W. (2011). Influence of a collapsed coastal landfill on metal levels in sediments and biota—a portent for the future? *Journal of Environmental Monitoring,* **13**, 1961-1974.

Pope, N. D. & Langston, W. J. (2011). Sources, distribution and temporal variability of trace metals in the Thames Estuary. *Hydrobiologia,* **672**, 49-68.

Portnoy, J. W. & Valiela, I. (1997). Short-term effects of salinity reduction and drainage on salt-marsh biogeochemical cycling andSpartina (cordgrass production. *Estuaries,* **20**, 569-578.

Potts, P. J., Webb, P. C., Williams-Thorpe, O. & Kilworth, R. (1995). Analysis of silicate rocks using field-portable X-ray fluorescence instrumentation incorporating a mercury(II) iodide detector: a preliminary assessment of analytical performance. *Analyst,* **120**, 1273-1278.

Power, M., Attrill, M. J. & Thomas, R. M. (1999). Heavy metal concentration trends in the Thames Estuary. *Water Research,* **33**, 1672-1680.

Putyrskaya, V., Klemt, E., Röllin, S., Astner, M. & Sahli, H. (2015). Dating of sediments from four Swiss prealpine lakes with 210Pb determined by gamma-spectrometry: progress and problems. *Journal of Environmental Radioactivity,* **145**, 78-94.

Quevauviller, P. (1998). Operationally defined extraction procedures for soil and sediment analysis I. Standardization. *TrAC Trends in Analytical Chemistry,* **17**, 289-298.

Quevauviller, P. & Donard, O. F. X. (1991). Organotin stability during storage of marine waters and sediments. *Fresenius' Journal of Analytical Chemistry,* **339**, 6-14.

Quinn, G. P. & Keough, M. J. (2002). *Experimental Design and Data Analysis for Biologists*, Cambridge University Press. 537 pp.

Radu, T. & Diamond, D. (2009). Comparison of soil pollution concentrations determined using AAS and portable XRF techniques. *Journal of Hazardous Materials,* **171**, 1168-1171.

Rainbow, P. S. (1995). Biomonitoring of heavy metal availability in the marine environment. *Marine Pollution Bulletin,* **31**, 183-192.

Ramsey, M. H. & Thompson, M. (1986). A predictive model of plasma matrix effects in inductively coupled plasma atomic emission spectrometry. *Journal of Analytical Atomic Spectrometry,* **1**, 185-193.

Rao, C., Sahuquillo, A. & Sanchez, J. L. (2008). A review of the different methods applied in environmental geochemistry for single and sequential extraction of trace elements in soils and related materials. *Water, Air, and Soil Pollution,* **189**, 291-333.

Raper, S. C. B. & Braithwaite, R. J. (2006). Low sea level rise projections from mountain glaciers and icecaps under global warming. *Nature,* **439**, 3.

Razali, N. M. & Wah, Y. B. (2011). Power comparisons of shapiro-wilk, kolmogorov-smirnov, lilliefors and anderson-darling tests. *Journal of Statistical Modeling and Analytics,* **2**, 21-33.

Read, A., Phillips, P. & Robinson, G. (1997). Landfill as a future waste management option in England: the view of landfill operators. *Resources, Conservation and Recycling,* **20**, 183-205.

Rees, A. B., Turner, A. & Comber, S. (2014). Metal contamination of sediment by paint peeling from abandoned boats, with particular reference to lead. *Science of The Total Environment,* **494–495**, 313-319.

Reid, M. & Spencer, K. (2009). Use of principal components analysis (PCA) on estuarine sediment datasets: The effect of data pre-treatment. *Environmental Pollution,* **157**, 2275-2281.

Relić, D., Đorđević, D., Sakan, S., Anđelković, I., Miletić, S. & Đuričić, J. (2011). Aqua regia extracted metals in sediments from the industrial area and surroundings of Pančevo, Serbia. *Journal of Hazardous Materials,* **186**, 1893-1901.

Remon, E., Bouchardon, J. L., Cornier, B., Guy, B., Leclerc, J. C. & Faure, O. (2005). Soil characteristics, heavy metal availability and vegetation recovery at a former metallurgical landfill: Implications in risk assessment and site restoration. *Environmental Pollution,* **137**, 316-323.

Renberg, I., Bindler, R. & Brännvall M-L. (2001). using the Historical Atmospheric Lead-Deposition Record as a Chronological Marker in Sediment Deposits in Europe. *The Holocene,* **11**, 511-516.

Revenko, A. G. (2002). X-ray fluorescence analysis of rocks, soils and sediments. *X-Ray Spectrometry,* **31**, 264-273.

Ribeiro, A. P., Figueiredo, A. M. G., Santos, J. O. d., Dantas, E., Cotrim, M. E. B., Cesar Lopes Figueira, R., V. Silva Filho, E. & Cesar Wasserman, J. (2013). Combined SEM/AVS and attenuation of concentration models for the assessment of bioavailability and mobility of metals in sediments of Sepetiba Bay (SE Brazil). *Marine Pollution Bulletin,* **68**, 55-63.

Robinson, P. (1980). Determination of calcium, magnesium, manganese, strontium, sodium and iron in the carbonate fraction of limestones and dolomites. *Chemical Geology,* **28**, 135-146.

Rodríguez-Germade, I., Rubio, B. & Rey, D. (2014). XRF scanners as a quick screening tool for detecting toxic pollutant elements in sediments from Marín harbour in the Ría de Pontevedra (NW Spain). *Marine Pollution Bulletin,* **86**, 458-467.

Rose, A. L. (2003). Effect of Dissolved Natural Organic Matter on the Kinetics of Ferrous Iron Oxygenation in Seawater. *Environmental Science & Technology,* **37**, 4877-4886.

Rothwell, J. J., Evans, M. G., Lindsay, J. B. & Allott, T. E. H. (2007). Scale-dependent spatial variability in peatland lead pollution in the southern Pennines, UK. *Environmental Pollution,* **145**, 111-120.

Rowell, D. L. (1994). *Soil Science: Methods & Application*, Routledge. 360 pp.

Rubio, B., Nombela, M. & Vilas, F. (2000). Geochemistry of major and trace elements in sediments of the Ria de Vigo (NW Spain): an assessment of metal pollution. *Marine Pollution Bulletin,* **40**, 968-980.

Ruiz-Fernández, A. C., Páez-Osuna, F., Hillaire-Marcel, C., Soto-Jiménez, M. & Ghaleb, B. (2001). Principal Component Analysis Applied to the Assessment of Metal Pollution from Urban Wastes in the Culiacán River Estuary. *Bulletin of Environmental Contamination and Toxicology,* **67**, 741-748.

Sakan, S. M., Dordevic, D. S., Manojlovic, D. D., Predrag, P. S., (2009). Assessment of Heavy Metal Pollutants Accumulation in the Tisza River Sediments. *Journal of Environmental Management,* **90**, 8.

Salomons, W. (1975). Chemical and Isotopic Composition of Carbonates in Recent Sediments and Soils from Western Europe. *Journal of Sedimentary Research,* **45**, 440-449.

Sastre, J., Sahuquillo, A., Vidal, M. & Rauret, G. (2002). Determination of Cd, Cu, Pb and Zn in environmental samples: microwave-assisted total digestion versus aqua regia and nitric acid extraction. *Analytica Chimica Acta,* **462**, 59-72.

Sauerbeck, D. R. (1991). Plant element and soil properties governing uptake and availability of heavy metals derived from sewage sludge. *Water, Air, and Soil Pollution,* **57-58**, 227-237.

Sauve, S., Hendershot, W. & Allen, H. E. (2000). Solid-solution partitioning of metals in contaminated soils: dependence on pH, total metal burden, and organic matter. *Environmental Science & Technology,* **34**, 1125-1131.

Schmutz, P. P. & Namikas, S. L. (2011). Utility of the Delta-T Theta Probe for Obtaining Surface Moisture Measurements from Beaches. *Journal of Coastal Research,* **27**, 478-484.

Schnug, E. & Lottermoser, B. G. (2013). Fertilizer-Derived Uranium and its Threat to Human Health. *Environmental Science & Technology,* **47**, 2433-2434.

Schwarzbauer, J., Heim, S., Brinker, S. & Littke, R. (2002). Occurrence and alteration of organic contaminants in seepage and leakage water from a waste deposit landfill. *Water Research,* **36**, 2275-2287.

Scrimshaw, M. D., Bubb, J. M. & Lester, J. N. (1996). Organochlorine Contamiantion of UK Essex Coast Salt Marsh Sediments. *Journal of Coastal Research,* **12**, 246-255.

SedNet (2004). Contaminated Sediments in European River Basins. *Abatement of water pollution from contaminated land, landfills and sediments.*

Şener, B., Süzen, M. L. & Doyuran, V. (2006). Landfill site selection by using geographic information systems. *Environmental Geology,* **49**, 376-388.

Shan, X. Q. & Chen, B. (1993). Evaluation of sequential extraction for speciation of trace metals in model soil containing natural minerals and humic acid. *Analytical Chemistry,* **65**, 802-807.

Shand, C. A. & Wendler, R. (2014). Portable X-ray fluorescence analysis of mineral and organic soils and the influence of organic matter. *Journal of Geochemical Exploration,* **143**, 31-42.

Sharma, R. K., Agrawal, M. & Marshall, F. (2007). Heavy metal contamination of soil and vegetables in suburban areas of Varanasi, India. *Ecotoxicology and Environmental Safety,* **66**, 258-266.

Shaw, T. J., Gieskes, J. M. & Jahnke, R. A. (1990). Early Diagenesis in Differing Depositional Environments: The Response of Transition Metals in Pore Water. *Geochimica et Cosmochimica Acta,* **544**, 1233-1246.

Sheahan, D. (2006). Impacts of climate change on pollution. In: Buckley, P. J., Dye, S. R., Baxter, J M., (Eds.), Marine Climate Change Impacts Annual Report Card 2006,. *Online Summary Reports, MCCIP, Lowestoft.*

Sheldon, R. W. (1968). Sedimentation in the estuary of the River Crouch, Essex, England. *Limnology and Oceanography,* **13**, 72-83.

Shennan, I. (1989). Holocene crustal movements and sea level changes in Great Britain. *Journal of Quaternary Science,* **4**, 4.

Shepard, F. P. (1954). Nomenclature Based on Sand-Silt-Clay Ratios. *Journal of Sedimentary Petrology,* **5**, 24.

Shukla, O. P. & Rai, U. N. (2009). Natural attenuation: A potential for environmental clean-up. *International Society of Environmental Botanists,* **15**.

Shuttleworth, E., Evans, M., Hutchinson, S. & Rothwell, J. (2014). Assessment of Lead Contamination in Peatlands Using Field Portable XRF. *Water, Air, & Soil Pollution,* **225**, 1-13.

Silvestri, S., Defina, A. & Marani, M. (2005). Tidal regime, salinity and salt marsh plant zonation. *Estuarine, Coastal and Shelf Science,* **62**, 119-130.

Simms, A. D., Woodroffe, C., Jones, B. G., Heijnis, H., Mann, R. A. & Harrison, J. (2008). Use of 210Pb and 137Cs to simultaneously constrain ages and sources of post-dam

sediments in the Cordeaux reservoir, Sydney, Australia. *Journal of Environmental Radioactivity,* **99**, 1111-1120.

Simpson, S. L., Apte, S. C. & Batley, G. E. (1998). Effect of Short-Term Resuspension Events on Trace Metal Speciation in Polluted Anoxic Sediments. *Environmental Science & Technology,* **32**, 620-625.

Simpson, S. L., Rosner, J. & Ellis, J. (2000). Competitive displacement reactions of cadmium, copper, and zinc added to a polluted, sulfidic estuarine sediment. *Environmental Toxicology and Chemistry,* **19**, 1992-1999.

Slack, R., Gronow, J. & Voulvoulis, N. (2005). Household hazardous waste in municipal landfills: contaminants in leachate. *Science of The Total Environment,* **337**, 119-137.

Smith, J., Nicholson, R. & Moore, P. (1973). Mercury in sediments from the Thames estuary. *Environmental Pollution,* **4**, 153-157.

Sneddon, J., Clemente, R., Riby, P. & Lepp, N. W. (2009). Source-pathway-receptor investigation of the fate of trace elements derived from shotgun pellets discharged in terrestrial ecosystems managed for game shooting. *Environmental Pollution,* **157**, 2663-2669.

Solomon, S., Qin. D., Manning. M., Chen. Z., Marquis. M., Averyt. K. B., Tignor. M. & Miller. H. L. 2007. *Climate Change 2007: The Physical Science Basis. Contribution of Working Group I to the Fourth Assessment Report of the Intergovernmental Panel on Climate Change,* (eds.)]. Cambridge, United Kingdom and New York, NY, USA: Cambridge University Press. 996 pp.

Speelmans, M., Vanthuyne, D. R. J., Lock, K., Hendrickx, F., Du, L. G., Tack, F. M. G. & Janssen, C. R. (2007). Influence of flooding, salinity and inundation time on the bioavailability of metals in wetlands. *Science of The Total Environment,* **380**, 144-153.

Spencer, K., Cundy, A., Davies-Hearn, S., Hughes, R., Turner, S. & MacLeod, C. (2008). Physicochemical changes in sediments at Orplands Farm, Essex, UK following 8 years of managed realignment. *Estuarine, Coastal and Shelf Science,* **76**, 608-619.

Spencer, K. L. (2002). Spatial variability of metals in the inter-tidal sediments of the Medway Estuary, Kent, UK. *Marine Pollution Bulletin,* **44**, 933-944.

Spencer, K. L., Cundy, A. B. & Croudace, I. W. (2003). Heavy metal distribution and early-diagenesis in salt marsh sediments from the Medway Estuary, Kent, UK. *Estuarine, Coastal and Shelf Science,* **57**, 43-54.

Sposito, G. 1987. Distinguishing Adsorption from Surface Precipitation. *Geochemical Processes at Mineral Surfaces.* American Chemical Society. 217-228 pp.

Stallard, M. O., Apitz, S. E. & Dooley, C. A. (1995). X-ray fluorescence spectrometry for field analysis of metals in marine sediments. *Marine Pollution Bulletin,* **31**, 297-305.

Statutory Instruments (2002). Landfill (England and Wales) Regulations. *SI 2002/1559.*

Suchkova, N., Darakas, E. & Ganoulis, J. (2010). Phytoremediation as a prospective method for rehabilitation of areas contaminated by long-term sewage sludge storage: A Ukrainian–Greek case study. *Ecological Engineering,* **36**, 373-378.

Sundaray, S. K., Nayak, B. B., Lin, S. & Bhatta, D. (2011). Geochemical speciation and risk assessment of heavy metals in the river estuarine sediments—A case study: Mahanadi basin, India. *Journal of Hazardous Materials,* **186**, 1837-1846.

Szava-Kovats, R. C. (2008). Grain-size normalization as a tool to assess contamination in marine sediments: Is the <63μm fraction fine enough? *Marine Pollution Bulletin,* **56**, 629-632.

Tabachnick, B. G. & Fidell, L. S. (2006). *Using Multivariate Statistics*, Pearson. 5th Edition. pp.

Tam, N. F. Y. & Yao, M. W. Y. (1998). Normalisation and heavy metal contamination in mangrove sediments. *Science of The Total Environment,* **216**, 33-39.

Tavakoly Sany, S., Salleh, A., Rezayi, M., Saadati, N., Narimany, L. & Tehrani, G. (2013). Distribution and Contamination of Heavy Metal in the Coastal Sediments of Port Klang, Selangor, Malaysia. *Water, Air, & Soil Pollution,* **224**, 1-18.

Teasdale, P. A., Collins, P. E., Firth, C. R. & Cundy, A. B. (2011). Recent estuarine sedimentation rates from shallow inter-tidal environments in western Scotland: implications for future sea-level trends and coastal wetland development. *Quaternary Science Reviews,* **30**, 109-129.

Tempest, J. A., Harvey, G. L. & Spencer, K. L. (2014). Modified sediments and subsurface hydrology in natural and recreated salt marshes and implications for delivery of ecosystem services. *Hydrological Processes,* **29**, 2346-2357.

Thamdrup, B. 2000. Bacterial Manganese and Iron Reduction in Aquatic Sediments. *In:* Schink, B. (ed.) *Advances in Microbial Ecology.* Springer US. 41-84 pp.

Thamdrup, B., Fossing, H. & Jørgensen, B. B. (1994). Manganese, iron and sulfur cycling in a coastal marine sediment, Aarhus bay, Denmark. *Geochimica et Cosmochimica Acta,* **58**, 5115-5129.

Thermo Scientific. 2011. Thermo Scientific. X-Ray Energy Reference. Available: http://www.niton.com/docs/literature/nitonperiodictable_fxl_2011jan24.pdf?sfvrsn=2 [Accessed 7th April 2104].

Tipping, E., Rothwell, J. J., Shotbolt, L. & Lawlor, A. J. (2010). Dynamic modelling of atmospherically-deposited Ni, Cu, Zn, Cd and Pb in Pennine catchments (northern England). *Environmental Pollution,* **158**, 1521-1529.

Tjallingii, R., Röhl, U., Kölling, M. & Bickert, T. (2007). Influence of the water content on X-ray fluorescence core-scanning measurements in soft marine sediments. *Geochemistry, Geophysics, Geosystems,* **8**, 1-12.

Tokalioğlu, Ş., Kartal Ş. & Birol, G. (2003). Application of a Three-stage Sequential Extraction procedure for the determination of extractable metal contents in highway soils. *Turkish Journal of Chemistry,* **27**, 333-346.

Topp, G. C., Davis, J. L. & Annan, A. P. (1980). Electromagnetic determination of soil water content: Measurements in coaxial transmission lines. *Water Resources Research,* **16**, 574-582.

Towett, E. K., Shepherd, K. D. & Cadisch, G. (2013). Quantification of total element concentrations in soils using total X-ray fluorescence spectroscopy (TXRF). *Science of The Total Environment,* **463–464**, 374-388.

Trimmer, M., Nedwell, D. B., Sivyer, D. B. & Malcolm, S. J. (2000). Seasonal benthic organic matter mineralisation measured by oxygen uptake and denitrification along a transect of the inner and outer River Thames estuary, UK. *Marine Ecology Progress Series,* **197**, 103-119.

Trimmer, M., Nicholls, J. C. & Deflandre, B. (2003). Anaerobic Ammonium Oxidation Measured in Sediments along the Thames Estuary, United Kingdom. *Applied and Environmental Microbiology,* **69**, 6447-6454.

Trivedi, P., Axe, L. (2000). Modeling Cd and Zn Sorption to Hydrous Metal Oxides. *Environmental Science and Technology,* **34**, 2215-2223.

Turner, A. (2013). Metal contamination of soils, sediments and dusts in the vicinity of marine leisure boat maintenance facilities. *Journal of Soils and Sediments,* **13**, 1052-1056.

Udayakumar, P., Jose, J. J., Krishnan, K. A., Kumar, C. S. R., Manju, M. N. & Salas, P. M. (2014). Heavy metal accumulation in the surficial sediments along southwest coast of India. *Environmental Earth Sciences,* **72**, 1887-1900.

US-EPA (2007). Field Portable X-Ray Fluorescence Spectrometry for the Determination of Elemental Concentrations in Soil and Sediment, Method 6200. *United States Environmental Protection Agency,* **Revision 0**.

Usero, J., Gamero, M., Morillo, J. & Gracia, I. (1998). Comparative study of three sequential extraction procedures for metals in marine sediments. *Environment International,* **24**, 487-496.

Valette-Silver, N. J. (1993). The Use of Sediment Cores to Reconstruct Historical Trends in Contamination of Estuarine and Coastal Sediments. *Estuaries,* **16**, 577-588.

Van Cappellen, P. & Wang, Y. (1996). Cycling of Iron and Manganese in Surface Sediments: A General Theory for the Coupled Transport and Reaction of Carbon, Oxygen, Nitrogen, Sulfur, Iron and Manganese. *American Journal of Science,* **296**, 197-243.

van der Wal, D. & Pye, K. (2004). Patterns, rates and possible causes of saltmarsh erosion in the Greater Thames area (UK). *Geomorphology,* **61**, 373-391.

Van Dyck, P. M. & Van Grieken, R. E. (1980). Absorption correction via scattered radiation in energy-dispersive x-ray fluorescence analysis for samples of variable composition and thickness. *Analytical Chemistry,* **52**, 1859-1864.

Vane, C. H., Chenery, S. R., Harrison, I., Kim, A. W., Moss-Hayes, V. & Jones, D. G. (2011). Chemical signatures of the Anthropocene in the Clyde estuary, UK: sediment-hosted Pb, 207/206Pb, total petroleum hydrocarbon, polyaromatic hydrocarbon and

polychlorinated biphenyl pollution records. *Philosophical Transactions of the Royal Society,* **369**, 1085-1111.

Veerasingam, S., Vethamony, P., Mani Murali, R. & Fernandes, B. (2015). Depositional record of trace metals and degree of contamination in core sediments from the Mandovi estuarine mangrove ecosystem, west coast of India. *Marine Pollution Bulletin,* **91**, 362-367.

Vernet, J. P. 1991. *Biological Availability of Metals in Sediments: Analytical Approaches. (Peter G. C. Campbell and Andre Tessier).* [Nriagu, J. (eds.)]. London: Elsevier. pp.

Vranken, M., Oenema, O. & Mulder, J. 1990. Effects of tide range alterations on salt marsh sediments in the Eastern Scheldt, SW Netherlands. *North Sea—Estuaries Interactions.* Springer. 13-20 pp.

Waldron, H. A. (1980). *Metals in the Environment,* London, Academic Press. 333 pp.

Ward, R. D., Teasdale, P. A., Burnside, N. G., Joyce, C. B. & Sepp, K. (2014). Recent rates of sedimentation on irregularly flooded Boreal Baltic coastal wetlands: Responses to recent changes in sea level. *Geomorphology,* **217**, 61-72.

Warith, M. & Sharma, R. (1998). Technical review of methods to enhance biological degradation in sanitary landfills. *Water Quality Research Journal of Canada,* **33**, 417-437.

Waste Management Paper 26B (1995). *Landfill Design, Construction and Operational Practice,* HMSO, London. 289 pp.

Weber, R., Watson, A., Forter, M. & Oliaei, F. (2011). Persistent organic pollutants and landfills-a review of past experiences and future challenges. *Waste Management & Research,* **29**, 107-121.

Weeks, J. M. & Comber, S. D. W. (2005). Ecological Risk Assessment of Contaminated Soil. *Mineralogical Magazine,* **69**, 601-613.

Weindorf, D. C., Paulette, L. & Man, T. (2013). In-situ assessment of metal contamination via portable X-ray fluorescence spectroscopy: Zlatna, Romania. *Environmental Pollution,* **182**, 92-100.

Weltje, G. J. & Tjallingii, R. (2008). Calibration of XRF core scanners for quantitative geochemical logging of sediment cores: Theory and application. *Earth and Planetary Science Letters,* **274**, 423-438.

Wentworth, C. K. (1922). A Scale of Grade and Class Terms for Clastic Sediments. *Journal of Geology,* **30**, 377-392.

Wheeler, A. (1969). Fish-life and pollution in the lower Thames: A review and preliminary report. *Biological Conservation,* **2**, 25-30.

Whiteley, J. D. & Pearce, N. J. G. (2003). Metal distribution during diagenesis in the contaminated sediments of Dulas Bay, Anglesey, N. Wales, UK. *Applied Geochemistry,* **18**, 901-913.

Williams, P. T. (2005). *Waste Treatment and Disposal,* Chichester, John Wiley and Sons Ltd. 2nd Edition. 382 pp.

Williams, T. P., Bubb, J. M., Lester, J. N., (1993). Metal Accumulation Within Salt Marsh Environments: A Review. *Marine Pollution Bulletin,* **28**, 14.

Windham, L., Weis, J. S. & Weis, P. (2001). Lead Uptake, Distribution, and Effects in Two Dominant Salt Marsh Macrophytes, Spartina alterniflora (Cordgrass) and Phragmites australis (Common Reed). *Marine Pollution Bulletin,* **42**, 811-816.

Windham, L., Weis, J. S. & Weis, P. (2003). Uptake and distribution of metals in two dominant salt marsh macrophytes, Spartina alterniflora (cordgrass) and Phragmites australis (common reed). *Estuarine, Coastal and Shelf Science,* **56**, 63-72.

Windom, H. L., Schropp, S. J., Calder, F. D., Ryan, J. D., Smith, R. G., Burney, L. C., Lewis, F. G. & Rawlinson, C. H. (1989). Natural trace metal concentrations in estuarine and coastal marine sediments of the southeastern United States. *Environmental Science & Technology,* **23**, 314-320.

Wolters, M., Bakker, J. P., Bertness, M. D., Jefferies, R. L. & MÖLler, I. (2005a). Saltmarsh erosion and restoration in south-east England: squeezing the evidence requires realignment. *Journal of Applied Ecology,* **42**, 844-851.

Wolters, M., Garbutt, A. & Bakker, J. P. (2005b). Salt-marsh restoration: evaluating the success of de-embankments in north-west Europe. *Biological Conservation,* **123**, 249-268.

Woods, A. M. (2009). *Tracing the Distribution of Heavy Metals in Sediments of the Pearl River Estuary. Durham University. Available at Durham E-Theses Online: http://etheses.dur.ac.uk/87/.*

Yamaguchi, N., Gazzard, D., Scholey, G. & Macdonald, D. W. (2003). Concentrations and hazard assessment of PCBs, organochlorine pesticides and mercury in fish species from the upper Thames: River pollution and its potential effects on top predators. *Chemosphere,* **50**, 265-273.

Yang, Y., Liu, Z., Chen, F., Wu, S., Zhang, L., Kang, M. & Li, J. (2014). Assessment of trace element contamination in sediment cores from the Pearl River and estuary, South China: geochemical and multivariate analysis approaches. *Environmental Monitoring and Assessment,* **186**, 8089-8107.

Yao, X., Xiao, R., Ma, Z., Xie, Y., Zhang, M. & Yu, F. (2015). Distribution and contamination assessment of heavy metals in soils from tidal flat, oil exploitation zone and restored wetland in the Yellow River Estuary. *Wetlands*, 1-13.

Yusof, N., Haraguchi, A., Hassan, M. A., Othman, M. R., Wakisaka, M. & Shirai, Y. (2009). Measuring organic carbon, nutrients and heavy metals in rivers receiving leachate from controlled and uncontrolled municipal solid waste (MSW) landfills. *Waste Management,* **29**, 2666-2680.

Zamorano, M., Molero, E., Hurtado, Á., Grindlay, A. & Ramos, Á. (2008). Evaluation of a municipal landfill site in Southern Spain with GIS-aided methodology. *Journal of Hazardous Materials,* **160**, 473-481.

Zenz, C. 1980. Vanadium. *In:* Waldron, H. A. (ed.) *Metals In The Environment.* London: Academic Press Inc. 333 pp.

Zhao, S., Feng, C., Wang, D., Liu, Y. & Shen, Z. (2013). Salinity increases the mobility of Cd, Cu, Mn, and Pb in the sediments of Yangtze Estuary: Relative role of sediments' properties and metal speciation. *Chemosphere,* **91**, 977-984.

Zhao, S., Wang, D., Feng, C., Wang, Y. & Shen, Z. (2014). Sequence of the main geochemical controls on the Cu and Zn fractions in the Yangtze River estuarine sediments. *Frontiers of Environmental Science & Engineering*, 1-9.

Zhu, Y., Weindorf, D. C. & Zhang, W. (2011). Characterizing soils using a portable X-ray fluorescence spectrometer: 1. Soil texture. *Geoderma,* **167–168**, 167-177.

Zhuang, W. & Gao, X. (2014). Integrated Assessment of Heavy Metal Pollution in the Surface Sediments of the Laizhou Bay and the Coastal Waters of the Zhangzi Island, China: Comparison among Typical Marine Sediment Quality Indices. *PLoS ONE,* **9**, e94145.

Zoumis, T., Schmidt, A., Grigorova, L. & Calmano, W. (2001). Contaminants in sediments: remobilisation and demobilisation. *Science of The Total Environment,* **266**, 195-202.

Zwolsman, J. J., Berger, G. & Van Eck, G. (1993). Sediment accumulation rates, historical input, postdepositional mobility and retention of major elements and trace metals in salt marsh sediments of the Scheldt estuary, SW Netherlands. *Marine Chemistry,* **44**, 73-94.

Zwolsman, J. J. G. & van Eck, G. T. M. (1999). Geochemistry of major elements and trace metals in suspended matter of the Scheldt estuary, southwest Netherlands. *Marine Chemistry,* **66**, 91-111.

Zwolsman, J. J. G., van Eck, G. T. M. & Burger, G. (1996). Spatial and Temporal Distribution of Trace Metals in Sediments from the Scheldt Estuary, South-west Netherlands. *Estuarine, Coastal and Shelf Science,* **43**, 55-79.

Appendix 1: ICP-OES Operational Conditions and LoD

Operational Conditions

Table 1: ICP calibration standards concentrations.

Standard	Concentration (mg kg^{-1})
1	0
2	1
3	2
4	5
5	10
6	20
7	50

Table 2: Elemental wavelengths used

Element	Wavelength Used (nm)
Al	396.152
Ca	315.887
Cd	228.802
Co	230.786
Cr	267.716
Cu	327.395
Fe	234.350
K	766.491
Li	670.783
Mg	280.270
Mn	259.372
Na	588.995
Ni	216.555
Pb	220.353
Sr	460.733
V	292.401
Zn	213.857

Table 3: Certified values for LGC6137 reference material (LGC Standards, 2008).

Element	Certified Concentration (mg kg^{-1})	Uncertainty (mg kg^{-1})
Ca	51100	2600
Cr	47	7
Fe	30700	1600
K	5010	1080
Li	42.5	6.5
Mg	11100	750
Mn	665	27
Na	7420	470
Pb	73	3.6
V	47	6.9
Zn	231	16

Limit of Detection (LoD)

Applicable standards were run to calibrate the instrument followed by triplicate measurements of concentrations in Table 4 in order to measure both reproducibility and signal intensity.

Table 4: Limit of Detection sample concentrations.

Matrix	Constituents	Concentrations (mg l^{-1})
Brackish	HNO_3.3HCl.12(2%NaCl)H_2O	0.001, 0.005, 0.01, 0.02, 0.04, 0.08, 0.1, 0.5, 1
Freshwater	HNO_3.3HCl.12H_2O	0.001, 0.005, 0.01, 0.02, 0.04, 0.08, 0.1, 0.5, 1, 2, 5, 10, 25, 50

As the relationship between signal intensity and contaminant concentration are theoretically linear, a simple linear regression model was obtained to determine the intensity response at a given concentration, determining a calibration model for values (given in mg L^{-1}) for each element at a given intensity. As each measurement was run in triplicate, the relative standard deviation (RSD%) could be calculated to quantify sample precision.

The average observed measurement for each concentration was then compared to actual concentration and a percentage recovery was calculated:

$$Recovery = \left(\mathrm{y}_{mean} \times y_{actual}\right) \times 100$$

Where y_{mean} is the average measured value and y_{actual} is the absolute value, thus calculating the accuracy of the calibration. From this calculation, concentrations that were recovered within 10% of the absolute value with an RSD% <10 were considered reproducible and above the LOD.

Table 6: Lowest reproducible concentration.

	Ag	Al	Ca	Cd	Co	Cr	Cu	Fe	Ga	K
Brackish	0.02			0.08	0.04	0.02	0.04		0.02	
Fresh		5	5					5		5

	Li	Mg	Mn	Na	Ni	Pb	Sn	Sr	Tl	V	Zn
Brackish	0.04		0.04		0.08	0.1	0.08	0.08	0.08	0.04	0.1
Fresh		5		10							

The values shown (Table 6) are show the lowest reproducible concentrations for the specific matrices and calibration standards. In order for these data to be representative of sediment concentrations, all values were given the same sample treatment as sediment data.

$$C_{ppm} = \frac{\left(C_{mg\,L^{-1}} \times V\right)}{M}$$

Where C_{ppm} is the representative value, $C_{mgL\text{-}1}$ is analytical LOD, *V* is the volume of analytical stock and *M* is the original mass of digestion. The analytical detection limits are therefore shown as (Table 7)

Table 7: Lowest reproducible concentration, corrected for sediment value.

	Ag	Al	Ca	Cd	Co	Cr	Cu	Fe	Ga	K
Brackish	2			8	4	2	4		2	
Fresh		500	500					500		500

	Li	Mg	Mn	Na	Ni	Pb	Sn	Sr	Tl	V	Zn
Brackish	4		4		8	10	8	8	8	4	10
Fresh		500		1000							

Samples < LoD

Table 8: Number of surface samples with values below LoD

	Ag	Cd	Co	Cr	Cu	Fe	K	Li	Mg	Mn	Na	Ni	Pb	Sr	Zn
Total Number	43	43	43	43	43	43	43	43	43	43	43	43	43	43	43
N <LOD	23	43	-	-	-	-	-	-	-	-	43	-	-	-	-
% <LOD	53	100	-	-	-	-	-	-	-	-	100	-	-	-	-

Table 9: Number of sediment core samples with values below LoD.

	Ag	Al	Ca	Cd	Co	Cr	Cu	Fe	Ga	K	Li
Total Number	245	245	245	245	245	245	245	245	245	245	245
N <LOD	64	5	5	245	5	4	9	5	7	4	4
% <LOD	26	2	2	100	2	2	4	2	3	2	2

	Mg	Mn	Na	Ni	Pb	Sr	V	Zn
Total Number	245	245	245	245	245	245	245	245
N <LOD	5	4	5	10	16	4	4	4
% <LOD	2	2	2	4	7	2	2	2

ICP Matrix Experimentation

Three test samples were initially run with standards containing a matrix resembling seawater (HNO_3.3HCl.12(3.4%NaCl)H_2O). The aim was that the matrix would contain the same concentration of EIE's as field samples. Recovery values for field representative CRM's can be seen in Table 10.

Table 10: LGC 6137 recovery values (%) for marine matrix samples.

	Ca	Cr	Fe	K	Li	Mg	Mn	Na	Pb	V	Zn
A	112	123	109	41	135	112	135	79	142	113	93
B	114	118	107	36	129	110	137	77	148	105	92
C	117	126	113	41	135	116	136	82	146	112	95
Average	**114**	**122**	**110**	**40**	**133**	**113**	**136**	**79**	**145**	**110**	**93**
RSD (%)	2.3	3.2	2.4	8.0	2.5	2.9	0.6	3.6	2.3	4.0	1.8

Elemental recovery values for Cr, K, Li, Mn, Na and Pb lie outside the 20% (80-120%) acceptable range whereas Fe, Mg, V and Zn recover well. Precision, represented by the relative standard deviation value (%) shows that the values are consistent, suggesting that the low accuracy is systematic across elements, and due to an overlying factor.

All test samples were therefore re-run with a modified matrix, based on a conservative estimate of the chemical composition of brackish outer estuary waters, HNO_3.3HCl.12(3.4%NaCl)H_2O. Recoveries can be seen in Table 11.

Table 11: LGC 6137 recovery values (%) for brackish matrix samples.

	Ca	Cr	Fe	K	Li	Mg	Mn	Na	Pb	V	Zn
A	117	85	108	84	99	106	102	88	105	90	94
B	127	75	115	71	91	111	95	91	90	81	88
C	124	84	113	82	98	112	99	90	102	87	90
Average	**123**	**81**	**112**	**79**	**96**	**110**	**99**	**90**	**99**	**86**	**90**
RSD (%)	4.1	6.5	3.3	8.4	4.8	3.1	3.7	1.6	7.9	5.4	3.5

Recoveries within the brackish matrix appear systematically more accurate than the marine matrix with the exception of Ca and V. Ca values recovered within a 20% limit with the marine matrix whereas they were outside these limits with the brackish matrix. V recoveries can be considered accurate with both matrices, however the marine matrix represents the concentration more accurately.

As the magnitude of contamination varied with trace and major elements, samples were also run with a 1:20 dilution to ensure the ICP could calibrate the elements. At these diluted concentrations, EIE presence did not have to be considered, as the dilution reduced their impact on the ICP torch, therefore a 'freshwater' matrix was used (HNO3.3HCl.12H_2O).

Table 12: Freshwater matrix CRM recovery values.

	Ca	Cr	Fe	K	Li	Mg	Mn	Na	Pb	Zn
A	118	78	113	89	99	114	100	114	105	90
B	120	87	116	104	110	116	101	116	98	99
C	119	78	118	88	99	116	99	116	97	92
Average (%)	**119**	**81**	**116**	**94**	**103**	**115**	**100**	**115**	**100**	**94**
RSD (%)	0.6	6.3	2.2	9.4	6.3	0.9	1.1	0.9	4.0	5.0

Freshwater standards (Table 12) show excellent recovery across the board, with all elements being within the 20% acceptance limit. However, for the sediment analysis, only major constituents (Ca, Fe, Mg, Na) will be analysed with this matrix as the samples will have to be diluted in order to bring them into range, reducing trace metal concentrations to levels below the detection limit.

These exploratory results show that different matrices have distinct impacts and that the analytical matrix calibration used within standards must closely match samples in order to accurately and precisely recover elemental data from ICP-OES. However, accurate recoveries are acceptable when using a brackish matrix and therefore will be used on samples likely to contain high concentrations of EIE's.

Appendix 2: Raw Surface Metal Data (mg kg^{-1})

Sample	Ag	Co	Cr	Cu	K	Li	Mg	Mn	Ni	Pb	Sr	Zn
A1	40	40	10	25	4928	26	4994	299	35	58	131	206
A2	15	41	10	20	4874	26	4707	266	33	129	104	121
A3	27	67	9	801	3166	11	3219	811	151	1035	156	2623
A4	35	48	10	29	6231	39	6288	311	37	53	172	124
A5	1	15	40	35	4522	31	10029	211	35	54	53	131
A6	1	14	37	33	4271	29	8986	220	34	48	77	132
A7	1	13	34	25	3948	27	8508	236	26	37	86	99
A8	1	17	32	30	3595	25	8266	253	30	42	91	109
B1	19	76	9	20	6574	66	5290	221	41	25	83	87
B2	20	48	9	26	4938	31	4414	290	34	53	123	106
B3	8	54	10	28	6516	44	6447	397	37	61	161	134
B4	1	15	44	36	4982	37	9460	274	37	50	92	130
B5	1	14	38	34	4110	29	8454	224	33	53	79	139
B6	1	14	33	29	3753	26	8335	240	30	44	96	108
B7	1	14	31	25	3537	24	7751	229	30	38	91	103
B8	1	14	32	26	3837	27	8320	264	26	34	110	95
C1	12	41	10	24	4802	28	4385	243	33	59	119	131
C2	7	38	9	21	4578	24	4080	367	33	72	95	135
C3	13	41	10	39	5643	22	6003	108	37	60	136	170
C4	11	56	10	32	7038	48	6590	478	39	64	181	140
C5	11	57	10	34	6647	47	6496	426	38	70	133	134
C6	1	15	36	32	4312	30	8728	218	33	38	81	114
C7	1	16	39	33	4554	31	8903	248	36	44	109	123
C8	62	15	37	35	3953	28	8555	252	33	55	100	132
C9	1	17	41	39	4611	33	9698	230	38	61	72	140
C10	1	15	41	34	4663	35	8782	266	34	49	89	117
D1	7	39	10	66	4759	28	4396	226	34	54	120	142
D2	11	38	10	21	4711	26	4522	290	32	53	126	118
D3	12	56	10	56	5766	32	6237	252	50	174	159	242
D4	12	52	10	31	6070	41	6171	298	35	65	115	118
D5	1	12	22	19	2416	16	5649	203	21	29	73	86
D6	1	14	28	25	3014	22	7055	225	26	42	82	98
D7	1	16	42	33	4773	35	8974	264	35	42	90	121
D8	1	14	42	37	3960	30	8919	215	33	65	74	120
D9	3	15	33	29	3775	26	7873	210	34	46	85	114
E1	10	35	10	24	4130	19	3971	264	30	57	104	125
E2	7	37	9	27	4433	29	4473	238	31	62	127	129
E3	10	39	10	37	4862	20	5488	98	34	79	130	131
E4	10	47	10	32	5256	31	5760	383	35	67	131	119
E5	1	13	28	24	3271	23	7425	233	27	35	98	95
E6	1	12	29	26	3207	22	7064	219	28	44	80	100
E7	1	15	34	31	3863	28	7986	217	30	38	75	114
E8	1	15	33	33	3120	22	7141	199	32	83	70	138
E9	1	14	31	29	3340	23	7616	204	29	48	79	122
F1	9	38	10	41	4603	23	4236	322	34	74	114	154
F2	7	42	10	32	4671	25	3998	291	36	100	99	168
F3	14	52	12	47	5366	28	6270	191	44	137	157	185
F4	8	48	11	27	5817	34	6569	511	39	59	172	128
F5	5	17	38	21	3380	24	5260	266	28	42	96	86
F6	5	18	36	21	3328	24	5285	245	49	48	94	89
F7	4	19	49	28	4905	35	5944	269	36	59	114	113
F8	3	20	46	26	4381	32	5898	294	34	44	114	103
F9	4	21	34	22	3049	20	4691	235	29	39	90	93
G1	3	36	12	35	3924	16	3653	298	31	111	147	196
G2	2	45	11	28	5354	31	4947	312	39	72	139	127
G3	3	39	12	44	4233	17	5482	285	40	1003	165	263

G4	3	41	12	88	3800	16	5314	426	37	255	224	313
G5	3	19	40	23	3631	27	6023	297	30	43	105	90
G6	5	18	37	22	2995	20	5308	237	28	54	74	92
G7	1	17	31	15	2816	17	4721	225	28	35	72	68
H1	2	41	12	25	4824	26	4908	308	32	68	154	148
H2	1	52	11	44	5332	36	5612	380	46	77	143	150
H3	1	55	11	52	6471	46	6041	469	44	226	137	257
H4	3	20	59	47	5536	44	6052	286	43	78	108	157
H5	3	20	52	43	4763	37	5928	293	37	61	103	139
H6	2	18	41	30	3653	26	5396	276	31	53	108	114
I1	25	39	11	28	4540	24	4728	346	35	57	163	161
I2	2	45	11	21	5424	32	5196	340	36	51	214	127
I3	3	39	11	57	3794	17	3406	377	36	132	131	143
I4	2	49	11	59	4672	27	4512	421	41	112	159	226
I5	2	68	11	29	6679	56	7692	259	53	51	117	133
I6	57	20	55	43	5149	42	5844	312	39	118	118	128
I7	2	21	56	56	5608	46	6115	356	40	62	151	143
J1	2	44	12	28	5413	30	4974	300	37	72	171	173
J2	1	35	11	35	3173	24	4019	408	30	95	133	115
J3	1	45	11	43	3971	24	4207	403	38	106	189	163
J4	1	39	11	19	2722	14	2542	245	27	61	79	95
J5	3	18	47	53	4523	33	5595	263	37	68	149	134
J6	3	21	54	45	5332	42	6070	311	38	63	163	131
K1	1	42	11	29	4970	28	4705	312	35	47	145	130
K2	1	42	11	28	4821	25	4726	344	38	63	143	124
K3	2	39	13	197	3495	18	3767	416	37	658	176	644
K4	1	54	11	32	5633	35	4799	475	37	63	95	125
K5	2	20	46	36	3933	29	5543	283	34	79	119	128
K6	2	19	50	45	4746	36	5717	296	35	61	121	125
L1	2	47	11	25	5687	35	4876	394	35	84	120	141
L2	2	41	11	26	2438	14	4164	799	22	64	213	103
L3	1	29	12	39	2491	2	2560	276	26	91	173	147
L4	1	48	12	23	3906	24	4980	309	45	36	83	102
L5	3	21	58	58	5327	41	6058	310	44	80	122	175
L6	2	19	56	55	5167	42	5799	284	39	77	107	142

Appendix 3: Sediment Core Carbon content

	Carbon (%)							
Depth	**Core H**	**Core G**	**Core F**	**Core E**	**Core D**	**Core C**	**Core B**	**Core A**
0	18.3		17.7				15.0	
5	16.4		15.4				10.9	
10	14.5		13.1				10.9	
15	11.3		13.7				10.7	
20	8.0		14.3				10.5	
25	9.1		12.1				9.7	
30	10.2		10.0				9.0	
35	9.6		10.5				9.0	
40	9.1		10.9				9.1	
45	9.2		11.3				8.7	
50	9.3		11.7				8.3	
55	9.3		10.2				8.1	
60	9.2		8.7				7.9	
65	9.5		8.6				7.5	
70	9.9		8.6				7.1	
75	9.8		8.6				6.3	
80	9.7		8.6				5.5	
85	9.5		7.9				5.4	
90	9.3		7.2				5.4	
95	9.0		6.4				4.7	
100	8.8		5.6				4.0	
110	9.3		3.9				5.3	
120	8.5		3.3				3.7	
130	8.3		5.3				3.1	
140	8.2		4.0				5.4	
150	9.2		4.0				4.7	
160	8.7		4.1				2.0	
170	8.6		4.2				1.4	
180	8.8		5.5				1.3	
190	9.0		4.3				2.4	
200	9.3		3.7				1.1	
220	8.5		3.3				2.0	
240	18.3		4.3				2.5	
260	16.4		3.0				3.6	
280	14.5		3.2				6.1	
300	11.3		4.9				4.2	
320	8.0		3.3				3.8	
340	9.1		2.9				4.8	
360	10.2		17.7				4.0	
380	9.6		15.4				4.7	
400	9.1		13.1				4.5	
420	9.2		13.7				5.1	

Appendix 4: Sediment Core pH Data

	pH							
Depth	**Core H**	**Core G**	**Core F**	**Core E**	**Core D**	**Core C**	**Core B**	**Core A**
0	7.95	7.95	7.77	7.5	7.71	7.54	7.50	7.99
10	7.91	7.81	8.14	7.82	7.64	7.95	7.76	8.46
20	8.08	7.68	7.51	7.73	7.9	8.06	7.87	8.25
30	8.18	7.66	7.96	7.81	7.78	8.14	7.93	8.05
40	8.18	7.79	7.80	7.8	8.34	8.06	7.98	8.38
50	8.78	7.81	7.71	7.73	8.58	8.02	8.26	8.16
60	8.85	7.83	8.53	7.89	8.26	8.29	7.97	8.59
70	8.89	7.72	8.49	7.98	8.46	8.15	8.36	8.46
80	8.78	7.9	8.55	8.23	8.61	8.48	8.11	8.31
90	8.94	7.62	8.37	8.42	8.54	8.31	8.16	8.69
100	8.88	7.78	8.24	8.02	8.62	8.3	8.17	8.65
110	8.80	8.61	8.37	8.61	8.75	8.34	8.18	8.85
120	8.61	8.56	8.53	8.52	8.63	8.11	8.56	8.76
130	8.68	8.62	8.48	8.5	8.43	8.36	8.24	7.71
140	8.62	8.3	8.78	8.16	8.48	8.69	8.48	8.12
150	8.92	8.36	8.81	8.58	8.46	8.28	8.26	8.51
160	8.83	8.63	8.72	8.36	8.48	8.29	8.37	8.1
170	8.53	8.46	8.63	8.39	8.31	8.43	8.39	8.27
180	8.67	8.41	8.36	8.24	8.03	8.4	8.55	8.26
190	8.89	8.28	8.39	8.44	8.44	8.25	8.34	8.59
200	8.72	8.62	8.66	8.23	8.42	8.43	8.69	7.96
220	8.72		8.53	8.4	8.34	8.1	8.47	7.92
240			8.30	8.32		8.39	8.15	8.07
260			8.47				8.46	8.05
280			8.61				8.17	8.43
300			8.48				8.29	8.54
320			8.48				8.36	
340			8.71				8.45	
360							8.29	
380							8.57	
400							8.62	
420							8.30	
440							8.50	

Appendix 5a: Sediment Core Metal Summary Statistics

Core A, n=36

	Mean	Median	Std. Deviation	Range	Minimum	Maximum
Al	28377.1	29533.0	4772.3	19793.8	16410.7	36204.6
Ca	28832.0	30435.7	13212.7	41685.0	8741.1	50426.1
Co	9.8	10.0	2.1	9.8	5.1	14.9
Cr	52.9	52.2	13.8	58.9	23.5	82.3
Cu	40.3	37.6	14.4	57.7	15.9	73.6
Fe	35537.6	35496.3	4640.9	21505.4	24942.4	46447.8
Ga	10.2	10.8	1.7	7.0	5.3	12.3
K	6449.9	6549.0	904.3	3861.8	3918.2	7780.0
Li	42.5	43.3	7.1	29.6	22.8	52.4
Mg	11195.8	11384.9	1581.5	7807.7	7053.2	14860.8
Mn	295.8	269.6	104.4	420.3	220.6	640.8
Na	10452.2	9871.0	5162.0	30229.3	5678.4	35907.7
Ni	32.5	32.9	6.5	27.1	15.2	42.3
Pb	99.3	94.6	31.8	166.9	37.8	204.7
Sr	82.4	79.6	22.2	74.2	49.5	123.6
V	85.1	90.3	13.3	51.2	48.0	99.2
Zn	138.5	119.1	56.7	208.0	54.3	262.3

Core B, n=42

	Mean	Median	Std. Deviation	Range	Minimum	Maximum
Al	17627.0	19341.2	6553.7	20621.5	7142.6	27764.1
Ca	24283.0	28457.5	12916.0	37925.5	5732.7	43658.2
Co	12.4	12.5	3.4	14.6	6.2	20.8
Cr	42.5	43.0	18.4	64.5	17.7	82.3
Cu	27.1	29.0	16.0	56.5	6.0	62.5
Fe	26815.4	27952.1	10027.9	31195.9	11977.0	43172.9
Ga	7.1	7.9	3.1	9.8	2.0	11.8
K	4866.4	5457.6	1542.5	4505.2	2313.4	6818.6
Li	28.7	31.5	10.7	31.2	11.5	42.7
Mg	7844.8	8507.4	2136.2	6858.0	4325.8	11183.7
Mn	324.2	247.4	189.9	829.0	159.5	988.5
Na	6664.3	7404.4	2194.8	6815.3	3415.5	10230.8
Ni	29.1	29.4	10.8	35.9	12.4	48.3
Pb	74.9	76.1	45.5	137.8	16.4	154.1
Sr	77.1	71.0	20.6	82.6	49.6	132.1
V	66.8	72.0	22.5	71.2	31.4	102.6
Zn	100.3	90.1	61.5	231.7	28.2	259.9

Core D, n=30

	Mean	Median	Std. Deviation	Range	Minimum	Maximum
Al	19281.3	20814.4	8183.3	28223.9	6704.2	34928.1
Ca	26272.8	25944.1	13862.9	45191.1	4802.2	49993.3
Co	9.8	9.8	3.7	13.5	4.0	17.6
Cr	37.8	41.3	17.9	60.4	12.0	72.4
Cu	24.2	23.4	15.6	49.9	5.0	54.9
Fe	30110.1	30681.8	12214.7	46331.2	14631.5	60962.7
Ga	8.3	8.2	3.5	11.6	2.9	14.4
K	4513.6	5059.4	1579.7	5143.3	2044.4	7187.7
Li	28.0	32.3	11.8	38.6	10.1	48.7
Mg	8940.7	10172.0	2740.8	7961.9	4741.6	12703.5
Mn	304.1	204.6	223.9	862.8	153.4	1016.1
Na	6694.6	6845.1	2345.6	8748.1	3227.1	11975.2
Ni	27.2	29.5	11.9	35.6	9.6	45.2
Pb	64.7	53.6	46.5	139.2	10.4	149.7
Sr	72.3	65.3	19.9	65.3	49.4	114.7
V	64.9	74.5	24.2	72.5	26.6	99.2
Zn	92.4	85.5	54.4	163.8	29.3	193.1

Core E, n=32

	Mean	Median	Std. Deviation	Range	Minimum	Maximum
Al	22730.2	25526.6	8996.3	28586.0	6625.5	35211.5
Ca	15728.7	6948.9	14965.2	42735.4	4840.3	47575.7
Co	11.9	11.7	4.9	20.7	4.9	25.6
Cr	46.8	52.0	19.6	65.4	14.6	80.0
Cu	30.7	31.2	17.8	61.2	5.1	66.3
Fe	34693.1	38454.4	13318.3	49668.3	11515.0	61183.3
Ga	9.7	10.9	4.2	12.9	2.6	15.5
K	5029.8	5787.2	1701.9	4771.7	2031.4	6803.0
Li	32.3	37.8	12.8	38.7	9.8	48.5
Mg	10017.2	11131.8	3014.8	9469.0	4164.2	13633.2
Mn	466.4	252.6	428.9	1556.0	161.6	1717.6
Na	7810.5	9002.1	3014.0	11542.4	38.6	11581.0
Ni	33.9	35.6	15.1	59.1	9.7	68.8
Pb	86.3	85.6	52.9	176.1	11.3	187.5
Sr	64.1	57.0	21.4	87.9	38.6	126.5
V	75.7	84.6	24.9	74.6	31.4	106.0
Zn	126.9	127.4	66.6	227.7	33.0	260.7

Core F, n=38

	Mean	Median	Std. Deviation	Range	Minimum	Maximum
Al	20140.6	24900.9	9822.5	31578.4	6025.8	37604.2
Ca	16220.4	8048.0	12992.4	32244.2	3839.0	36083.2
Co	12.0	12.6	3.5	17.4	7.0	24.4
Cr	40.2	43.7	26.5	82.0	6.5	88.5
Cu	26.8	22.8	20.4	64.8	3.7	68.5
Fe	27490.3	29619.6	12452.1	41456.5	10225.7	51682.2
Ga	8.4	9.0	3.0	9.4	3.9	13.3
K	4925.5	6001.2	2099.8	6194.3	1861.2	8055.5
Li	30.7	38.4	15.4	48.5	8.8	57.3
Mg	8281.5	9732.6	3000.6	9147.6	3499.1	12646.7
Mn	331.6	175.0	273.5	1206.6	142.5	1349.1
Na	6501.2	7269.7	2903.8	8872.0	2746.0	11618.0
Ni	25.8	25.6	16.5	54.4	2.6	57.0
Pb	62.7	55.3	51.5	164.8	4.2	169.0
Sr	56.9	55.1	18.8	92.8	30.6	123.3
V	67.7	82.6	31.8	96.3	21.7	118.0
Zn	98.6	97.8	63.5	182.6	22.1	204.8

Core G, n=29

	Mean	Median	Std. Deviation	Range	Minimum	Maximum
Al	21993.6	25169.3	11048.7	33969.7	4081.0	38050.7
Ca	14469.1	4765.0	15297.6	40125.3	1924.6	42049.9
Co	11.8	12.5	4.9	16.2	3.2	19.4
Cr	45.7	54.0	23.6	76.9	9.1	86.0
Cu	29.0	31.7	18.3	63.5	3.6	67.1
Fe	33396.1	41523.6	15298.6	42396.9	8855.7	51252.6
Ga	9.5	10.5	4.6	14.6	1.5	16.1
K	4691.7	5587.5	1931.2	5826.3	1381.2	7207.5
Li	31.0	37.6	15.4	47.7	5.6	53.4
Mg	8745.2	10203.5	3272.8	10484.7	3163.2	13647.9
Mn	394.3	336.0	278.3	927.6	124.7	1052.3
Na	7449.1	8103.9	3553.5	11393.5	2198.6	13592.1
Ni	31.2	37.3	14.6	41.1	7.7	48.8
Pb	77.1	78.2	51.9	147.4	7.8	155.2
Sr	59.9	56.8	16.2	62.8	33.7	96.4
V	74.0	89.6	31.5	89.7	21.5	111.3
Zn	101.9	113.2	50.8	153.6	27.1	180.7

Core H, n=33

	Mean	Median	Std. Deviation	Range	Minimum	Maximum
Al	24116.9	23128.0	5129.4	20890.7	18354.5	39245.2
Ca	28919.8	35461.8	14471.8	42775.9	5098.0	47873.9
Co	10.0	9.2	2.5	9.3	7.1	16.4
Cr	51.5	46.5	15.2	54.6	36.0	90.6
Cu	40.8	36.3	12.0	39.2	28.8	68.0
Fe	31679.8	29594.1	6949.4	27170.5	22373.3	49543.8
Ga	6.9	6.4	2.0	7.3	4.6	11.9
K	5823.9	5662.5	875.3	4414.4	4501.1	8915.5
Li	36.7	34.8	7.4	32.3	28.5	60.8
Mg	9140.4	8730.5	1450.5	5775.0	7720.7	13495.7
Mn	338.0	269.9	180.6	859.9	206.5	1066.5
Na	7859.9	7543.0	1182.9	6213.9	6167.3	12381.3
Ni	32.6	29.6	7.8	29.5	24.6	54.2
Pb	92.3	88.7	16.6	66.2	65.9	132.1
Sr	88.2	89.4	27.3	125.5	43.1	168.6
V	75.6	71.4	13.5	49.7	60.3	110.0
Zn	139.5	134.2	32.2	114.6	87.8	202.4

Appendix 5b: Raw Sediment Core Metal Data

Core A (mg kg $^{-1}$)

Depth (cm)	Al	Ca	Co	Cr	Cu	Fe	Ga	K	Li	Mg	Mn	Na	Ni	Pb	Sr	V	Zn
0	21259	34071	9	59	53	37865	8	4993	32	10662	418	8470	30	114	86	68	159
5	34900	21036	12	82	61	41859	12	6682	49	11593	641	7669	42	114	76	95	197
10	28753	18398	13	76	58	40325	11	5951	42	11377	585	7475	41	112	66	91	194
15	29944	16869	15	75	52	46011	11	6274	43	11913	624	9267	42	100	73	96	188
20	30086	8741	10	67	47	43173	11	6385	44	12154	330	10879	40	95	70	96	164
25	30753	10086	11	57	40	46448	12	6585	45	12603	298	10914	38	67	70	93	154
30	27035	25424	8	72	69	33969	10	6504	42	11438	287	9822	33	138	82	91	261
35	31521	14635	11	64	74	34043	11	6743	46	11841	221	9896	38	132	55	94	234
40	31006	17605	12	60	65	38740	11	7546	46	13864	269	13847	39	129	62	99	262
45	27501	18337	11	57	52	35485	10	6473	43	11261	281	9926	35	112	64	93	213
50	30946	19318	10	68	62	35903	12	6838	47	11393	299	9885	38	125	71	95	216
55	29122	20055	11	58	49	36021	10	6681	43	11738	250	10363	35	127	64	90	179
60	34004	14809	11	61	39	38150	12	7423	50	12594	239	10454	37	124	55	99	156
65	33514	11330	14	62	39	35555	12	7324	50	14861	232	35908	39	205	50	99	176
70	31786	10885	10	62	38	37373	12	7158	48	11870	241	10236	36	135	49	97	147
75	30167	13004	11	60	40	35240	11	6802	46	11924	229	9629	36	121	53	93	147
80	26308	25294	7	46	37	31361	9	6895	39	12967	235	22767	27	95	81	79	121
85	26938	29216	9	46	35	33310	10	6328	42	10721	239	8733	30	94	73	84	117
90	25373	33606	8	43	32	31596	9	6192	40	10346	237	8619	28	90	82	80	105
95	32965	33914	9	52	38	34535	11	7306	49	11906	263	9290	32	102	86	93	108
100	27112	32611	9	45	38	33086	9	6291	41	11197	235	9982	29	100	80	84	116
110	27351	32365	10	45	35	34691	11	6513	42	10902	263	10223	32	94	80	85	106
120	30221	38714	9	48	32	35156	11	7047	46	11727	277	9470	32	89	94	87	104
130	27610	15857	11	53	42	36346	10	6422	42	11954	228	10777	35	114	54	88	167
140	27028	37304	10	44	30	34091	10	6243	43	11135	289	8644	30	83	90	80	92
150	33737	39753	10	53	34	36708	12	7584	52	11125	277	9857	36	88	106	92	107
160	31879	41689	9	50	30	34680	11	7253	49	10596	271	9554	29	84	104	89	94
170	36205	47254	10	50	31	37988	12	7780	52	11735	272	10716	32	82	119	91	89
180	25580	31655	8	44	35	32019	9	6103	40	10602	245	9937	29	92	79	80	104
190	31851	36736	11	50	33	35508	12	7173	49	11261	271	9983	33	89	94	90	99
200	31576	45621	10	46	30	37607	11	6976	47	11246	271	10431	32	80	111	85	88
220	22620	49899	9	37	28	36197	8	5625	35	9957	284	8709	28	72	113	69	81
240	19795	46803	8	30	21	29825	7	4951	30	8345	268	6401	23	51	115	60	66
260	20694	45934	7	31	19	27357	7	4926	31	7699	270	5823	20	47	120	60	62
280	18029	50426	6	26	16	26192	6	4307	26	7488	254	5678	17	38	124	51	54
300	16411	48698	5	23	16	24942	5	3918	23	7053	256	6045	15	38	117	48	57

Core B (mg kg $^{-1}$)

Depth (cm)	Al	Ca	Co	Cr	Cu	Fe	Ga	K	Li	Mg	Mn	Na	Ni	Pb	Sr	V	Zn
0	22192	36764	13	49	30	31447	9	6349	37	9436	320	9474	35	54	132	77	131
5	24940	13095	16	55	34	37324	10	6129	39	9995	647	8466	37	65	68	81	128
10	20664	8447	14	61	40	31393	10	5843	38	8987	310	7815	37	80	62	82	133
15	22274	6692	19	71	44	35007	11	6149	40	9232	888	7622	48	93	61	92	176
20	24565	6556	16	82	59	36934	11	6454	41	9798	544	8622	44	120	61	99	178
25	24870	14648	18	82	62	38306	10	6016	38	9959	743	8057	46	128	71	88	197
35	24718	7274	17	65	57	39593	11	6146	39	10435	567	9748	41	149	58	92	204
40	25817	5733	21	63	53	41430	12	6681	42	10195	989	9515	48	133	58	103	222
45	25650	6937	15	60	48	38602	11	6675	43	10832	364	9683	43	143	61	100	260
50	27764	8771	15	62	44	43173	11	6573	42	11184	367	10231	41	154	61	95	184
55	20018	8734	15	55	40	39779	9	5905	35	9705	335	9187	39	139	60	85	162
60	22638	6930	13	56	30	34512	9	5662	33	9457	245	8314	36	133	50	84	123
65	17205	7855	16	53	40	31956	8	5250	31	9161	473	8640	38	128	50	77	151
70	24991	6091	13	63	36	32079	10	6448	40	9773	249	8526	35	108	52	80	134
75	27146	10054	16	58	41	41052	11	6819	42	10620	389	9367	40	134	62	95	146
80	21833	15951	14	51	31	33305	10	6336	37	8988	307	7705	36	109	65	83	121
85	23064	21534	15	49	31	36000	9	6007	37	9836	327	8006	34	95	71	81	109
90	23235	21591	14	49	33	37340	10	6575	39	9249	302	8043	34	92	75	88	104
95	20872	32705	12	43	30	30891	8	5880	34	9221	246	7740	29	73	84	69	90
100	17070	32131	11	39	29	26482	7	5161	30	7607	242	6241	28	88	91	67	79
110	21133	27295	11	45	29	27176	9	6000	35	8606	258	7187	29	81	81	75	82
120	20215	37187	14	37	20	20973	7	5187	31	7768	220	5887	30	53	86	65	61
130	15061	35351	11	34	20	19834	6	4521	26	7283	226	5894	24		84	61	62
140	18431	16785	13	47	34	31686	9	5590	32	8886	275	7905	32		67	78	126
150	21884	29204	13	43	29	26089	8	5669	34	8285	241	6654	33		82	78	100
160	10064	29985	8	22	11	14811	3	2882	16	5613	178	4419	16	30	63	41	39
170	8646	32758	6	19	6	12425	2	2544	13	4841	169	3435	13	16	66	34	31
180	7974	32231	6	18	6	12257	2	2360	12	4489	160	3488	12	18	64	31	28
190	16265	23385	10	38	21	23352	7	4591	26	7409	232	6017	24	18	66	64	80
200	8580	31770	7	19	8	12491	2	2558	13	4597	161	3416	14	19	66	33	29
220	7143	31566	9	18	8	11977	2	2313	12	4326	172	3510	15	20	71	34	38
240	18665	27711	12	40	26	28728	7	5326	30	8409	249	7676	28	21	82	66	90
260	9231	34344	10	21	8	14762	3	2833	14	4754	202	3639	17	22	82	38	33
280	14243	32557	10	31	20	19963	5	4056	23	6943	207	6118	22	22	75	55	59
300	10332	37710	11	22	9	17168	4	2959	16	5692	214	4429	19	22	83	41	38
320	9312	39127	9	22	8	15060	3	2815	15	5249	217	3770	16	21	94	40	34
340	10233	43658	9	22	14	17549	4	3064	17	5731	223	4483	17	20	109	41	37
360	8050	37951	9	20	8	13743	3	2575	14	4888	206	3717	17	21	94	37	37
380	10451	42866	9	24	10	17626	4	3215	17	5727	232	4419	19	37	118	44	40
400	10994	42127	9	24	9	17029	4	3335	18	5363	239	4054	18	20	123	43	43
420	11038	34888	9	28	12	16901	4	3522	19	5356	249	4273	20	28	110	46	52
440	10866	40935	9	25	10	18038	4	3419	19	5598	233	4507	18	23	118	45	43

Core D (mg kg $^{-1}$)

Depth	Al	Ca	Co	Cr	Cu	Fe	Ga	K	Li	Mg	Mn	Na	Ni	Pb	Sr	V	Zn
0	21151	28719	14	47	29	38036	9	5804	34	11192	592	11975	39	54	100	76	128
5	22831	7939	13	58	40	41463	10	5423	36	11953	417	10506	41	84	62	83	152
10	24407	5996	13	72	53	43364	10	5270	35	11542	345	10138	39	129	54	89	156
20	20843	4930	17	58	55	45341	10	4833	32	10128	792	8917	43	150	51	91	193
25	27154	5342	14	55	46	44416	13	5763	38	11560	587	8069	43	108	50	87	184
30	34928	6025	15	61	40	51418	14	6375	45	12703	785	8017	45	122	51	97	182
35	30456	4802	18	63	42	44112	14	6130	44	10646	1016	8269	45	132	53	99	182
40	29023	15342	13	53	37	60963	14	6245	40	12633	396	8713	40	130	68	88	155
45	23466	14158	11	57	36	30736	9	5423	36	10964	191	7475	32	125	49	84	118
50	23239	28150	12	48	34	31222	9	5614	37	10644	216	6725	33	106	72	81	118
55	21362	21054	11	43	37	33251	8	5568	34	10629	206	7773	31	111	59	83	112
65	20785	21990	11	41	24	34109	8	5393	33	10400	203	8005	31	82	58	74	92
70	27745	23157	9	46	30	34415	12	6101	40	11206	217	8055	31	73	64	82	96
75	24914	26550	9	42	21	30628	11	5982	37	10216	210	6668	28	54	68	75	77
80	34805	25106	12	54	37	36982	14	7188	49	12667	231	8526	37	101	74	93	123
85	25268	22556	10	43	25	33004	11	5993	37	11204	213	8015	32	73	62	79	94
90	18025	21486	10	37	23	26092	7	4849	29	8569	178	6965	25	52	55	70	79
95	18354	32377	9	33	16	22621	7	4302	25	8050	173	6279	23	33	67	59	59
100	15334	31305	9	28	14	20734	6	3690	21	7469	169	5455	22	34	60	54	53
110	13296	25338	10	27	15	21279	5	3458	20	7055	165	5424	23	27	55	55	51
120	12491	29383	7	19	9	16896	6	3099	17	6142	153	4007	16	18	60	38	38
130	12285	35459	7	20	11	20106	6	3220	18	7128	185	6361	17	27	81	40	49
140	10778	44576	5	17	7	17421	6	2610	15	5916	194	3709	13	15	98	33	34
150	14461	49993	6	21	9	22231	7	3358	19	7071	225	4854	17	20	115	41	43
160	10382	41253	4	16	6	16471	5	2654	14	5339	190	3424	12	13	101	32	34
170	6704	43957	5	15	6	15164	3	2044	10	4788	177	3369	11	14	97	32	35
180	9269	40758	6	17	7	17355	3	2385	13	5718	170	4654	13	17	88	37	37
190	9372	43932	6	18	6	24045	4	2419	13	5151	177	3674	11	14	95	35	35
200	7864	43438	5	15	5	14632	3	2066	11	4742	170	3592	11	10	95	32	32
220	7447	43113	4	12	5	14796	5	2149	11	4792	181	3227	10	11	108	27	29

Core E (mg kg $^{-1}$)

Depth (cm)	Al	Ca	Co	Cr	Cu	Fe	Ga	K	Li	Mg	Mn	Na	Ni	Pb	Sr	V	Zn
0	29214	35985	14	52	29	39367	13	6587	44	11359	649	10689	38	54	127	83	132
5	23265	6684	15	56	42	38441	12	5946	38	11114	541	11092	42	85	67	80	144
10	25351	7880	16	65	45	45542	12	5600	37	12149	715	10820	48	103	63	84	180
15	27468	6957	20	77	61	48793	13	6221	41	12481	1169	11581	56	141	69	101	209
20	30224	7469	19	80	64	50481	14	6154	39	13633	1718	11193	69	144	61	94	257
25	25702	6055	26	71	66	44150	11	5786	38	11390	1709	10172	66	145	56	100	261
30	23286	7697	18	63	54	43004	10	5260	35	11113	767	9395	45	162	54	90	205
35	34360	6506	11	65	46	40774	15	6691	48	12855	341	8886	41	93	51	89	187
40	31781	5794	16	64	44	44772	15	6395	46	11497	830	9153	45	130	55	103	194
45	35211	6621	18	66	50	50012	15	6803	48	13288	1174	10913	51	161	58	106	195
50	27135	6601	17	59	41	61183	14	6048	39	12190	773	9836	44	187	60	99	178
55	34702	6761	12	67	39	51165	15	6772	46	13386	377	9744	40	150	57	99	205
60	23719	5692	11	51	36	36292	9	5539	37	11613	216	9002	36	112	46	85	134
65	23769	5670	12	49	34	40677	10	5950	36	11149	240	9401	36	111	46	93	123
70	32693	6296	13	54	31	43682	14	6791	45	13147	280	9603	38	96	50	92	127
75	29037	5494	9	48	27	34457	12	5997	39	11630	190	8925	33	77	44	80	111
80	28600	6396	11	54	33	39376	13	6141	41	12179	313	9525	36	106	51	89	132
85	27272	5574	12	53	28	37986	11	6493	41	10775	253	8068	35	86	49	95	111
90	25986	4840	12	53	28	33596	11	6217	40	10031	232	7440	34	75	43	90	116
95	26255	5348	10	49	28	35401	10	5787	38	10689	199	7897	33	72	42	89	112
100	23312	6941	11	47	34	38468	9	5157	33	11070	281	9587	32	161	44	82	134
110	20225	8046	9	40	24	26493	7	4878	30	9486	194	7091	28	56	39	75	119
120	17629	13985	12	34	18	23645	6	4092	25	8680	179	6597	27	53	40	64	75
130	16134	21359	10	30	17	20335	9	4048	25	7751	206	5542	24	42	57	57	67
140	28275	8414	12	54	36	38659	13	6218	41	11193	402	9815	37	109	58	90	163
150	10405	43985	7	21	10	18767	4	2767	15	6397	198	4707	17	24	94	43	47
160	9856	39692	7	21	8	16768	4	2602	15	5659	197	4224	15	20	88	42	47
170	8432	47576	6	16	7	15700	3	2188	11	5223	172	4043	12	15	95	34	37
180	6626	35694	6	19	6	11515	3	2061	10	4164	162	3136	18	13	92	31	33
190			7	20	9		4	2572	14		193	39	15	22	87	41	51
200	7634	39397	6	16	6	13702	3	2159	11	4447	168	3248	11	16	87	34	35
220	6897	40609	6	16	5	13034	3	2033	10	4359	185	2966	10	14	95	33	34
240	6912	41300	5	15	7	13946	3	2031	10	4453	168	3416	10	11	92	32	34

Core F (mg kg $^{-1}$)

Depth (cm)	Al	Ca	Co	Cr	Cu	Fe	Ga	K	Li	Mg	Mn	Na	Ni	Pb	Sr	V	Zn
0	26870	32341	11	52	31	35423	9	6836	44	10137	448	9285	38	56	123	83	133
5	28390	7223	14	62	42	38156	9	6701	45	10838	679	10272	44	72	66	88	142
10	27194	8873	14	67	44	41327	9	6469	43	10767	518	9464	45	97	67	94	163
15	30302	5727	14	86	57	43193	10	6389	44	11899	545	9389	47	123	55	102	177
20	29080	5079	15	89	65	42354	10	6453	44	10909	774	11255	52	132	59	108	182
25	28692	5056	14	86	68	45179	9	6285	42	10987	596	9501	46	150	54	100	196
30	29773	6071	13	78	66	39427	9	6159	42	10216	525	7640	41	125	51	95	185
35	26745	4176	13	64	53	36520	8	5844	39	10081	566	8403	42	121	43	87	181
40	29802	4997	15	65	55	45387	10	6657	43	11408	545	10560	47	138	55	105	200
45	32553	4748	16	67	51	45576	11	7146	49	11449	720	10295	48	136	57	109	201
50	27776	4310	16	60	47	41763	9	6384	43	10399	865	9756	46	143	51	100	188
55	37604	5027	24	76	49	51682	13	8056	57	12647	1349	11618	57	169	63	118	205
60	34044	4609	14	65	36	33272	10	7379	52	11663	202	9328	43	102	45	102	131
65	27727	4623	14	50	31	31089	13	7101	45	11270	169	7512	28	90	37	87	100
70	26141	4299	15	50	31	30843	13	7006	44	10876	170	7600	30	89	37	93	104
75	24773	4446	14	43	26	29537	11	6377	38	10756	167	8011	26	61	35	83	103
80	25029	4514	14	49	32	29548	12	7023	43	9703	178	7473	28	89	38	90	111
85	26079	4629	15	46	26	32316	12	6828	41	9888	200	7977	28	77	37	88	100
90	28755	3839	13	49	24	32648	13	7288	46	9946	165	7413	28	58	37	92	99
95	26071	4065	13	45	22	30168	12	6661	40	9762	160	7126	25	55	34	83	96
100	20884	4628	11	36	18	29691	10	5529	32	9498	149	6018	20	45	31	72	75
110	18024	11522	10	30	16	24552	9	4720	28	9155	175	5165	17	30	37	62	69
120	13540	16842	8	22	11	17086	7	3446	20	8094	147	4128	12	18	36	45	62
130	11910	24955	8	21	13	20068	7	3366	19	6419	163	4425	12	42	54	43	68
140	10977	34880	10	15	8	13515	6	2740	15	6053	171	3377	12	11	67	36	39
150	11080	25703	10	12	6	17217	5	2483	13	4933	167	3665	9	9	68	31	29
160	8081	27674	13	11	7	15164	5	2321	13	4735	171	3412	14	11	55	31	34
170	9170	36083	9	13	7	14771	5	2603	15	4915	188	3016	14	13	76	32	33
180	15987	13351	10	26	15	21717	8	4115	24	6773	161	4567	15	28	38	54	60
190	12632	30592	9	13	8	14881	5	2572	14	5043	173	3824	9	17	63	33	37
200	8290	32796	10	11	7	12647	5	2409	13	4406	175	3107	13	9	68	31	34
220	7513	33096	8	10	10	12381	4	2275	11	4100	164	2783	7	7	73	27	28
240	9198	33648	9	14	8	15346	5	2762	15	5169	181	3496	12	15	72	35	38
260	6045	31484	7	7	4	10226	4	1861	9	3519	143	2746	3	5	71	22	22
280	6109	32977	7	8	5	11188	4	1988	10	3738	165	2793	4	6	81	25	25
300	10075	30440	10	17	11	16991	6	3103	17	5344	261	4359	12	24	75	39	50
320	6026	31685	7	7	4	10742	4	1879	9	3499	149	2842	3	4	73	23	24
340	6398	35366	7	7	4	11040	4	1955	9	3704	153	3446	4	7	79	23	24

Core G (mg kg $^{-1}$)

Depth (cm)	Al	Ca	Co	Cr	Cu	Fe	Ga	K	Li	Mg	Mn	Na	Ni	Pb	Sr	V	Zn
0	20859	16572	11	48	32	34352	9	5588	33	11196	293	13592	35	54	78	77	123
5	24136	6915	14	61	38	41524	11	5582	38	11174	406	9293	39	84	59	86	144
10	28415	6525	19	69	45	48686	13	6036	40	13072	1036	10754	48	102	63	91	166
15	37929	5804	13	86	67	51253	16	7087	50	13648	407	12639	47	124	70	109	162
20	29538	3786	19	81	64	42221	14	6190	42	10550	899	9516	49	152	57	96	181
25	26743	3318	16	57	46	44866	11	5730	38	10856	625	9732	40	122	48	91	142
30	25759	7105	16	72	49	46003	11	5910	38	12391	618	12842	45	116	63	92	159
35	25169	4765	17	58	41	45290	11	5723	37	10488	540	11330	40	129	53	95	143
40	24086	3214	19	59	40	47485	10	5104	34	10204	964	9755	43	155	46	90	151
45	26853	4487	12	55	45	50463	11	5604	38	11472	287	11152	39	139	50	98	127
50	33286	2708	12	62	35	38434	15	6707	48	10384	233	7390	39	122	46	104	125
55	26705	3108	13	51	35	41962	10	5409	38	11165	211	8722	37	108	41	88	113
60	38051	3332	15	65	33	43717	16	7207	53	11003	354	8104	44	101	51	111	121
65	35099	3046	13	56	28	41766	15	6196	46	10314	365	6929	37	75	44	98	103
70	31732	2691	15	54	30	45762	14	6090	44	9738	414	7802	38	78	46	103	112
75	20235	1925	12	44	23	31610	9	4363	30	7553	301	5818	31	54	34	76	92
80	34826	4007	12	54	28	41254	14	6219	44	10794	336	8796	36	66	46	91	108
85	27879	3045	13	50	27	36349	12	5808	39	9128	357	7480	36	67	42	88	101
90	32722	3140	19	64	43	45896	14	6459	46	10188	1052	9830	47	153	52	105	155
95	21908	3162	14	53	38	42106	10	4916	33	9620	342	8450	37	122	46	90	122
110	11726	31935	6	20	12	15920	6	2732	16	5963	173	3771	16	23	65	38	57
130	8492	36859	5	15	6	12118	5	2361	12	4800	151	3113	12	13	79	31	33
140	5477	29198	3	9	5	9150	4	1668	7	3435	125	2469	9	13	66	22	27
150	4766	36826	6	12	4	10082	2	1538	6	3398	139	2881	10	8	78	28	31
160	9145	39177	8	19	11	14810	4	2277	12	5113	162	3522	14	16	78	38	43
170	4637	35380	5	11	4	8856	2	1495	6	3333	136	2199	8	8	71	25	30
180	4081	35666	5	11	4	9268	1	1381	6	3163	151	2480	8	8	78	26	27
190	8849	42050	5	13	5	14047	5	2324	11	4845	175	2791	10	9	91	28	28
200	8712	39857	5	14	5	13241	5	2356	12	4622	180	2872	11	12	96	30	32

Core H (mg kg $^{-1}$)

Depth (cm)	Al	Ca	Co	Cr	Cu	Fe	Ga	K	Li	Mg	Mn	Na	Ni	Pb	Sr	V	Zn
0	39245	47874	13	66	38	49544	12	8915	61	13496	452	12381	48	66	169	104	163
5	24139	5155	12	56	39	36227	7	5662	37	10159	429	9334	38	69	56	82	125
10	32946	5789	15	77	48	49294	11	7098	50	12198	568	10241	49	106	68	107	172
15	37078	6598	16	91	58	49315	12	7300	54	12429	730	8958	54	122	66	110	202
20	32058	6303	13	91	68	40840	11	6642	46	11594	526	8988	45	116	56	98	183
25	25049	5098	16	77	67	36467	8	5656	37	9834	1066	9013	47	116	53	91	180
30	28204	5619	13	75	65	35134	9	6146	42	9537	417	7618	37	127	50	88	168
35	19597	6016	14	61	61	36321	6	4501	29	9566	570	8289	36	132	44	77	172
40	22144	5683	9	61	57	34144	7	5128	34	9452	321	7532	35	108	43	78	163
45	20250	15121	10	49	49	31100	5	5045	32	8835	247	7163	30	102	55	70	161
50	28122	23934	8	56	53	29501	8	6498	41	9613	237	7585	33	100	74	83	193
55	20516	33465	7	40	30	22373	5	5119	30	7800	207	6167	25	82	81	65	133
60	21576	37889	9	41	36	22644	5	5413	33	7984	208	6546	30	74	95	66	182
65	24777	35740	8	45	39	25807	6	6071	37	8355	218	7100	28	88	94	71	134
70	24214	39837	9	46	42	27437	7	6071	37	8823	233	7325	30	78	102	74	154
75	23128	38663	8	41	36	26426	7	5816	35	7928	229	6839	27	83	98	68	130
80	18566	36089	9	39	33	25859	5	4978	29	8143	232	7242	28	95	87	64	134
85	25857	38934	9	49	36	31394	8	6316	40	9664	262	8087	32	93	102	80	144
90	27153	35462	10	50	38	30789	8	6824	42	9357	262	8125	33	96	101	81	148
95	23372	32138	9	46	34	27690	7	5902	36	8357	236	7553	30	82	87	73	126
100	26769	37508	10	51	39	31479	7	6612	41	9907	265	8580	32	96	97	81	146
110	18780	29703	9	41	34	26236	5	5008	30	7906	217	7227	28	92	76	63	120
120	20736	32759	8	44	33	28009	5	5396	33	8482	242	7468	27	89	83	69	112
130	21522	32977	9	47	40	29261	6	5710	35	9008	270	7876	29	100	84	72	151
140	20487	36474	10	40	33	27857	6	5230	32	8290	266	7247	25	89	94	64	108
150	23316	42463	9	39	30	31548	6	5515	34	8571	285	7543	28	77	114	68	94
160	22685	42365	8	40	31	29812	6	5840	35	8117	287	7453	28	81	124	66	96
170	19778	41606	8	36	29	29301	5	5144	31	7858	276	7175	27	74	117	61	88
180	18354	35370	9	39	31	26172	5	4876	29	7783	254	6829	25	86	89	62	115
190	24399	43498	9	47	32	31738	7	5913	36	8731	297	8158	30	86	120	71	109
200	20520	39337	9	39	29	28384	5	5243	31	7954	275	7036	27	80	108	63	101
220	19168	40914	8	37	29	27739	5	5081	30	7721	274	7081	26	78	113	60	91
231	21354	37972	8	44	31	29594	6	5516	33	8181	298	7616	28	82	110	66	104

Appendix 6: Lithium Normalised Downcore Metal Plots

Aluminium (Al/Li)

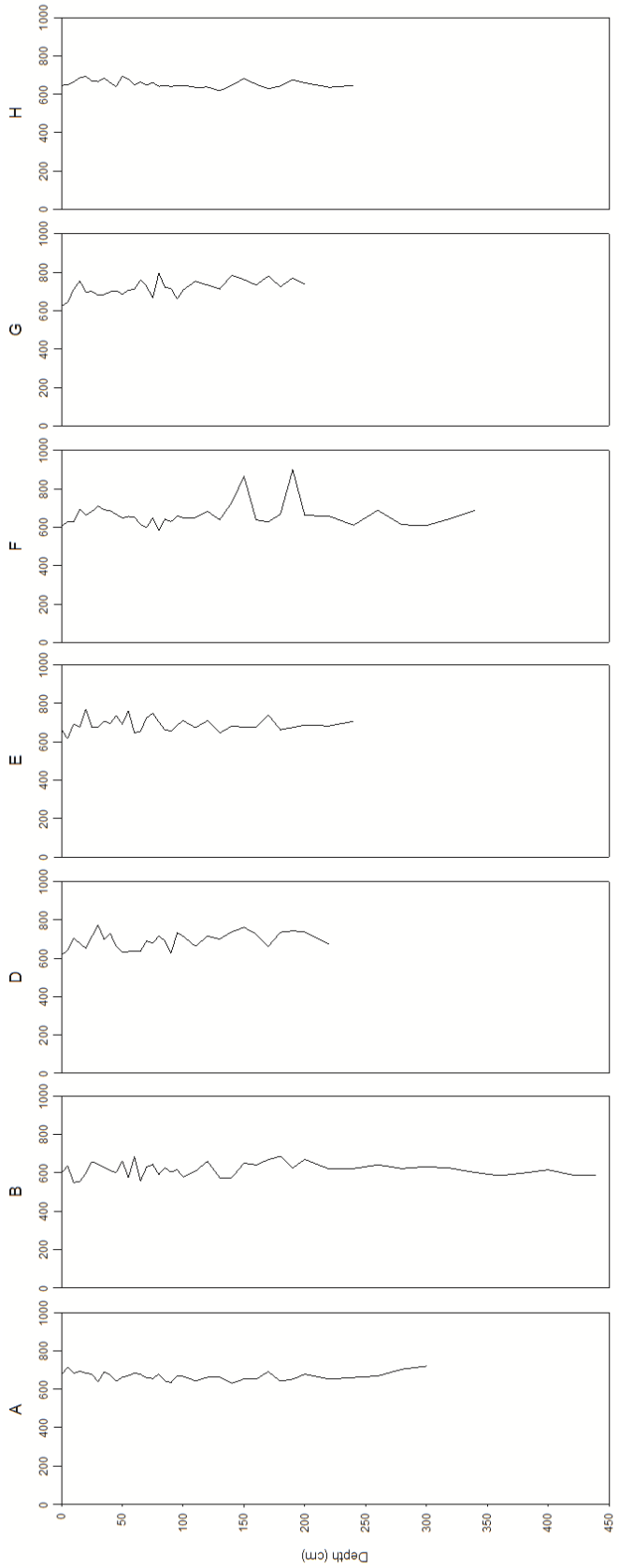

Calcium (Ca/Li)

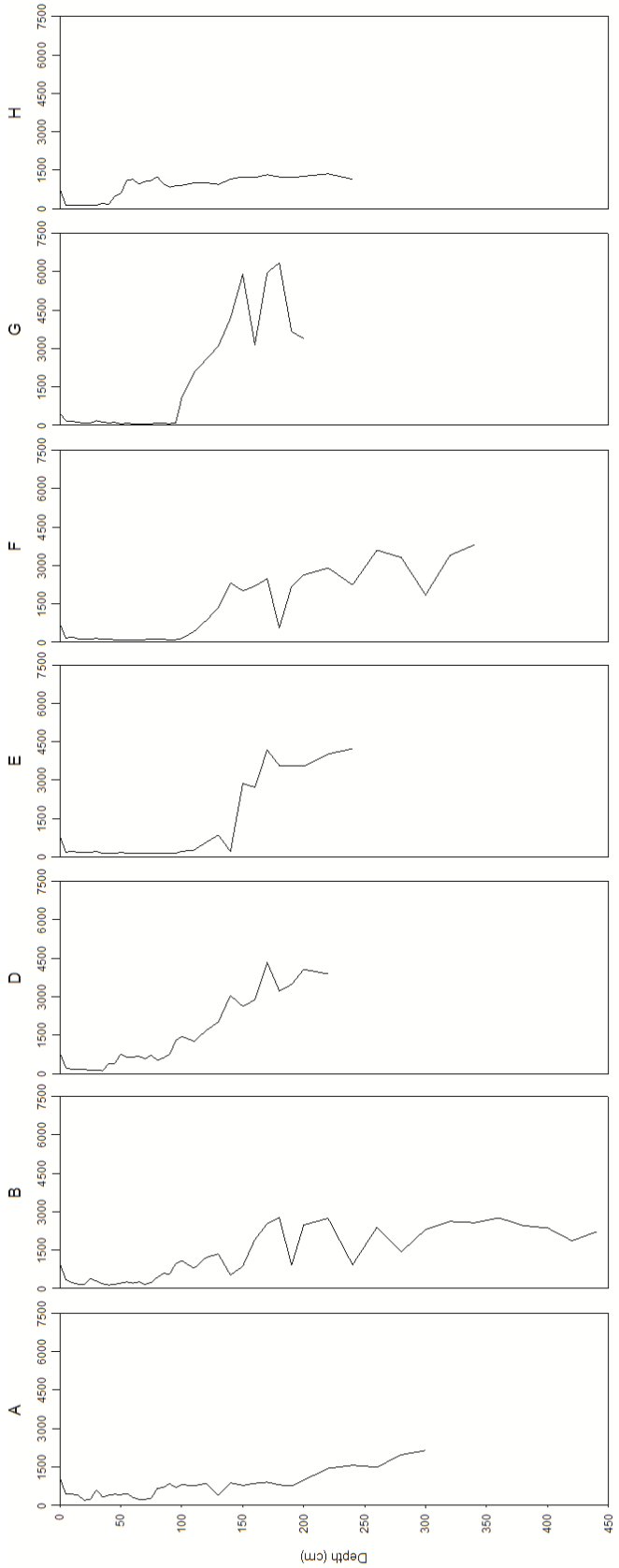

Cobalt (Co/Li)

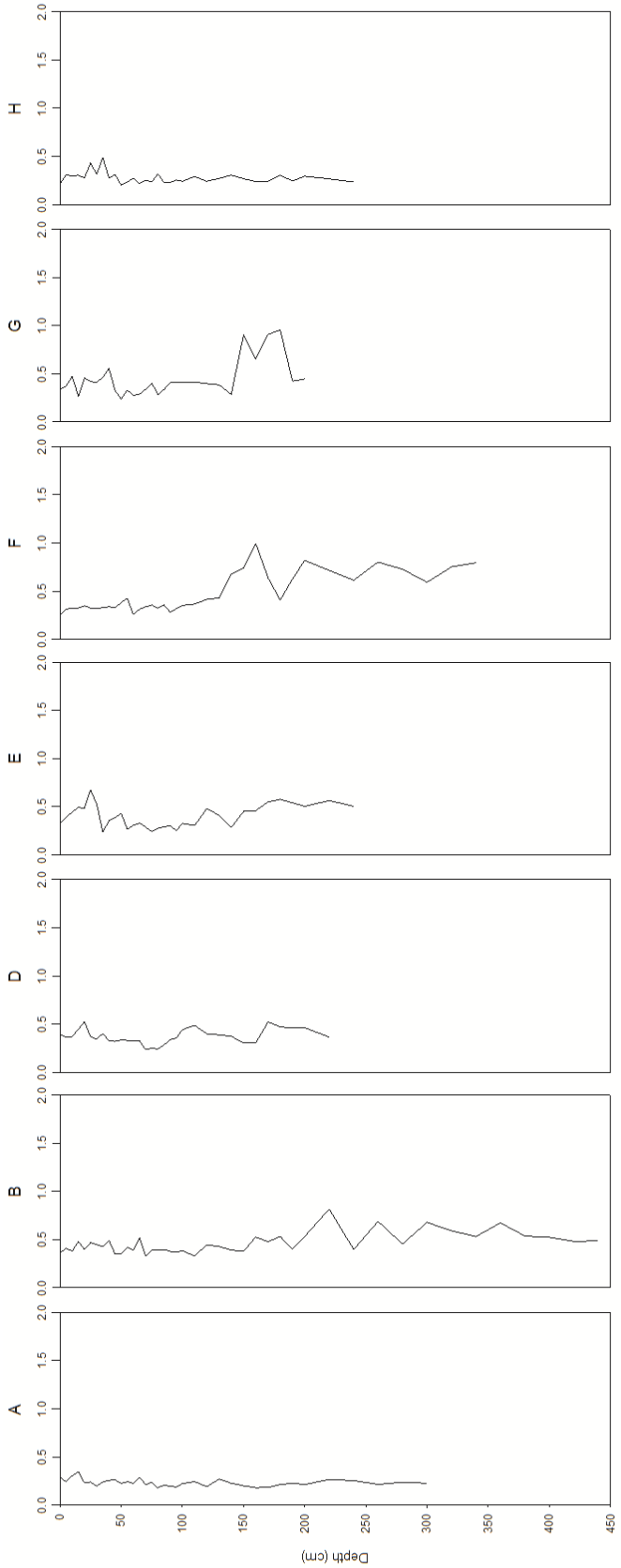
H
G
F
E
D
B
A
0.0
0.5
1.0
1.5
2.0
0
50
100
150
200
250
300
350
400
450
Depth (cm)

Chromium (Cr/Li)

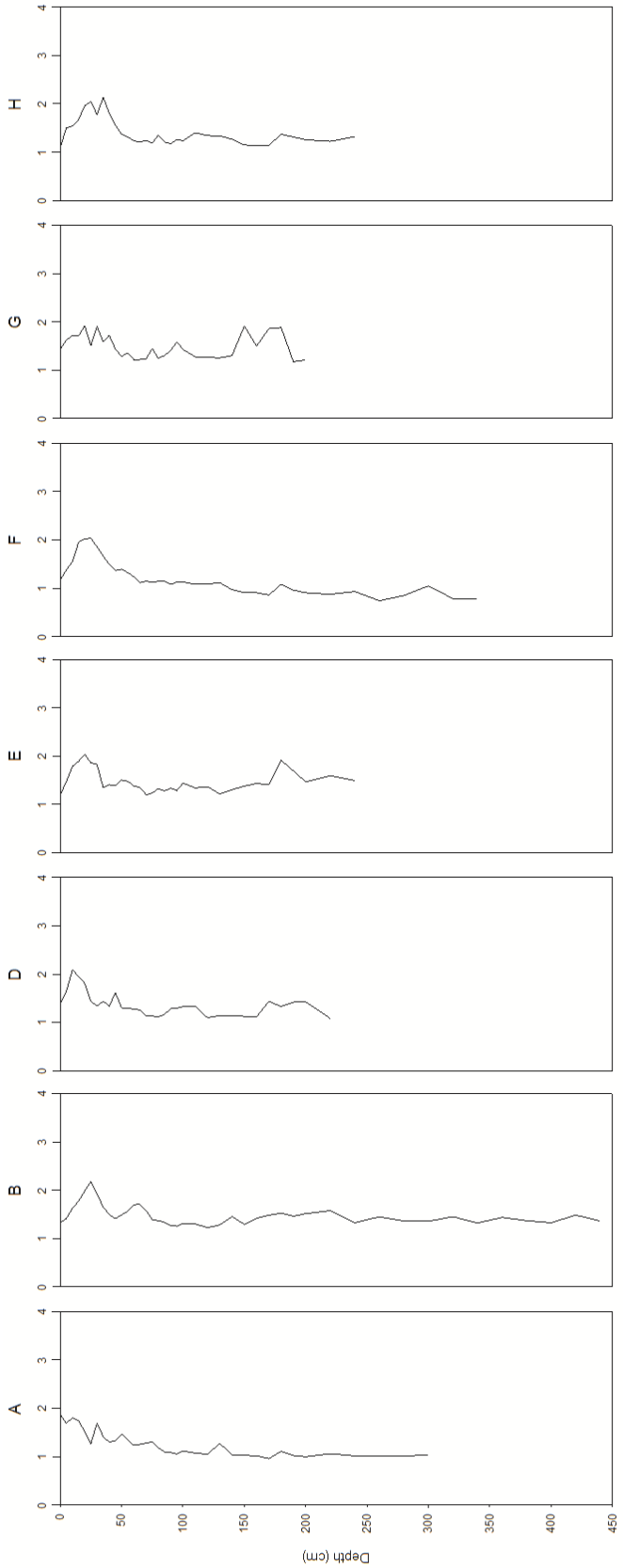

Copper (Cu/Li)

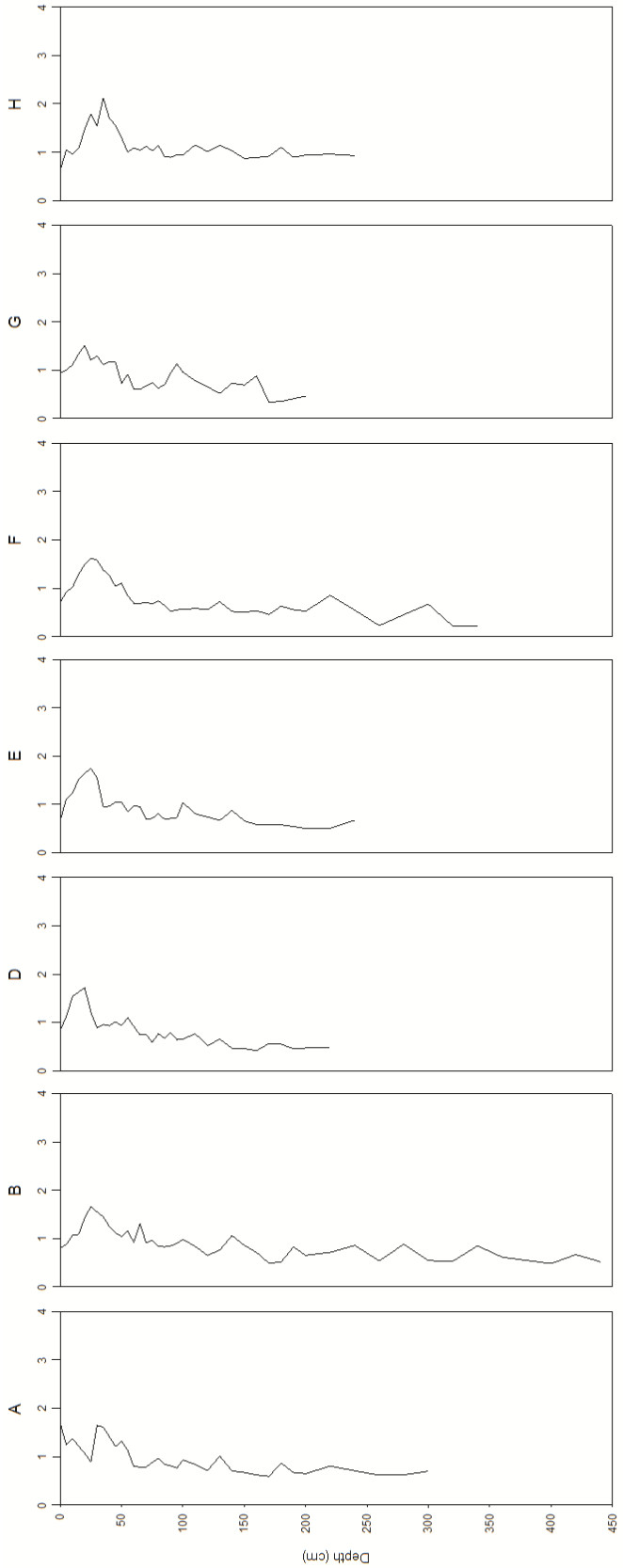

Iron (Fe/Li)

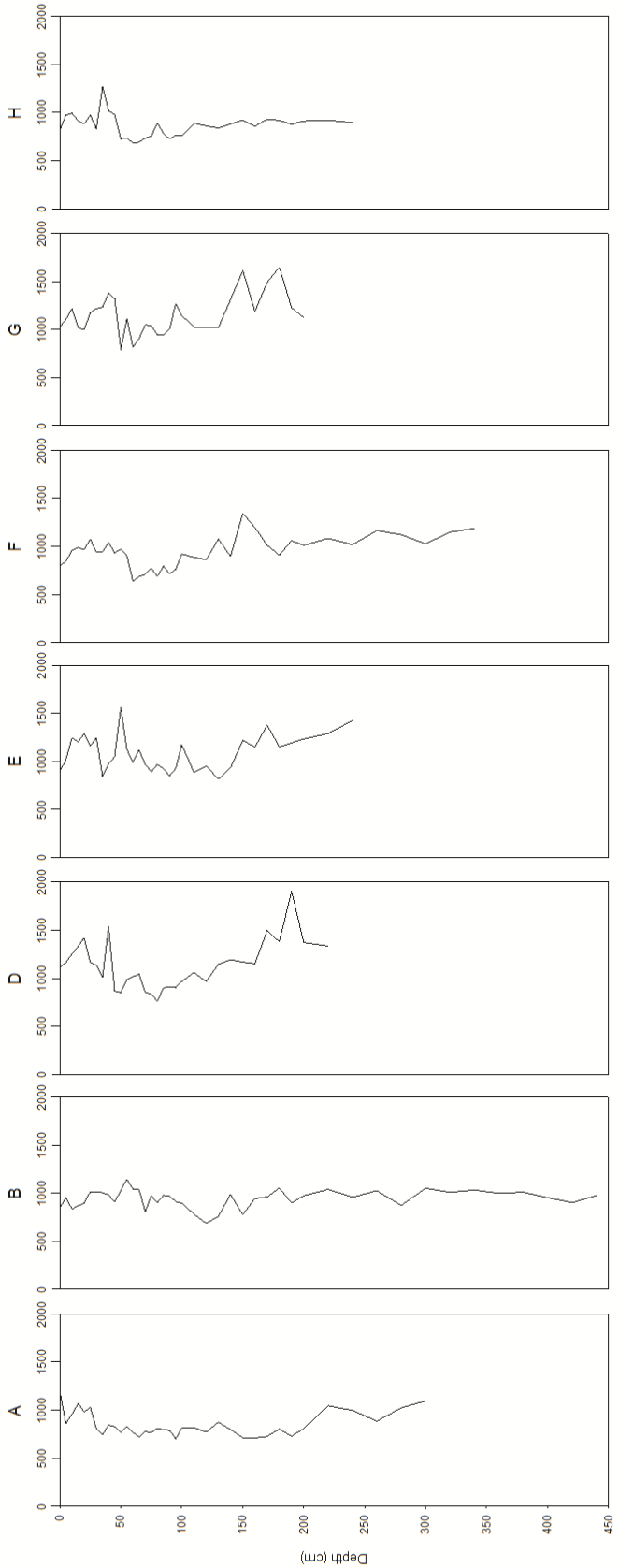
H
G
F
E
D
B
A
0
500
1000
1500
2000
0
50
100
150
200
250
300
350
400
450
Depth (cm)

Gallium (Ga/Li)

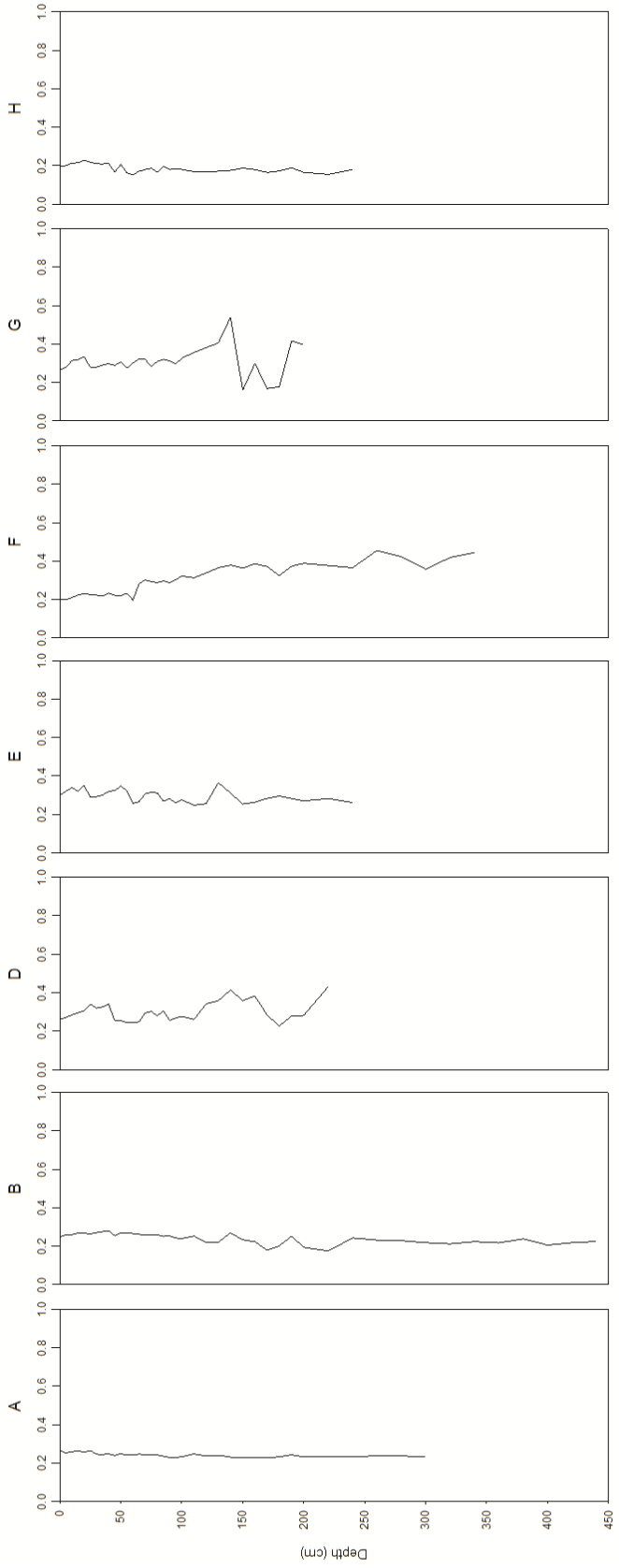

Mercury (Hg/Li)

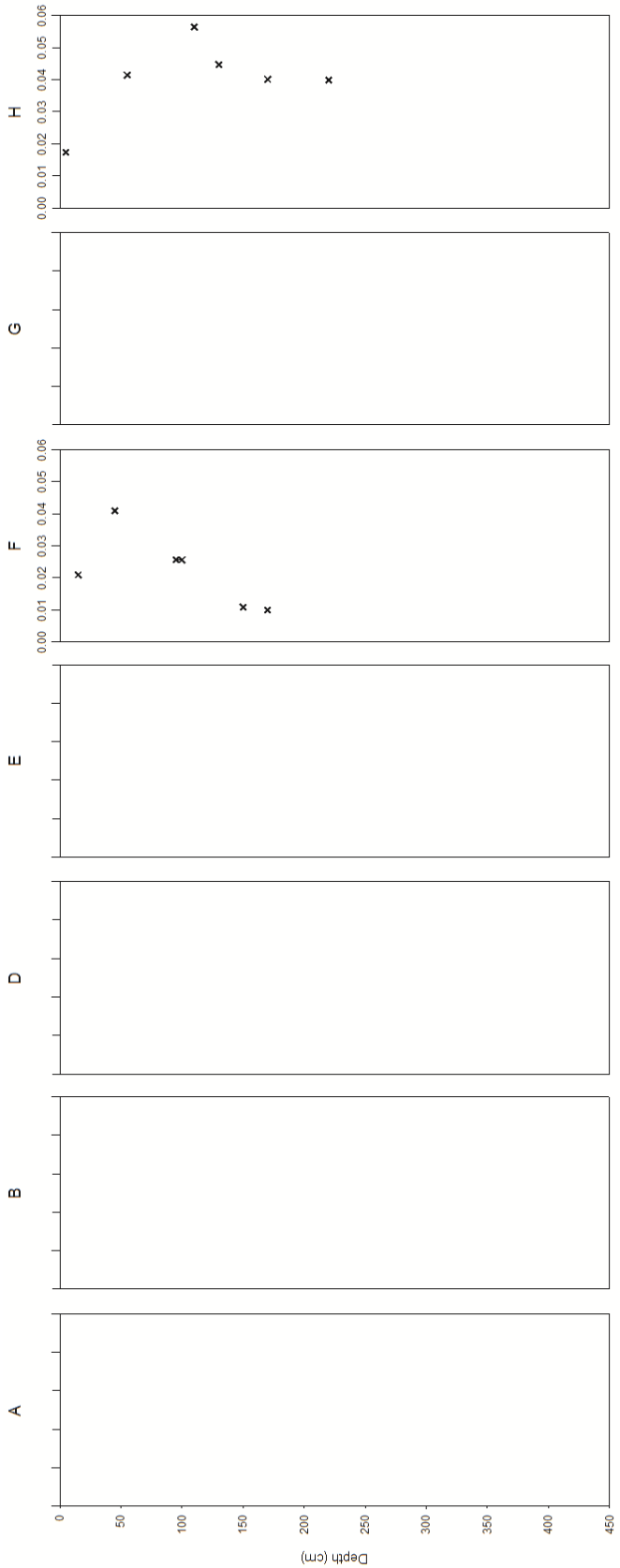

Potassium (K/Li)

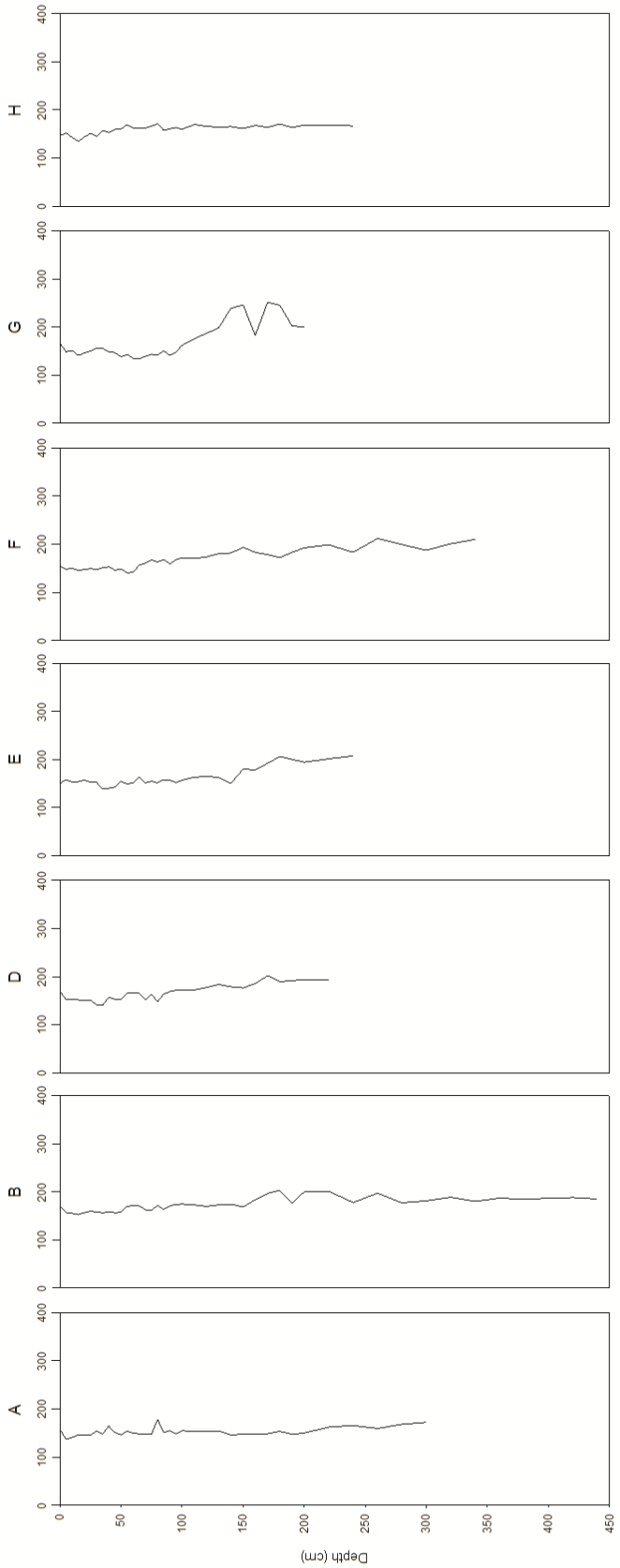

Magnesium (Mg/Li)

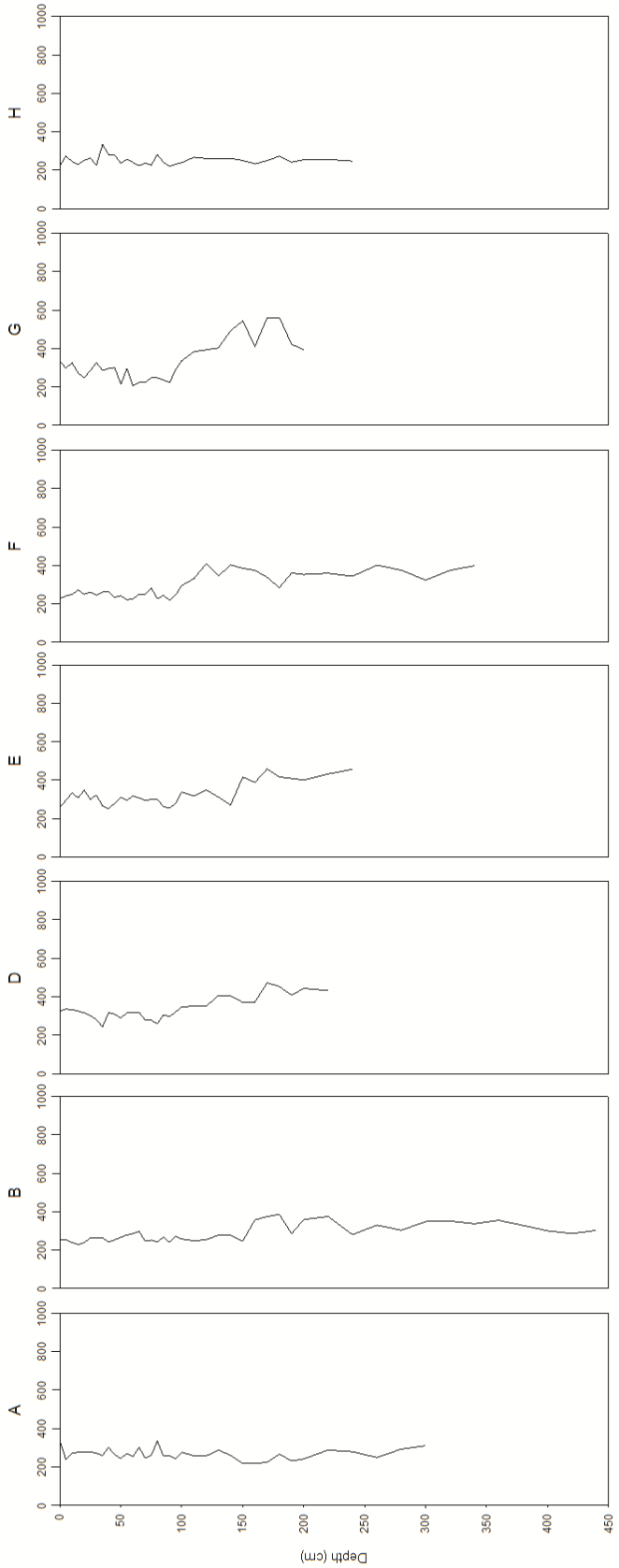

Manganese (Mn/Li)

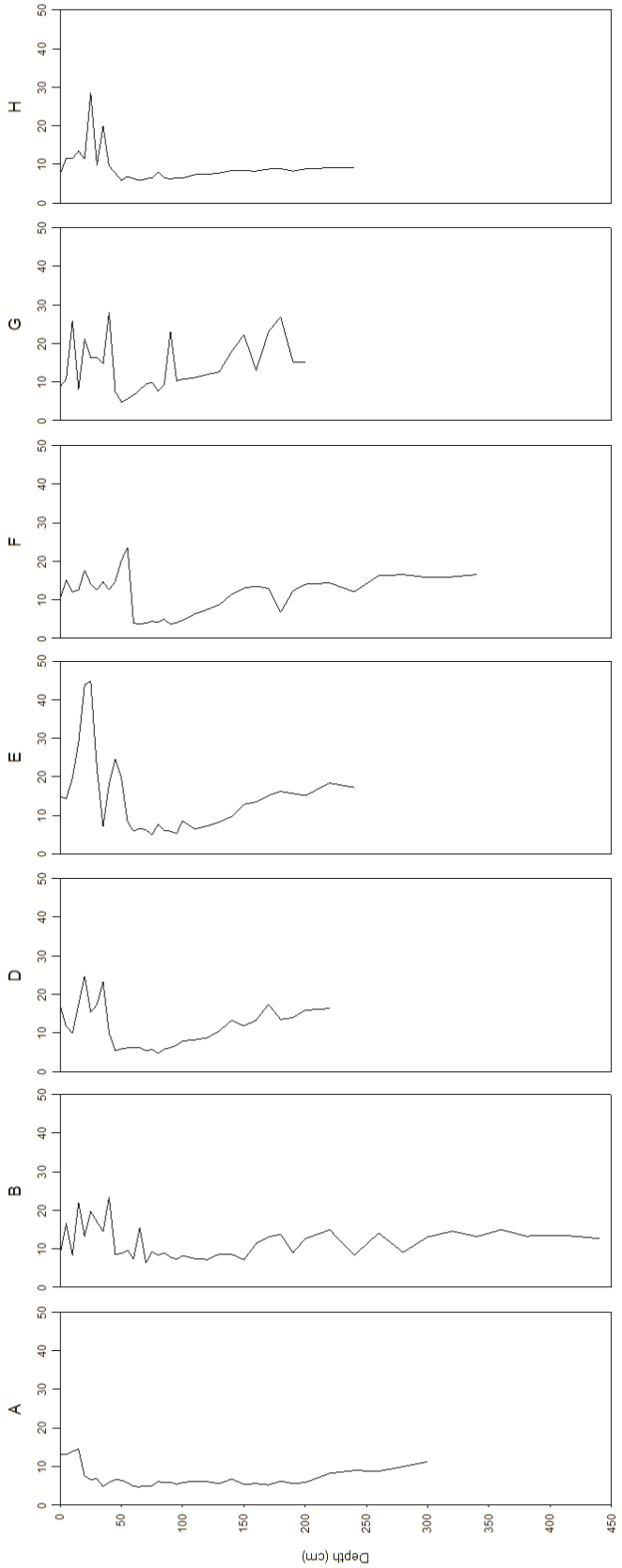

Sodium (Na/Li)

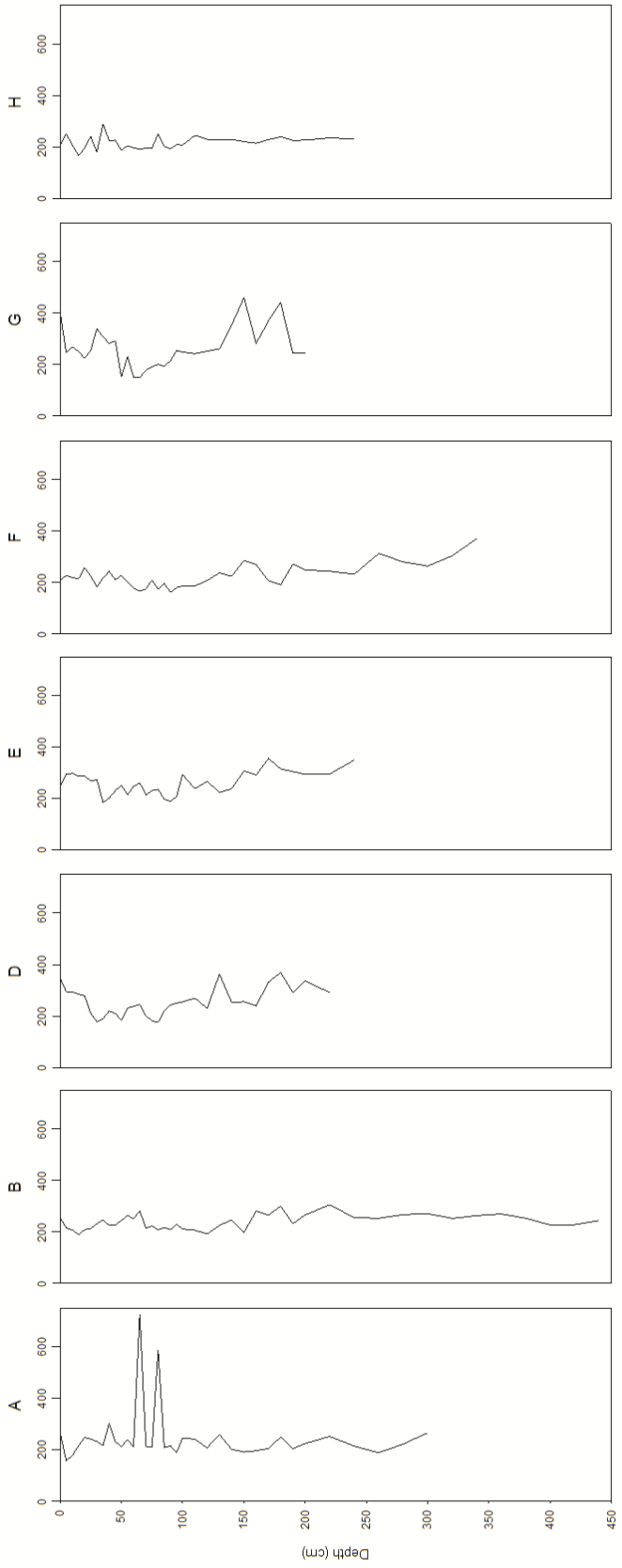
H
G
F
E
D
B
A
0
200
400
600
0
50
100
150
200
250
300
350
400
450
Depth (cm)

Nickel (Ni/Li)

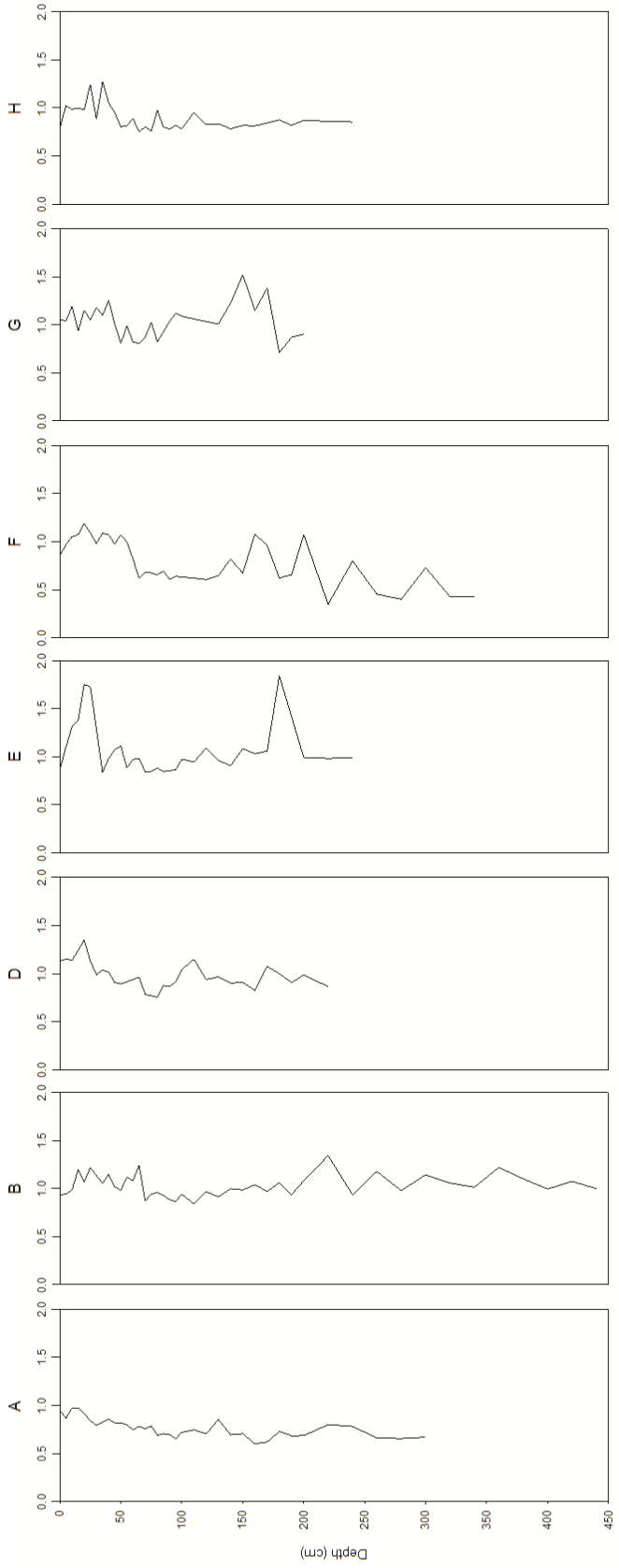
H
G
F
E
D
B
A
0.0
0.5
1.0
1.5
2.0
0
50
100
150
200
250
300
350
400
450
Depth (cm)

Lead (Pb/Li)

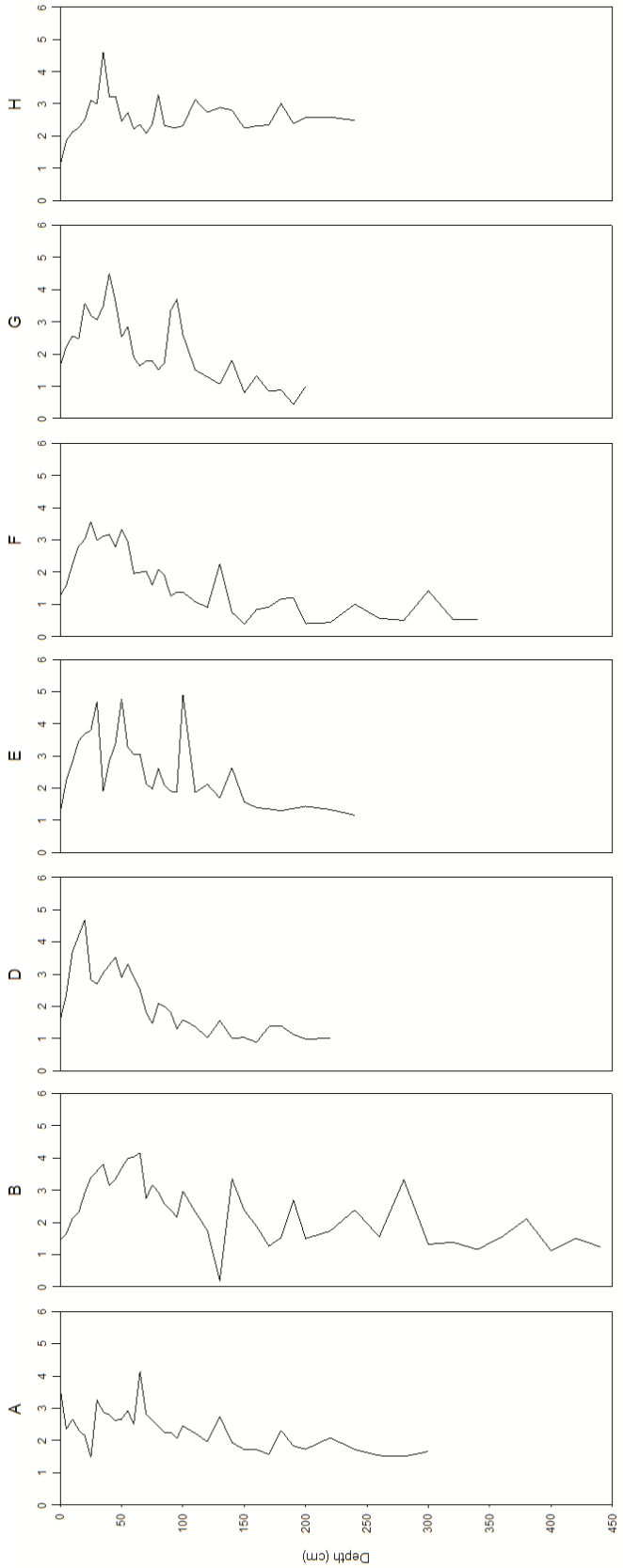

Strontium (Sr/Li)

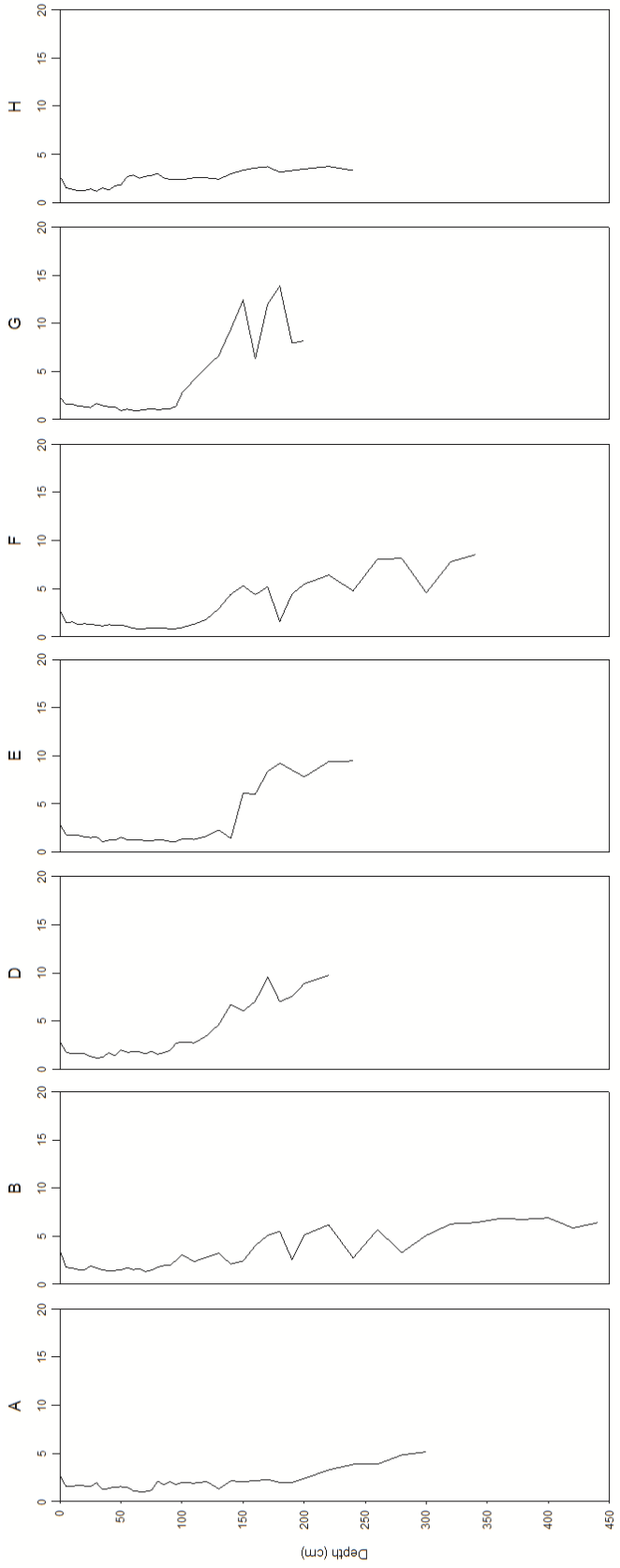

Vanadium (V/Li)

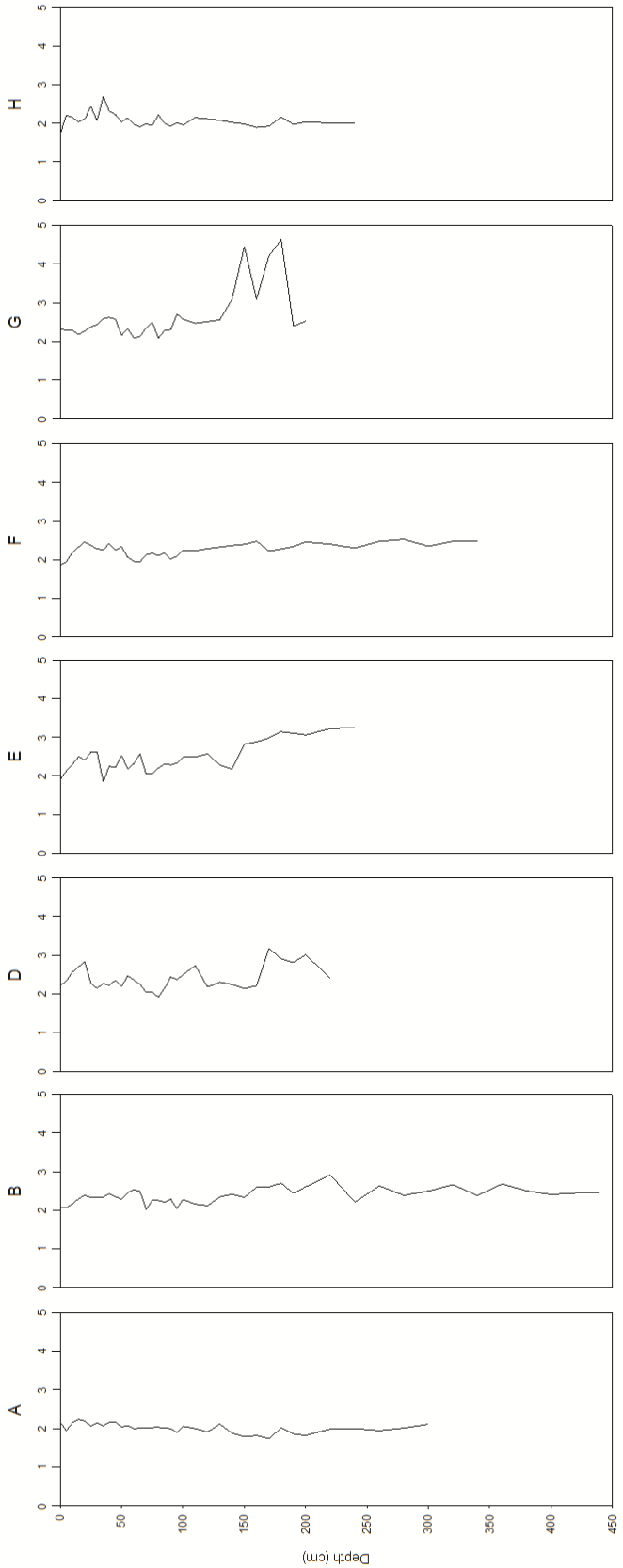

Zinc (Zn/Li)

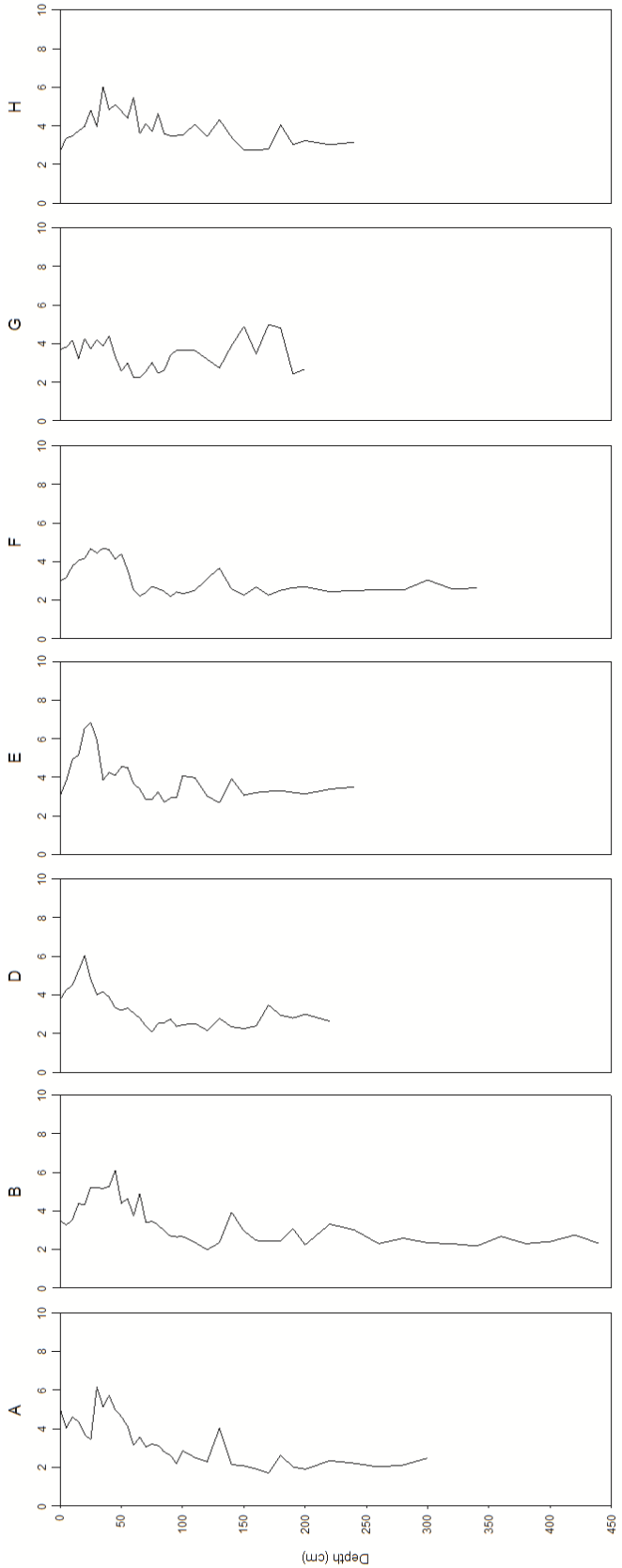

Appendix 7: Downcore Enrichment Values

Aluminium (Al/Li)

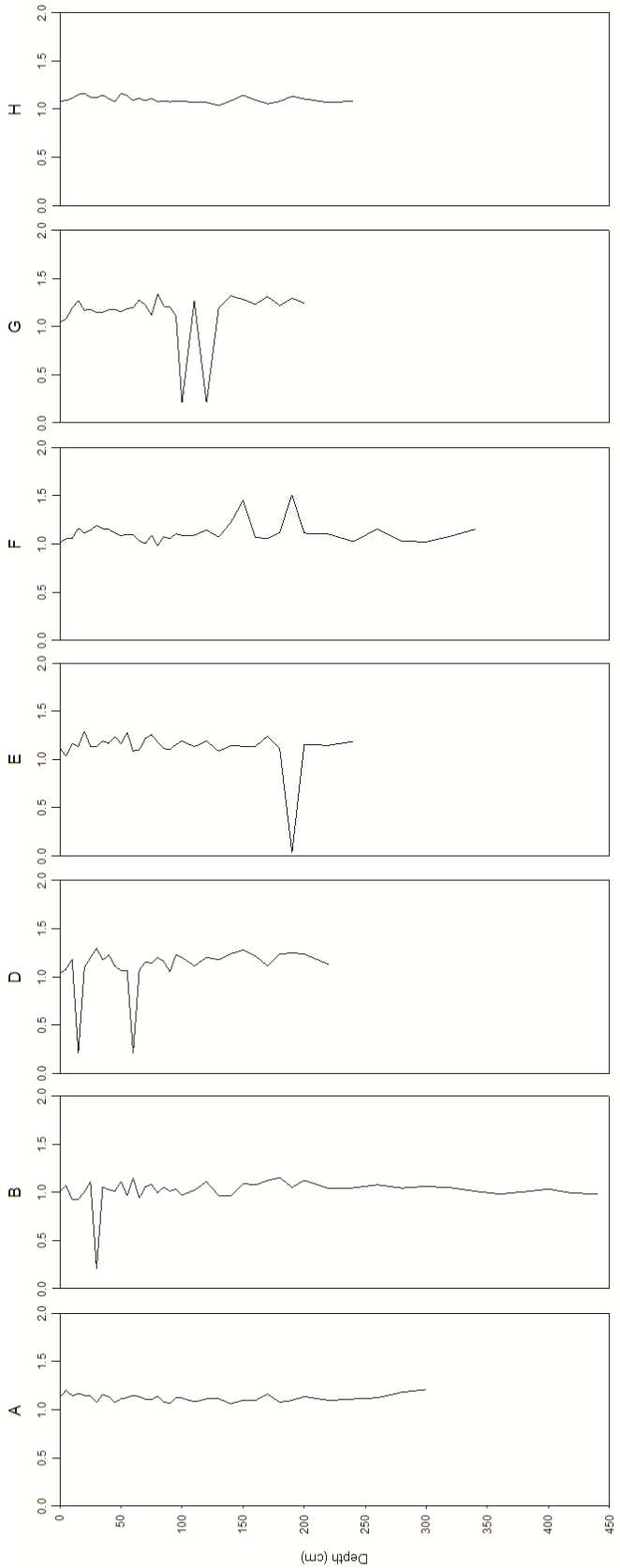

Calcium (Ca/Li)

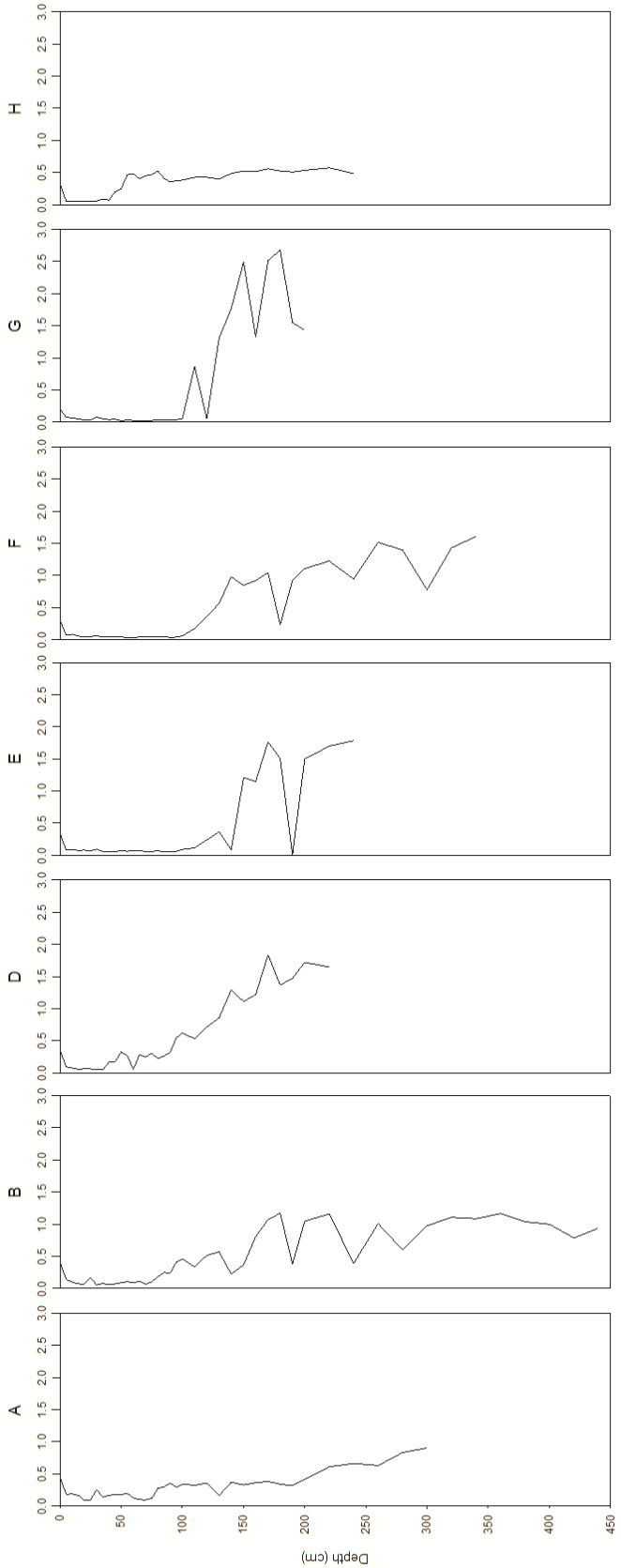

Cobalt (Co/Li)

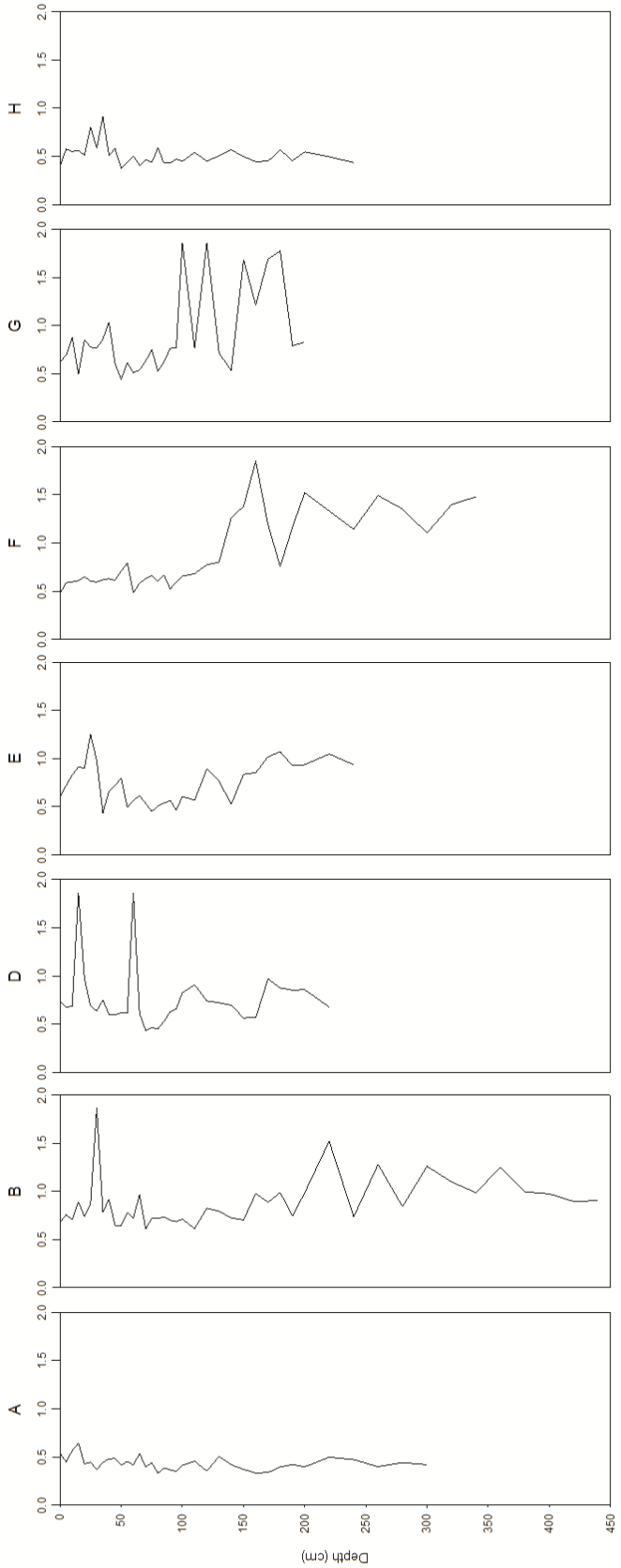
H
G
F
E
D
B
A
0.0
0.5
1.0
1.5
2.0
0
50
100
150
200
250
300
350
400
450
Depth (cm)

Chromium (Cr/Li)

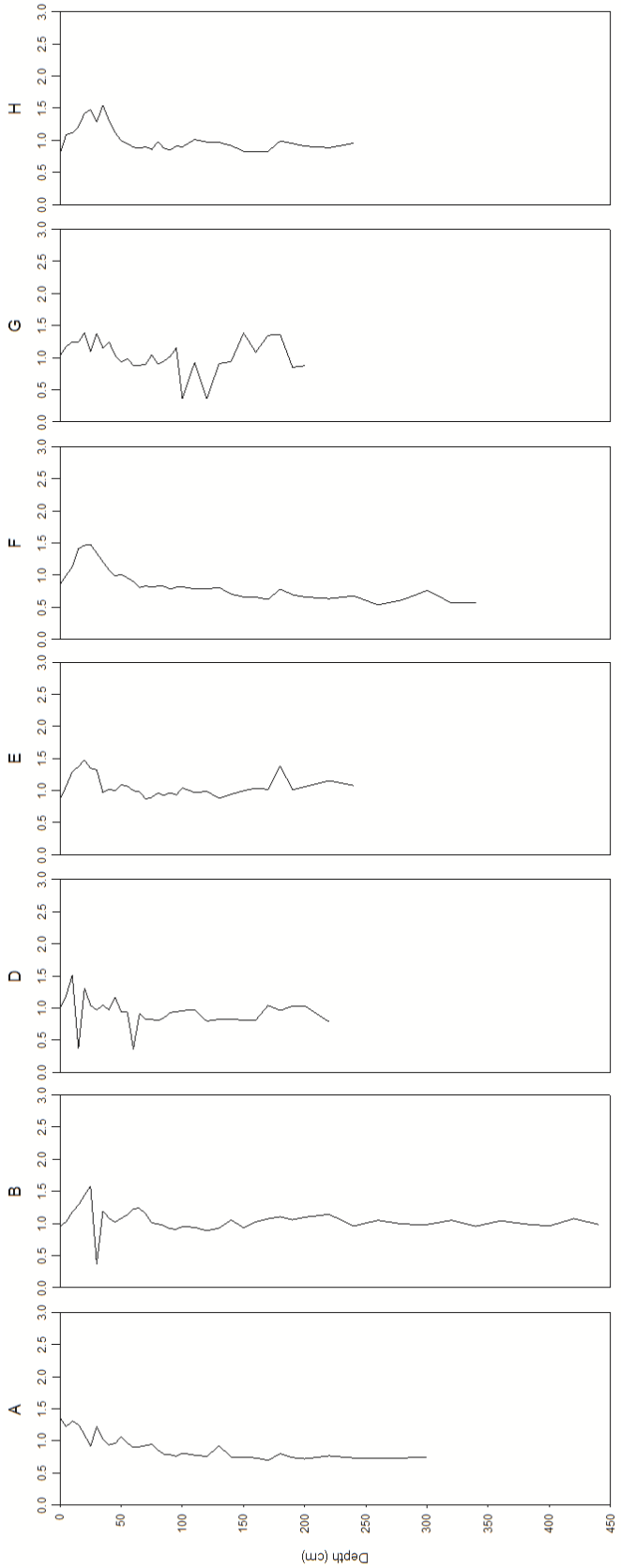

Copper (Cu/Li)

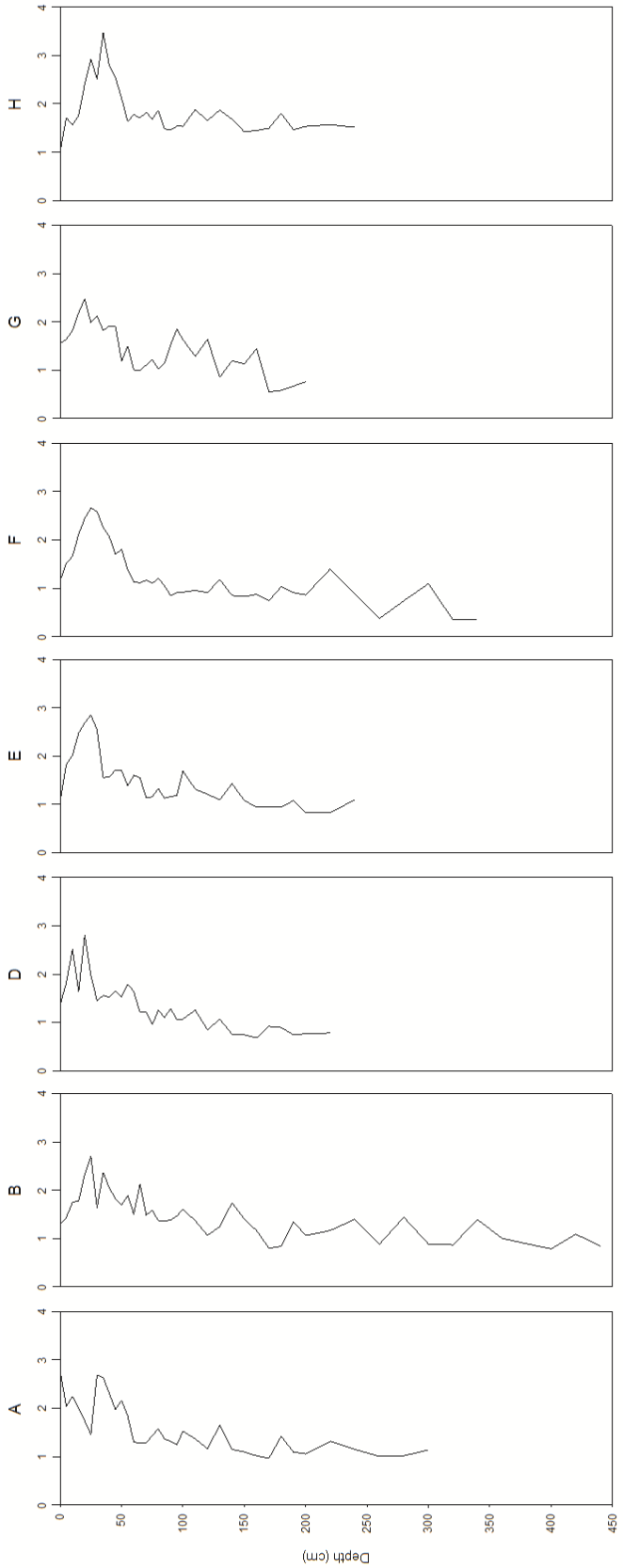

Iron (Fe/Li)

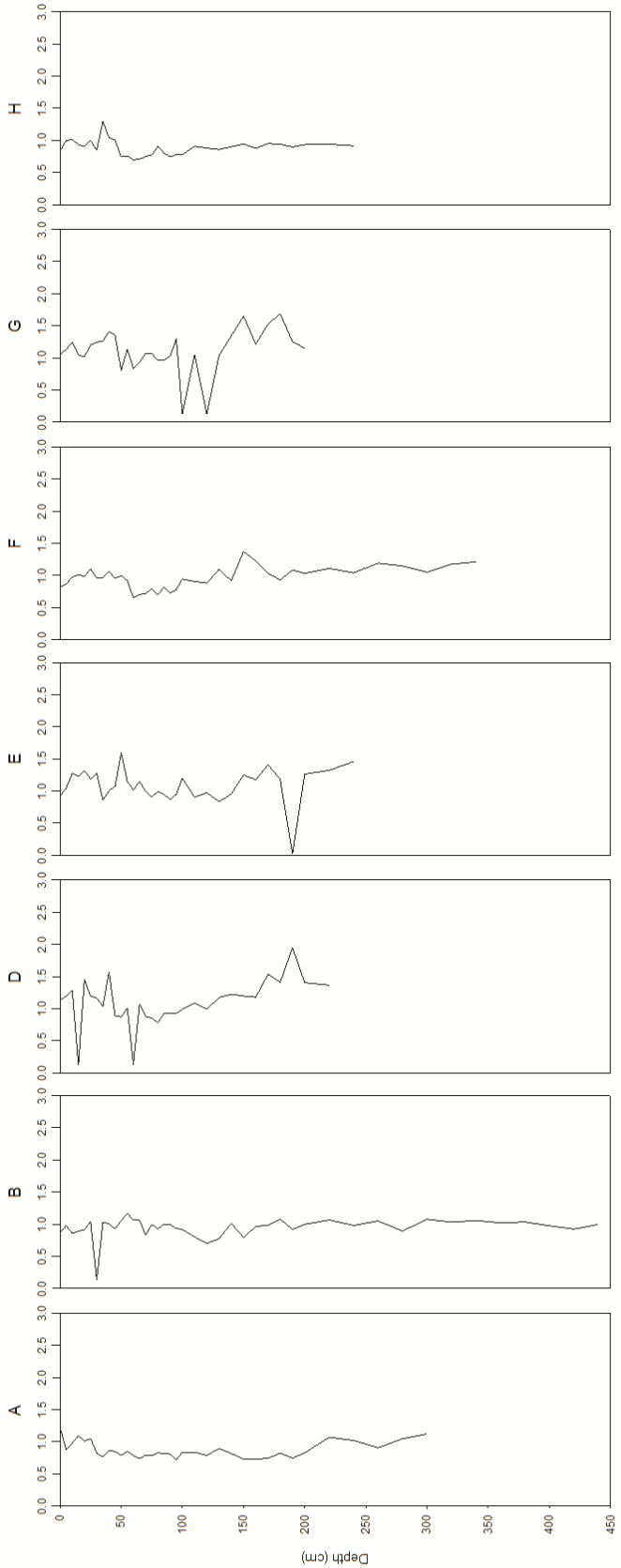
H
G
F
E
D
B
A
0.0
0.5
1.0
1.5
2.0
2.5
3.0
0
50
100
150
200
250
300
350
400
450
Depth (cm)

Gallium (Ga/Li)

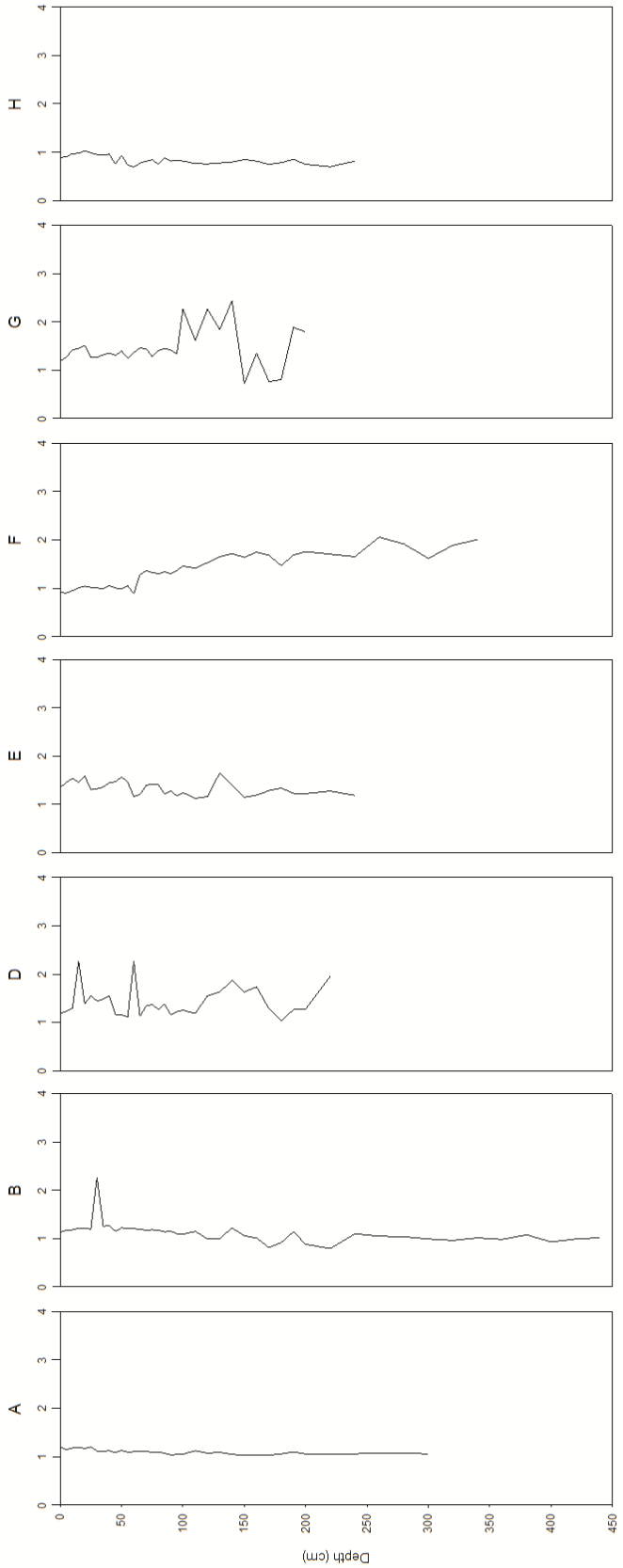

Potassium (K/Li)

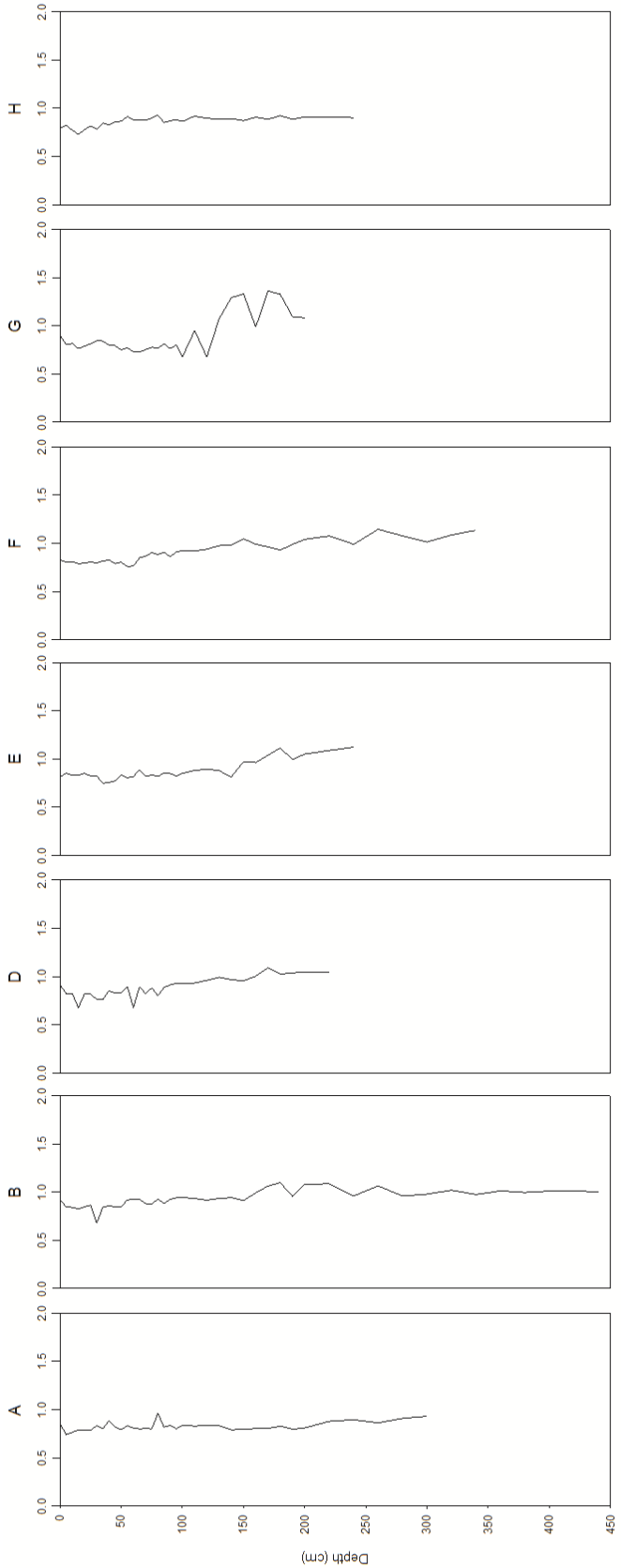

Magnesium (Mg/Li)

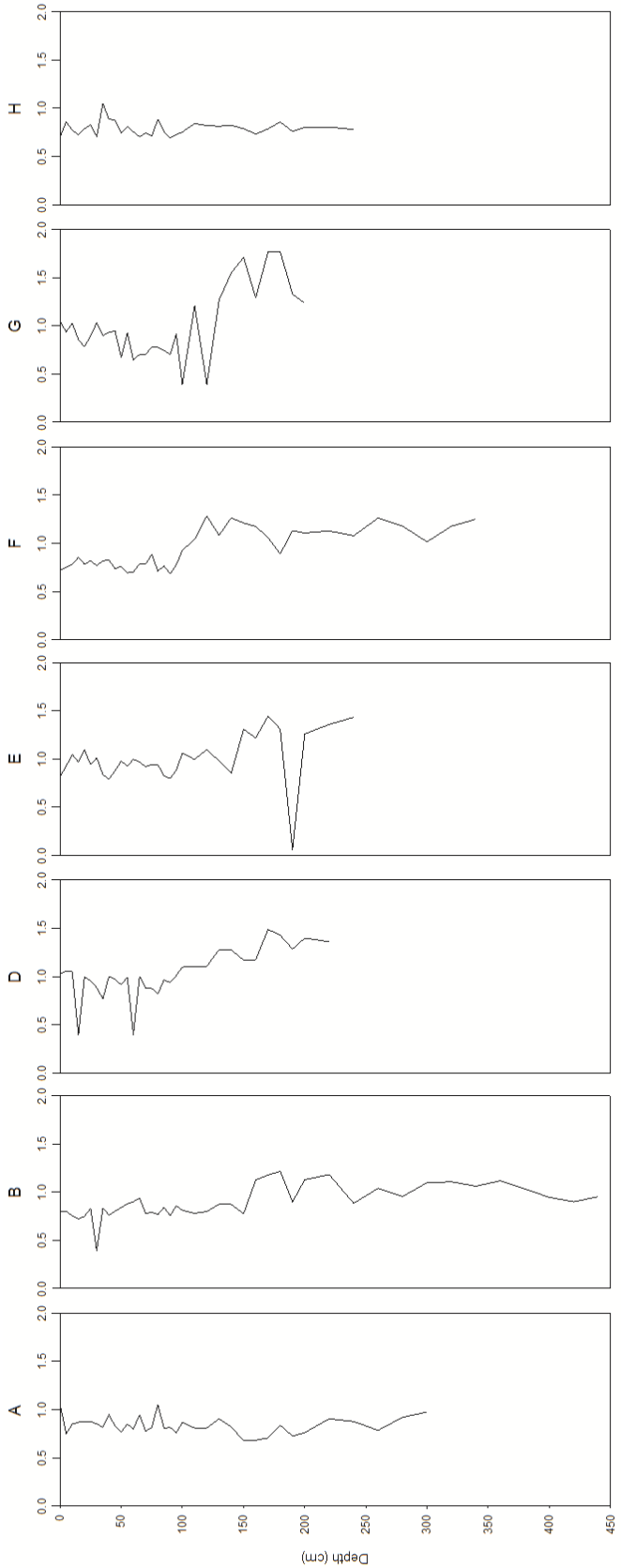

Manganese (Mn/Li)

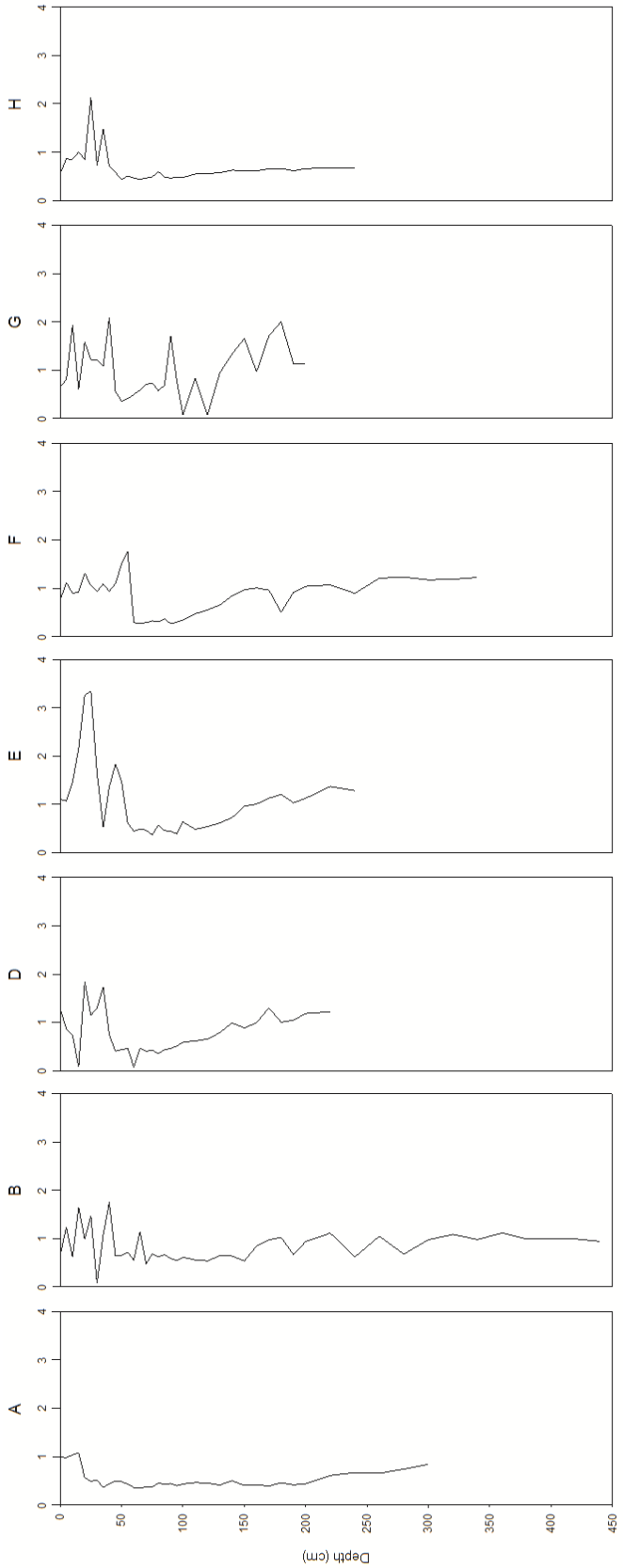

Sodium (Na/Li)

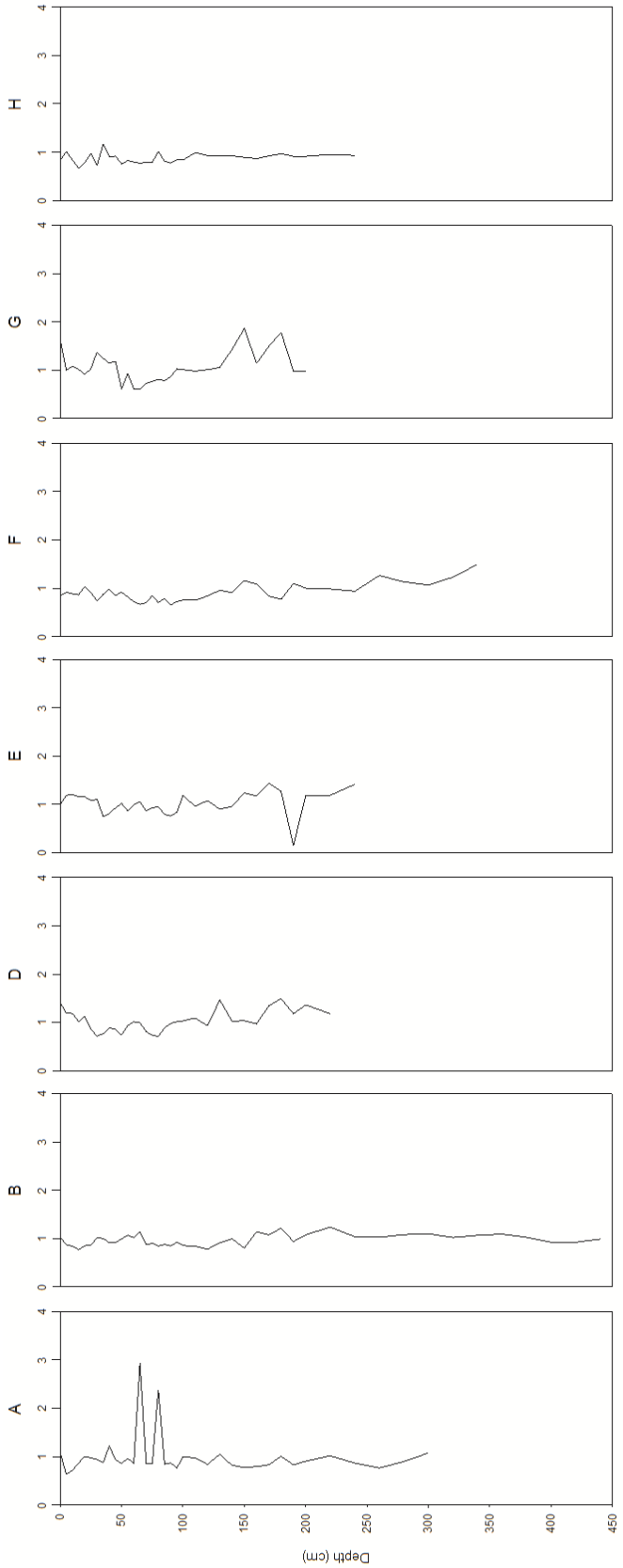

Nickel (Ni/Li)

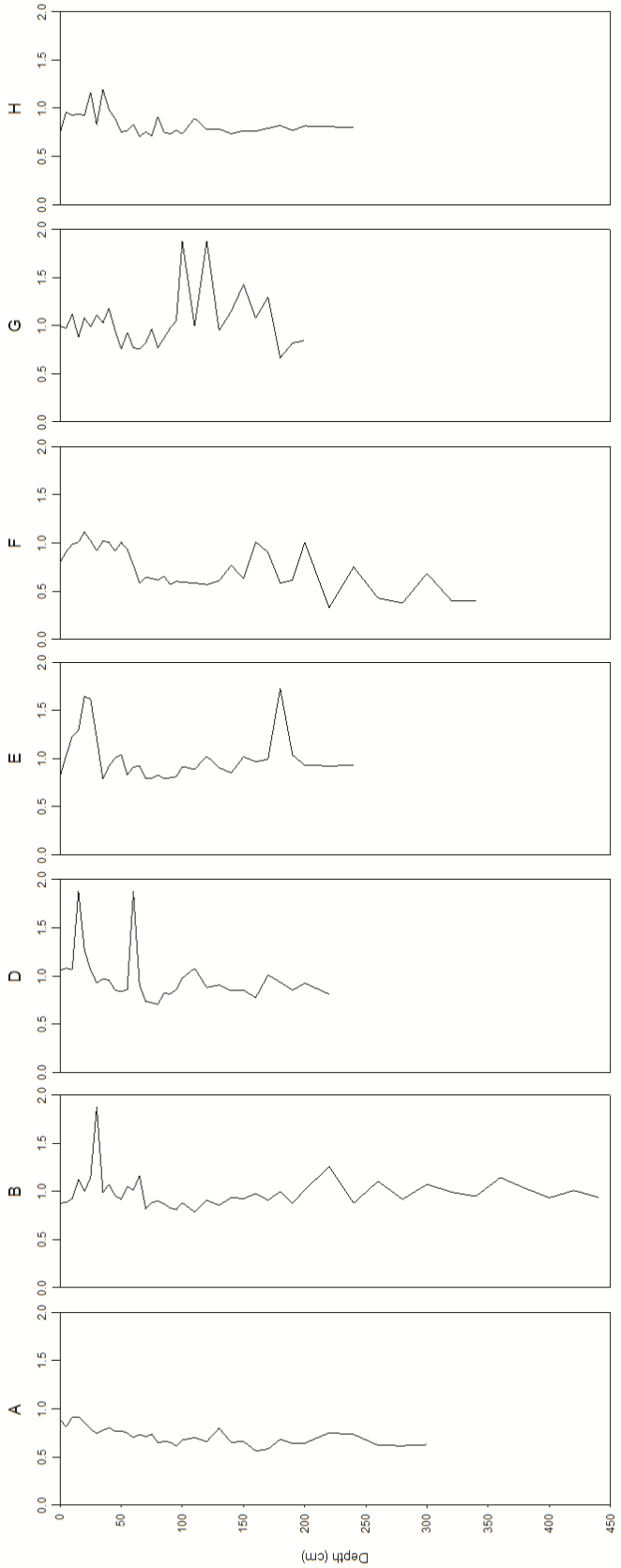
H
G
F
E
D
B
A
0.0
0.5
1.0
1.5
2.0
0
50
100
150
200
250
300
350
400
450
Depth (cm)

Lead (Pb/Li)

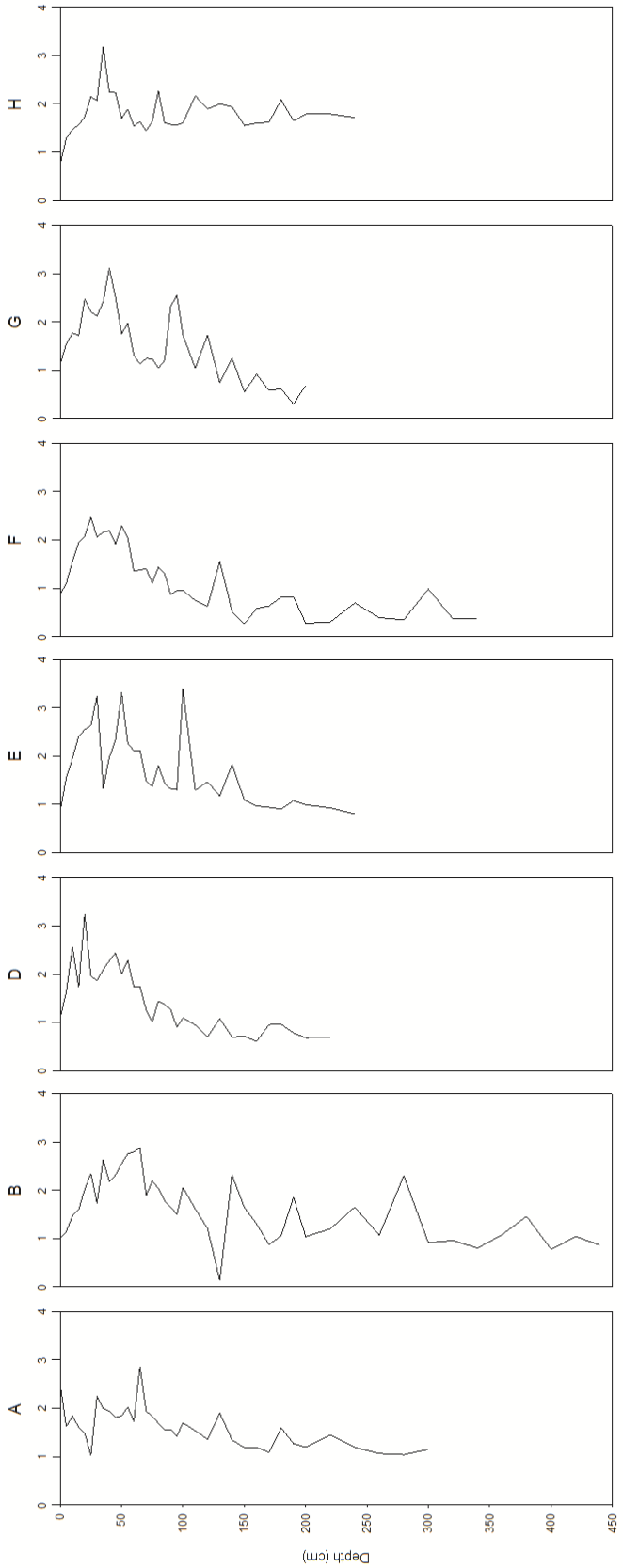

Strontium (Sr/Li)

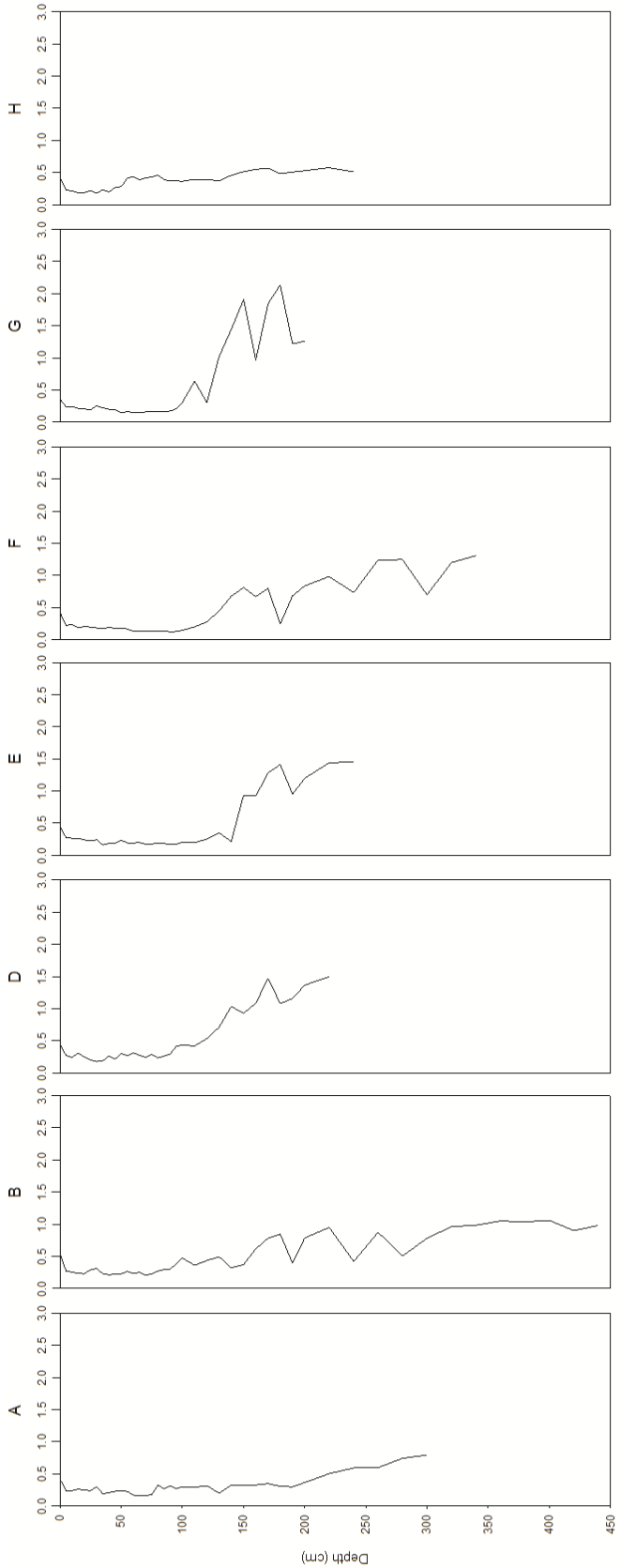

Vanadium (V/Li)

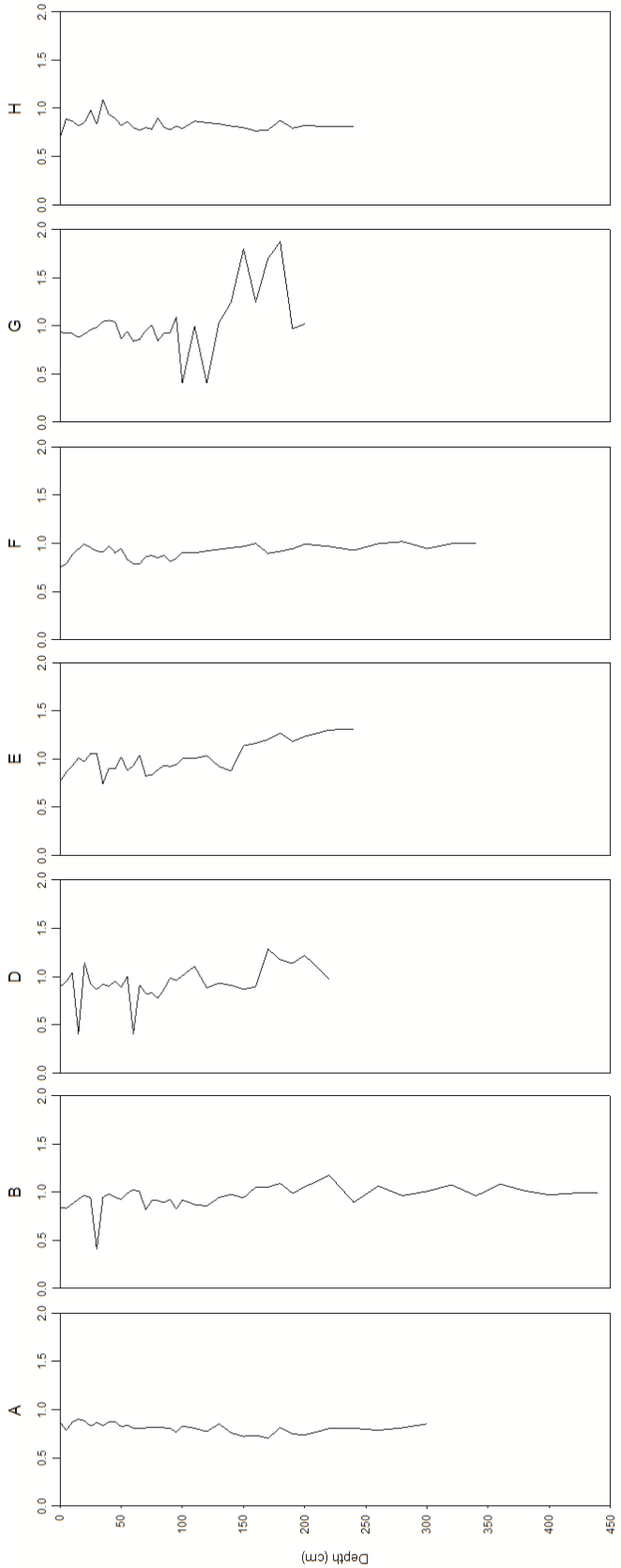

Zinc (Zn/Li)

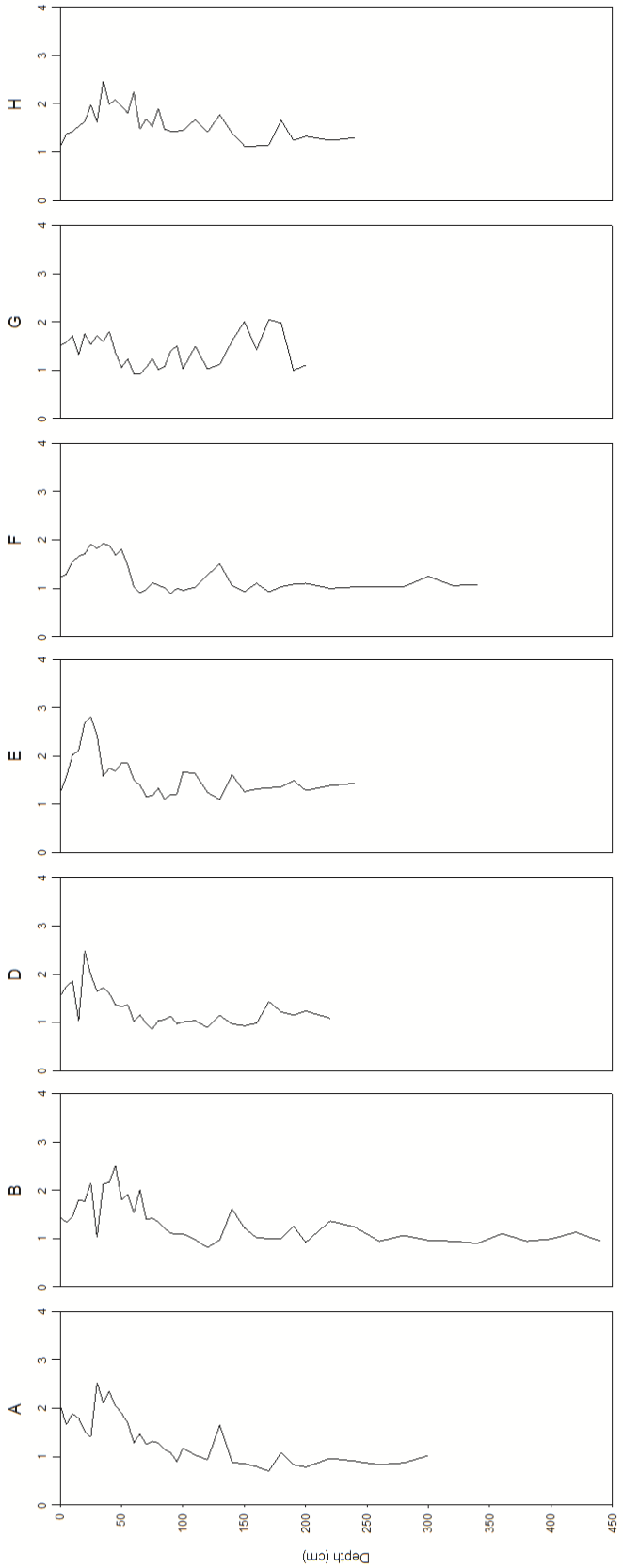

Appendix 8: Moisture Impact Concentrations

Concentration (mg kg $^{-1}$)	Moisture Content (%)												
	0	**12.8**	**13.5**	**20**	**25**	**31**	**42**	**50**	**60**	**70**	**78**	**90**	**100**	**110**
As	30	24	25	25	25	18	20	13	14	31	16	17	19	16
Ca	12847	11340	12238	12238	11504	9298	12439	63	9866	11160	11290	10359	9678	10716
Cr	49	30	34	34	32	26	25	12660	37	35	30	12	11	
Cu	253	208	221	210	194	182	157	19	124	196	145	124	145	121
Fe	36687	29100	31906	30061	28366	26281	22377	144	18840	27402	18157	18960	20580	18360
K	8617	7448	7977	7855	7198	5988	7801	20240	5982	7315	7006	6588	5911	6583
Mn	323	225	250	224	213	182	139	7956	147	153	116	94	86	76
Mo	9	6	6	6	6	6	4	171		8		4		
Pb	182	146	158	149	177	131	115	117	99	117	110	97	99	98
S	6734	5706	6472	6310	4676	4671	6962	7057	4359	5871	5990	5280	4461	5521
Sr	283	224	246	232	221	207	188	183	155	171	171	153	155	140
Ti	2870	2638	2765	2766	2597	2163	2789	2913	2431	2659	2645	2454	2303	2561
V	90	76	87	78	83	67	92	89	85	87	84	84	78	81
Zn	374	292	311	295	273	260	225	240	190	283	220	551	210	186

Appendix 9: Correction Results

	Moisture Content (%)												
	0	**10**	**15**	**20**	**25**	**30**	**40**	**50**	**60**	**7**	**075**	**85**	**90**
	Concentration (mg kg $^{-1}$)												
As	115	102	111	115	120	92	111	73	96	91	111	135	118
Cu	82	76	81	82	78	77	72	70	75	67	70	86	75
Fe	90	80	89	89	86	84	78	74	79	77	81	92	86
Mn	73	58	65	62	60	54	45	58	42	56	37	36	33
Pb	99	90	98	98	121	94	89	95	96	91	92	100	102
Sr	103	91	102	102	100	98	97	100	99	94	96	103	97
V	68	65	75	71	78	66	99	100	101	107	109	107	116
Zn	103	91	97	98	93	93	88	99	96	87	95	106	97